THESIS

EFFECT OF FIRE AND FIRE FOLLOWING AN EARTHQUAKE ON STEEL REDUCED BEAM SECTION MOMENT CONNECTIONS

Submitted by

Collin Turbert

Department of Civil and Environmental Engineering

In partial fulfillment of the requirements

For the Degree of Master of Science

Colorado State University

Fort Collins, Colorado

Summer 2013

Master's Committee:

Advisor: Hussam Mahmoud

Rebecca Atadero
Allan Kirkpatrick

ABSTRACT

EFFECT OF FIRE AND FIRE FOLLOWING AN EARTHQUAKE ON STEEL REDUCED BEAM SECTION MOMENT CONNECTIONS

The main objective of this research is to investigate the behavior of steel frames with reduced beam sections (RBS) during a fire as well as during the combined events of fire following an earthquake (FFE). Historical events and recent disasters have clearly demonstrated that the occurrence of these two events (fire and FFE) within steel framed buildings represents a probable scenario that warrants further investigation. Accurate analytical evaluation of the structural behavior of steel buildings under fire, and to a lesser extent an earthquake, is difficult due to the many complex and uncertain phenomena involved. Detailed numerical modeling of the overall structural system has been shown to provide the most reliable simulation results under current research development. However, detailed analysis is generally computationally expensive and as such not practically applicable. In addition, the nonlinear behavior of entire structures is complex and not fully understood. Therefore, detailed numerical models of the overall structural system often have difficulty capturing local failure modes. This research provides a practical analytical approach to perform accurate numerical evaluation of steel structures under fire and FFE and to closely investigate its characteristic behavior. The approach utilized is to limit the focus on localized compartment fires and investigate the behavior of a single beam-column subassembly within the chosen compartment. By limiting the focus of the study the numerical models can be simplified by utilizing specifically appropriate subassembly models for the analysis.

Using the finite element program ABAQUS, two different beam-column subassemblies with RBS were created and analyzed. The subassemblies are representative of actual connections in two steel special moment resisting frames that were designed for the highly seismic Los Angeles region. The frames selected for analysis are an 8-story 4-bay frame and a 16-story 4-bay frame and the selected subassemblies are located at the exterior of the frames at the mid and lower levels, respectively. Both subassemblies were analyzed under fire alone to determine their structural behavior during the event as well as allow for a better understanding of the influence the seismic demand has on the behavior of the connection when exposed to FFE. For the FFE simulations both models were analyzed under a suite of earthquake ground motions followed by a fire simulation. For the fire analysis portion of both simulations (fire alone and FFE) a sequentially coupled thermo-mechanical modeling technique, which includes representative constraint elements to simulate the restraint imposed by the frame is employed. The results of the study highlight the significance of including realistic boundary conditions during fire simulations and points towards the possibility for the occurrence of substantial damage in unprotected steel frames during fire as well as protected steel frames during fire following an earthquake.

TABLE OF CONTENTS

LIST OF TABLES

LIST OF FIGURES

CHAPTER 1
INTRODUCTION

1.0 Statement of the Problem

The National Fire Protection Association (NFPA) reported that in the year 2011 there were over 484,500 structure fires in the United States (U.S.) alone, resulting in 2,640 civilian deaths and over $9.7 billion in property damage (NFPA, 2013). Even with these astounding numbers the response of structures, particularly steel framed buildings, exposed to fire loading remains a relative unknown. Numerous historical events have emphasized the need for a better understanding of the response of steel-framed structures during realistic fire scenarios. Traditional building-code design provisions for fire resistance in steel-framed buildings are highly prescriptive and empirically based, simply specifying a required fire resistance rating (FRR) value for the various components of the building. These values are based on the importance, occupancy type, size, and construction material of the building and does not account for the effects of realistic fire behavior which includes complex structural and thermal interactions between building components. As a result structural engineers have both limited means and opportunities to devise, assess and implement alternative solutions for fire resistance that may be more cost-effective than conventional methods. This has created a demand for a better understanding of the actual response of steel structures when exposed to the elevated temperatures of a fire.

The response of steel-frame structures to multi-hazard events involving fire, such as fire following an earthquake, is also a field that has a relatively small knowledge base. The occurrence of fires igniting during and immediately following a seismic event is a significant issue in highly active seismic regions and represents a relevant design scenario. Structures which have been exposed to earthquake-induced damage are particularly vulnerable to the effects of fire loading and the combination of events represents a plausible scenario that isn't often considered during the design process. The current seismic design approach allows a certain degree of damage during severe earthquakes leaving the structure more vulnerable to fire loading. Furthermore, the ability of emergency response personnel to respond to the fire following a seismic event is hampered due to the earthquake-induced impairment to water supplies, transportation and communications as well as the existence of multiple fires. These factors combined with certain building characteristics and density, and meteorological conditions can create a situation in which the subsequent fire is the predominant agent of damage. Records from historical earthquakes confirm that given the right conditions the damage caused by the ensuing fire can be much worse than the damage caused by the seismic action itself, this being true for both single buildings and whole regions. For example, it is estimated that the losses due to the fires after the 1906 San Francisco (California, USA) earthquake (Figure 1-1) were 10 times larger than that due to the ground motion; in addition, for the 1923 Tokyo (Japan) earthquake it was estimated that 77% of lost buildings were destroyed by fire. Despite these facts, large fires following earthquakes remain a problem that has not been sufficiently addressed. This is clearly demonstrated by the more recent events including the 1994 Northridge (California, USA), 1995 Kobe (Japan), and 2011 Japan (Figure 1-2) earthquakes. These historical accounts have shown that the combined hazard of fire following an earthquake can lead to catastrophic scenarios characterized by structural collapse, hazardous materials release, loss of life, and the inability to provide emergency medical need.

Figure 1-1. Fire caused from the 1906 San Francisco earthquake
(Golden Gate NRA, Park Archives, PAM Negative Collection, GOGA 35256.2085)

Figure 1-2. The city of Natori in northern Japan engulfed in flames following the 2011 earthquake
(STR/AFP/Getty Images)

This study presents a new simulation methodology for the assessment of steel frames with reduced beam section (RBS) connections exposed to fire as well as fire following an earthquake. In addition, work completed on the set up of the Colorado State University (CSU) Engineering Research Center (ERC) fire testing furnace is presented in Appendix D.

1.1 Objectives and Scope of Research

The objective of the research described in this thesis is to develop an improved understanding of the performance of steel-moment resisting frames with reduced beam section connections in fire as well as fire following an earthquake through a series of finite element studies. More specifically, the objectives of the research are to better understand force and deformation demands on these connections, as well as to characterize the strength and deformation capacity of the connections at elevated temperatures. Specific research objectives developed for the study include the following:

1. To quantify force and deformation demands in two beam-column subassemblies taken from representative steel special moment-resisting frames (SMRF) during exposure to fire as well as a seismic event representative of the maximum considered earthquake (MCE) followed by exposure to fire.
2. To determine the expected temperature distributions within the two beam-column subassemblies when exposed to a representative compartment fire.
3. To evaluate the effect of earthquake-induced damage in reduced beam section connections on the structural response of the connections during post-earthquake fire exposure.
4. To develop a new methodology for representing mechanical restraint against thermal expansion on beam-column subassemblies during fire exposure, considering cases with and without preexisting earthquake induced damage.
5. To provide an analytical case study for evaluating the adequacy of current building code provisions, considering the potential failure modes during fire and post-earthquake fire exposure.

To realize the above mentioned objectives, numerical finite element models were developed to investigate the response of steel-moment resisting frames with reduced beam section connections on the local connection level. Three dimensional continuum element models were developed for analyzing the connection level response of two beam-column subassemblies. The two analyzed subassemblies were taken from an eight-story 4-bay frame and a sixteen-story 4-bay frame designed for the Los Angeles region. The models were evaluated under a series of realistic scenarios that accurately simulate the occurrence of a fire as well as fire following an earthquake. The models employ a sequentially coupled thermo-mechanical methodology that includes representative mechanical boundary conditions which allow for the incorporation of the restraint imposed by the surrounding frame. In addition to conducting numerical simulations, the scope of work includes the development of a fire testing furnace and its corresponding test setup at the Engineering Research Center (ERC) at Colorado State University (CSU). The test setup is designed to allow for testing of beam-column connections under seismic and fire demand. The findings of the study provide a valuable design tool for structural engineers and offer insight into the expected behavior of steel moment-resisting frames designed with RBS connections when exposed to fire as well as fire following an earthquake.

1.2 Organization of Thesis

This thesis includes six different chapters. Chapter 1 introduces the problem statement and objectives of this research. Chapter 2 provides a background and literature review in reference to evaluating steel frames with reduced beam section connections for fire loading as well as fire following an earthquake. Chapter 3 provides background information on the modeling framework employed for this research. Chapter 4 focuses on the finite element modeling techniques utilized for this study. Chapter 5 presents the results of the finite element model simulations. Chapter 6 provides a summary of the work as well as conclusions and recommendations based on the findings of the study. Appendix A summarizes the most relevant experimental testing that has been performed on RBS moment connections. Appendix B provides design calculations performed on the two selected beam-column subassemblies. Appendix C contains relevant information on the selection and scaling of the earthquake ground motion records used for this study. Appendix D provides relevant information on the experimental setup of the ERC fire testing furnace.

CHAPTER 2
BACKGROUND AND LITERATURE REVIEW

2.0 Introduction

This chapter presents the relevant background material that was used for this study. Extensive research has been done on the behavior of steel structures during earthquakes as well as fires; however the combination of the two events has seen very little attention. Because of this knowledge on the behavior of steel structures subjected to fire following an earthquake must be drawn from numerical and experimental testing that has been done on each event independently as well as the few studies performed on the combined events. The following sections provide a brief overview of each event as well as the current state of knowledge on the combined hazard. The extensive amount of work that has been performed on steel structures during an earthquake require that the background on seismic performance only focuses on reduced beam sections (RBS) connections. Section 2.1 discusses the development, performance and observed failure modes of RBS connections under seismic action. Following this discussion Sections 2.2 and 2.3 provide an introduction to the fundamental knowledge of the response of steel structures to building fires as well as fire following an earthquake, respectively. Section 2.4 of this chapter presents the current code of practice for the design of steel structures for both seismic and fire demand. The final section provides a brief summary of the chapter.

2.1 Reduced Beam Section Connections

Following the 1994 Northridge earthquake extensive work was undertaken to gain a better understanding of the behavior of special moment-resisting frame (SMRF) steel connections. Brittle failures observed in moment connections of SMRFs moment connections after the earthquake raised concerns over material properties, connection geometry, design parameters and weld quality. Figure 2-1 provides two examples of typical failures observed in the Northridge earthquake. Even though total collapse of buildings with steel moment frames did not occur during the event, the response of the structures indicate that severe damage and even complete failure could have occurred if the earthquake had a longer duration. This was confirmed by the 1995 Kobe earthquake which struck the city of Kobe, Japan a year after the Northridge earthquake and resulted in far more severe damage. The earthquake caused partial or total collapse of numerous buildings with steel moment frame, confirming that the response of steel moment connections during a severe seismic event was not as good as previously believed to be. These two earthquakes resulted in the implementation of a number of research initiatives, most notably the SAC project (Venture, 2000), being created to examine the reasons for the poor response of these connections and develop better seismic design and retrofitting techniques. From these studies it was found that high stress concentrations at the welded flanges and the vulnerability of the connections to large ductility demands were the two primary causes of the observed failures. These findings led structural engineers to change the seismic design philosophy so that connections remain nominally elastic at the column face while forcing the inelastic deformation to occur in a portion of the beam outside the joint.

Figure 2-1. Failures Observed in Steel Moment Connections during the Northridge Earthquake (Engelhardt, 2000)

Concluding the research efforts undertaken as a result of the Northridge and Kobe earthquakes recommendations for the detailing and design of steel connections in seismically prone regions were prescribed in FEMA 350 and FEMA 351. One of the most economical and widely used connections presented in the new guidelines was the reduced beam section connection, commonly referred to as the dogbone connection. This connection relies on the removal of portions of the beam flange in the region just outside the beam-column joint which ensures that yielding occurs at the reduced portion so as to limit the moment that can develop at the face of the column. Numerous shapes of the cutouts have been studied including tapered cut, constant cut and radius cut, the later proving to be the most effective and popular configuration. For the purpose of this study the radius cut configuration was utilized and as such was the main focus of this literature review. Figure 2-2 provides a depiction of a RBS connection as well as typical detailing requirements. A significant amount of research and testing has been performed on RBS connections, the following sections summarize the most important experimental and analytical work and the key observations that can be drawn from the work.

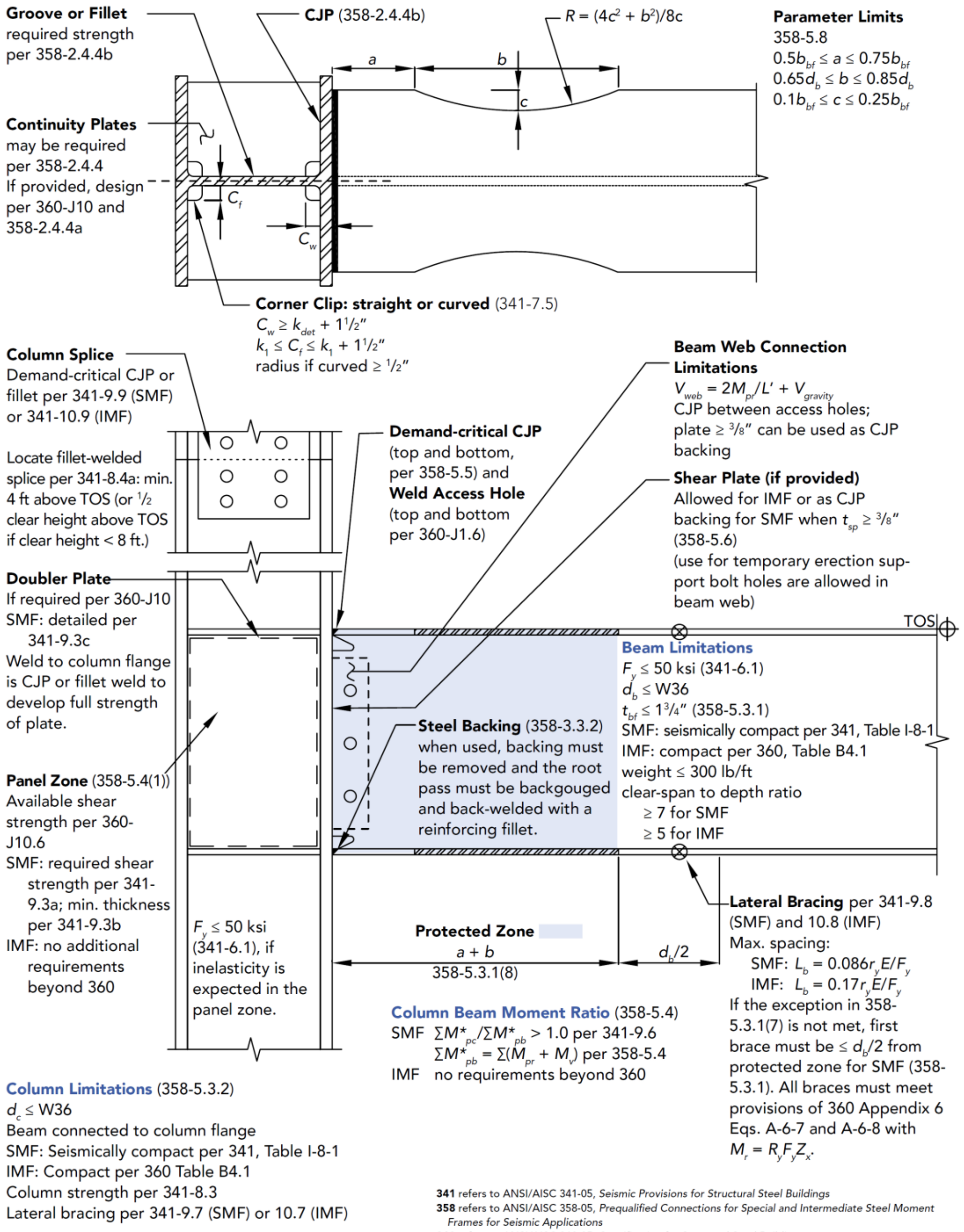

341 refers to ANSI/AISC 341-05, *Seismic Provisions for Structural Steel Buildings*
358 refers to ANSI/AISC 358-05, *Prequalified Connections for Special and Intermediate Steel Moment Frames for Seismic Applications*
360 refers to ANSI/AISC 360-05, *Specification for Structural Steel Buildings*

Figure 2-2. Reduced Beam Section (RBS) Moment Connection
(Kochalski and Erickson, 2007)

2.1.1 Experimental Work

Experimental testing of RBS connections subjected to seismic loading has been extensively investigated by various researchers. The response of the connection in these tests has been satisfactory in meeting the AISC 358-10 required connection design parameters, which has lead researchers to consistently assert that the use of RBS connections is appropriate in steel moment resisting frames in high seismic regions (Iwankiw and Carter 1996, Zekioglu 1997, Tremblay et al. 1997, Engelhardt et al. 1998). In addition to the flange reduction most RBS specimens incorporated substantial enhancements in detailing and welding procedures. Improved practices with respect to weld backing bars and weld tabs being the most notable of the changes. Backing bars at the top flange of the beams were seal welded to the columns and backing bars at the bottom flange removed, back gouged and sealed with a fillet weld. In most cases weld run-off tabs were also removed from the specimens. Additionally, welding electrodes with improved notch toughness values compared to the E70T-4 electrode commonly used prior to the Northridge earthquake were employed. Consequently, although the reduction of flange width in the beam is the most recognizable feature of these types of connections, the many detailing and welding improvements applied to the test specimens play a major role in the success during testing. Figure 2-3 and 2-4 provides two examples of a RBS connection specimen that underwent cyclic loading and the observed response.

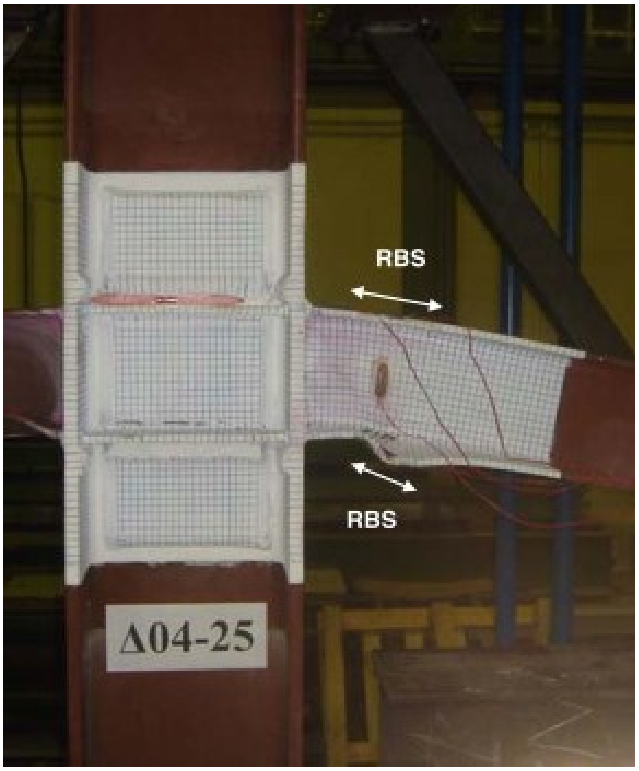

Figure 2-3. Buckling of Beam Bottom Flange
(Pachoumis et al, 2010)

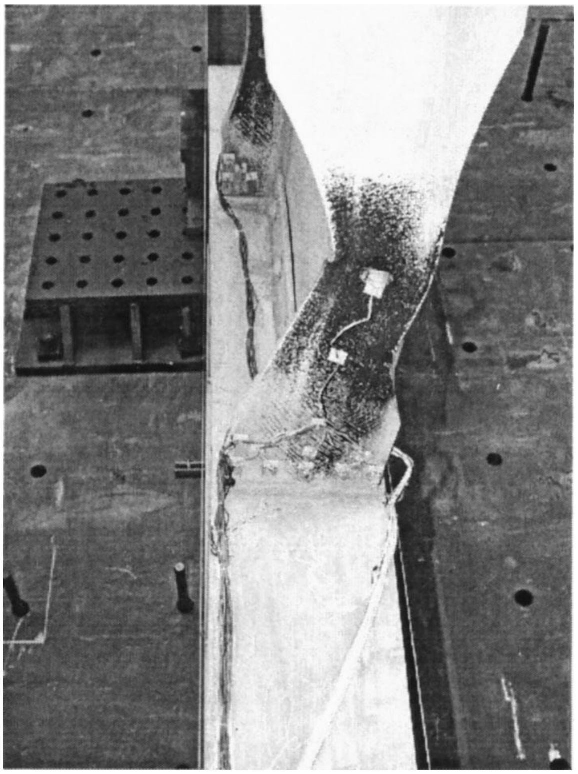

Figure 2-4. Lateral Torsional Buckling of the Beam
(Chi and Uang, 2002)

Despite the excellent performance, some key general observations can be drawn regarding the behavior of RBS connections. For example, many tests resulted in lateral torsional buckling of the beam which ultimately led to extensive strength degradation in the joint. The inability of the reduced portion of the flange to support the web resulted in web local buckling in some tests. Furthermore, column twisting was also observed in deep column connections as a result of lateral torsional buckling of the beam. Appendix A provides a listing of the most important experimental work done on RBS connections and includes important features of each test including member size and shape, connection details, plastic rotation achieved and failure modes. In addition to work done by private researchers the appendix includes tests completed under the SAC Phase 2. It should be noted that the table originated from a study by Engelhardt

(1999) and was updated/revised for this study. As a consequence to the observed general behavior, current seismic design guidelines ensure that such undesired behavior does not occur (FEMA-350).

2.1.2 Numerical Studies

In addition to the extensive experimental work that has been performed on reduced beam section connections numerous researchers have utilized numerical techniques to analyze the behavior of the connection. The following sections provide an overview of the most notable analytical work performed on RBS connections as well as frames with RBS connections.

2.1.2.1 Connection Level

Numerous numerical studies have been performed to supplement the experimental work done on the local behavior of RBS connections. Nonlinear finite-element modeling was performed by Zekioglu et al. (1997) confirming experimental results that the target beam plastic rotation is able to be achieved by RBS connections. These results were confirmed by finite-element analysis performed by Engelhardt et al. (2003), Gilton et al. (2005), and Gilton and Uang (2005) which also found that compared to connections without the RBS strains in the critical regions of the joint were significantly larger.

Expanding on previous research a stiffness matrix for two dimensional beam elements with RBS was derived by Kim and Engelhardt (2007) taking transverse shear deformations into consideration. The stiffness matrix they developed is provided in Figure 2-5. In addition, Kim and Engelhardt developed a methodology to calculate an effective moment of inertia of a beam with a RBS which allows for accurate simulation of beams with RBS in structural analysis software that doesn't allow specifically defined stiffness matrices to be included. This was achieved by comparing the moment–rotation relationship of a standard beam to a beam with a RBS assuming an idealized anti-symmetric rotation condition.

$$[D]^{-1} = \begin{bmatrix} \frac{EA}{L}k_a & 0 & 0 \\ 0 & \frac{EI}{L}\frac{s_{ii}}{s_{ii}^2 - s_{ij}^2} & -\frac{EI}{L}\frac{s_{ij}}{s_{ii}^2 - s_{ij}^2} \\ 0 & -\frac{EI}{L}\frac{s_{ij}}{s_{ii}^2 - s_{ij}^2} & \frac{EI}{L}\frac{s_{ii}}{s_{ii}^2 - s_{ij}^2} \end{bmatrix} = \begin{bmatrix} \frac{EA}{L}k_a & 0 & 0 \\ 0 & \frac{EI}{L}k_{ii} & \frac{EI}{L}k_{ij} \\ 0 & \frac{EI}{L}k_{ij} & \frac{EI}{L}k_{jj} \end{bmatrix}$$

Figure 2-5. Stiffness Matrix of a RBS Beam
(Kim, 2007)

Uang et al. (2001) used the results of 55 experimental tests performed on RBS connection to evaluate the cyclic instability of the connections. They performed regression analyses to determine the correlation between the response parameters of strength degradation rate and plastic rotation capacity to the slenderness parameters used to determine the likelihood of buckling. These regression analyses led the authors to assert that the selected response parameters are strongly linked to the slenderness ratio of web local buckling. Furthermore, it was found that the slenderness ratio related to lateral torsional buckling played an insignificant role in the behavior of the response parameters. Based on these finding equations relating the response parameters to the slenderness ratios for web and flange local buckling were established. This allows designers to determine the width to thickness ratio of web local buckling based on a target plastic rotation capacity determined necessary for the expected seismic demand. The author also looked into the effects of a concrete slab on the plastic rotation capacity of RBS beams, stating that is would increase both capacity and strength when subjected to positive bending. This did not hold true under negative bending where it was found that the slab provided negligible enhancement to the plastic rotation capacity of the beam. These studies provide useful information on modeling techniques that were used for this study. In addition, work by Selamet and Garlock (2010) provided detailed information on modeling techniques for 3-D structural connections under fire loading including suggestions on element types, integration order, meshing, material properties, contact configuration, and solving techniques that were taken into consideration.

2.1.2.2 Steel Moment Resisting Frames with Reduced Beam Section Connections

In addition to the numerical studies on the local performance of RBS connections, a number of studies have been conducted to investigate the global response of steel frames with RBS connections during a seismic event. Shen et al. (2000) provided useful information on the performance of these frames with emphasis given to predicting values for both roof and inter-story drift ratios, the structural demand imposed on the frames, as well as the locations and degree of plastic deformations throughout the structure.

The effects of radius cut RBS connections on the elastic lateral stiffness of steel moment frames was investigated by Grubbs (1997) using finite element models. From this analysis the author was able to develop a simplified approach for modeling the RBS region in the frame using a single prismatic frame element with an effective moment of inertia that is representative of the moment of inertia in the reduced section of the beam. An equation for determining the moment of inertia was also provided and was developed in such a way that any cut out configuration can be evaluated. Comparable work was performed by Iwankiw and Mohammadi (2004) who utilized conjugate beam theory and numerical integration techniques to determine the mechanical properties of 40 beams with RBS. The authors then performed a regression analysis using the results of the study to formulate an equation for determining the shear and bending stiffness of beams with RBS. However, the equation does not account for transverse shear deformations and is only applicable to member sizes that are within the range of the beams studied.

The response of steel frames of various heights with reduced beam sections during a seismic event was extensively examined by Lee and Foutch (2004). The authors were able to include the P-Δ effects of the gravity frames, panel zone flexibility and the effects of the ductile connections. The results of this study were used during the development of the FEMA-350 (2000) provisions used for the performance based design of steel framed structures. Figure 2-6 provides a depiction of the moment-rotation curve they utilized to model the RBS.

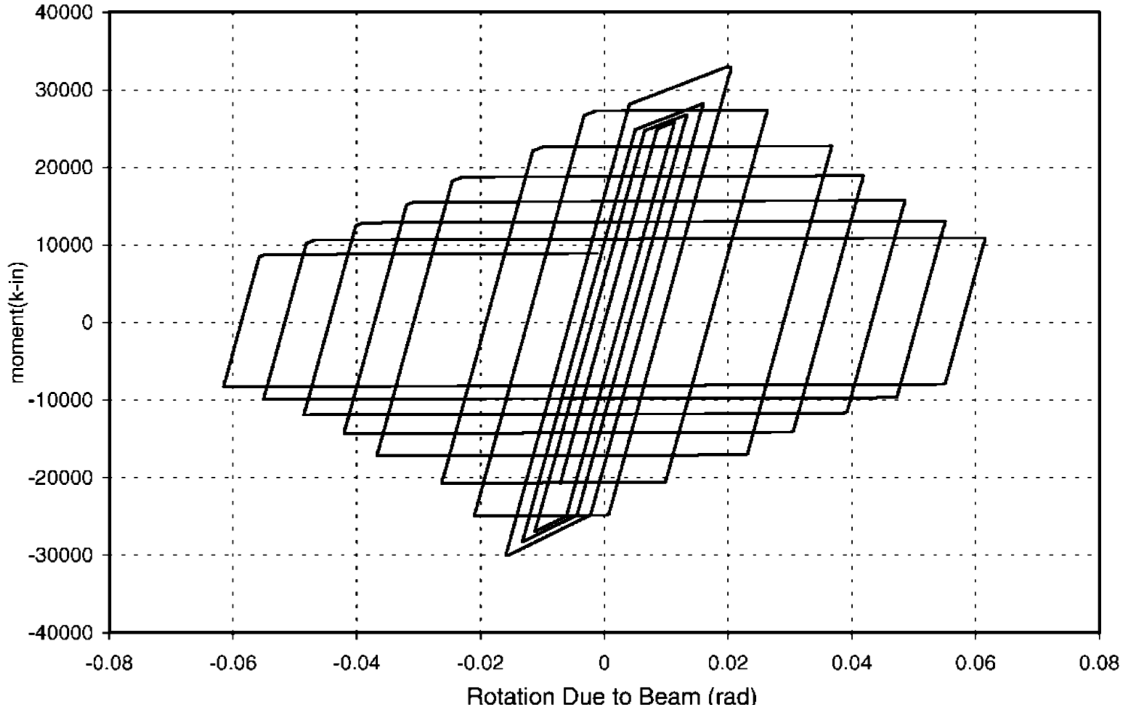

Figure 2-6. Model of moment-rotation behavior of RBS connection
(Lee and Foutch, 2004)

Further work on the modeling of the RBS was performed by Kitjasateanphun et al. (2001) who developed two models for use in nonlinear analysis of frames. The authors found that the seismic behavior of the frame is particularly sensitive to how the RBS is modeled. A study performed by Jin and El-Tawil (2005) with the objective of developing a better understanding of global behavior of frames with RBS and critiquing the recently published FEMA-350 (2000) design specifications was performed. The authors utilized nonlinear pushover analysis as well as transient dynamic analyses of three different lateral load resisting frames of varying heights with RBS connections to determine the expected global response. The analyses provided further confirmation that frames with reduced beam section are capable of economically providing satisfactory seismic performance in highly seismic regions in spite of characteristically low overstrength.

2.2 Effect of Fire on Steel

Steel structures have a history of poor performance when exposed to building fires. Structural fires can easily reach temperatures of up to 1800 °F and have a significant effect on the loadbearing capacity of structural elements. The yield strength of steel is reduced by up to 50% at temperatures of 1000 °F and as much as 95% when exposed to temperatures as high as 1800 °F. In addition to losing practically all of its load-bearing capacity steel also has an extremely high rate of thermal conductivity and a high coefficient of thermal expansion creating a less than ideal response to fire loading.

The behavior of steel during a fire is further complicated because of the complex nature of simulating the behavior of steel structures under fire which must include the simulation of the fire behavior, the heat transfer to the structure and the structural response of the building. Because of this, fire analysis involves many engineering fields including material science, chemical and mechanical engineering, engineering statistics and structural engineering. Each field has its own relevance to fire safety, including different measures used to control both the risk of fire ignition and growth, as well as the possible implications of a fire. For structural engineers the primary behavioral effect in structural assessment is the degradation of stiffness and strength of structural materials at high temperatures and the potential for localized structural failure to trigger global collapse.

The following sections provide relevant background material for this study related to the response of steel structures exposed to fire. Case studies from past building fires are examined and the relevant observations and implications discussed. A brief overview of all the components involved in the simulation of buildings exposed to fire is presented. These include simulation of the fire behavior, heat transfer mechanisms between the fire and the structure and the response of steel structures to fire.

2.2.1 Case Studies of Past Fire Events Involving Steel Structures

Experimental studies and analytical simulations are essential in the evaluation of the behavior and performance of steel structures exposed to fire. Experimental work on steel under elevated temperatures has been carried out in many different forms from the steel material level to individual members, however very limited work has been done on the global level. Tests on full structural assemblies are limited due to the technical and financial difficulties associated with such experiments. Because of this the performance of real buildings that have experienced fires provides important and much needed information about the response of structures on the global level. Table 2-1 provides a summary of several noteworthy fire events involving steel buildings. The subsequent sections provide a more in-depth discussion of the fires for some of the more notable events.

Table 2-1. Summary of Past Major Fire Disasters of Steel Buildings

Structure	Location	Date	Stories	Fire Description	Fire Resistance	Damage	Reference
One New York Plaza	New York, USA	1970	50	Ignited on the 49th floor and spread to the top floor. 6 hrs.	Sprayed fire protection to steelwork that flaked away	Connection bolt failure, beam failure at 33nd and 34th floor	NIST, 2002
First Interstate Bank	Los Angeles, USA	1988	62	Ignited at the 12th floor and spread to four floors above. 3 hrs. 40 min	Sprayed fire protection to steelwork. Automatic sprinklers system not yet activated	Four floors destroyed and one partially damaged	FEMA 1988
Broadgate Phase 8	London, UK	1990	14	The fire lasted 4.5 hours including 2 hours where the fire exceeded 1000°C (1832°F).	Sprayed fire protection, only partial at that stage in construction	No collapse of any of the floors, columns or beams	Newman, 1991
Credit Insurance Building	Churchill Plaza, UK	1991	12	Ignited on the 8th floor and as external glazing failed spread up to the tenth floor	Spray- applied protection on the composite floor beams. Board fire protection on Columns	Burnout of 8th-10th floor, no collapse	Beitel, 2002
One Meridian Plaza	Philadelphia, USA	1991	38	Fire began on the 22nd floor and spread up to the 30th floor	Passive fire protection, automatic sprinklers system	Burnout of 22nd-29th floor, No collapse	Routley, 1991
World Trade Center	New York, USA	2001	101	Plane crashes caused multiple floor fires above the impacted floors. 1.5 hrs.	Passive fire protection, automatic sprinklers system	Total Collapse	FEMA, 2002
Parque Central	Caracas, Venezuela	2004	56	Fire began on the 34th floor and spread upward to all the floors above. 17 hrs.	Passive fire protection, sprinkler system malfunctioned	Burnout of 34th-56th floor, No collapse	Moncada, 2005
Windsor Building	Madrid, Spain	2005	32	Ignited at the 21st floor, spreading to all regions above the 2nd level. 18 to 20 hrs.	Passive fire protection, no sprinklers, steel columns above 17th floor unprotected.	Total failure of building with extensive slab failure above the 17th Floor.	NILIM, 2006

Details of the fire, protection and response of the structures for the Broadgate Phase 8 and the Windsor building fires are discussed in more detail in Sections 2.2.1.1 and 2.2.1.2. Emphasis is given to these events because of the significant observations that can be taken from the response of the steel framework during the fires.

2.2.1.1 Broadgate Phase 8

In 1990, a fire ignited within a construction hut on the first level of a partially completed 14-story steel-frame office building at the Broadgate development in London (British Steel, 1999). Flame temperatures during the fire were estimated to be over 1800°F. At the time of the fire, much of the steel framework was unprotected and as a result an approximate area of 131 feet by 65 feet was damaged beyond repair. However, investigators noted that the heat-affected framework responded in a ductile manner, and that the system as a whole remained stable because of excellent load redistribution. In addition, the integrity of the composite floor slab was maintained throughout the duration of exposure. Following the fire, a metallurgical investigation indicated that temperatures in the steel framework did not exceed 1100°F. A metallurgical study was also performed on the bolts of the steel connections finding that the peak temperature was less than 1000 °F which could have been attained during the manufacturing process.

Beams that had large permanent displacements showed signs of local buckling in the bottom flange and web regions near the end supports. This behavior was thought to be predominately influenced by mechanical restraint against thermal expansion provided by the surrounding structure. Steel columns that were fully exposed to ambient thermal heating because fire-proofing had not been applied at that point in construction also showed signs of local buckling distortion and subsequent axial shortening of up to 4 inches. The column deformations were thought to have been the result of the rigid transfer beams in the upper level of the building restraining thermal expansion of the heat-affected column regions. Figure 2-7 shows the local buckling distortions in a heat-affected column. The investigators noted that the heavier exposed column sections within the fire compartment showed no signs of permanent deformation, most likely attributed to the larger volume-to-surface area aspect ratios that resulted in lower steel temperatures.

Figure 2-7. Local Buckling of the Column
(Newman, 2000)

2.2.1.2 Windsor Building

On February 12th, 2005 one of the most devastating fire disasters in history occurred in the Windsor building in Madrid, Spain. The fire ignited at approximately 11pm on the 21st floor of the 32 story office building and quickly progressed to the top floor by 1am the next day. The top ten floors were eventually totally engulfed in flames and it gradually spread to the lower floors ultimately reaching downward to the 4th floor by 9am. The fire wasn't under control until almost 2pm giving the fire a total duration between 18 and 20 hours.

The building was constructed in 1979 and had 32 stories with a total height of 348 feet. The building was a composite steel and reinforced concrete structure that had a concrete core and waffle slabs supported by steel beams and perimeter columns as well as internal concrete columns. The structure was built based on the 1970's Spanish design codes which had very little specifications regarding fire protection. The building was under renovation when the fire occurred, which included the installation of sprinklers, fire protection of perimeter steel columns and interior beams, fire walls, fire insulation of floors and perimeter cladding and exterior stairs. The renovations had been implemented on the ground floors all the way to the 17th floor but no protection had been installed higher up.

Structural damage was significant on the top 11 stories with perimeter steel columns including exterior bays of waffle slabs having almost completely collapsed. The reinforced concrete core maintained its strength and is thought to have prevented total collapse of the structure. The partial collapse mechanisms reported in NILIM (2005) were as follows:

1) The steel columns near the fire buckled due to material degradation under elevated temperatures.
2) The axial loads of the buckled columns were redistributed to adjacent structures.
3) The number of deteriorated columns increased due to the developing fire; however the waffle slab worked as a cantilever and prevented structural collapse.
4) The fire spread and the waffle slabs reached their load capacity as a cantilever for the extended supporting area and collapsed.
5) The floor collapse induced failure of other floors and waffle slabs were ripped off at the connections to the core.

It was found that a mechanical floor between the 16th and 17th floors provided enough redundancy to prevent further failure of the lower floors. Figure 2-8 provides a before, during and after picture of the structure.

Figure 2-8. Before, During and After Pictures of the 2005 Windsor Building Fire
(Meyer, 2012)

2.2.2 Fire Simulation Methodologies

The behavior of building fires are largely governed by the amount of fuel available, the flow of oxygen and the temperature of the fire. Building fires are caused from a wide range of scenarios but the initial ignition only occurs when a fuel temperature is raised above its combustion point and oxygen is available. Once the initial combustion of the fuel source begins it releases heat, increasing the temperature of the surrounding environment. As the adjoining fuel sources reach their combustion point the fire grows engulfing the surrounding environment until it becomes fully developed. It continues to burn at this extreme temperature until the fuel sources are exhausted and the fire begins to decay and eventually burn out. This process is depicted in Figure 2-9 which represents a typical time-temperature curve of a natural fire.

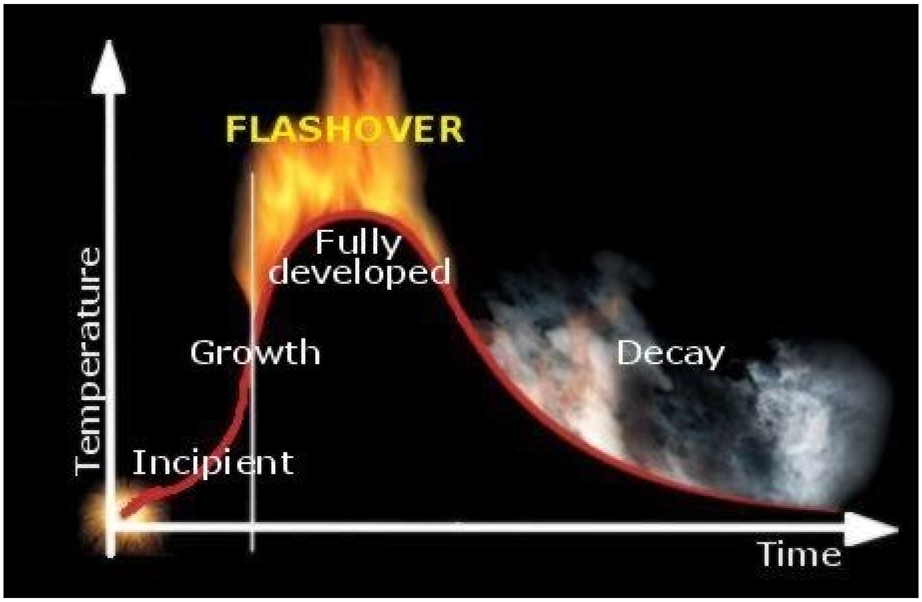

Figure 2-9. Typical Fire Compartment Behavior
(Lars, 2013)

As discussed earlier the fire curve can be divided into three main phases, growth, fully developed and decay. The flashover point is defined as the transition of the fire from growing to fully developed; this typically involves the fire spreading from the area of localized burning to all combustible surfaces within the compartment. After flashover the heat release rate remains at a maximum as long as fuel and oxygen supplies last. This is particularly important because once a building fire reaches the flashover point it is almost impossible for firefighters to stop it and sprinklers are designed to only work at the growth phase of the fire. This leaves sprayed-on fire proofing material as the only defense against a fully developed fire.

Because of the intricate nature of building fires, simulating the response of buildings and their components under fire loading is extremely complicated. Most countries around the world use simple fire resistance tests that utilize standardized fire curves to evaluate the behavior of building components and structural members during a fire. These standard curves provide a simple means of assessing a specimen’s response against a common set of performance criteria subject to closely defined thermal and mechanical loading under prescribed loading and support conditions. This methodology has several shortcomings and has been heavily criticized by the structural engineering community because it does not take into account any of the physical parameters affecting fire growth and development. In addition it cannot be used to analyze the response of a complete structure and neglects the important interaction between components. This has lead researchers to start to use more realistic and complex methods for simulating the response of structures to fire loading. The following sections provide a brief overview of compartment fires which are typical of most buildings, standard fire curves and more realistic parametric fire curves.

2.2.2.1 Compartment Fires

For the purpose of this study, focus has been given to compartment fires in office buildings since they are the most common type of fires seen in buildings. Compartment or room fires are typically categorized as a pre-flashover fire, which never reaches the flashover point and has the most influence on life safety, or a post-flashover fire, which reaches the flashover point and is critical when considering structural integrity. Pre-flashover fires are dependent on the rate of fire growth and the upper layer gas temperatures in the compartment, whereas post-flashover fires change behavior drastically and produce very turbulent flow of gases and high temperatures in the compartment. These high temperatures and increased duration make post-flashover fires the main focus of structural analysis. In order to accurately capture the behavior of post-flashover fires they must be understood at all stages including combustion and initiation, the pre-flashover phase and finally the post-flashover phase.

The combustion of organic material is an irreversible exothermic chemical reaction between atmospheric oxygen, hydrocarbons, and heat that results in the release of water vapor, carbon dioxide, and heat which is represented by the following equation (Bhowmick et al., 2011):

$$fire + 5O_2 + C_3H_8 \rightarrow 2CO_2 + 4H_2O + heat \qquad \text{(Equation 2-1)}$$

Where the heat of the combustion products is much larger than the heat of the reactants, and combustion of 2.2 lbm of O_2 results in releasing 12,000 Btu of heat. This equation provides an idealization of the phenomenon since complete combustion is almost impossible in reality. The presence of a variety of other reactants such as solid carbon and carbon monoxide gas prevent complete combustions. During this process the release of heat from the reactants usually results in the production of light in the form of either glowing or a flame. (Bhowmich, 2011)

In order to facilitate the chemical reaction of combustion, kinetic energy in the form of heat is needed to initiate the oxidation of the hydrocarbon. In building fires, the initial combustion reaction is generally initiated by heat from an external source. The amount of heat required to ignite a given material is a function of its thermal inertia, which is related to thermal conductivity, density, and specific heat (Bhowmich, 2011). An object with a lower thermal inertia is quicker to ignite, or requires a lower amount of heat to initiate the combustion reaction, than an object with a higher thermal inertia value.

Once the necessary kinetic energy has been reached for ignition, the heat from the resulting flames is most often sufficient to maintain the combustion reaction, resulting in established burning. This can be thought of as a positive feedback loop in which volatile compounds created by the flames are mixed with oxygen to continue the process, until one of the initial reactants (oxygen or combustible material) runs out. The local rate of combustion in building fires varies spatially meaning that combustion only occurs in areas where O_2-containing air mixes with gaseous fuels, usually in areas above the already-existing flame, where convective movement of combustion products in the plume meet their maximal heat (Feasey, 2002).

During the pre-flashover stage, a convection plume of hot gas rises vertically from the burning object. The hot gas spreads horizontally along the ceiling boundary forming an upper layer or zone. As the combustion process continues, more and more hot gas is expelled into the upper layer. Confined by the boundaries of the compartment, the upper layer begins to extend downward toward the source until it reaches the level of an open door or window. As the hot air flows out of the compartment through the opening, it creates a vacuum effect that draws in fresh oxygen-rich air to fuel the combustion process. Temperatures in the upper layers rise as combustion of the fuel source continue, creating a surge of radiant heat flux to the surrounding environment (Feasey, 2002). Once the critical threshold of radiant heat flux is reached, ignition of any combustible entities in the surrounding area will ignite, causing a sudden rise in both temperatures and rate at which heat is released. This period in the fire is termed the flashover stage. Once flashover has occurred the rise in temperatures and heat fluxes will cause any exposed combustible surfaces to pyrolyse which results in the emission of large amounts of combustible gas (Feasey, 2002). This causes the airflow in the compartment to become turbulent.

At this stage, the post-flashover fire is governed by either ventilation, said to be a ventilation-controlled burning, or combustible fuel, termed a fuel-controlled burning.

2.2.2.2 Standard Fire Curves

The typical methodology for determining the performance of structural members and various nonstructural building components during a fire is based upon fire resistance testing. These tests utilize standard fire curves that have been established by the industry, most notably ASTM E-119 (ASTM, 2000), ISO 834 (ISO 1975) and the Eurocode Standard Fire Curve model (EC1, 2002). Figure 2-10 provides a comparison of these three fire curves.

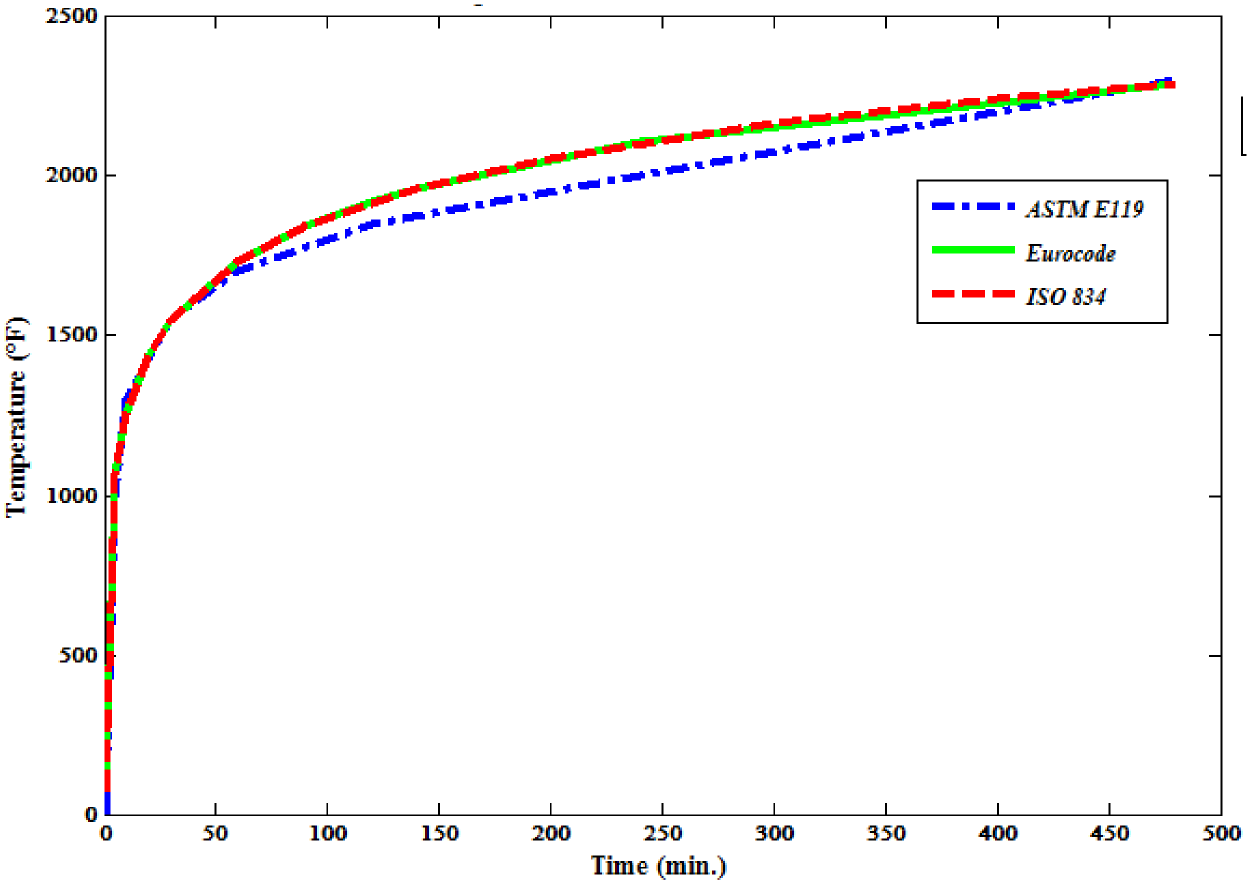

Figure 2-10. Comparison of Standard Fire Curves

The standard fire curve used in the United States comes from the ASTM E119 - Standard Test Methods for Fire Tests of Building Construction and Materials, which was one of the first published tests that established a fire resistance rating for steel members through a prescribed method. This test also served as a basis for the determination of fire resistance ratings in other tests such as ISO 834 and various European codes. The basic principle behind standard fire resistance testing is to expose a single structural member or assembly to a standard fire curve with designated fuel load and intensity. Results are based on the highest temperature seen by the unexposed surface of the member being tested and if that member fails in a way that creates the release of hot gases. In addition to these requirements the E119 standard test for wall systems also includes if the wall can withstand the pressure of fire hose following the fire. A fire resistance rating is then assigned to the specimen based on the time it took to fail.

These standard tests have numerous shortcomings that limit the amount of useful information that can be obtained from them. The standard fire curves were based on fuels that were commonly found in buildings at the time when the tests were first published in the early 1900s. This has proven rather unconservative since it has been shown that modern fuel sources can create fires with considerably faster rates of growth and higher radiative fractions which can have an impact on the fire spread rates (NIST, 2005). Another consideration is the addition of automatic sprinkler systems, which can limit the growth phase of the fire and is not often considered during standard fire testing today. The physical limitations of standard furnaces are another major weakness of these tests. A typical furnace only allows for specimens to be tested individually and cannot accommodate and include the interaction of structural systems or the implementation of boundary loads (gravity, lateral, etc.). End restraints and loading conditions are very difficult to accurately replicate in a furnace making it difficult to test anything other than very basic structural elements. These tests are outdated providing a prescriptive rating that reflects a time when prescriptive design was primarily used but the recent shift towards performance-based design has created a need for other methods.

2.2.2.3 Parametric Fire Curves

In addition to the previously discussed standard fire curves many codes and standards are now including parametric fire curves. These fire curves provide a simplified design procedure to estimate the ambient temperature in post-flashover compartment fires. These curves are able to consider the ventilation conditions, compartment size, thermal properties of compartment walls and ceilings, and the fuel load. Figure 2-11 provides a depiction of a typical parametric fire curve:

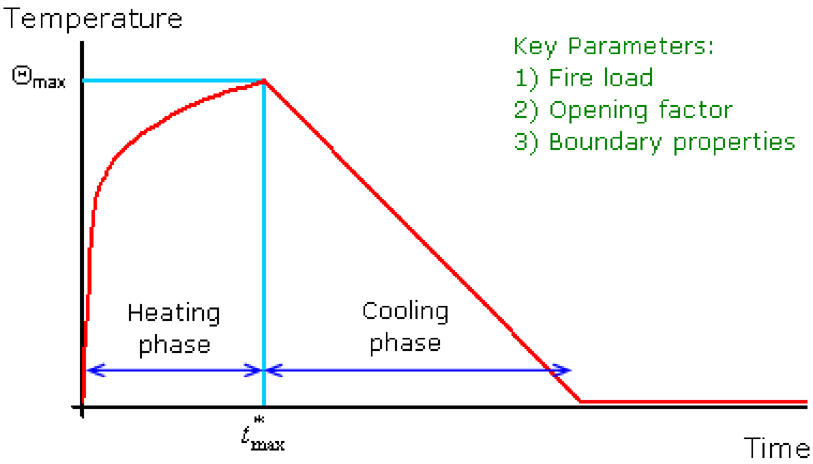

Figure 2-11. Typical Parametric Fire Curve
(BS EN, 1991)

In comparison to the previously discussed standard fire curves, parametric fires provide a more realistic estimate of the compartment temperature to be used in the structural fire design. While this methodology provides a much more realistic fire scenario it should be noted that there are several assumptions:

1. Complete combustion occurs and is contained within the boundaries of the compartment.
2. The temperature within the compartment is uniform.
3. Estimated values for thermal inertia are typically used.
4. The flow of heat through the compartment walls is assumed to only occur in one direction.

One of the most common parametric fire curve used by engineers to predict the temperature of a compartment fire is the BS EN 1991-1-2 which is included in EN 1991 Eurocode 1 Actions (EC1, 2004). This curve utilizes the following equation for the heating phase of the fire:

$$\Theta_g = 20 + 1325\left(1 - 0.324e^{-0.2t^*} - 0.204e^{-1.7t^*} - 0.472e^{-19t^*}\right)$$

$$O = {A_v\sqrt{h_{eq}}}/{A_t} \quad \Gamma = \left(\frac{O}{b}\right)^2 \left(\frac{1160}{0.04}\right)^2 \quad b = \frac{\Sigma(b_j A_j)}{A_t - A_v}$$

(Equation 2-2)

$$t^* = t\Gamma$$

Where,

Θ_g is the gas temperature in the fire compartment [°C]

b is the thermal inertia of linings [$J/m^2 s^{½} K$]

O is the opening factor [$m^{1/2}$]

t is the time [hr.]

For the cooling phase of the fire the curve utilizes the following:

$$\Theta_g = \begin{cases} \Theta_{max} - 625(t^* - t^*_{max}x) & for\ t^*_{max} \leq 0.5 \\ \Theta_{max} - 250(3 - t^*_{max})(t^* - t^*_{max}x) & for\ 0.5 < t^*_{max} < 2 \\ \Theta_{max} - 250(t^* - t^*_{max}x) & for\ t^*_{max} \geq 2 \end{cases}$$

(Equation 2-3)

$$x = \begin{cases} 1.0 & for\ t_{max} > t_{lim} \\ t_{lim}\,{\Gamma}/{t^*_{max}} & for\ t_{max} = t_{lim} \end{cases}$$

It should be noted that this model is not without limitations. In order to use the curves derived from the model. the compartment being analyzed must meet the following requirements:

1) Maximum area of 5380 ft^2 for the compartment floor
2) Maximum height of 13 ft.
3) Roof without openings
4) Compartments with mainly cellulosic type fire loads
5) Compartment linings with thermal inertia between 100 and 2200 $J/m^2s^{1/2}K$

The most influential factor in the Eurocode parametric fire curve is the ratio of openings to wall area, which is termed the opening factor. Almost every parametric fire equation includes some form of this parameter since it is typically the controlling factor for the behavior of the fire. It provides a representation of the amount of ventilation that the fire will experience (Ma and Pentti, 2000). Because of the numerous variables and equations used to develop the heating and cooling phases of the fire curves, they can be challenging to replicate for design purposes. Furthermore, the decay curve of the Eurocode parametric fire curve has been shown to be an inaccurate representation of time-temperature characteristics during the cooling phase seen in most fires (Zehfuß and Hosser, 2007).

As a result of the complexities and inefficiencies of the European parametric curve previously described, a simple fire curve, termed the BFD curve, was developed by researchers with data obtained from over 142 natural fire tests (Barnett, 2002). While the European parametric curve consists of at least three equations for both the heating and cooling phases of the fire, there are two basic equations that describe the BFD curve. The input parameters needed for the BFD equation can be found in published fire data, design codes or by calculation.

The two equations are presented below:

$$T_g = T_a + T_m e^{-z}$$

$$Z = {(log_e t - log_e t_m)^2}\Big/{S_c}$$

(Equation 2-4)

Where,

T_g is the gas temperature at any time t (°C)
T_a is the ambient temperature (°C)
T_m is the maximum gas temperature generated above T_a (°C)
t is the time from start of fire (min)
t_m is the time at which Tm occurs (min)
S_c is the shape constant for the time-temperature curve

There are several other parametric fire curve models that are commonly used by engineers. The first is the design fires presented in The Swedish Design Manual, which presents two models for fully developed fires. The first model represents a ventilation-controlled fire where the rate of combustion during the initial phase is determined by the ventilation in the compartment. The second model assumes that there is an excess of inflowing air and because of this the driving factors in this fire are the properties of the combustible material. Other parametric fire curves that must be addressed are the "short duration, high intensity" and the "long duration, low intensity" fire curves that were provided through previous coursework in structural fire protection and defined in the SFPE Handbook for Fire Protection Engineering. In addition to the curves mentioned in this review there are several more parametric fire curves that have been presented by researchers over the last several decades. Each parametric fire curve has characteristics that make it unique from others. In order to fully understand the inputs into structural fire engineering, one must recognize what parameters and characteristics make up each fire including the maximum temperature, intensity of fire, heating phase, cooling phase, and time to maximum temperature.

In addition to the previously mentioned design and parametric curves, it is worth noting that more complex and realistic fire models exist. These include Zone Models which utilize relatively simple computer models to split the selected fire compartment into distinct zones and utilize conservation of mass and energy to provide a more realistic prediction of fire behavior. The most advanced and sophisticated fire modeling technique in current practice is computational fluid dynamics (CFD) models which are based on the fundamental equations of fluid flow. These models were deemed out of the scope of this research and as such they were not explored with much detail.

2.2.3 Heat Transfer Mechanics

Heat transfer during a fire event can be attributed to three transport mechanisms: conduction, convection, and radiation, which are illustrated schematically in Figure 2-12. The following section provides a brief discussion regarding each of these processes.

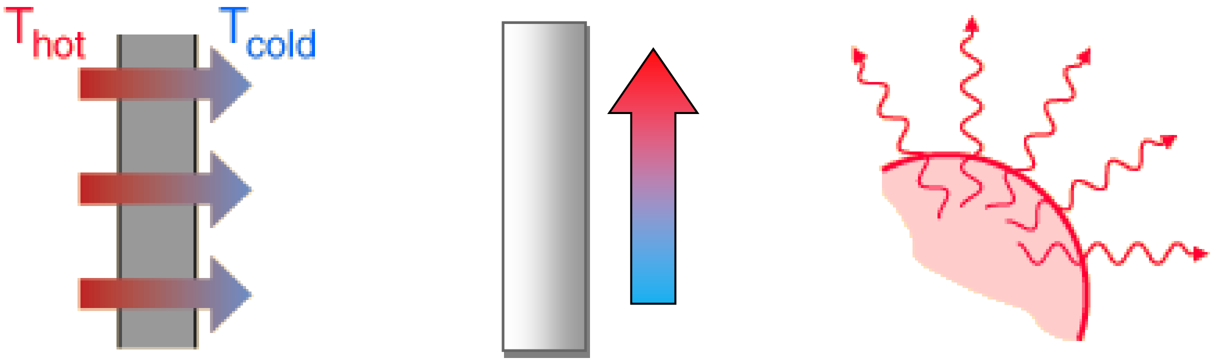

Figure 2-12. Conduction, Convection and Radiation
(Nouanegu et al, 2009)

2.2.3.1 Conduction

Conduction is the heat transfer mechanism that occurs within solid materials. During conduction the heat flows through the actual body of the member as opposed to other heat transfer mechanisms which involve heat transfer between moving matter. Conduction can occur in any type of appreciable matter including liquids and gases. The most commonly discussed form of conduction for structural analysis occurs in solids and is caused by a combination of diffusion of free electrons and vibrations of the molecules in a lattice or photons. In gases and liquids conduction is caused by the collision and diffusion of the molecules within the substance during random motion. Conduction of heat is an important factor in the ignition of solid surfaces, and in the fire resistance of various structural members and components. The general three-dimensional heat-conduction relationship neglecting convection is presented in Equation 2-5.

$$\frac{\partial}{\partial x}\left(\mathrm{K}_{xx}\frac{\partial T}{\partial x}\right)+\frac{\partial}{\partial y}\left(\mathrm{K}_{yy}\frac{\partial T}{\partial y}\right)+\frac{\partial}{\partial z}\left(\mathrm{K}_{zz}\frac{\partial T}{\partial z}\right)+Q=\rho c\frac{\partial T}{\partial t} \qquad \text{(Equation 2-5)}$$

Where,

K_{xx}, K_{yy}, and K_{zz} are the thermal conductivity of the material in the x, y, and z directions, respectively, (generally assumed as a uniform value of k for isotropic materials), in W/(m-K), where K is temperature in Kelvins ([K] = [°C]+273.15)

$\frac{\partial T}{\partial x}$, $\frac{\partial T}{\partial y}$, and $\frac{\partial T}{\partial z}$ are the temperature gradients within the solid in Cartesian space, in K/m

Q is the heat generated (positive value) or lost (negative value) per unit time, per unit volume, in $\mathrm{W/m^3}$

ρ is the mass density of the material, in $\mathrm{kg/m^3}$

c is the specific heat of the material, in J/(kg-K)

$\frac{\partial T}{\partial t}$ is the time rate of temperature change in the solid, in K/s

2.2.3.2 Convection

Convection is heat transfer that occurs through the movement of fluids and is an important factor in flame spread throughout a building as well as the upward movement of smoke and hot gas.

The rate of heating or cooling for a solid body immersed in a fluid environment is highly dependent on the fluid velocity at the boundary surface. In a building compartment fire, convective heat transfer is driven by buoyancy forces that arise from temperature gradients in the heated air. This process is referred to as natural convection. Newton's law of cooling is used to express the amount of heat flow that occurs due to convection:

$$q_h = h(T - T_\infty) \qquad \text{(Equation 2-6)}$$

Where,

q_h is the heat flow by convective heat transfer, in W/m^2
h is the convection heat-transfer coefficient (or film conductance), in W/(m^2-K)
T is the temperature of the solid, in K
T_∞ is the free stream temperature, in K

Considering conservation of energy, the general three-dimensional heat transfer relationship for conductive and convective transport mechanisms becomes:

$$\frac{\partial}{\partial x}\left(\mathrm{K}_{xx}\frac{\partial T}{\partial x}\right) + \frac{\partial}{\partial y}\left(\mathrm{K}_{yy}\frac{\partial T}{\partial y}\right) + \frac{\partial}{\partial z}\left(\mathrm{K}_{zz}\frac{\partial T}{\partial z}\right) + Q = \rho c\frac{\partial T}{\partial t} + q_h\left(\frac{A_h}{V_b}\right) \qquad \text{(Equation 2-7)}$$

Where,

A_h is the area of the boundary surface involved in convective heat transfer, in m^2
V_b is the volume of the solid body, in m^3

2.2.3.3 Radiation

Radiation occurs through the transfer of energy by electromagnetic waves which are able to move through a vacuum or any transparent liquid or solid. This mechanism becomes particularly important when analyzing the behavior of a structural fire because it is the main mechanism for heat transfer between the various components. It accounts for the transfer of heat from the flames of the fire to the surfaces of the fuel sources, from the hot smoke and gases to the various building components, and from a burning building to the surrounding structures. It has been shown that an idealized thermal radiator, often referred to as a blackbody, will emit energy at a rate directly proportional to its surface area and proportional to the fourth power of the absolute temperature of the body. This relationship can be seen in Equation 2-8:

$$q_{black\ body} = \sigma T_e^4 \qquad \text{(Equation 2-8)}$$

Where,

$q_{black\ body}$ is the heat flow by radiation from a black body radiator, in W/m^2
σ is the proportionality constant, referred to as the Stefan-Boltzmann constant, equal to 5.67x10^{-8} W/(m^2-K^4)
T$_e$ is the temperature of the emitting surface, in K

The majority of surfaces, such as steel beam or column, do not radiate as much energy as the ideal blackbody. Even so the amount of radiation emitted is still generally proportional to the fourth power of the temperature of the body. A parameter referred to as emissivity (ε), which relates the radiation of any given surface to that of an ideal black surface, is introduced to account for this difference. The emissivity between two walls is defined by the following equation:

$$\varepsilon = \frac{1}{\left(\frac{1}{\varepsilon_e}+\frac{1}{\varepsilon_r}-1\right)} \qquad \text{(Equation 2-9)}$$

Where,

ε is the resultant emissivity
ε_e is the emissivity of the emitting surface
ε_r is the emissivity of the receiving surface

The Society for Fire Protection Engineering Task Group on Fire Exposures (SFPE, 2004) recommends a resultant emissivity of 1.0 for compartment fire exposure since the affected surfaces will likely be covered in soot. In addition to the emissivity of a material the fact that not all of the radiation leaving one surface will hit another surface must be taken into consideration. Some radiation that leaves the first surface will be lost to the surrounding environment since electromagnetic waves travels in straight lines. To account for this a geometric view factor (φ) is introduced and defined as follows:

$$\varphi = \frac{1}{A_1} \iint_A \frac{\cos\theta_i \cos\theta_j}{\pi R_{ij}^2}\, dA_i dA_j \qquad \text{(Equation 2-10)}$$

Figure 2-13 illustrates the components of the geometric view factor for two areas.

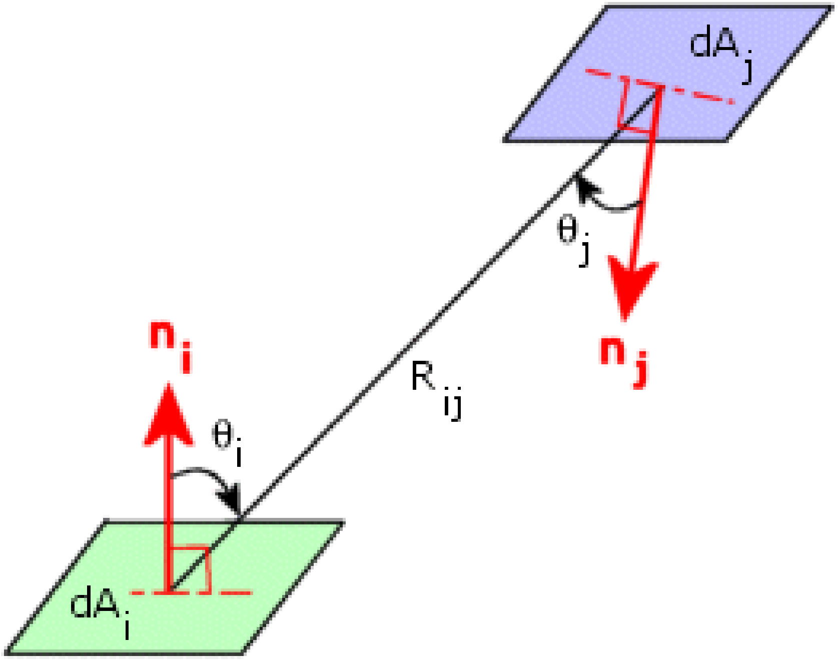

Figure 2-13. Radiation View Factors
(View, 2013)

The resultant heat flow for a typical surface taking the efficiency of the emitting surface as a radiator into consideration then becomes:

$$q_r = \varphi \varepsilon_r \sigma \left(T_e^4 - T_r^4\right) \qquad \text{(Equation 2-11)}$$

Where

q_r is the resultant heat flow by radiation from a gray body radiator, in W/m^2

T_r is the temperature of the receiving surface, in K

Considering conservation of energy, the general three-dimensional heat transfer relationship becomes:

$$\frac{\partial}{\partial x}\left(K_{xx}\frac{\partial T}{\partial x}\right) + \frac{\partial}{\partial y}\left(K_{yy}\frac{\partial T}{\partial y}\right) + \frac{\partial}{\partial z}\left(K_{zz}\frac{\partial T}{\partial z}\right) + Q = \rho c\frac{\partial T}{\partial t} + q_h\left(\frac{A_h}{V_b}\right) + q_r\left(\frac{A_r}{V_b}\right) \qquad \text{(Equation 2-12)}$$

Where

A_r is the area of the boundary surface involved in radiative heat transfer, in m^2

2.2.4 Behavior of Steel Structures Exposed to Fire

Understanding the behavior of steel structures exposed to fire is an involved topic and requires an in-depth understanding of several areas, including the properties of structural steel at elevated temperatures as well as the expected response of steel connections and frames exposed to thermal loading. The following sections provide an overview of the temperature dependent properties of steel followed by a review of previous research performed on steel connections and frames exposed to fire.

2.2.4.1 Thermomechanical Properties of Steel

The properties of structural steel vary drastically with increase in temperature and accurate modeling of these properties is one of the most critical aspects in analyzing the behavior of steel structures during a fire. The mechanical and thermal properties of interest for the purpose of this study include the coefficient of thermal expansion, modulus of elasticity, yield strength, specific heat and thermal conductivity. Similar to room temperature properties, the properties of structural steel at elevated temperatures are also obtained from laboratory testing. A review of the most prominent studies on the mechanical and thermal properties of structural steel at elevated temperatures and the constitutive models developed to predict these temperature dependent properties are provided in this section.

Harmathy and Stanzak (1970) presented elevated-temperature properties of two structural steels, ASTM A36 and CSA G40.12, and a prestressing steel, ASTM A421, up to 1200°F from steady-state tensile tests. Stress-strain curves up to 12-percent strain for the two types of steel were obtained from these tests. Harmathy and Stanzak evaluated ultimate and yield strength of these steels from the stress-strain relationships as well as the elongation and reduction in area of the tested steels. Figure 2-14 shows the Stress-Strain curves for ASTM A36 steel derived from these tests. The next notable work was performed by Cooke (1988), who presented data on the mechanical properties at elevated temperatures of hot-rolled structural steel providing a meaningful discussion on the physical meanings of these properties. The properties analyzed included modulus of elasticity, Poisson's ratio, thermal expansion, and stress-strain relationships. It was concluded that a Poisson's ratio of 0.3 and coefficient of linear thermal expansion of 7.78×10-6/°F are generally acceptable for fire analyses.

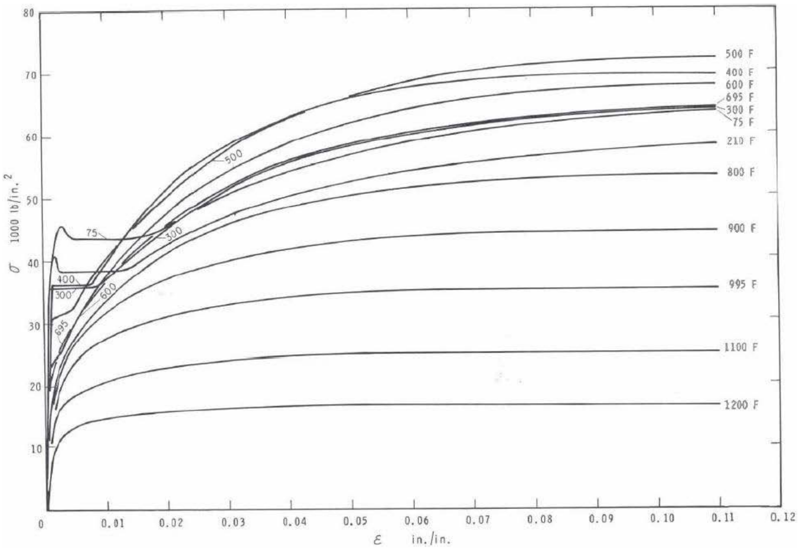

Figure 2-14. Stress-Strain Curves for ASTM A36 Steel
(Harmathy and Stanzak, 1970)

Kirby and Preston (1988) tested Grade 43A and Grade 50B steel up to 1650°F using both the steady-state and transient methods to provide elevated-temperature data for structural fire engineering applications. Stress-strain relationships can be further derived from the results. Li et al. (2003) conducted steady-state tests up to 1290°F to examine high temperature properties of two kinds of widely used steel in China: 16Mn steel and 20Mn TiB steel. The authors discussed the obtained yield and tensile strengths, modulus of elasticity, and coefficient of thermal expansion. Based on the obtained test data, equations were developed that can be used to predict the elevated temperature properties of structural steel.

Chen and Young (2005) performed experimental testing on stainless steel at elevated temperatures of up to 1800 °F and provided stress-strain curves determined from both steady-state and transient tensile tests. The properties obtained included modulus of elasticity, ultimate strength, ultimate strain and thermal elongation, yield strength with varying strain levels. In addition the authors also derived a unified equation for each of these properties at elevated temperatures. The stress strain curve from the test results as well as from the derived equations is shown in Figure 2-15.

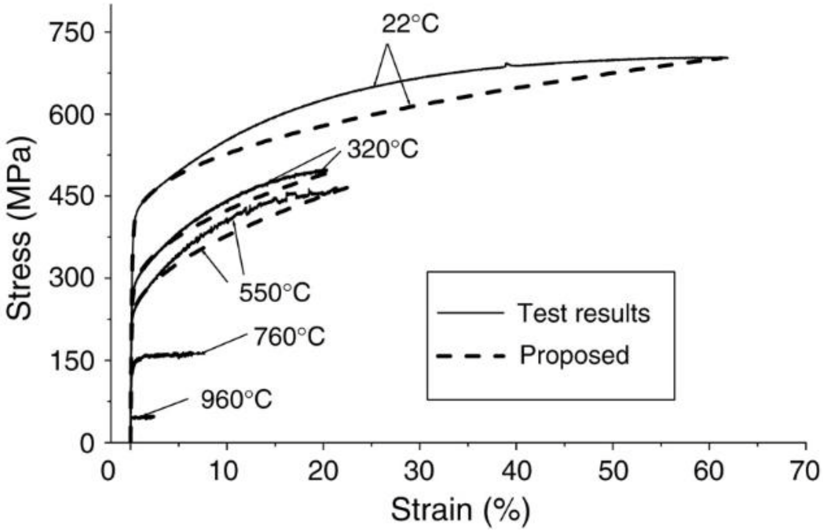

Figure 2-15. Stress-Strain Curves of Stainless Steel Type EN 1.4301 at Elevated Temperatures (Chen and Young, 2005)

The mechanical properties of structural steel recovered from the World Trade Centers (WTC) site at ambient temperature and high temperatures were analyzed following the attack on September 11, 2001. The high-temperature tensile behavior of steel specimens collected from 15 different steel members: three perimeter columns, four core columns, three truss components, and five truss seats, was characterized. The tested properties were then used for modeling of structural response of the towers to WTC fire. Qutinen (2007) carried out tensile tests to study the behavior of mechanical properties of different steel grades during and after elevated temperatures using both steady-state and transient methods. Qutinen's test results were presented with a comparison to Eurocode 3 (2005). Most of the results of the steel tested agreed with Eurocode 3 quite well, although the yield strength reduction factors of the cold-formed material were clearly higher than those given in Eurocode 3. The study showed that the mechanical properties after cooling largely returned to the nominal values of the steel that had never been heated. Yu (2006) tested Grade 50 structural steel at elevated temperatures up to 1470°F using the steady-state method with two loading rates. The stress-strain curves of the steel up to 10-percent strain were obtained (Figure 2-16) and the static yielding behavior of the steel at different temperatures was examined.

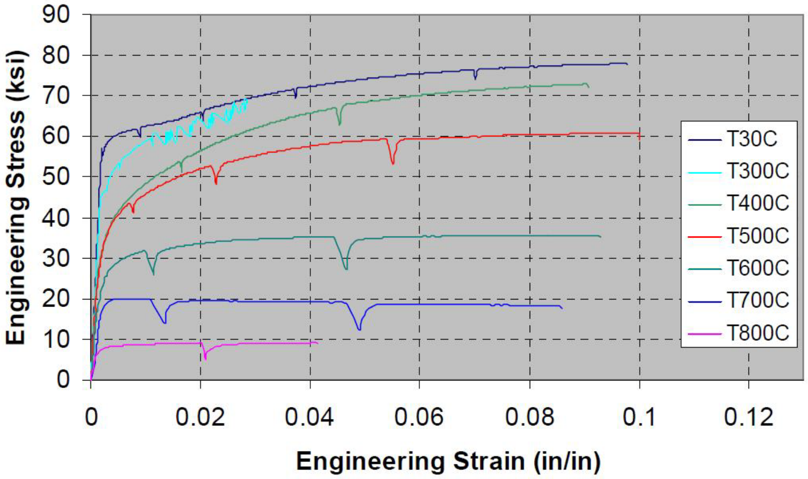

Figure 2-16. Stress-Strain Curves of Grade 50 Steel at Elevated Temperatures
(Yu, 2006)

From previous research conducted on structural steel properties at elevated temperatures, it can be observed that in general the key mechanical properties of steel including yield strength, ultimate tensile strength and modulus of elasticity all decrease as temperature increases. In addition, the reduction rates of strength and modulus of elasticity vary significantly in different temperature ranges. At temperatures lower than 750°F the reduction is relatively small while at higher temperatures the material degradation is remarkably more significant. Further, it can also be observed that at different temperatures the shapes of stress-strain curves are also quite different. For most structural steels, with temperature increase the yield plateau gradually disappears, and the strain-hardening portion of the stress-strain curve shortens significantly which makes the curve similar to an elastic-perfectly plastic curve.

In addition to the research performed on the behavior of steel at elevated temperatures, several constitutive relationships exist that provide a means for estimating temperature dependent properties. The most notable are presented in the American Society of Civil Engineers (ASCE) *Structural Fire Protection* Manual (ASCE 1992) and the European Committee (EC) for Standardization *General Rules – Structural Fire Design, EN1993-1-2* (Wickstrom, 2005), commonly referred to as Eurocode 3. These models were compared in great detail with data obtained from several previous studies by Kodur et al. (2010). Several conclusions can be drawn from their work regarding the high-temperature constitutive relationships for structural steel; the first being that there is not a significant variation in ASCE and EC constitutive models for high-temperature thermal properties below 1290°F. However, significant variations exist for temperatures above 1290°F.which can be seen in Figure 2-17.

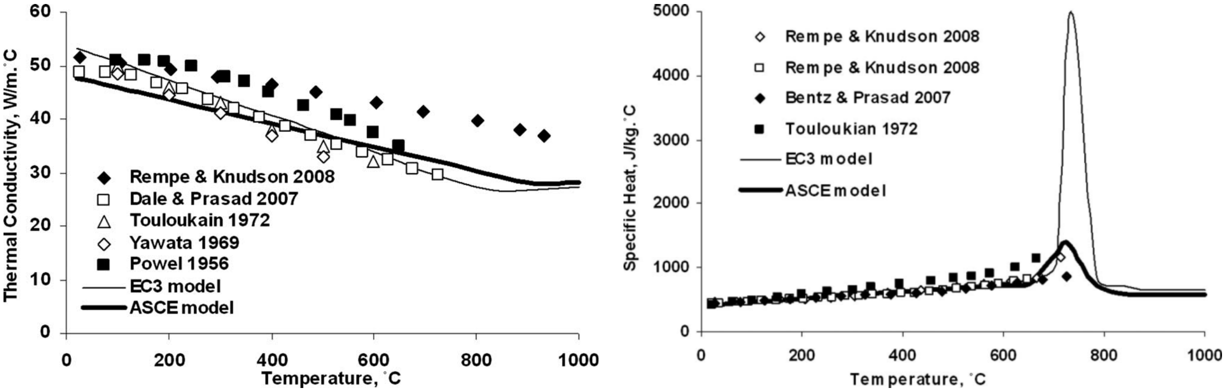

Figure 2-17. Thermal Properties of Steel as Predicted by Different Models and Measured in Different Tests (Kodur et al., 2010)

The study also found that there was a significant variation in high-temperature constitutive models for stress strain relationships as specified by the ASCE manual, Eurocode 3, and research performed by Poh (2001). These variations in high temperature constitutive models result in different fire resistance predictions. A comparison of the yield strength and elastic modulus are shown in Figure 2-18.

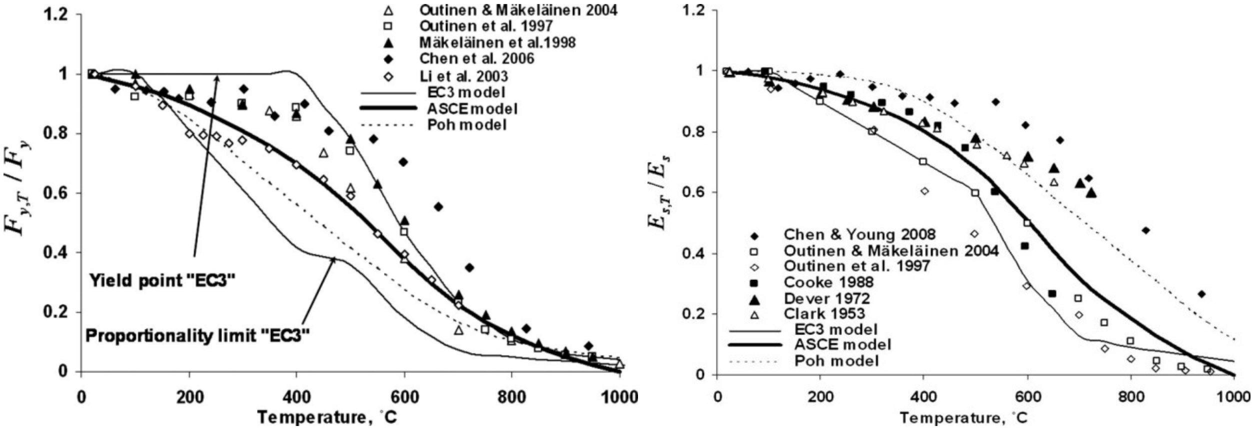

Figure 2-18. Mechanical Properties of Steel as Predicted by Different Models and Measured in Different Tests (Kodur et al., 2010)

In addition to these conclusions it was found that high-temperature creep has a substantial effect on the fire resistance of structural steel. Despite its significance, high temperature creep in structural steel is not explicitly accounted for in most stress-strain relationships. In some situations this might lead to unconservative fire resistance predictions. The use of the Eurocode high-temperature stress strain relationship gives a more realistic fire resistance prediction than does the use of ASCE stress strain relations, primarily due to the fact that the Eurocode temperature-stress-strain relationship partially takes high-temperature creep into account.

It is worth noting that the information for high temperature material properties presented above is only for the heating phase of fires. This is because most material tests were conducted under either transient or steady-state tests with increasing temperature. There is a lack of data on material properties in the cooling phase, which is critical for modeling the response of steel structures under realistic fires. Because of this the material properties used for this project were assumed to be the same for the heating and cooling phases.

2.2.4.2 Experimental Work

Early work on the behavior of steel structures subjected to fires typically focused on simply supported specimens (Olsen 1980, Vandamme and Janss 1981, Aasen 1985, Janss and Minne 1981, Lie and Almand 1990, and Franssen et al. 1998). Most of these tests were conducted on very small and slender column members and contained some uncertainty about end fixity achieved by the test boundary conditions. Ali et al. (1998) and Ali and O'Connor (2001) conducted numerous small-scale tests to evaluate the effects of axial restraints on the fire resistance of steel columns. Their test results indicated that axial restraints could significantly reduce the fire resistance of steel columns, further emphasizing the importance of accurately representing the boundary conditions for thermal loading.

Liu et al. (2002) conducted an experimental investigation on steel beams in fire. In this research, the experimental program was designed to study the effect of beam end restraint and catenary action. Test beams were connected to test columns by two types of connections in which the horizontal restraint stiffness could be changed by varying boundary supports of the supporting columns. The columns and the top flanges of the test beams were insulated by a ceramic fiber blanket. The experimental program included 20 fire tests on steel beams, three main load ratios of 0.3, 0.5 and 0.7 and three levels of axial restraint of 8kN/mm, 35kN/mm and 62kN/mm. During the tests, gas temperature in the furnace was controlled to closely follow the ISO834 standard fire temperature curve. Temperature distribution in the beam was obtained by measuring temperatures on the beam bottom flange, web and top flange and beam deflections were also measured. The effects of axial restraint were examined by studying axial force-temperature behavior for different levels of axial stiffness. From all these test results, the researcher made the following conclusions: connection restraint can increase fire resistance of a steel beam by reducing mid-span moment during fire conditions. Catenary action was much more noticeable in end-plate moment connections than web-cleat shear connections. Catenary action is more significant in the condition of lower load levels, higher axial restraint and larger deflection.

Mesquita et al (2005) examined the lateral torsional buckling performance of laterally unrestrained steel beams at high temperatures. The beams tested in this research had no axial restraint at the beam ends. Transient tests were conducted so that critical temperatures were determined for beams with different effective lengths. In 2007, Li and Guo (2007) studied the response of restrained steel beam members exposed to heating and cooling by conducting two full scale beam tests. The setup used for these tests can be seen in Figure 2-19.

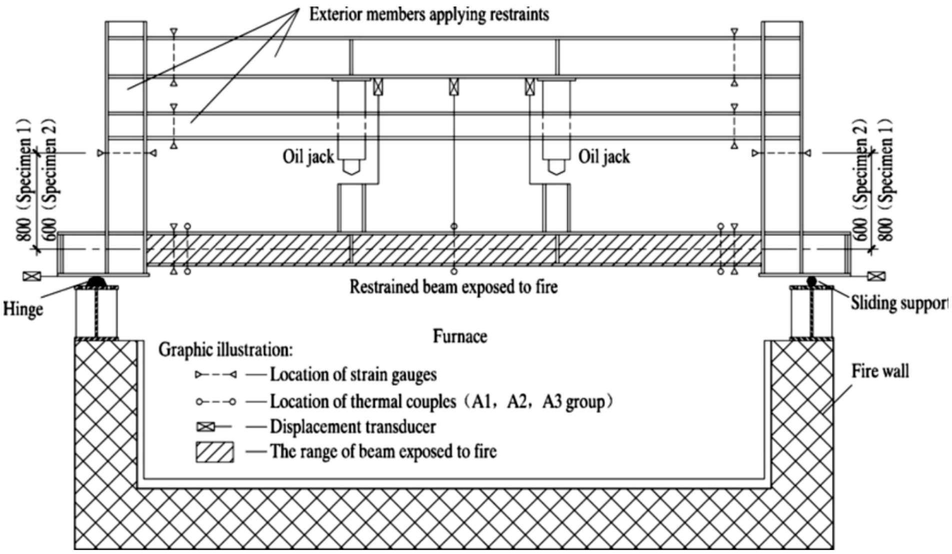

Figure 2-19. Li's Test Setup and Arrangement of Instruments (Li and Guo, 2007)

Ceramic blankets were used to cover the top flanges of the test beams in order to simulate the insulating effects of the concrete slabs on the steel beams. The fire was turned off after about 20 minutes of heating, and the air in the furnace cooled down naturally to ambient temperature. The axial forces in the beam were estimated by measuring beam end horizontal displacements. From the results of this experimental investigation it was concluded that the behavior of the restrained beams during a fire can be quite different from the behavior of an isolated beam. During the initial heating phase the axial restraint against thermal expansion creates an axial compression force, followed by an axial tension force due to catenary action that occurred as the beam deflected. The researchers also observed large increases in tensile force in restrained beams and little recovery of vertical deflections during the cooling phase of the fire. More recently, Choe et al. (2011) used experiments on several full-scale steel members (W10×68, W8×35, and W14×53) to validate detailed 3D finite-element models. The study provided useful recommendations for loading conditions and modeling techniques.

In 1990, a series of large-scale fire tests were conducted at the BHP Research Laboratories in Melbourne, Australia to evaluate the fire performance of an existing 41-story steel frame office building (British Steel, 1999). The tests were conducted using a purpose built test structure that was representative of a 40 feet by 40 feet corner bay of the actual building and included a 13 feet by 13 feet compartment designed to resemble a typical office environment. A total of four fire tests were conducted. Two of the tests were focused on studying the performance of the existing sprinkler system. The third test was designed to assess the fire resistance of the existing composite slab. In the fourth test a simulated office fire was conducted to evaluate the behavior of bare steel beams taking into consideration the influence of thermal shielding from a conventional suspended ceiling system. The office fire produced a peak atmospheric temperature of 2240 °F. Steel temperatures in the shielded beams reached 1170 °F. The peak beam displacement, measured at mid-span, was recorded as 4.7 inches, and it was noted that most of this deflection was recovered after the test. The study concluded that the thermal shielding from a conventional suspended ceiling system could significantly enhance the fire resistance of a steel frame floor system during fire exposure.

As a companion study to the previously mentioned fire tests, BHP Research Laboratories also carried out a series of large-scale fire tests to collect temperature data resulting from the combustion of furniture in a typical office compartment (British Steel, 1999). The compartment used in the test was furnished with typical office fixtures including desks, chairs, carpet, computer terminals, and paper. Atmospheric temperatures were recorded on either side of the ceiling and steel temperatures were monitored in the unprotected steel beams and in free-standing columns. Peak gas temperatures below the ceiling ranged from 1500-2125 ºF, with the smallest values happening near regions of damaged glazing. The atmospheric temperatures above the ceiling ranged from 650-1335 ºF, with the higher values occurring in the vicinity of ceiling breach locations. The maximum recorded temperature in the unprotected beams was 806ºF.

One of the most significant experimental programs investigating fire behavior of steel buildings was the Cardington program, in which a full-scale eight-story steel framed structure was studied under fire exposure at the Cardington, UK research facility of the Building Research Establishment (Cardington, 1998). The steel building tested at Cardington was constructed with composite floors, and a number of steel beams in the composite floors were not fire protected and would not have satisfied US prescriptive fire protection requirements. Despite the absence of fire protection, the floor system and the entire structure was capable of sustaining severe fire exposure without collapse. The Cardington tests demonstrated the potential for significant cost saving in fire protection while still maintaining the safety of the steel structure under fire exposure. One of the important outcomes of the Cardington research was the conclusion that the key behavioral factor that affects the ability of a floor system to survive a fire is the development of tensile catenary and membrane action resulting from the large vertical displacements, which normally occur in a fire (Figure 2-20).

Figure 2-20. Floor System Response in Cardington Fire Test (Cardington, 2003)

This highly beneficial system behavior of a full composite floor system is not recognized in current US standards and typical practice, where fire protection requirements for structural steel beams are based on a standard fire test of isolated floor assemblies. Cardington and other related research have clearly shown that the fire behavior of a structural system is completely different from that seen in the standard fire test of a single structural element or assembly (Usmani et al. 2001).

2.2.4.3 Numerical Studies

The use of numerical modeling to analyze steel specimen behavior during a fire is a relatively new field, only receiving significant attention with recent improvement of computational capability. Yin and Wang (2004) performed a numerical study examining the behavior of restrained steel beams at elevated temperatures with an emphasis on large deformations. The authors included a parametric study that evaluated the influence of different load levels, rotational and axial restraint stiffness values, beam spans, and non-uniform and uniform temperature distributions. Experimental test results were used in validating the finite element model in ABAQUS. It was concluded that catenary action can enable steel beams to endure elevated temperatures without collapsing as long as reliable axial restraints are provided. Among the variables studied, axial restraint stiffness was found to be the most important factor in affecting beam deflection and catenary force. Yin and Wang (2005) presented a simplified hand calculation method to determine the catenary tensile force in beams. The temperature was assumed to be uniform across the section and along the span. A deflection shape of the beam was assumed according to the load type in order to determine beam elongation. This allowed the beam axial force to be determined when combined with thermal expansion. An incremental approach was used when material becomes plastic.

Moss et al. (2002) performed analysis to study the effect of support conditions on the fire behavior of steel and composite beams. The finite element software SAFIR was used to analyze beams with pin-roller, pin-pin, fixed-slide and fixed-fixed supports. Standard fire curves from the International Organization for Standardization (ISO) was used in analysis. It was found that beam behavior is very different with the change of support conditions. They concluded that stress conditions relative to the temperature reduced yield strength was a key variable in the beam behavior. Similar sized composite beams and steel beams were found to have similar behavior at elevated temperature.

Dai et al. (2010) used ABAQUS to simulate fire tests on 10 different restrained beam-column subassemblies using various types of connections, which were then validated with previously performed experiments. Details of the simulation methodology implemented to attain numerical stability and accurately capture the in depth structural performance was presented, as well as failure modes observed in the connections and the mid-span deflections and axial loads seen in the beams. Selamet and Garlock (2011) used nonlinear finite element models to examine the local buckling of floor beams for different connection types at elevated temperatures. The authors then compared the results to the AISC design equation for plate buckling under ambient and elevated temperatures, showing that at elevated temperatures the code overestimates the capacity.

2.3 Fire Following an Earthquake

Records of post-earthquake fire damage from several large magnitude seismic events illustrate the significance of the combined event of fire following an earthquake. Fire loss following the 1906 earthquake in San Francisco, California was estimated to be roughly ten times greater than loss associated with the ground shaking alone. In the aftermath of the 1923 Tokyo earthquake in Japan, an estimated three quarters of the buildings were lost and 56,000 deaths were attributed to post-earthquake building fires. Damage estimates for more recent seismic events, such as the 1994 Northridge earthquake in southern California and the 1995 Great Hanshin earthquake in

Kobe, Japan, range into the tens to hundreds of billions of US dollars (Scawthorn, 2008). Faggiano (2007) reported that nearly 7,000 buildings in Kobe were destroyed by post-earthquake fires alone.

2.3.1 Numerical Studies

The behavior of steel structures damaged by an earthquake and then subjected to fire has provided a new spark of interest in the engineering field. Although the work in this area is still limited, recent efforts have been geared towards investigating the scenario. The following section provides a brief summary of relevant studies on post-earthquake fire modeling.

Cousins and Smith (2004) used historical data from earthquakes in three New Zealand cities to develop a probabilistic model for estimating loss due to post-earthquake fire, and to characterize the relative impact of post-earthquake fire on total loss for a given event. Ren and Xie (2004) used historical data to develop a probabilistic model for post-earthquake fire ignition, and linked the algorithm to a geographical information system (GIS) in order to provide emergency response personal with a simulation tool for predicting post-earthquake fire spread.

Faggiano et al. (2007) utilized sequentially coupled heat transfer-stress analyses to evaluate the effect of residual destabilizing forces on the response of an unprotected steel portal frames during fire exposure. Nonlinear dynamic response history analyses were used to characterize peak and residual drift demands in the frame for various levels of seismic intensity. A thermo-mechanical post-earthquake fire model was then built in the deformed configuration to evaluate the effect of second-order destabilizing gravity loads. The study found that a sidesway collapse mechanism could be developed in the frame for cases with low residual stability indices, i.e. large ratio of second-order destabilizing gravity load to elastic restoring force. Additional research on fire following an earthquake has been conducted by Faggiano (2005, 2008, 2010) whom proposed an investigative approach for assessing the fire resistance of steel structures damaged by earthquakes in relation to different structural damage levels.

Yassin et al. (2008) investigated the post-earthquake fire-resistance of single-bay, single-story and single-bay, two-story steel moment-frames using the nonlinear finite element software SAFIR. The residual destabilizing forces in the damaged buildings were modeled with an idealized lateral load pattern that was scaled to various levels of intensity. Thermal insulation for the frames was assumed to be damaged during dynamic response, and was therefore neglected from the component heat transfer analyses. This meant that the heat transfer analyses was performed using the bare steel sections. Ambient fire exposure for the simulation utilized the temperature history from the ASTM E119 (ASTM, 2000) standard fire curve. The study found that residual second-order destabilizing forces in the damaged building could exacerbate lateral drift demands in the frames during ambient thermal heating.

Scawthorn (2008) used a probabilistic model to estimate potential fire loss arising from a hypothetical M7.8 earthquake in southern California. In the scenario, approximately 1,600 ignitions would occur that would require intervention of fire-fighting personnel. In roughly 1,200 of these fires, the first responding engine would not be able to adequately contain the fire, which would ultimately spread to adjacent buildings and potentially destroy several city blocks. The estimated loss would range from 40-100 billion US dollars. Lee and Davidson (2008) developed a physics-based approach for modeling post-earthquake fire spread that considers (1) evolution of fire within a room; (2) room-to-room spread within a building, and (3) building-to-building spread by flame impingement and radiation from window flames and branding. Kelly and Tell (2011) proposed a statistical model for predicting the number of fire ignitions following an earthquake based on historical data for earthquakes from 1906 to 1989 in Alaska and California.

2.3.2 Earthquake Record Selection

Table 2-2 provides an overview of the steps involved in a response-history analysis and summaries how various codes handle each step.

Table 2-2. Response History Analysis Comparison (Haselton, 2012)

Step for Response History Analysis	Design/Assesment Method			
	ASCE 7-05	ASCE 7-10	LATBSDG (2008)	PEER TBI (2009)
Explicit Goal	-	P[C] < 10% for MCE$_R$	Well-degined NL behav., func. For service motion, low P[C] for MCE.	Low risk of collapse, modest residual drift, no cladding failure.
Ground Motion Intensity	Sa_geoMean	Sa_maxDir	Sa_geoMean	Sa_geoMean or Sa_maxDir
Ground Motion Level for Assessment	2/3 MCE	2/3 MCE$_R$	MCE, service-level	MCE, service-level
Target Spectrum	-	-	-	-
General Approach	UHS	UHS with risk adjustment	UHS	UHS or multiple CMS
Notes	Limited by deterministic cap.		Limited by deterministic cap	Limited by deterministic cap
Ground Motion Selection	-	-	-	-
Number of Motions	≥7 (or 3) pairs		≥7 pairs	≥7 pairs
Types of Motions	Recorded and/or simulated		Recorded and/or simulated	Recorded and/or simulated
Other	None		"Appropriate numer" of motions with directivity effects	Directivity if needed
Scaling/Modification of Motions to Match Target Spectrum	-	-	-	-
General Approach	Scaling (spectral matching not mentioned)		Scaling or spectral matching	Scaling or spectral matching
Specific Instructions for Far-Field Sites	SRSS is above 1.17x target spec.	SRSS is above target spectrum	SRSS is above 1.17x target spectrum	"Match records to the target spectrum"
Specific Instructions for Near-Fault Sites	None	Average of FN is above target	None	None
Period Range for Matching	0.2T - 1.5T		02.T - 1.5T	Not specified
Applications of Ground Motions to Structural Model	-	-	-	-
Far-Field Sites	Just apply horizontal motions together, no rules for orientation		Orient motions randomly; no need for multiple orientations of GMs.	"Apply along principle directions" (but no GM rotation mentioned)
Near-Fault Sites	No rules for orientation	Apply in FN/FP directions if site > 5km from fault	Apply in FN and FP directions	Apply in FN and FP directions if directivity effects dominate
Treatment of Vertical Ground Motion	Not considered		Not considered	Included in rare cases
Response Metrics and Acceptance Criteria (at MCE or 2/3 MCE)	-	-	-	-
Peak Interstory Drifts	$\mu < 1.25*\text{limit}$		$\mu < 0.03$	$\mu < 0.03$, max < 0.045
Residual Interstory Drifts	No limit		No limit	$\mu < 0.01$, max < 0.015
Deformations for Deformation-Controlled Actions	$\mu <$ limit		$\mu <$ limit	No limit (except to keep within reliable analysis range)
Force for Force-Controlled Actions (Critical, well-defined mech.)	Maximum force is used for designs based on overstrength factor		$\mu <$ limit	$\max(\mu+1.3\sigma,\ 1.2\mu) \le \varphi F_{n,e}$
Force for Force-Controlled Actions (Critical, no well-defined mech.)				$1.5\mu \le \phi Fn,e$
Force for Force-Controlled Actions (Non-Critical)				$\mu \le \phi Fn,e$
Loss in Story Strength	No limit		No limit	Less thant 20% loss
Treatment of Collapse Cases	Unclear. Average drift limits suggest collapses are not allowed		Not discussed. Average drift limits suggest collapses are not	Collapses are not allowed
Other	None		None	Response in reliable analysis
Notes	None		None	For the multiple CMS, use response envelope for the various anchor periods
Other Design Uses of Response History Analysis Predictions	-	-	-	-
Design of Non-Structural Components	Not specified		Not specified	Not specified

2.4 Code of Practice

With the increase in multi-hazard events, awareness of fire and life safety and the technological advances and innovations for building design, the field of structural engineering is expanding each day. Codes and standards provide guidelines, regulations and techniques that govern structural design. Table 2-3 provides a brief overview of the codes and standards pertaining to this project, which include the design of RBS connections as well as the structural design for seismic and fire loading.

Table 2-3. Summary of Codes and Specifications

Code	Organization	Date	Relevance
Recommended Seismic Design Criteria for New Steel Moment-Frame Buildings	FEMA 350	2000	Provides recommended guidelines for the design and construction of steel moment frame buildings and alternative performance-based design criteria. A series of pre-qualified connection details, as well as a detailed procedure for performance evaluation, is included.
Recommended Specifications and Quality Assurance Guidelines for Steel Moment-Frame Construction for Seismic Applications	FEMA 353	2000	Provides recommended specifications for the fabrication and erection of steel moment-frames for seismic applications. The recommended design criteria contained in FEMA 350, FEMA 351, and FEMA 352 are based on the standards contained in this document.
State of the Art Report on Connection Performance	FEMA 355D	2000	Summarizes the current state of knowledge of the performance of different types of moment-resisting connections under large inelastic deformation demands. It includes information on fully restrained, partially restrained, and partial strength connections, both welded and bolted, based on laboratory and analytical investigations.
Fire Resistance of Structural Steel Framing	AISC 19	2003	Covers the design of fire resistant steel framing, including building code requirements, fire protection methods and materials, standard fire resistance tests, and the associated rating system. Provides detailed guidance for the selection of rated designs for columns, beams, and trusses, complemented with comprehensive design examples and W/D tables for common protection configurations.
Seismic Provisions for Structural Steel Buildings	AISC 341	2005	Provides information on connection detailing and member design requirements for structural steel and composite systems in high-seismic applications.
Quantification of Building Seismic Performance Factors	FEMA P695	2009	Presents a recommended methodology for reliably quantifying building system performance and response parameters for use in seismic design. The parameters or "seismic performance factors" addressed include the response modification coefficient (R factor), system overstrength factor, and deflection amplification factor.
NEHRP Recommended Seismic Provisions	FEMA P-750	2009	Resource for introducing new knowledge, innovative concepts, and design methods to improve the national seismic standards and codes. Presents consensus approved modifications to the reference standard, a completely rewritten commentary that explains how to design using the reference standard and a series of resource papers that focus on emerging seismic design concepts and methods for exposure to and trial use by the design community and on issues that have proven historically difficult or complex to adequately codify.
Prequalified Connections for Special and Intermediate Steel Moment Frames for Seismic Applications	AISC 358	2010	Presents connections which have been prequalified for use in special and intermediate steel moment frames, without the need for additional testing. The standard addresses three types of connections – the reduced beam section (RBS) connection, the bolted unstiffened extended end plate (BUEP) connection, and the bolted stiffened extended end plate (BSEP) connection.
Steel Construction Manual	AISC	2010	Provides information on design requirements and methodology used for steel structures as well as dimensions and properties of various types of steel sections.
Seismic Design Manual	AISC	2010	Governs the design, fabrication and erection of structural steel members and connections in the seismic force resisting systems (SFRS), and splices and bases of columns in gravity framing systems of buildings and other structures with moment frames, braced frames and shear walls.
Minimum Design Loads for Buildings and Other Structures	ASCE 7	2010	Provides loading requirements and information on seismic analysis including earthquake record selection and scaling.
International Building Code	ICC	2012	A large portion of the code deals with fire prevention. It differs from the related International Fire Code in that the IBC addresses fire prevention in regard to construction and design.
Fire Code	NFPA 1	2012	Requirements cover the full range of fire and life safety issues from fire protection systems and equipment and occupant safety in new and existing buildings to hazardous materials, flammable and combustible liquids, LP-Gas, and more.

2.5 Summary

Relevant background material for the study was presented in this chapter, the following list provides a summary of the key points that were addressed:

- The behavior of reduced beam sections during a seismic event has been extensively investigated and is relatively well understood. These connections have been shown to provide acceptable behavior on both the local connection level as well as the global frame level during an earthquake.
- A description of the various components that are needed for assessing the structural performance of steel buildings during a fire was presented. This included a discussion of past fire events, the different methodologies for simulating a typical office compartment fire, the heat transfer mechanisms involved in an office compartment fire, as well as a summary of previous experimental and analytical work that has been performed on steel structures exposed to fire. In addition to these discussions an emphasis was placed on the material modeling of structural steel at elevated temperatures.
- A brief discussion of the numerical studies that have been performed on steel structures exposed to fire following an earthquake was presented. An overview on the selection and scaling of earthquake records was also provided. An emphasis was placed on the recent study by Braxtan and Pessiki (2009, 2011a, 2011b) on the seismic performance of spray-applied fire-resistive insulation. This study was highlighted because the results played a significant role in the development of this study.
- A brief overview of the codes and standards pertaining to this project were presented including a description of their specific relevance to this project.

CHAPTER 3
MODELING FRAMEWORK

3.0 Introduction

The main objective of this research is to investigate the behavior of steel frames with reduced beam sections (RBS) during a fire as well as during the combined events of fire following an earthquake (FFE). Historical events and recent disasters have clearly demonstrated that the occurrence of these two events (fire and FFE) within steel framed buildings represents a probable scenario that warrants further investigation. Accurate analytical evaluation of the structural behavior of steel buildings under fire, and to a lesser extent an earthquake, is difficult due to the many complex and uncertain phenomena involved. Detailed analytical modeling of the overall structural system has been shown to provide the most reliable simulation results under current research development. However, detailed analysis is generally computationally expensive and as such not practically applicable. In addition, the nonlinear behavior of entire structures is complex and not fully understood. Therefore, detailed analytical models of the overall structural system often have difficulty capturing local failure modes. One of the main objectives of this research is to present a practical approach to perform accurate numerical evaluation of steel structures under fire and FFE and to closely investigate its characteristic behavior. The approach taken is to limit the focus on localized compartment fires and investigate the behavior of a single beam-column subassembly within the chosen compartment. By limiting the focus of the study, the numerical models can be simplified by utilizing specifically appropriate subassembly models with proper boundary conditions for the analysis.

Using the finite element (FE) program ABAQUS (ABAQUS 2012), two different beam-column subassemblies with RBS are created and analyzed. The subassemblies are taken from two steel special moment resisting frames (SMRFs) that are designed for the highly seismic Los Angeles region. The frames selected for analysis are an eight-story 4-bay frame and a sixteen-story 4-bay frame and the selected subassemblies are located at the exterior of the frames at the mid and lower levels, respectively. Both subassemblies are analyzed under fire alone to determine their structural behavior during the event as well as allow for a better understanding of the influence the seismic demand has on the behavior of the connection when exposed to FFE. For the FFE simulations, both models are analyzed under a suite of earthquake ground motions followed by a fire simulation. For the fire analysis portion of both simulations (fire alone and FFE), a sequentially coupled thermo-mechanical modeling technique is employed, which includes representative constraint elements to simulate the restraint imposed by the frame.

Section 3.1 provides an overview of the methodology used for both the fire and FFE analysis. In addition a description of how the mechanical boundary conditions for simulating the constraints imposed by the frame is presented. Section 3.2 describes the configuration of both frames as well as the selected subassemblies. Section 3.3 describes the selection and scaling of the suite of ground motion records used for the FFE models. Section 3.4 discusses the selection of the time-temperature curve and provides background information on its development. Finally, Section 3.5 summarizes the material properties used for the analysis.

3.1 Simulation Methodology

The following sections provide a brief description of the simulation methodology used for the numerical analysis performed for this study. This overview is provided so the reader understands all the components involved in the simulations prior to them being discussed in the remaining sections of the chapter. Detailed information on the finite element modeling techniques employed for these analyses can be found in Chapter 4. Figure 3-1 provides a visual overview of the simulation methodology for the both the fire and FFE analysis.

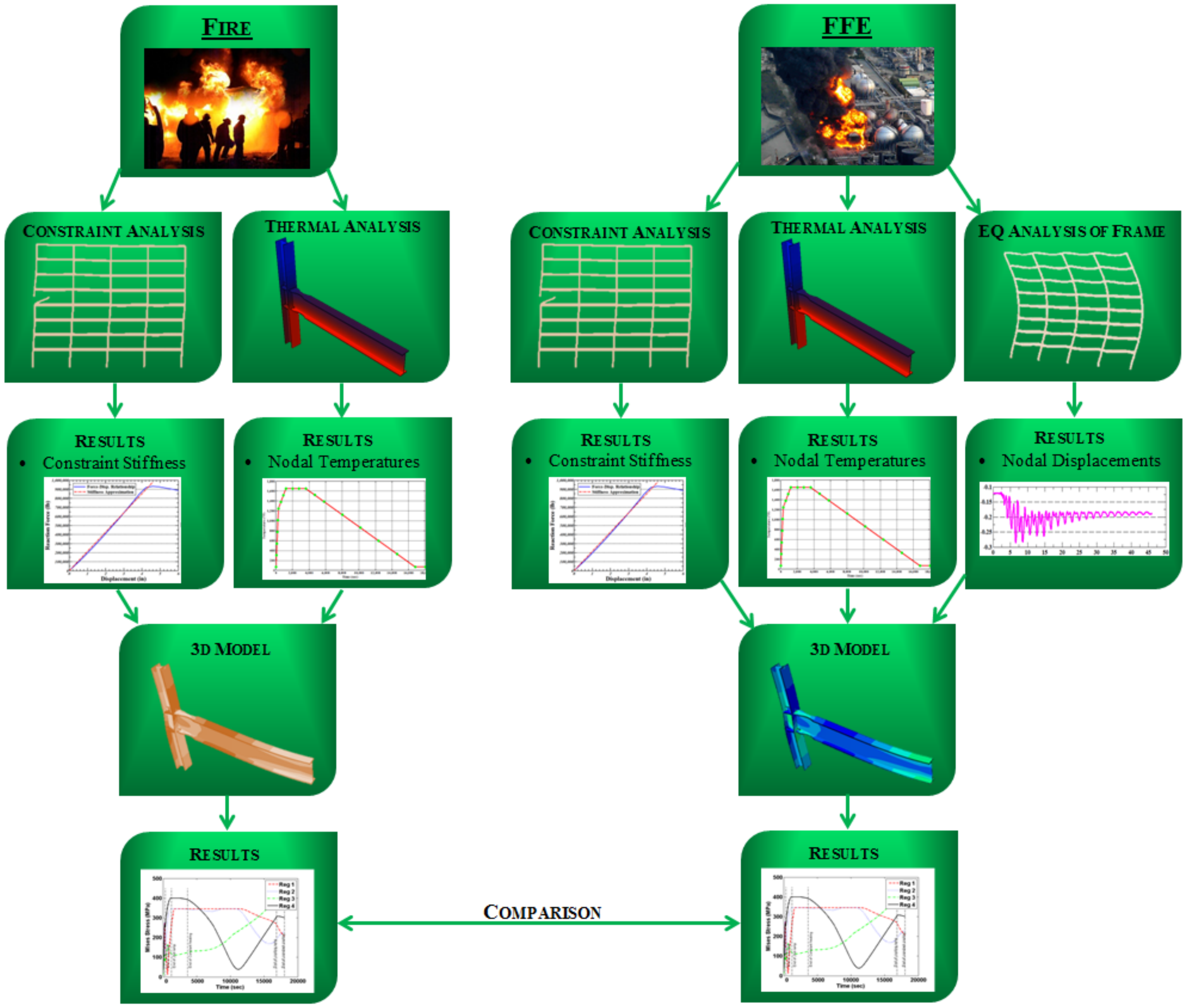

Figure 3-1. Simulation Methodology for the Assessment of RBS Connections under Fire and FFE

3.1.1 Fire Following an Earthquake Simulation

A multi-step sequential analysis is developed to determine the selected beam-column subassemblies responses to the seismic and subsequent thermal loading from the FFE scenario. The procedure is designed to transfer the imposed stresses and strains from the initial analysis step (earthquake) to the next (fire) in order to capture the effect of residual damage from the earthquake. This was accomplished by developing a two-step finite element model using the program ABAQUS. Information on the finite element models are provided in detail in Chapter 4. The first step of the analysis was to simulate the response of the subassemblies to earthquake loading. This is accomplished by applying nodal displacement histories to the tips of the beam and column of the subassemblies. The nodal displacement histories are obtained from a dynamic analysis that is performed on each frame under the suite of ground motions selected for this study. The earthquake simulation procedure is shown schematically in Figure 3-2.

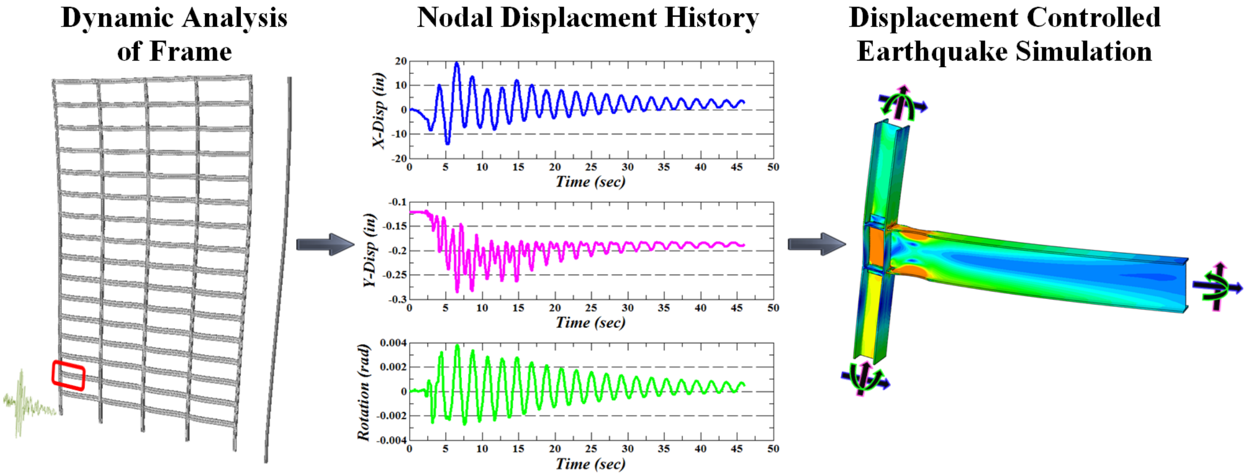

Figure 3-2. Schematic of Earthquake Analysis

The second step of the analysis involves simulating the post-earthquake fire and investigating the effects of temperature-induced material degradation and restrained thermal expansion on the beam-column subassemblies behavior. This is realized through a thermo-mechanical stress analysis utilizing nodal temperature data from a sequentially coupled heat transfer simulation. This required a thermal analysis of each subassembly be performed to determine the expected temperature distribution within the members. Once this step is completed, nodal temperatures are imported directly from the results as a predefined temperature field into the thermo-mechanical stress analysis.

For the thermal analysis damage to the fire proofing is assumed to have occurred in the RBS region of the beam during the preceding earthquake. This is based on observed damage patterns from several experimental studies conducted by Braxtan and Pessiki (2009, 2011a, 2011b) as well as Keller and Pessiki (2012), which indicated that the spray-applied fire resistive material (SFRM) in moment-frame beam hinge regions debonded, cracked, and spalled during inelastic seismic response, leaving the bare steel exposed to the ambient temperature. Depictions of some of the damaged specimen from the study are shown in Figure 3-3.

Figure 3-3a. Damaged SFRM insulation at beam hinge region after cyclic loading
(Keller and Pessiki, 2012)

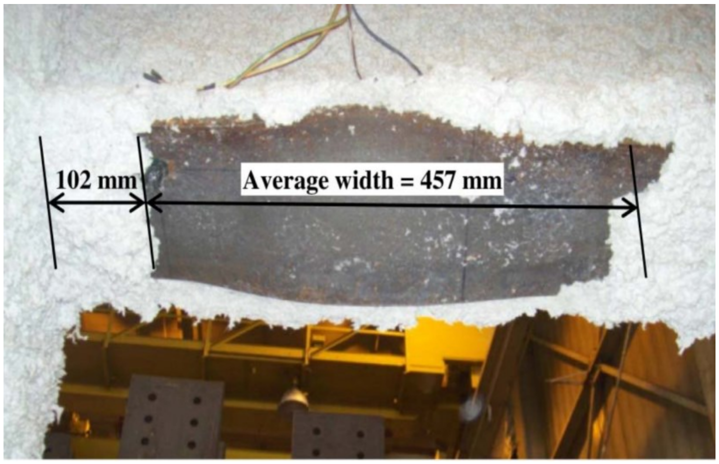

Figure 3-3b. SFRM damage on the underside of bottom beam flange after cyclic loading
(Braxton and Pessiki, 2011)

The RBS portion of the beam is selected because preliminary results from this study as well as existing experimental and numerical work that has been performed on similar connections indicate that plastic hinges would form in that region. A detailed description of the studies performed by Braxton and Pessiki (2009, 2011a, 2011b) and Keller and Pessiki (2012) as well as a summary of experimental and numerical work on RBS connections is provided in Sections 2.3.2 and 2.1 respectively.

The thermal analysis is accomplished by constraining the surface temperature of the RBS to follow the values of a selected time-temperature curve. This means that conduction is the only heat transfer mechanism considered in the analysis. While this is a rather significant simplification, the uncertainty associated with modeling the ambient temperature of a typical office fire as well as the computational costs associated with realistic simulations required its use. The exclusion of convection and radiation is thought to have a negligible effect on the results of the analysis based on numerical and experimental testing that suggests that the surface temperature of exposed steel closely follows the ambient temperature of the compartment it is contained within (Garlock 2005, Takagi 2007, and Villaverde 2011). Plots taken from these studies comparing the surface temperature of exposed steel members to the applied fire curve are shown in Figure 3-4.

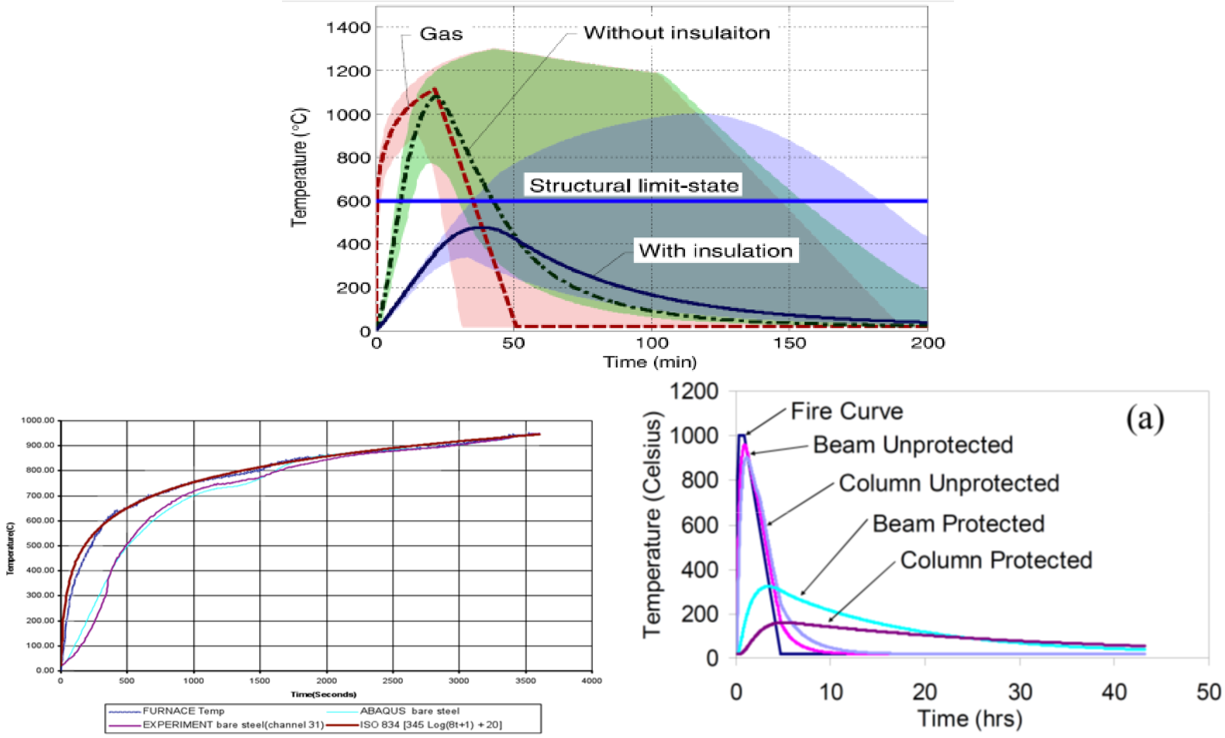

Figure 3-4. Surface Temperature of Unprotected Steel Compared to the Applied Time-Temperature Curve (Takagi 2007, Villaverde 2011, Garlock 2005)

In order to accurately capture the demands imposed by the surrounding frame on the subassemblies during the fire, elements are placed at the ends of the columns and beams to provide planar restraints (axial, lateral, and rotational) representative of the remainder of the frame. These elements provided a way of capturing the fully-coupled transient restraint stiffness that is provided by the remainder of the frame without having to include the entire structure in the model. This technique has never been employed in thermo-mechanical analysis before so the implemented approach had to be developed specifically for this study. Further details on the development of this methodology can be found in Section 3.1.3.

3.1.2 Fire Simulation

The same technique used to simulate the fire in the FFE analysis was also employed in the fire analysis. Both beam-column subassembly models were exposed to thermal loading in their undamaged states in order to determine the expected temperature distributions within the joint. These temperature distributions were then imported into the thermo-mechanical analysis of the subassemblies. This process is depicted in Figure 3-5.

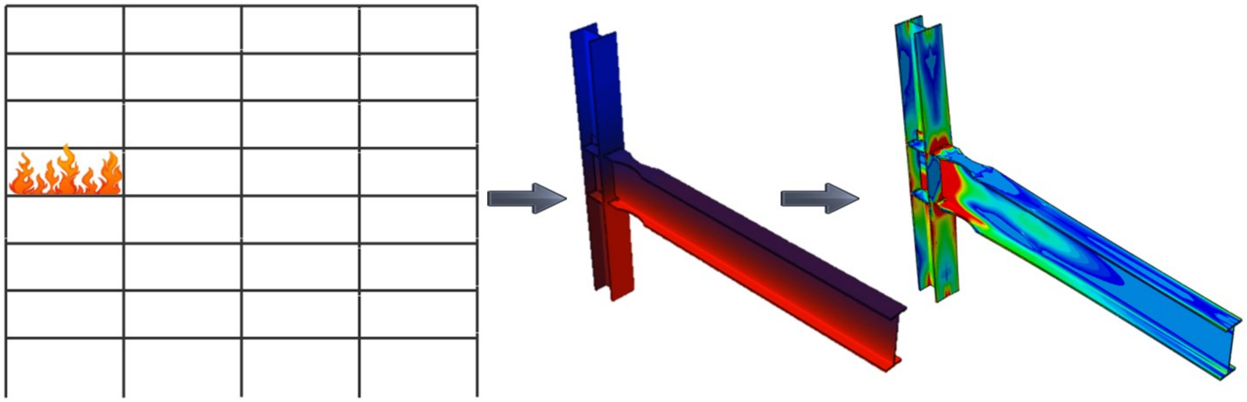

Figure 3-5. Schematic of Fire Analysis

For the thermal analysis, the beam-column subassemblies were assumed to have no passive fire protection in place. This approach was selected because it was thought to provide the most value to the research being performed. This is a result of relatively little data existing on the behavior of unprotected steel members when exposed to fire as well as the simplistic nature of the current design approach for fire safety. While the current prescriptive methodology that requires passive fire protection has proven adequate, its simplistic nature has led to numerous criticisms, particularly from the steel industry, which bares the largest financial burden from the cost of fire protection. The most notable issue is that the current practice does not provide any tangible basis on how real fires affect structures, leaving the actual risk of structural failure due to fires a relative unknown. Furthermore, a widespread perception exists that in some cases the prescriptive requirements are overly conservative and are not cost effective. These criticisms are further supported by real events including the Broadgate Phase 8 Fire (British Steel, 1999) and experimental testing done at the Cardington, UK test facility (Cardington, 1998) which demonstrated that unprotected steel frames could still exhibit acceptable behavior under fire loading. The outcome of such criticism is a recent shift towards performance-based fire engineering, which is starting to take hold, particularly in Europe, Japan, Australia, and New Zealand. This new performance based approach could offer engineers more opportunities to formulate alternative solutions for fire resistance. Because of this it was decided that neglecting the passive fire protection would offer useful insight into the behavior of the connections under fire loading and provide more value to the engineering community.

The restraint provided by the frame is implemented in the fire analysis in the same manner as the FFE analysis. However, in addition to the realistic restraints used in the FFE analysis two other restraint models are implemented to study the influence of the boundary conditions on the response of the beam-column subassemblies. This includes a fully restrained model where the tips of the beam and column are fixed in all six degrees of freedom (DOFs). This is representative of a scenario where the surrounding frame does not allow for thermal expansion of the subassembly. The second model uses representative restraints at the tips of the beam and column in the planar axial and rotational DOF's and fixed the lateral DOF's. This is employed to analyze the effect that the horizontal constraint at the column tips and vertical constraint at the beam end has on the response of the subassembly. This is particularly significant because lateral constraint has not been considered in previous work on fire and as such its impact on the response of the subassembly is a complete unknown.

3.1.3 Mechanical Boundary Conditions

A realistic boundary condition model is developed to capture the transient mechanical restraint provided by the frame during the fire simulation. For this approach additional finite element models are developed for both steel frames and their restraint properties are examined throughout the entirety of the fire simulation. For the FFE models a dynamic earthquake simulation is performed on each frame prior to being analyzed throughout the fire simulation to capture the residual earthquake damage. ABAQUS is utilized to develop and run the analysis of the finite element models of both frames. The simulation is terminated at twenty representative times throughout the fire simulation and a series of displacement-controlled analyses are performed to evaluate the restraint provided by the framework surrounding the subassemblies. The locations where the analysis is terminated and the frames analyzed is depicted in Figure 3-6.

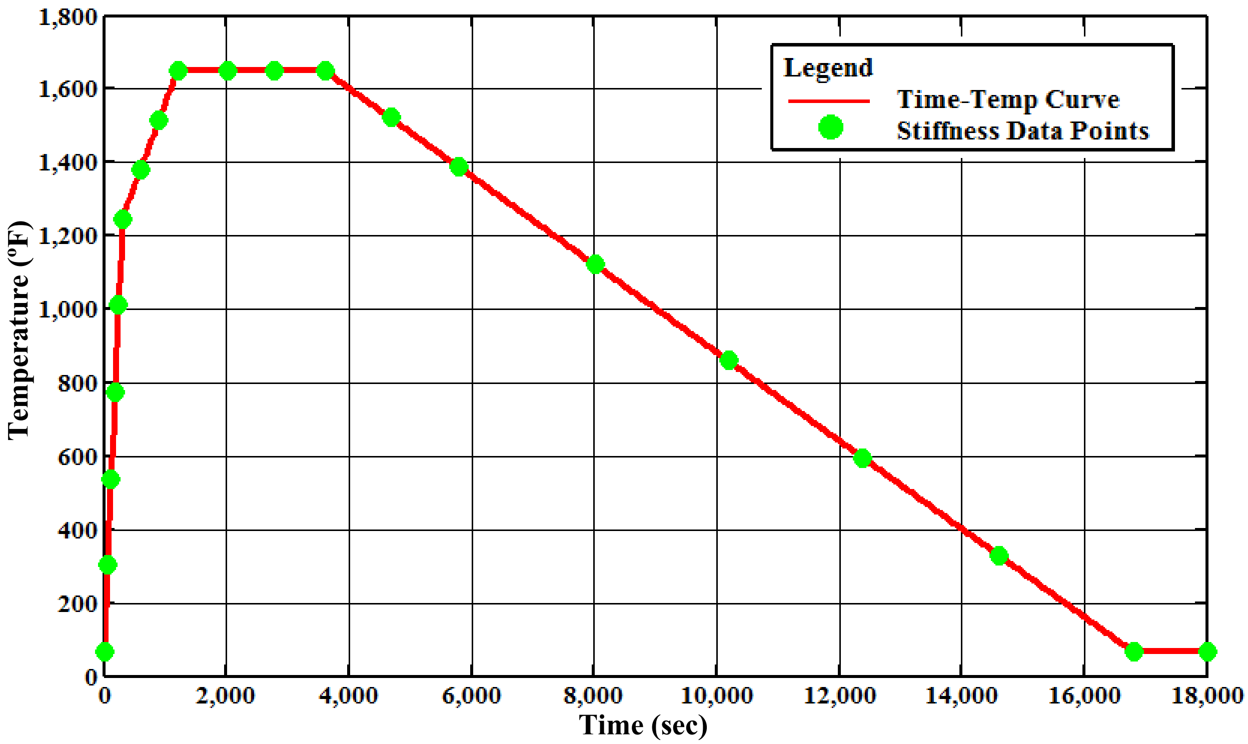

Figure 3-6. Fire Simulation Stiffness Points

The response data is then used to calibrate linear restraint elements used for the subassemblies beam and column boundary conditions throughout the fire simulation. A depiction of this procedure can be seen in Figure 3-7. These elements are updated throughout the analysis to capture the evolution of restraint provided by the frame over the duration of the fire.

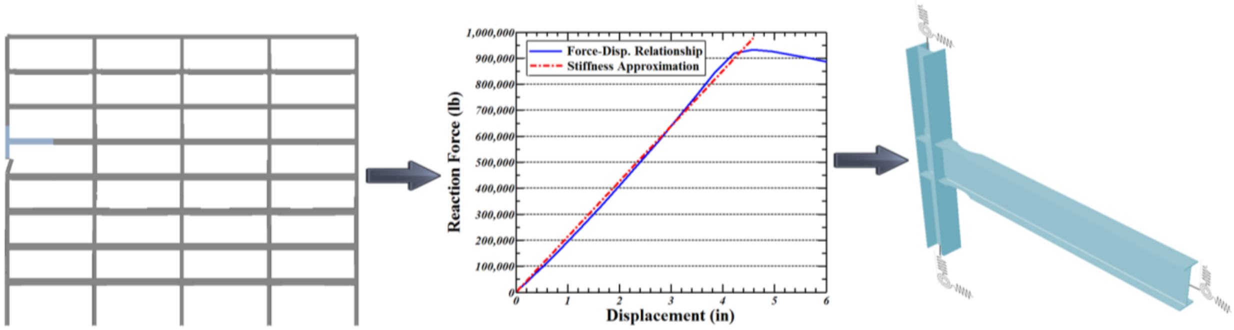

Figure 3-7. ABAQUS Stiffness Model Configuration

3.2 Configuration of the Analyzed Structures

One of the primary objectives of this study is to evaluate the adequacy of current U.S. building code provisions for preventing structural failures during fire exposure. The selection of the test structures is an integral aspect of the research project, an overview of the structural configuration and the design checks performed on the structures are provided in this section. The goal of this task is to select and verify the design of two structures that would be representative of a typical steel moment-frame office building located near Los Angeles, California. The design standards used for verifying the design of the structures are presented in Section 3.2.1. The building configurations are presented in Section 3.2.2 and the configuration of the selected beam-column subassemblies are provided in Section 3.2.3. Floor dead and live loads are discussed in Section 3.2.4, and the seismic design loads are presented in Sections 3.2.5. Section 3.3.6 provides information on the design approach for fire safety implemented on both frames.

3.2.1 Design Standards

Various provisions were used for verifying and analyzing the design of the lateral frames used for this study, a list of the most notable are presented below. All design loads were obtained by assuming the structures to be standard office buildings located in a region near Los Angeles.

- 2010 California Building Code
- 2006 International Building Code
- AISC Steel Construction Manual 14th Edition
- ANSI/AISC 358-10: Prequalified Connections for Special and Intermediate Steel Moment Frames for Seismic Applications
- ANSI/AISC 341-10: Seismic Provisions for Structural Steel Buildings

- ANSI/AISC Steel Design Guide 19: Fire Resistance of Structural Steel Framing
- ASCE/SEI 7-10: Minimum Design Loads for Buildings and Other Structures
- FEMA-350: Recommended Seismic Design Criteria for New Steel Moment-Frame Buildings
- FEMA-695: Quantification of Building Seismic Performance Factors

3.2.2 Building Configuration

The two structures considered in this study are an 8-story, 4-bay (longitudinal) by 4-bay (transverse) steel frame and a 16-story, 4-bay (longitudinal) by 4-bay (transverse) steel frame. The structures were designed by Jin and El-Tawil (2004) to evaluate the seismic performance of steel frames with RBS connections. The lateral load resisting system for both buildings are special moment resisting frames (SMRF) specified along the perimeter of the structures. For the purpose of this study these SMRFs are selected to be analyzed in more detail. The RBS connections are sized according to provisions in FEMA 350, which requires 50% beam flange reduction for the majority of the connections. Doubler plates are used for panel zone reinforcement when required. The structural configuration for the buildings is shown in Figure 3-8. The figure provides member sizing for interior and exterior columns and beams for the analyzed perimeter special moment resisting frames.

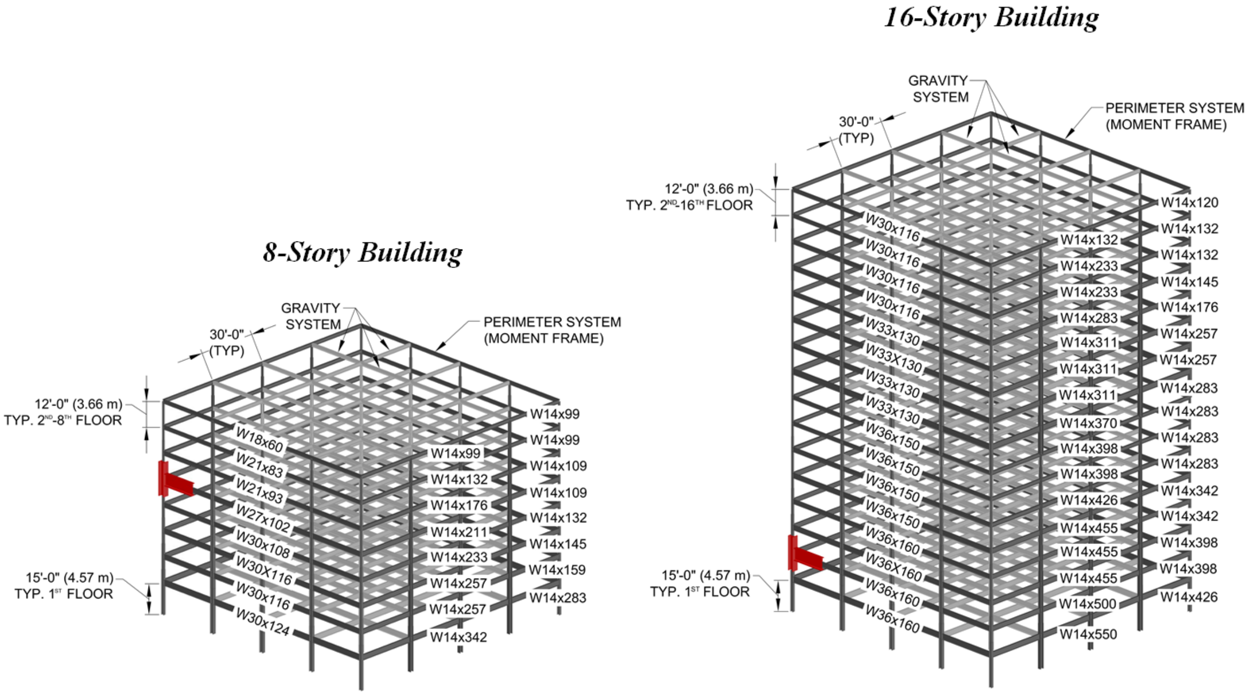

Figure 3-8. Configuration of 8-story and 16-story Buildings

The columns are wide-flange 50 ksi steel members sized as shown in Figure 3-8, with the interior columns all having the same member size. Column splices, which are designed to carry bending and uplift forces due to the lateral excitation, are located at 6-feet above the center-line of the beam to column joints. The column bases are fixed at the ground level. The floor system is comprised of wide-flange 50 ksi steel beams with each outer frame assumed to resist one half of the seismic mass associated with the entire building.

Business Group B is selected for the occupancy classification for both structures in accordance with IBC-06 Section 304, and is assumed to utilize type 1B non-combustible construction material in accordance with IBC-06 Section 602. For both structures the height of the topmost occupied floor is located more than 75 feet from the lowest level of fire department access meaning that they qualify as high-rise structures and are subject to the additional design requirements of IBC-06 Section 403.

3.2.3 Connection Design

Beam-column subassemblies at the fifth floor of the eight-story frame and second floor of the sixteen-story frame are selected to be analyzed in detail to assess the local behavior of the connections. These subassemblies are highlighted in red in Figure 3-8. The eight-story beam-column subassembly consists of a W27x102 beam welded to a W14x109 column. The sixteen-story beam-column subassembly consists of a W36x160 beam welded to a W14x398 column. The reduced portions of both beams are designed based on the procedures outlined in FEMA-350. In addition, the configuration of the weld access holes, backing bars, continuity plates, and all other applicable details are designed to meet the specifications of current code practice (FEMA-350, AISC 341, AISC 358, AISC Steel Construction Manual, AISC 341). Figure 3-9 provides a detailed illustration of the connections, the design calculations used for member detailing can be found in Appendix B.

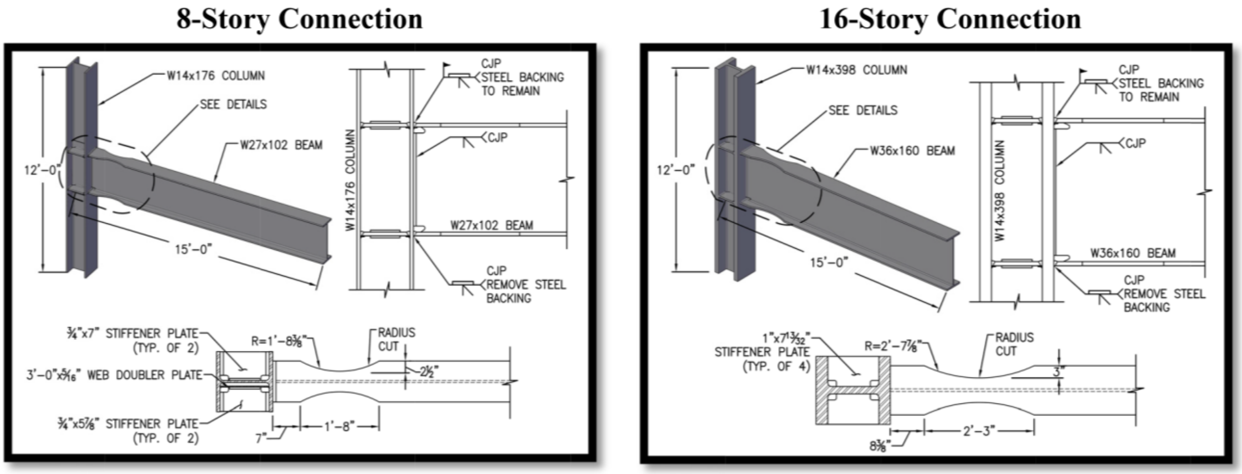

8-Story Connection

16-Story Connection

Figure 3-9. Beam-Column connection configuration

3.2.4 Floor Dead and Live Load

The seismic mass of the structure was determined according to ASCE 7-10 and takes into consideration the steel framing, floor slabs, ceiling/flooring, partitions, mechanical and electrical components, roofing and a penthouse located on the roof. The seismic mass is based on a total dead load of 124 psf for the floor levels and 106 psf for the roof. A live load of 80 pounds per square foot is assumed for both structures based on the guidelines of ASCE 7-10.

3.2.5 Seismic Design

IBC-06 and ASCE/SEI 7-10 define the seismic hazard for a structure in terms of an associated pseudo-acceleration response spectrum, where pseudo-acceleration (or spectral acceleration) demand is defined in Equation 3-1:

$$S_\tau = SD_\tau \omega_n^2 \qquad \text{(Equation 3-1)}$$

Where,

S_τ is the spectral acceleration demand for ground shaking calculated at period T
SD_τ is the peak displacement demand for ground shaking calculated at period T
ω_n is the natural frequency of vibration for the dynamic system equal to$2\pi/T$

For seismic design of structural systems, ASCE/SEI 7-10 defines various levels of seismic hazard with corresponding response spectra, this includes a design earthquake (DE) spectrum as well as maximum considered earthquake (MCE) spectrum. The design earthquake demand is taken as two-thirds of the MCE demand. When evaluating a structure, it is suggested that systems are designed for DE ground motions and collapse evaluation is performed using the corresponding set of MCE ground motions. The purpose of this study is to evaluate the structures for collapse so the MCE demand is utilized. The seismic provisions of ASCE/SEI 7-10 define the MCE demand in terms of mapped values of short-period spectral acceleration, S_S, and 1-second spectral acceleration, S_1, site coefficients F_a and F_v, and a standard response spectrum shape. In order to facilitate a practical approach for determining spectral acceleration values ASCE/SEI 7-10 provides geographically mapped values. These mapped values assume an inherent damping ratio (ζ) of 5% and Site Class B (rock). Once the spectral acceleration values are determined site modification factors F_a and F_v taken from IBC-06 Section 1613.5.2 are then used to adjust the MCE spectral acceleration to account for the effect of soil conditions on ground motion response. These adjusted values are referenced as S_{ms} and S_{m1} and multiplied by 2/3 to determine the DE spectral acceleration parameters S_{DS} and S_{D1}. Finally, the long-period transition period T_L is taken from Figures 22-12 through 22-16 of ASCE/SEI 7-10. Once these values are determined, the next step is to use the procedure outlined in Figure 3-10 to determine DE response spectrum. These values are then multiplied by 3/2 to obtain the MCE response spectrum.

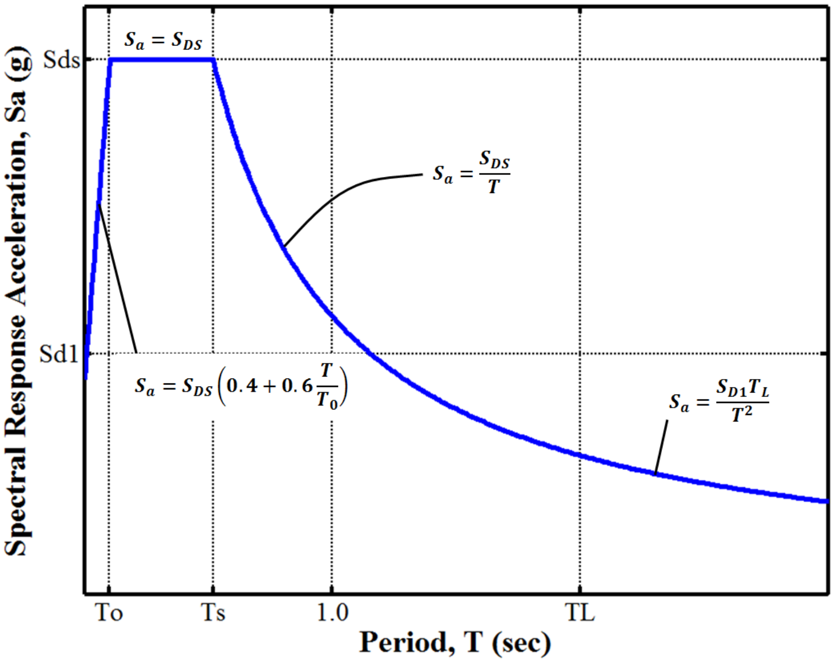

Figure 3-10. Design Response Spectrum

Where,

$$T_0 = 0.2\frac{S_{D1}}{S_{DS}}$$

$$T_s = \frac{S_{D1}}{S_{DS}}$$

For the purpose of this study the USGS U.S. Seismic Design Maps application was utilized to determine all applicable values for defining the response spectra. Short (S_S) and 1-second period (S_1) MCE spectral acceleration demands for both structures are taken as 1.50g and 0.60g, respectively, where g is defined as gravitational acceleration. For both test structures site class D (stiff soil) conditions are assumed, and the site coefficients for the acceleration-controlled (F_a) and velocity-controlled (F_v) response regions are taken as 1.0 and 1.3, respectively. The assumption of site class D conditions is consistent with the ASCE/SEI 7-10 recommendations for when soil profiles are not known in sufficient detail.

3.2.6 Fire Safety Design

Fire protection for the building is assumed to be a combination of active protection systems (automatic sprinklers) and passive fire protection (spray-applied fire-resistive insulation) based on the prescriptive guidelines of IBC-06. Since the test structure qualifies as a high-rise building, as defined in IBC-06, all floors are required to be protected with an automatic sprinkler system in accordance with IBC-06 Section 403.2. In addition, since the primary usage of the building is for office rental space, the California Building Code requires that the structure be equipped with a heat and smoke monitoring system capable of relaying information to emergency response and fire-fighting personnel. The construction classification for the building is assumed to be Type 1B non-combustible material in accordance with IBC-06 Section 602. For this type of construction, IBC-06 Table 601 requires that the structural components provide a minimum fire resistance of 2-hours. In order to meet this requirement, the structural steel framework is assumed to be passively protected with a proprietary two-hour fire-rated dry-mix spray-applied fire-resistive insulation.

3.3 Ground Motion Records

3.3.1 Ground Motion Selection

The suite of earthquake records used for this study are selected, normalized, and scaled following the guidelines of FEMA-P695 (2008). A total of ten earthquake records are chosen consisting of five far-field and five near-field records. These records are taken from the FEMA P695 Ground Motion Records Sets; when selecting the records, the following objectives are taken into consideration:

- **Source of Records**: Emphasis is given to ground motions that are obtained and scaled from individual recorded events. All records selected for the far-field and near-field set come from actual events and no two records within each set are from the same event.
- **Strength of Ground Motions**: The records should represent a very strong ground motion corresponding to the maximum considered earthquake demand. Priority is given to records with the highest peak ground acceleration (PGA) and velocity (PGV) values.
- **Large Number of Records:** Importance is placed on selecting a sufficient number of records so the set is statistically sufficient. It is imperative that the results of the analysis adequately describe both the median value and record-to-record variability of the imposed structural demand. Numerous studies, which are described in Section 2.3.2, have been performed to determine how many records are necessary; these studies are taken into consideration when selecting the number of records along with considerations for computational expense and time constraints.
- **Structure Type and Site Hazard Independence:** The records should be broadly applicable to evaluation of a variety of structural systems and site locations. Importance

is placed on selecting records such that the set has a large variability in site class, epicentral distance, frequency values, and source type.

Table 3-1 provides a summary of the records selected for this study.

Table 3-1. Summary of Selected Ground Motions

Record	Type	Earthquake	Year	M_w	Site Class	Source Type	Epicentral Distance (km)	Lowest Freq. (Hz)	PGA (g)	PGV (cm/s)
1	NF	Erzican	1992	6.7	D	Strike-slip	9	0.13	0.49	95.5
2	NF	Kocaeli	1999	7.5	B	Strike-slip	5.3	0.13	0.22	29.8
3	NF	Imperial Valley	1979	6.5	D	Strike-slip	6.2	0.13	0.76	44.3
4	NF	Loma Prieta	1989	6.9	C	Strike-slip	7.2	0.25	0.51	45.5
5	NF	Northridge	1994	6.7	D	Thrust	10.9	0.11	0.87	167.3
6	FF	Duzce	1999	7.1	D	Strike-slip	41.3	0.06	0.82	62
7	FF	Kobe	1995	6.9	D	Strike-slip	46	0.13	0.24	38
8	FF	Loma Prieta	1989	6.9	D	Strike-slip	9.8	0.13	0.53	35
9	FF	San Fernando	1971	6.6	D	Thrust	39.5	0.25	0.21	19
10	FF	Northridge	1994	6.7	D	Thrust	26.5	0.13	0.48	45

While all the objectives are considered during the selection process, no single set of records can fully meet all of the requirements of each objective. This is largely due to inherent limitations in available data. Large magnitude events are rare and few existing earthquake ground motion records are strong enough to be considered large magnitude. For instance, in the United States strong-motion records first started being recorded after the 1933 Long Beach earthquake, but only a few records were obtained from each event until the 1971 San Fernando earthquake. Furthermore, strong motion instrumentation networks only provide coverage for a relatively small fraction of high seismicity regions. Considering the size of the earth, the available sample of strong motion records from large magnitude earthquakes is relatively limited and likely biased by records from more recent events that occurred in areas with numerous recording stations.

3.3.2 Scaling of Ground Motions

For the purpose of this study, the selected ground motion records were scaled in accordance with the procedure outlined in FEMA P695 Section A.8. The first step in scaling the ground motions was to normalize both the near-field and far-field record sets. Each set is normalized by peak ground velocity in accordance with the methodology presented in FEMA P695. Normalization by peak ground velocity is a simple way to remove undesirable variability between records that are caused from differences in source type, site conditions, distance to source, and event magnitude while still maintaining the record-to-record variability required for accurately predicting collapse fragility. This is done by determining the median PGV for each set and then scaling each record such that the specific record PGV matches the median value. The formulas used for this process are provided in Equation 3-2:

$$\begin{aligned} NM_i &= Median\left(PGV_{PEER_i}\right)/PGV_{PEER_i} \\ NTH_{1,i} &= NM_i \times TH_{1,i} \\ NTH_{2,i} &= NM_i \times TH_{2,i} \end{aligned} \qquad \text{(Equation 3-2)}$$

Where,

NM_i is the normalization factor of both horizontal components of the ith record
PGV_{PEER_i} is the peak ground velocity of the ith record (PEER database)
$Median\left(PGV_{PEER_i}\right)$ is the median of PGV_{PEER_i} values of records in the set
$NTH_{1,i}$ is the normalized ith record, horizontal component 1
$NTH_{2,i}$ is the normalized ith record, horizontal component 2
$TH_{1,i}$ is the record I, horizontal component 1 (PEER database)
$TH_{2,i}$ is the record I, horizontal component 2 (PEER database)

Once the record sets are normalized, the next step is to scale the records based on the MCE design response spectrum. For this step, each set of normalized records are collectively increased or decreased in strength as required to determine median collapse. The same scaling factor is applied to each record in the set such that 50 percent of the records cause collapse of the analysis model of interest. This is done by scaling each set of records such that the median value of the scaled record set matches the MCE demand at the fundamental period of the structure of interest. Figure 3-11 provides a depiction of both ground motion record sets response spectra scaled to the MCE design spectrum for both the 8 and 16 story frames. When looking at the figures it should be noted that the fundamental period of the 8 and 16 story frames are 1.548 seconds and 2.664 seconds, respectively. Appendix C provides more detailed description of the normalization and scaling of the earthquake record sets.

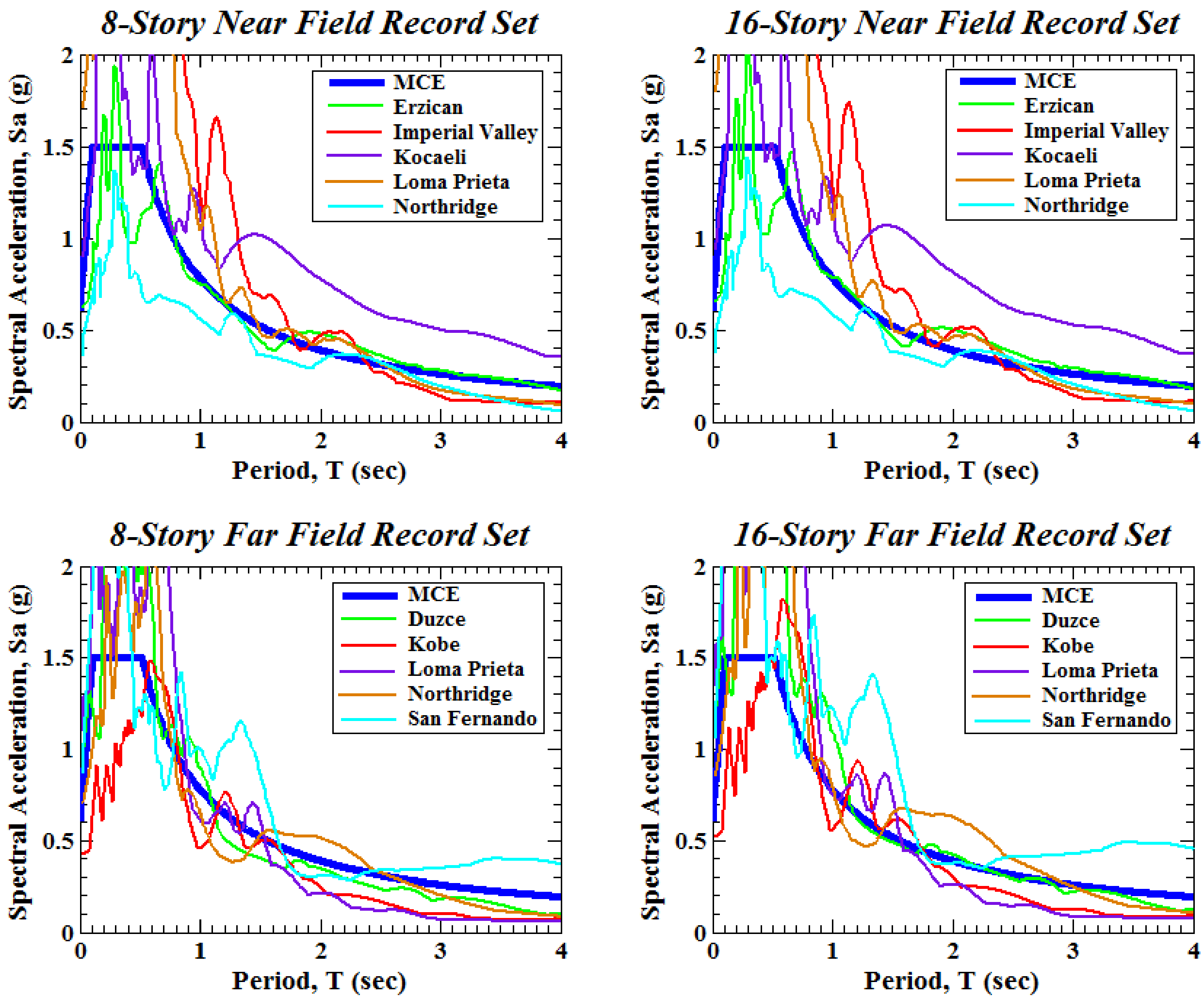

Figure 3-11. Scaled Ground Motion Response Spectra

3.4 Fire Time-Temperature Curve Selection

In this study a realistic fire time-temperature curve, which includes a cooling phase, is used instead of the more traditional standard fire curves such as those presented in ASTM E-119 and ISO-834. The selected curve is taken from a study by Quiel and Garlock (2008) and provides an accurate representation of a typical compartment fire seen in office buildings. The realistic time-temperature curve used for this study can be seen in Figure 3-12 compared to the standard fire curve presented in ASTM E-119.

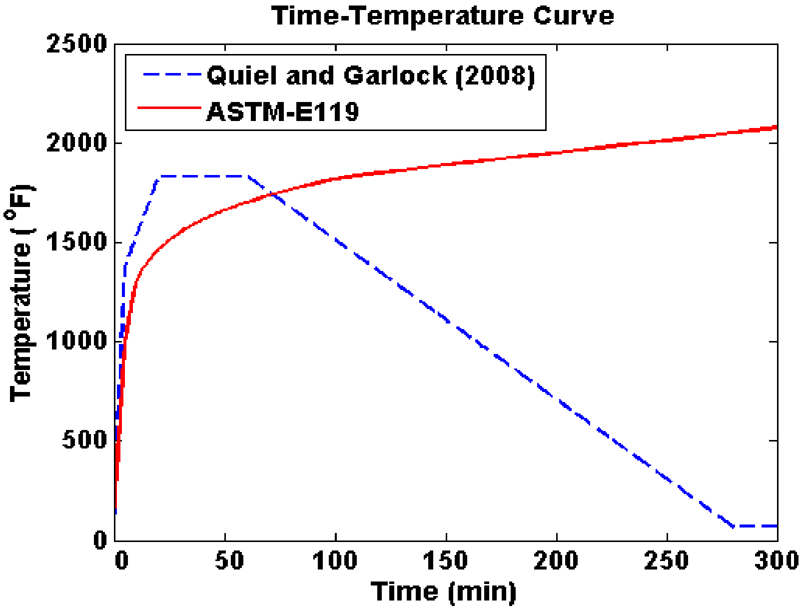

Figure 3-12. Time-Temperature curve comparison

3.5 Material Properties

3.5.1 A992 Steel

The material properties for the earthquake and fire simulation models are based on ASTM A992 steel for the beams and columns and include damage modeling, density, inherent damping, and temperature dependent values for mechanical and thermal properties. ASTM A992 steel is a structural steel alloy commonly used for steel beams within the United States, it has become the industry standard for all structural beams. Like most carbon steels the density of ASTM A992 steel is approximately 0.2836 lb./in^3 (ASTM 2011). According to ASTM (2011) specifications A992 steel has a tensile yield strength of 50 ksi, a tensile ultimate strength of 65 ksi, and a strain to rupture of 18% for a 7.9 inch specimen and 21% for a 2.0 inch specimen. The American Institute of Steel Construction states that "ASTM A992 (F_y = 50 ksi, F_u = 65 ksi) is the preferred material specification for wide-flange shapes, having replaced ASTM A36 and A572 grade 50." (AISC 2012)

The increased strength of the weld material is taken into consideration by increasing the yield stress of the material in the weld regions to 58 ksi. Because of the mechanical properties of A992 steel matching both the yield and tensile strengths of the weld material to the base metal was not possible. Because of this the filler metal was selected such that it is said to be overmatched. This is common practice within the industry and likely scenario for this application. The selected weld material is based on E70 filler metal, which has a yield stress of 58 ksi and ultimate tensile strength of 70 ksi. This means the weld has a yield stress value that is 8 ksi greater than the A992 steel and a tensile ultimate strength of 70 ksi which is 5 ksi greater than the value for A992 steel.

The Johnson-Cook constitutive damage model is selected for inclusion of damage initiation in the material model (Johnson and Cook, 1983 and 1985). The three key material responses used in this model are strain hardening, strain-rate effects, and thermal softening. The Johnson-Cook constitutive model combines these three effects in a multiplicative manner as shown in Equation 3-3:

$$\sigma_Y = \left[A + B\left(\varepsilon_{eff}^P\right)^N\right](1 + C \ln \delta\varepsilon)[1 - (T_H)^M] \quad \text{(Equation 3-3)}$$

Where,

ε_{eff}^P is the effective plastic strain
$\delta\varepsilon = \frac{\delta\varepsilon_{eff}^P}{\delta\varepsilon_0}$ where $\delta\varepsilon_0$ is the strain rate used to determine A, B and N
$T_H = \frac{T - T_R}{T_M - T_R}$ is the homologous temperature
T_M is the melting point
T_R is the reference temperature when determining A, B and N
$\Delta T = \frac{1}{\rho C_P} \int \sigma d\varepsilon_{eff}^P$ where ρ is mass density and C_P is specific heat

This model is expanded to include fracture based on cumulative damage. The cumulative damage fracture model is provided by Equation 3-4:

$$\varepsilon^F = \left(D_1 + D_2 exp\left[D_3 \frac{P}{\sigma_{eff}}\right]\right)(1 + D_4 ln\delta\varepsilon)(1 + D_5 T_H) \quad \text{(Equation 3-4)}$$

Where:

$D = \sum \frac{\Delta\varepsilon_{eff}^P}{\varepsilon^F}$ and failure occurs when $D = 1$
σ_{eff} is the effective stress
P is the mean stress (pressure)

Because insufficient data exists on damage modeling of A992 steel the values used for this study are taken from data presented on 4340 steel in Johnson and Cook (1985). While 4340 steel does differ slightly in composition from A992 steel they are similar enough that the effect of the differences in the analysis are thought to be negligible.

3.5.2 Temperature-Dependent Mechanical Properties

The temperature-dependent mechanical properties are adopted from Eurocode 3 (2005) and included yield strength, elastic modulus, and coefficient of thermal expansion. Figure 3-13 provides a plot of the yield strength and modulus of elasticity taken from Eurocode 3 along with values taken from the ASCE fire protection manual (1992) and Poh (2001) constitutive models and various experimental studies. As seen in the plots both the yield strength and elastic modulus decrease as the temperature increases. This behavior is attributed to the nucleus of the iron atoms in the steel moving apart as the temperature rises, causing a decrease in bond strength. This loss of bond strength is the cause of the reduction of yield strength and elastic modulus.

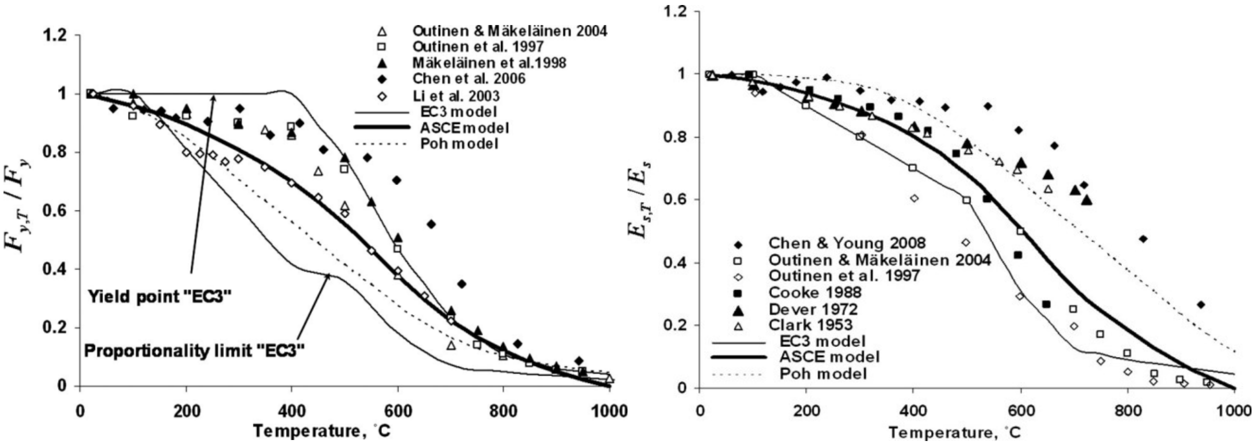

Figure 3-13. Mechanical Properties of Steel as Predicted by Different Models and Measured in Different Tests (Kodur et al., 2010)

When evaluating the values for yield strength and modulus of elasticity at temperatures above 300°C it can be seen that there is a significant variation not only between the test data but also between the various constitutive models. The variation in test data is largely attributed to variable heating and loading rates during the various tests. For example, when a small heating rate is used the specimen will be subjected to stresses at higher temperatures for longer periods of time. This will cause factors such as high-temperature creep to influence the resulting temperature-stress-strain curves of the tested specimen. The variation in constitutive models is primarily due to the large variation in the test data used to compile the models.

When comparing the Eurocode model to the ASCE and Poh models it can be seen that there is less reduction in yield strength, particularly at lower temperatures. The Eurocode model assumes no reduction in steel yield strength up to 400°C while ASCE model assumes a loss of 30% and the Poh model a loss of 40%. However, when comparing the modulus of elasticity it can be seen that the Eurocode model provides a higher reduction. The plot of yield stress also shows that the Eurocode distinguishes between the yield limit and the proportionality limit. The yield limit is the point after which the stress-strain relationship becomes both nonlinear and inelastic whereas the proportionality limit is the end of the linear portion of the stress-strain curve, after which point the stress-strain relation remains elastic but becomes nonlinear. This is not included in either the ASCE or Poh models which both assume a set value as the limit between linear-elastic and inelastic material response. The proportionality limit in the Eurocode stress-strain curves is used to capture viscoelastic behavior which is partly due to creep effects. This simplification enables the stress-strain curves of the Eurocode to partly account for high-temperature creep strain at elevated temperature. However, for the purpose of this study the proportionality limit is not included in the material model because of the computational cost associated with its inclusion. The relationships provided in Eurocode 3 for yield strength and modulus of elasticity that is employed in this study is presented in Equations 3-5 and 3-6.

$$\frac{E_{s,T}}{E_s} = \begin{cases} 1.0, & T < 100℃ \\ c_1 T + c_2, & 100℃ \leq T < 500℃ \\ c_3 T + c_4, & 500℃ \leq T < 600℃ \\ c_5 T + c_5, & 600℃ \leq T < 700℃ \\ c_7 T + c_8, & 700℃ \leq T < 800℃ \\ c_9 T + c_{10}, & 800℃ \leq T < 1{,}200℃ \\ 0.0, & 1{,}200℃ \leq T \end{cases} \qquad \text{(Equation 3-5)}$$

$$\frac{F_{y,T}}{F_y} = \begin{cases} 1.0, & T < 400℃ \\ c_{11} T + c_{12}, & 400℃ \leq T < 500℃ \\ c_{13} T + c_{14}, & 500℃ \leq T < 600℃ \\ c_{15} T + c_{16}, & 600℃ \leq T < 700℃ \\ c_{17} T + c_{18}, & 700℃ \leq T < 800℃ \\ c_{19} T + c_{20}, & 800℃ \leq T < 900℃ \\ c_{21} T + c_{22}, & 900℃ \leq T < 1{,}200℃ \\ 0.0, & 1{,}200℃ \leq T \end{cases} \qquad \text{(Equation 3-6)}$$

Where:

$$\begin{array}{llll} c_1 = -1 \times 10^{-3} & c_2 = 1.1 & c_3 = -2.9 \times 10^{-3} & c_4 = 2.05 \\ c_5 = -1.8 \times 10^{-3} & c_6 = 1.39 & c_7 = -4 \times 10^{-4} & c_8 = 0.41 \\ c_9 = -2.25 \times 10^{-4} & c_{10} = 0.27 & c_{11} = -2.2 \times 10^{-3} & c_{12} = 1.88 \\ c_{13} = -3.1 \times 10^{-3} & c_{14} = 2.33 & c_{15} = -2.4 \times 10^{-3} & c_{16} = 1.91 \\ c_{17} = -1.2 \times 10^{-3} & c_{18} = 1.07 & c_{19} = -5 \times 10^{-4} & c_{20} = 0.51 \\ c_{21} = -2 \times 10^{-4} & c_{22} = 0.24 & & \end{array}$$

The stress-strain relationship implemented in this study assumes elastic perfectly plastic material behavior. The degradation of yield stress with increased temperature follows the Eurocode 3 model, however the computational expense associated with utilizing their stress-strain model resulted in assuming the simplified elastic perfectly plastic behavior. The temperature dependent stress-strain relationship used for this study can be seen in Figure 3-14.

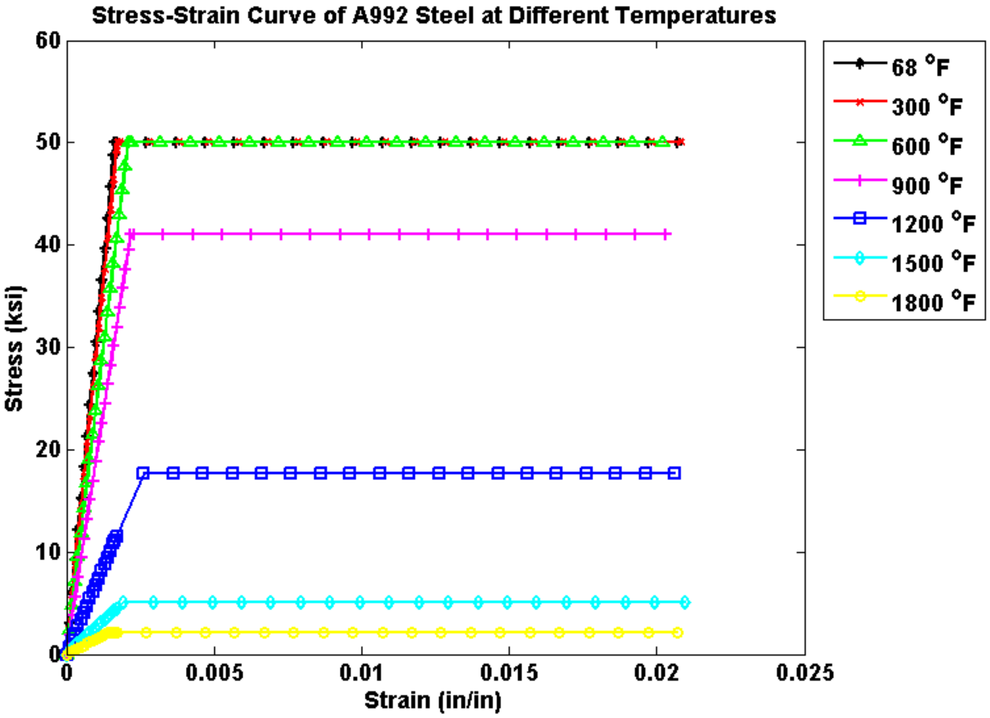

Figure 3-14. A992 steel temperature dependent stress-strain relationship

The deformation properties that influence the fire response of steel structures are thermal strain and high-temperature creep. For the purpose of this study high-temperature creep is not included; however the thermal strain model presented by Eurocode 3 was implemented. This model can be seen in Equation 3-7.

$$\begin{aligned}
&For\ T < 750℃\\
&\qquad \frac{\Delta\ell}{\ell} = 1.2\times10^{-5}T + 0.4\times10^{-8}T^2 - 2.416\times10^{-4}\\
&For\ 750℃ \le T \le 860℃\\
&\qquad \frac{\Delta\ell}{\ell} = 1.1\times10^{-2} \qquad\qquad \text{(Equation 3-7)}\\
&For\ 860℃ < T \le 1200℃\\
&\qquad \frac{\Delta\ell}{\ell} = 2\times10^{-5}T - 6.2\times10^{-3}
\end{aligned}$$

Figure 3-15 provides a depiction of the thermal strain values presented in Eurocode 3 as well as values from several other constitutive models and test data. It can be seen that the thermal strain of steel increases with temperature up to nearly 750°C, at which point a phase change takes place and the thermal strain becomes nearly constant up to 800°C. After this point the thermal strain starts to increase again. When comparing the Eurocode and ASCE models there are very little difference up to 700°C. However, between 700°C and 850°C the ASCE model assumes a continuously increasing thermal strain while the Eurocode model accounts for the phase change that occurs by assuming a constant thermal strain within this range.

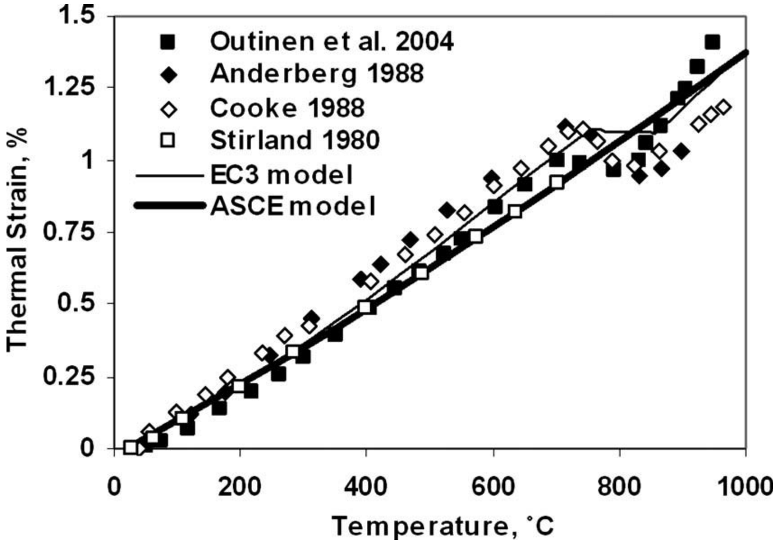

Figure 3-15. Thermal Strain of Steel as Predicted by Different Models and Measured in Different Tests (Kodur et al., 2010)

3.5.3 Temperature-Dependent Thermal Properties

The main thermal properties that influence the temperature rise in steel are thermal conductivity and specific heat. For the purpose of this study relationships for these properties are taken from Eurocode 3 (2005), which provides empirical equations as a function of temperature. Those relationships are presented in equations 3-8 and 3-9:

$$\begin{aligned} &For\ T < 800℃ \\ &\qquad k_s = 54 - 3.33 \times 10^{-2} T \\ &For\ T \geq 800℃ \\ &\qquad k_s = 27.3 \end{aligned} \qquad \text{(Equation 3-8)}$$

$$
\begin{aligned}
&For\ T < 600°\mathrm{C} \\
&\qquad c_s = 425 + 7.73 \times 10^{-1}T - 1.69 \times 10^{-3}T^2 + 2.22 \times 10^{-6}T^3 \\
&For\ 600°\mathrm{C}\ \leq T < 735°\mathrm{C} \\
&\qquad c_s = 666 + \frac{13002}{738 - T} \\
&For\ 735°\mathrm{C}\ \leq T < 900°\mathrm{C} \qquad\qquad\qquad\qquad \text{(Equation 3-9)} \\
&\qquad c_s = 545 + \frac{17820}{T - 731} \\
&For\ 900°\mathrm{C}\ \leq T < 1200°\mathrm{C} \\
&\qquad c_s = 650
\end{aligned}
$$

These equations are plotted in Figure 3-16 along with values presented by the ASCE (1992) model and various test data. It can be seen that thermal conductivity decreases with temperature in an almost linear fashion, and there is little variation between the models presented in Eurocode and the ASCE fire protection manual. It can also be seen that specific heat models vary considerably above 700°C. In general, the specific heat of steel increases with increase in temperature with a large spike occurring around 750°C. The increase in specific heat with temperature is due to individual atoms in the steel moving farther apart, thus achieving a higher energy state. The spike in the specific heat at around 750°C is due to the phase change that occurs in steel in which the atoms transition from a face centered cubic to a body centered cubic structure. This process absorbs considerable energy in the form of heat, which causes the spike around 750°C. The variation between the test data and the models shown in Fig. 3-16 is partly due to the fact that the majority of the existing data on specific heat originates from studies carried out on iron and nonstructural steel alloys. Additionally, the maximum temperature reached in these studies of iron and nonstructural steel is below 750°C so the full range of temperatures observed in fire conditions is not captured.

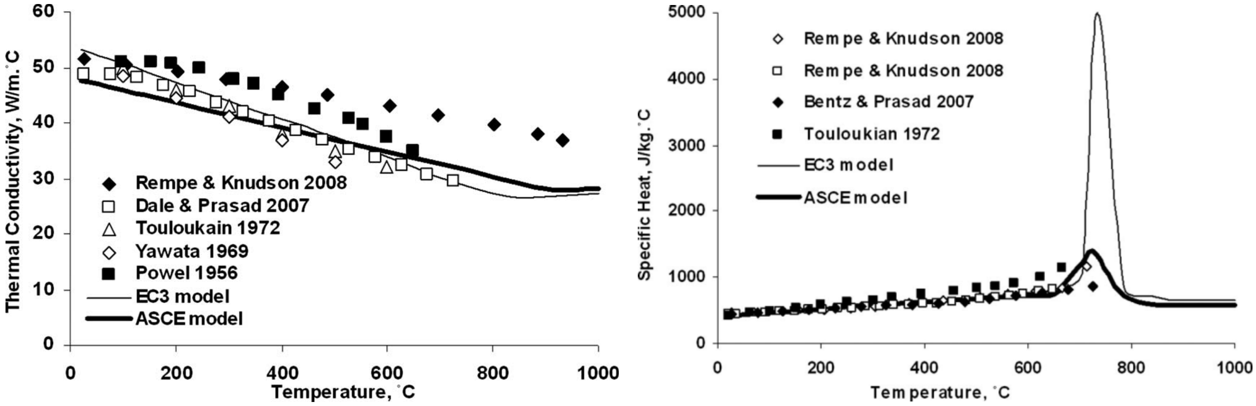

Figure 3-16. Thermal Properties of Steel as Predicted by Different Models and Measured in Different Tests (Kodur et al., 2010)

3.6 Summary

The general methodology employed for this research is presented in this chapter, along with a description of the analyzed structures, a discussion on the selected ground motion records and time-temperature curve and finally a description of the employed material model. A summary of the key points presented in this chapter are provided below:

- A description of the research methodology employed for this study is presented including a description of the various components involved in the simulations.
- An overview of the simulation methodology used for the FFE and Fire analyzes is presented as well as an introduction to how the constraint boundary conditions were determined.
- The two frames used for the analysis are taken from a study by Jin and El-Tawil (2004) and the configuration and design are verified with current code provisions.
- A total of ten ground motions are selected from the FEMA-695 Ground Motion Record Set and scaled in accordance with that document.
- The time-temperature curve used for this project are taken from a study performed by Maria Garlock (2008) and scaled to represent a typical office compartment fire.

- ASTM A992 structural steel was selected for all structural members within the frame and properties for the material were obtained from the Eurocode 3 (2005) provisions.

CHAPTER 4
FINITE ELEMENT MODELS

4.0 Introduction

This section describes the nonlinear multi-degree-of-freedom (MDOF) finite element models developed to analyze the response of steel special moment resisting frames (SMRF) with reduced beam sections (RBS) when exposed to fire as well as fire following an earthquake (FFE). All models used in this study were developed and executed using the general purpose finite element (FE) program ABAQUS (2012). The study required developing 3-D continuum element models for both of the previously described beam-column subassemblies as well as 2-D line element models of both frames that the subassemblies were taken from. Section 4.1 provides a description of the development and implementation of the line element models. Section 4.2 discusses the modeling techniques implemented for the 3-D continuum element models. A description of the validation models used to confirm the finite element modeling techniques implemented for this study are discussed in Section 4.3. Finally a brief summary of the chapter is provided in Section 4.4.

4.1 Line Element Models

4.1.1 Overview

The development of 2-D line element models was required in order to determine nodal displacements used in the seismic simulation portion of the 3-D FFE analysis as well as for defining the restraint stiffness values used for the 3-D fire simulations. Models were developed for both the 8-story and 16-story frames discussed in the previous chapter. The models employ line elements for the entire frame, which allows the variation in member sizing, and mechanical and thermal properties to be incorporated while still keeping the computational cost at a minimum. Element length was based on a mesh convergence study, which is described in further detail in Section 4.3.6. In order to capture the reduction in flange width in the reduced beam sections, variable cross sections were utilized. A depiction of this can be seen in Figure 4-1 along with a rendered visualization of both line element models. Both models included a leaning column for simulating the P-Δ effects generated by the interior gravity frames, panel zone models for representing the behavior of the region where the columns and beams meet, as well as an inherent damping model. Each of these components is discussed in further detail in the proceeding sections followed by a description of the various simulations that were performed on the line element models.

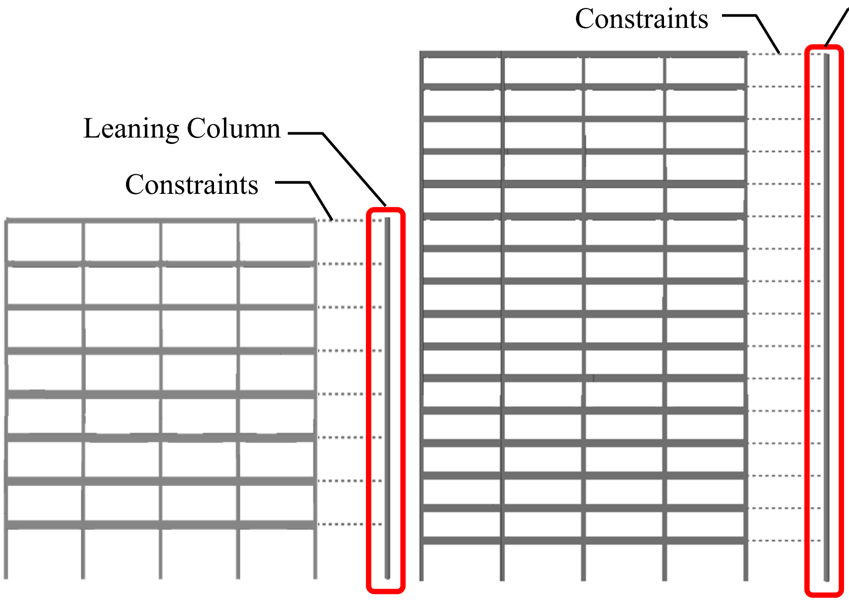

Figure 4-1a. Rendered Depiction of 8-Story and 16-Story Finite Element Frame Models

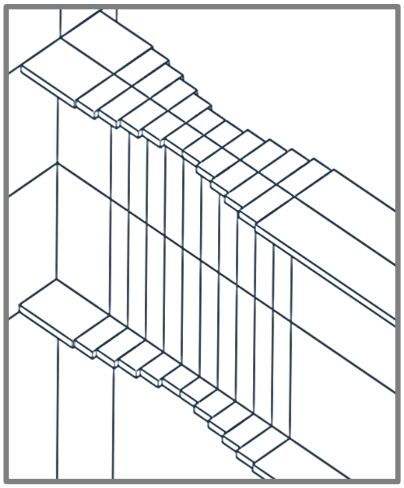

Figure 4-1b. RBS Variable Cross Section

4.1.2 Leaning Column Model

The analysis accounted for second-order destabilizing gravity loads in the system associated with the interior gravity frames by using a leaning column substructure. This allows the P-Δ effects to be incorporated without overestimating the gravity force demands acting directly on the SMRF. The leaning column substructure is depicted in Figure 4-1 linked to the SMRFs.

4.1.3 Panel Zone Model

Panel zone flexibility was taken into account by modeling the joint regions using the scissor model technique outlined by Foutch (2002). As shown in Figure 4-2 the sections of the beams and columns that are contained within the panel zone region is modeled as rigid bodies that are then connected by a hinge at the shared center node. A rotational spring is then introduced to tie the beam and column together and simulate the stiffness of the panel zone.

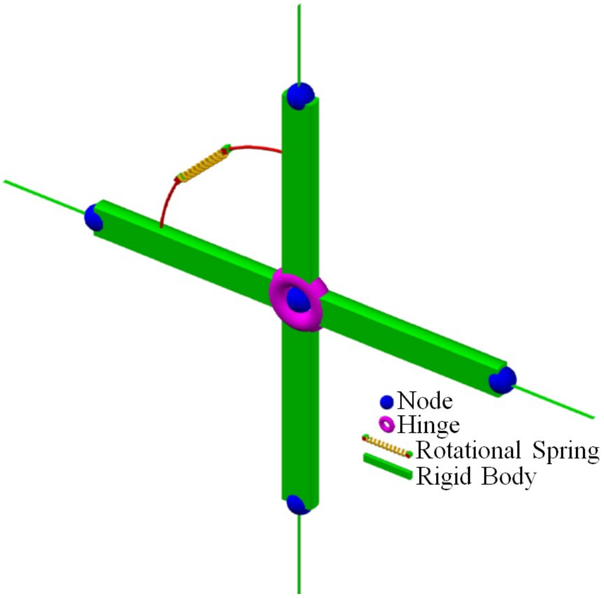

Figure 4-2. Scissor Panel Zone Model Configuration

The rigid links stiffen the structure but the rotational spring adds flexibility and combined they provide a simple, yet accurate representation of the panel zone. When compared to a simple centerline model that doesn't consider panel zone flexibility the model has been shown to provide better estimates of shears, moments and axial forces in the members of the entire frame (Foutch, 2002). The equations for determining the stiffness of the panel zone spring are based on the yield properties of the panel zone which are presented in Equation 4-1.

$$\gamma_y = \frac{F_y}{\sqrt{3}G} = \theta_y$$
$$M_y = V_y d_b = 0.55 F_y d_c t d_b \qquad \text{(Equation 4-1)}$$
$$K_\theta = \frac{M_y}{\theta_y}$$

Where,

F_y = the yield strength of the panel zone
G = the shear modulus
d_c = depth of the column
t = thickness of the panel zone which is the thickness of the web of the column plus the thickness of the doubler plates if they are included
d_b = depth of the beam
K_θ = panel zone rotational spring stiffness

4.1.4 Damping Model

Inherent damping mechanisms in the structural system were accounted for using the conventional Rayleigh mass and stiffness-proportional equivalent viscous damping model. The basis of this model comes from assuming the damping matrix to be proportional to the mass and stiffness matrix as follows:

$$[C] = \alpha[M] + \beta[K] \qquad \text{(Equation 4-2)}$$

Where,

α = the mass-proportional damping coefficient
β = the stiffness-proportional damping coefficient

From this equation one can apply relationships between modal equations and othrogonality conditions to rewrite it as follows:

$$\xi = \frac{\alpha}{2\omega_i} + \frac{\beta\omega_i}{2} \qquad \text{(Equation 4-3)}$$

Where,

ξ = the critical-damping ratio
ω_i = is the natural frequency of the structure for mode i

The alpha and beta constants can then be solved by assuming a critical-damping ratio for two of the modes of vibration of the structures and determining the natural frequency of the structure at those modes through an eigenvalue analysis. For both frames a value of 2% of critical damping in the first and third modes of vibration was assumed. The natural frequency values for these two modes were determined by performing a modal analysis on both frames with ABAQUS. Once the frequencies were determined Equation 4-3 was solved for both modes and the alpha and beta constants determined. The model was then implemented by specifying these constants in the material properties defined in the ABAQUS models.

4.1.5 Thermal Analysis

In order to run the restraint stiffness analysis, the temperature distribution throughout the frame during the fire had to be determined. This was completed by running a thermal analysis on both frames for both the Fire and FFE scenarios. These models captured the temperature distribution within the frames which was then loaded into the thermo-mechanical portion of the restraint stiffness analysis. Models were created for both frames for both scenarios (fire and FFE) and a single step transient heat transfer simulation was performed. In this type of analyses the temperature field is calculated without knowledge of the stress/deformation state of the frames and allows the determined temperature field to be read into the stress analysis as a predefined field. A single story single bay fire located in the compartment directly below the selected beam-column subassemblies was assumed for both scenarios. For the FFE analysis the temperature of the RBS region of the beams within the compartment were constrained to follow the selected time-temperature curve. This region is highlighted in red in Figure 4-3 and is representative of the area where damage to fire protection is expected due to the high inelastic demand during earthquake loading. The selection of this region as well as the choice to neglect convection and radiation in the analysis is discussed in more detail in Section 3.1.1. For the Fire analysis the temperature of the entire compartment was constrained to follow the selected time-temperature curve. This assumes that no passive fire protection is present on the entire frame, which was selected based on the rationale provided in Section 3.1.2. A depiction of the region constrained to follow the time-temperature curve for the Fire analysis is also shown in red on Figure 4-3.

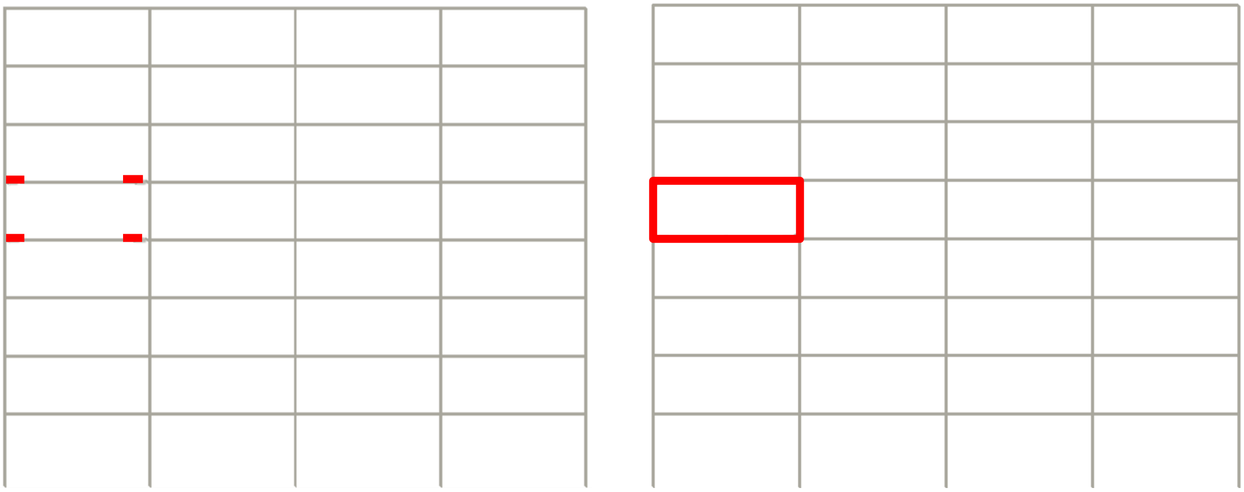

Figure 4-3. Location Constrained to Follow Time-Temperature Curve for FFE (left) and Fire (right) for the 8-Story Frame

For this analysis standard linear heat transfer line elements (DC1D2: 2-node heat transfer link) were utilized for the entire frame. The line element frame models were discretized based on a mesh convergence study which included comparing the results of thermal, earthquake, and thermomechanical analysis of both frames for each scenario under consideration. The mesh convergence study is discussed in further detail in Section 4.3.6.

4.1.6 Earthquake Analysis

For the earthquake portion of the FFE analysis of the beam-column subassemblies nodal displacement values from the line element frame models were used as boundary conditions to simulate the earthquake. These nodal displacement values were obtained by conducting a dynamic earthquake simulation on both frames for each earthquake record in the ground motion record set. The first step in these models was to apply the gravity load demands that were presented in Section 3.2.4 on the frames. Floor and roof loads were applied to the SMRFs to model tributary gravity loads expected to be present on the frames. Concentrated loads were applied to the leaning column substructure to model the tributary gravity load demands from the rest of the structure. The load factors were adjusted in accordance with FEMA P695 to represent probable loading conditions. The gravity load case used for the dynamic analysis is presented in Equation 4-4.

$$1.05D + 0.25L \qquad \text{(Equation 4-4)}$$

Where,
D is the dead load demand
L is the live load demand

The gravity loads were applied by defining non-structural mass values along the beams of the frame and point loads on the leaner column. Once these were in place, a general static step was performed on the frame to apply the gravity acceleration boundary condition. Seismic analysis of the frames was then performed using a general nonlinear dynamic step. This step employed a transient fidelity application which uses small time increments to accurately resolve the vibrational response of the frames, keeping numerical energy dissipation at a minimum. The default Hilber-Hughes-Taylor time integration technique was used for all of the analysis. This time integration operator is an extension of the Newmark β-method and is an implicit application. This means that the operator matrix must be inverted and a set of simultaneous nonlinear dynamic equilibrium equations are solved at each time increment. The solution is obtained using the iterative Newton method, which has the advantage of being unconditionally stable for linear systems. For the analysis the frames were modeled with nonlinear, distributed plasticity, cubic-formulation, beam-column elements (B33: 2-node linear beam in a plane).

4.1.7 Restraint Stiffness Analysis

In order to evaluate the restraint stiffness properties of the steel frames for the fire simulation of the beam-column subassemblies a series of displacement controlled analyses on the frame models were performed. These analyses were used to evaluate the force-displacement relationship for the frame surrounding the beam-column subassemblies in all three planar degrees of freedom. The response data was then used to calibrate the mechanical properties of connector elements that were utilized in the 3-D models to provide restraint to the subassemblies during the fire simulation portion of the analysis. For the FFE models both frames were analyzed under the suite of ground motion records followed by the fire simulation. The fire simulation was terminated at twenty points throughout the time-temperature curve to analyze the force-displacement relationship of the frame surrounding the selected beam-column subassemblies. Once the analysis was terminated a small portion (0.005”) of the beam-column subassembly was removed from the location being analyzed (beam or column tips) and a displacement boundary condition was introduced to the now unconnected portion of the frame. The displacement boundary condition was set to follow an amplitude curve so the entire force-displacement relationship could be captured. The reaction force created by the applied displacement was then recorded and used to determine the initial restraint stiffness value at that point in the time-temperature curve. For the fire models, the same procedure was utilized but the initial earthquake simulation was excluded.

This analysis was performed for both the fire and the FFE analyses for both frames. All three planar degrees of freedom (axial, lateral, and rotational) were analyzed for both tips of the column and the beam. In order to accomplish this task a total of 3,960 models had to be created, ran, and analyzed. Because of the large number of models a MATLAB code was developed for creating all the necessary input files. The code included the creation of a unique displacement boundary condition amplitude curve for each model as well as updating the point in the time-temperature curve the analysis was to start, the degree-of-freedom (DOF) being analyzed and the location being considered. Once finished the force-displacement relationship were analyzed, this was done manually because the variability in the results required that special attention be given in interpreting the stiffness properties.

All of the frame elements were assigned nonlinear, distributed plasticity, cubic-formulation, beam elements (B33: 2-node linear beam in a plane). The first step of the analysis was to apply the gravity loads to the frame; this was done in the same manner described in Section 4.1.6. For the FFE models the next step was to perform the earthquake simulation, which was also done using the same methodology described in Section 4.1.6. Next, the fire simulation was executed using a transient dynamic analysis that uses the nodal temperature values from the previously described thermal analysis. The same time incrimintation and modeling technique used for the earthquake step of the simulation was employed for the fire step. The force—displacement analysis was then performed using a general static step.

The results from the above analysis were used to calibrate the restraints used during the thermo-mechanical analysis of the RBS subassemblies. The inclusion of transient restraints at the beam and column ends allows for realistic representation of the effect of the surrounding frame on the expansion and contraction of the subassemblies. This technique was validated by comparing the response of the entire frame of the structures to models of the beam-column subassembly with the determined restraints. Various loading scenarios were applied to both models and displacement values were compared to ensure the same response was being captured. Very good agreement between the models was achieved; the largest variation in displacement values from all the simulations was 7.2%. Figure 4-4 provides a depiction of the transient restraint stiffness for the 16-story subassembly for one of the FFE scenario.

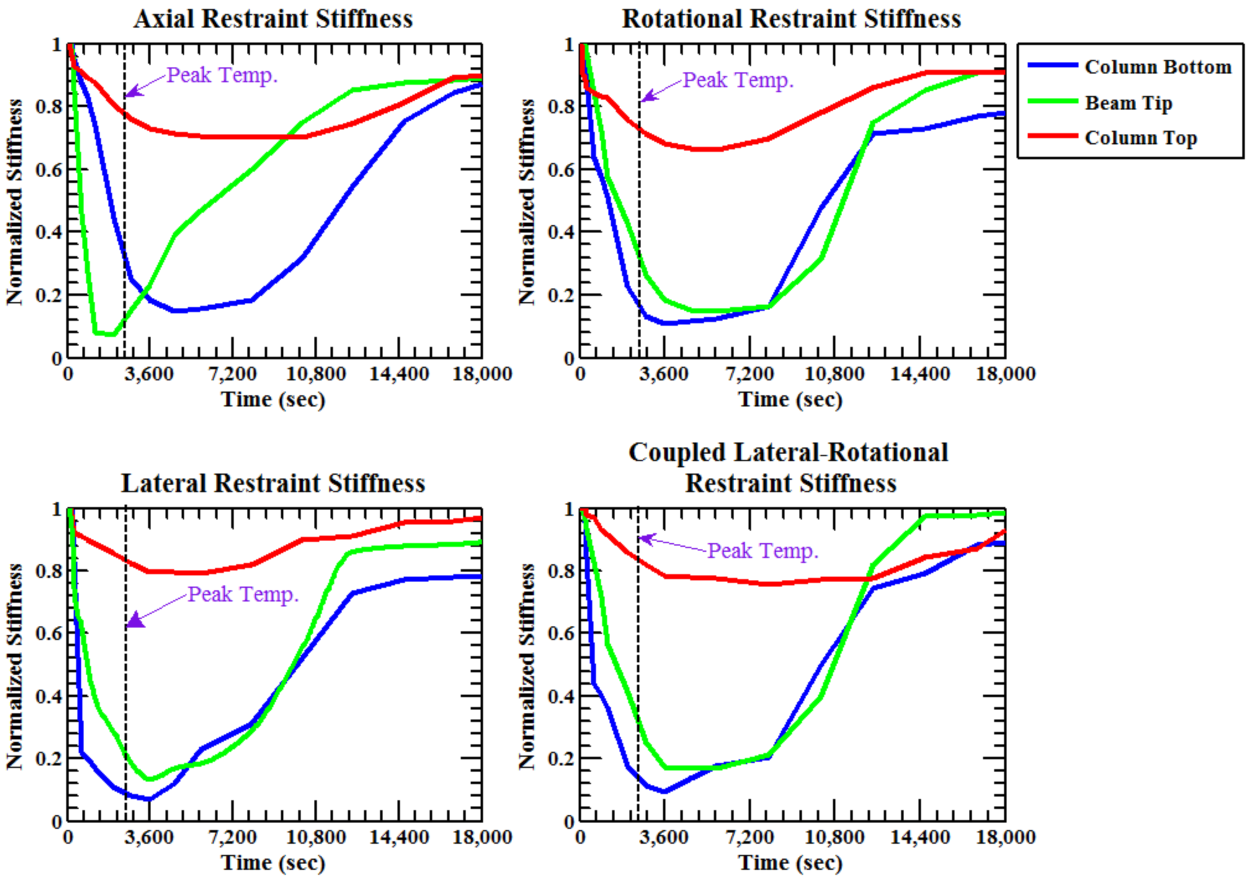

Figure 4-4. Normalized Restraint Stiffness Values for 16-Story FFE (1992 Erzican) Model

4.2 Continuum Element Models

4.2.1 Overview

The 3-D finite element models used for the detailed analysis of the selected beam-column subassemblies were also created using the program ABAQUS. Three dimensional solid models of both subassemblies were developed in the graphical software package AutoCAD (AutoCAD, 2012) and imported into ABAQUS workspace as 3-D deformable continuum parts. These parts were then discretized and meshed using 3-D brick elements for all of the subassembly components. A depiction of the mesh for both subassemblies is provided in Figures 4-5 and 4-6.

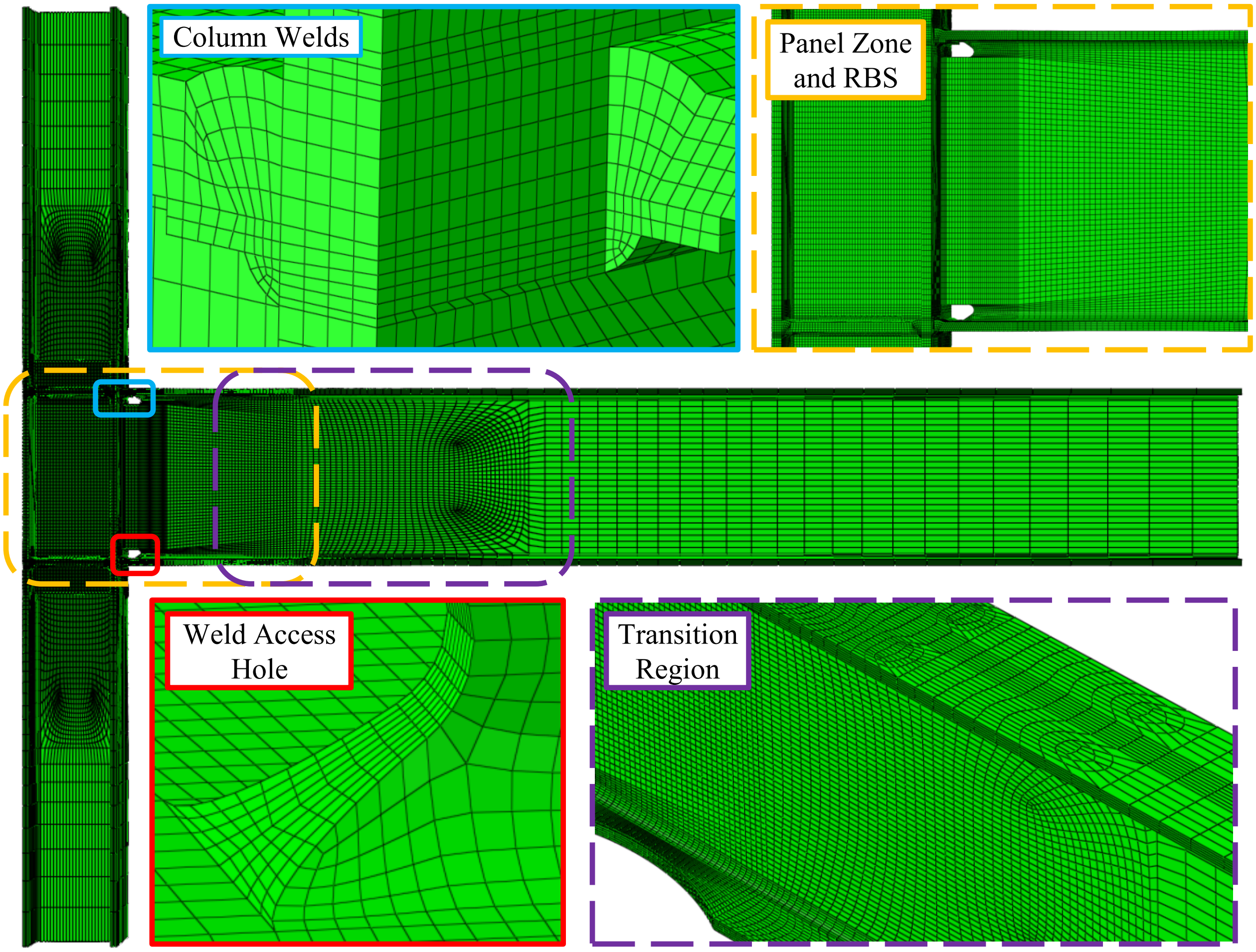

Figure 4-5. Mesh Discretization for 8-Story Beam-Column Subassembly

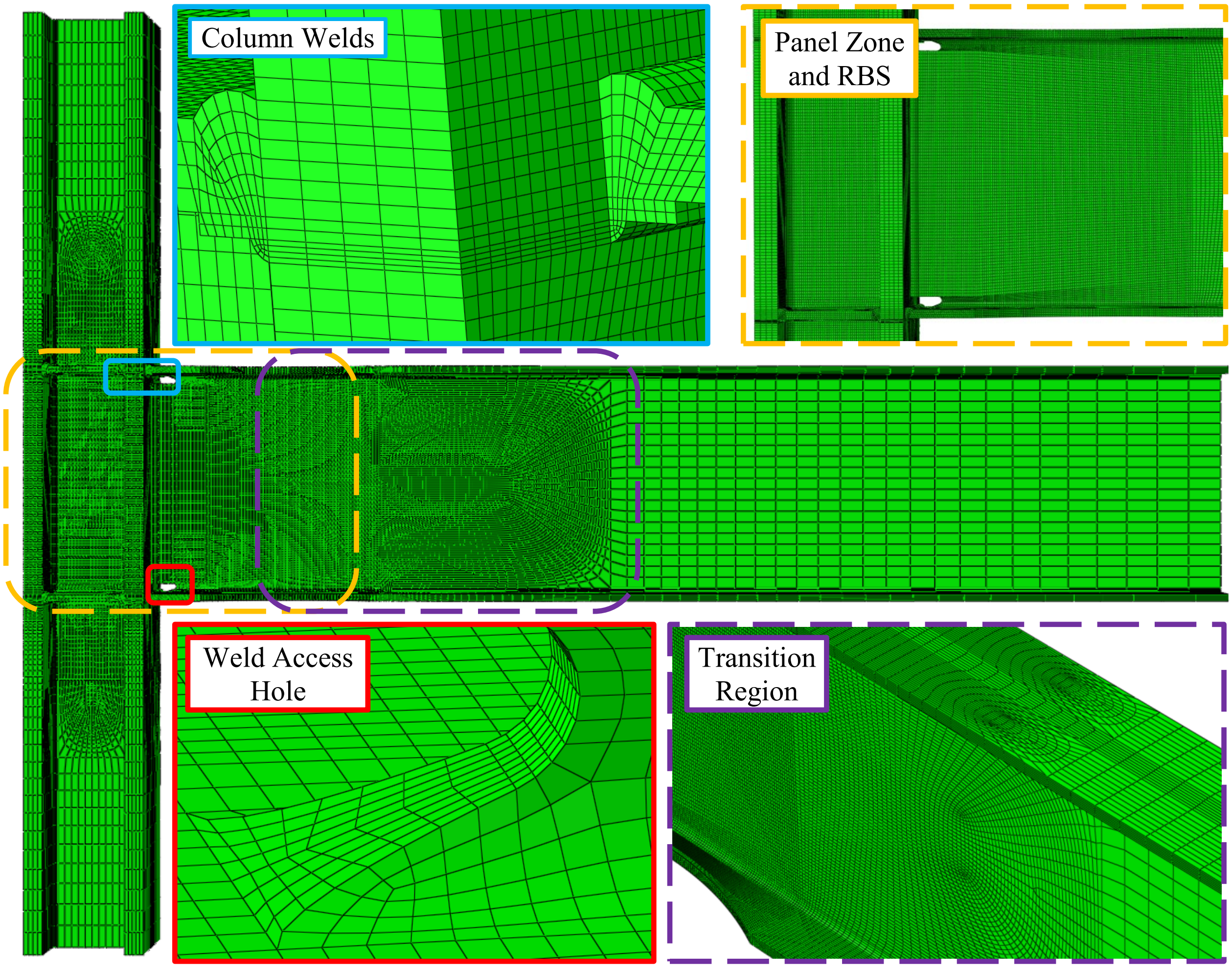

Figure 4-6. Mesh Discretization for 16-Story Beam-Column Subassembly

Mesh discretization for the 3-D beam-column subassemblies was based on suggestions by Garlock (2010), practical considerations regarding the computational expense of the numerical simulation, and a mesh convergence study performed on both subassemblies. For the mesh convergence study, the mesh of the subassemblies was reduced until convergence was reached for stress values in the critical regions of the model, which included the weld access hole, beam-column welds, reduced beam section of the flange, and several points within the panel zone region of the column. Section 4.3.6 provides a detailed description of the mesh convergence study. For the thermal analysis of the 3-D subassemblies the models were discretized for compatibility with the earthquake and fire simulation.

The composite floor slab was excluded from the mechanical simulations in order to simplify the models. However, the lateral restraint provided by the floor slab was implicitly included by restraining the upper flange of the beams outside of the protected hinge region for lateral motion. Geometric nonlinearity was considered in all mechanical analyses by implementing a large displacement formulation. ABAQUS adopts a large strain formulation for 3-D solid elements by default. When the optional parameter “NLGEOM” is activated, the locations of all nodes are updated after each analysis increment. This option was activated for all mechanical analyses so that local instability and large deformation effects would be captured. It should be noted that the analysis did not consider the residual stress demands in the steel sections due to fabrication. These stresses were thought to be less important in the critical heat-affected regions since the elevated steel temperatures during the fire simulation effectively anneal the residual stress field (Buchanan, 2002).

The analysis of both subassemblies subjected to fire and FFE consists of two sequentially coupled steps: (1) heat transfer analysis (thermal analysis), and (2) mechanical analysis (fire and FFE analysis). The heat transfer analysis is conducted first to obtain temperature distributions throughout the subassemblies over the course of the specified time-temperature curve. Details of the heat transfer analysis are provided in Section 4.2.2. Once the heat transfer analysis is completed, the nodal temperatures computed within the subassemblies are then used in the mechanical analysis to compute the structural response of the subassemblies during the fire simulation portion of the analyses. The details of the mechanical analysis for the fire and FFE simulations are provided in Sections 4.2.3 and 4.2.4, respectively. In the analysis approach used for this research the heat transfer analysis is said to be sequentially coupled to the mechanical analysis. This approach assumes that the mechanical analysis has no effect on the heat transfer analysis. This simplification may introduce errors in some situations. For example, if the structural analysis predicts large deformation of a member, parts of the member may move closer or farther from the fire and thereby affect heat transfer to the member. However, in most practical situations, it is been shown that a sequentially coupled heat transfer and mechanical analysis provide accurate results. A brief summary of the various 3-D continuum element models is provided in Table 4-1.

Table 4-1. Summary of 3-D Continuum Element Models

Model	Subassembly	Element Type	# of Elements	Approx. Run Time	Earthquake Simulation	Fire Simulation	Constraint Type
Thermal Analysis	8-Story	DC3D8	388,443	2 hrs.	NA	Heat Transfer	NA
	16-Story	DC3D8	595,588	3 hrs.	NA	Heat Transfer	NA
Fire Analysis	8-Story	C3D8R	388,443	3 days	NA	Dynamic, Implicit	Realistic
	8-Story	C3D8R	388,443	3 days	NA	Dynamic, Implicit	No Lateral
	8-Story	C3D8R	388,443	2.5 days	NA	Dynamic, Implicit	Fixed
	16-Story	C3D8R	595,588	5 days	NA	Dynamic, Implicit	Realistic
	16-Story	C3D8R	595,588	5 days	NA	Dynamic, Implicit	No Lateral
	16-Story	C3D8R	595,588	4 days	NA	Dynamic, Implicit	Fixed
FFE Analysis	(10) 8-Story	C3D8R	388,443	6 days/EQ	Static (for all 10 records)	Dynamic, Implicit	Realistic
	(10) 16-Story	C3D8R	595,588	8 days/EQ	Static (for all 10 records)	Dynamic, Implicit	Realistic

4.2.2 Heat Transfer Analysis

For the thermal analysis of the beam-column subassemblies the structural steel and weld was modeled using an analytical mesh of 8-node, quadratic, continuum heat transfer elements (type DC3D8: 8-node linear brick). The selection of the element type was based on the work of Lee et al. (2006), which concluded that when modeling temperature propagations in steel, the DC3D8 quadratic elements provide superior convergence compared to a conventional first-order elements. The expected compartment fire exposure was modeled by constraining the surface temperature of the beam-column subassemblies in selected regions to follow the time-temperature curve discussed in Section 2.4. Surface temperature values in the selected regions were constrained by specifying a temperature boundary condition that follows the selected time-temperature curve on the exposed surfaces of the subassemblies. The exposed surfaces were selected based on the reasoning presented in Sections 3.1.1 and 3.1.2. For the fire analysis passive fire protection was not included in the simulation and because of this the interior flange of both the beam and column were selected to act as the exposed surface constrained to follow the time-temperature curve. For the FFE models the bottom and top flanges within the RBS of the beam was selected to follow the time-temperature curve. These regions are depicted in Figure 4-7. The heat transfer simulation was executed within a single heat transfer analysis step, which was discretized into real time increments of 30 seconds.

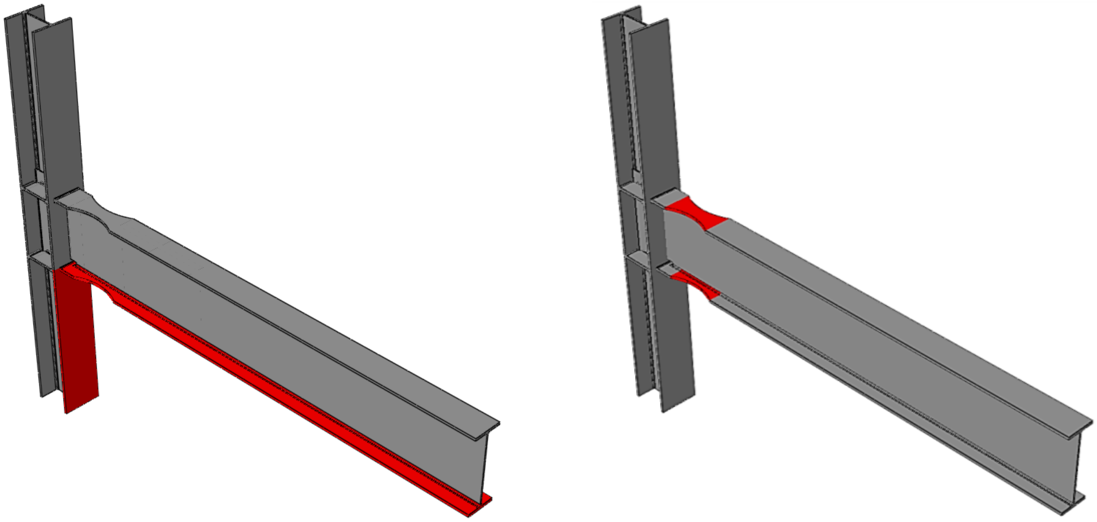

Figure 4-7. Regions Constrained to Follow Time-Temperature Curve for Fire and FFE Analysis

4.2.3 Fire Analysis

For the fire analysis the 3-D beam-column subassemblies were modeled using 8-node, quadratic, reduced-integration, continuum stress analysis elements (C3D8R: 8-node linear brick, reduced integration, hourglass control). The selection of the element type was based on work by Garlock (2010) as well as recommendations in the ABAQUS user manual (ABAQUS 6.12). A more comprehensive description of the selected element type is provided in Section 4.2.5. For the fire simulation the FE program ABAQUS was used to perform a multi-step mechanical stress analysis on both subassembly models. The nodal temperatures from the heat transfer analysis were imported directly into the fire analysis as a predefined field. A quasi-static dynamic analysis was then performed on each subassembly using the default backward Euler time integration method. In order to save computational cost during the fire analysis the quasi-Newton solution method was utilized instead of the default Newton method for the time incrementation scheme. The selection of this modeling technique is based on suggestions from various researchers (Garlock 2010, Keller 2012, and Engelhardt 2011), computational cost and suggestions in the ABAQUS user manual (ABAQUS 6.12). If more information on the modeling techniques is desired a detailed description can be found in the ABAQUS user manual.

For each subassembly three models were created with the three restraint configurations discussed in Section 3.1.3 and 4.1.7. For the fully fixed model a boundary condition was placed on the tips of the beam and column to fix the ends in all degrees of freedom. For the realistic restraint model as well as the axial and rotational restraint model the frame stiffness was introduced into the analysis through a basic connector element. For the connector elements a translational type of "cartesian" and rotational type of "rotation" was selected which allowed the coupled stiffness matrix and yield force for the element to be directly specified. Utilizing this element type allowed for the fully coupled stiffness of the surrounding frame to be incorporated, which is not possible with simple spring elements. The coupled stiffness includes not only the axial, lateral, and rotational stiffness values but also the lateral-rotational stiffness. In order to capture the change in restraint stiffness throughout the fire, elements with different stiffness values were created and a model change interaction to add and remove the elements at the correct instance in the analysis was utilized. A depiction of this process is provided in Figure 4-8.

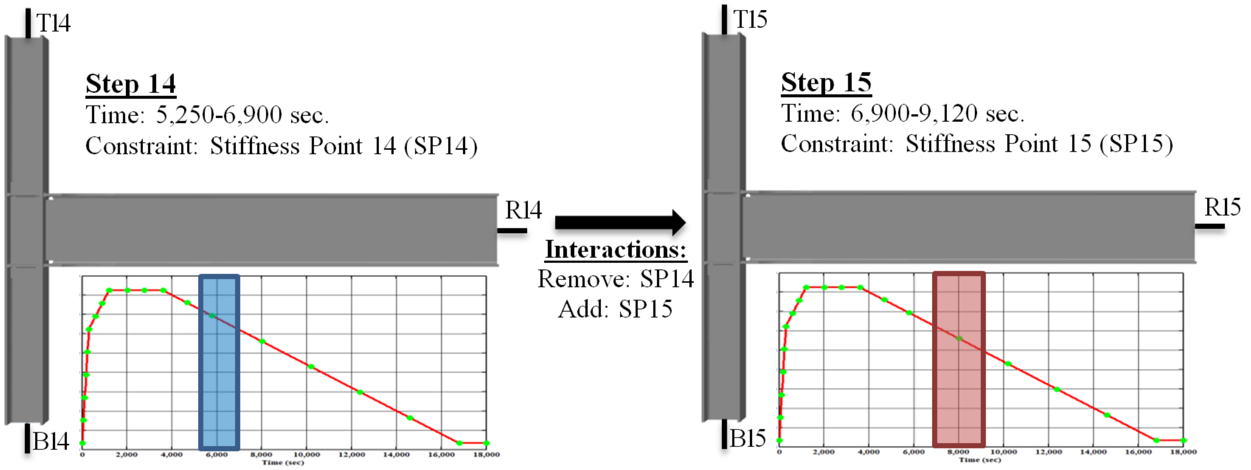

Figure 4-8. Variation of Constraint Stiffness during the Fire Analysis

4.2.4 Fire Following an Earthquake Analysis

For the FFE analysis the three-dimensional beam-column subassemblies were modeled using 8-node, quadratic, reduced-integration, continuum stress analysis elements (C3D8R: 8-node linear brick, reduced integration, hourglass control). The selection of the element type was based on work by Garlock (2010) as well as recommendations in the ABAQUS user manual (ABAQUS 6.12). A detailed description of the element can be found in the following section. For the earthquake simulation a separate model for each ground motion record was created, making a total of twenty models (10 for the 8-story subassembly, 10 for the 16-story subassembly). A nonlinear static analysis step was implemented to replicate the seismic demand on each subassembly. For each model the nodal displacement histories obtained from the corresponding line element model was specified as a time-dependent boundary condition on the tips of the column and beam. Forcing the tips of the subassemblies to follow the exact displacement histories obtained from the line element simulations allows the seismic demand to be imposed on the joint without having to include the entire frame. The default Newton method was used for the time incrementation scheme and no additional modeling techniques were employed for the analysis. More information on the general static analysis used for the earthquake simulation can be found in the ABAQUS user manual (2010). Once the earthquake simulation was finished the tip boundary conditions were released and the initial constraint elements were introduced. For the fire simulation portion of the analysis the same modeling procedures described in Section 4.2.3 were employed.

4.2.5 Continuum Element Selection

The use of reduced-integration continuum stress analysis elements is recommended primarily because the element is not susceptible to numerical shear locking. Shear locking occurs when the interpolation functions are not able to model the deformations in the element causing it to be over constrained. When correctly modeled a block of material under a pure bending moment will deform into a curved shape. If one envisions straight lines on the surface of the element when the bending action occurs it is intuitive that the horizontal lines will bend to curves while the vertical lines will rotate but remain straight. As such the angle between the horizontal and vertical line will remain at 90° after bending as predicted by classical beam theory (Timoshenko, 1997). However, on fully integrated first order elements the edges of the element are not allowed to bend into a curve. This creates tensile stresses at the top surface of the element and compressive stresses at the bottom surface under pure bending. Furthermore, the element will not be able to maintain the 90° angle between horizontal and vertical lines causing an artificial shear stress to be introduced. A depiction of this phenomenon is provided in Figure 4-9.

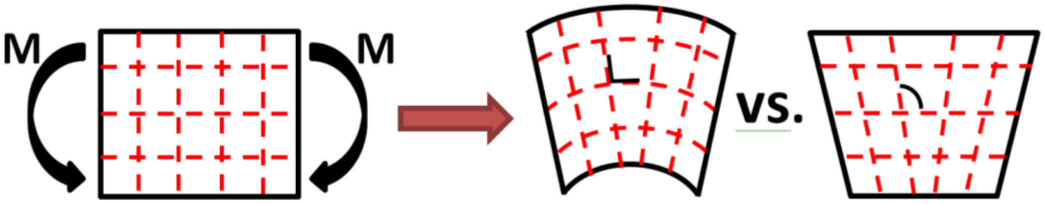

Figure 4-9. Deformation of Reduced Integration (left) and Fully Integrated (right) First Order Element under Pure Bending

However, the use of these elements creates another issue known as hourglassing. Hourglassing can occur in continuum elements that utilize a single-point reduced integration scheme. While a reduced integration approach can significantly improve the computational cost of a numerical simulation and prevent shear locking, it also makes the element susceptible to the zero energy shear deformation mode because strain demands are only monitored along the neutral axis. Because of this behavior, particular attention must be given to mesh density in critical regions to ensure hourglassing does not occur.

4.3 Modeling Technique Validation

4.3.1 Overview

Experimental test data and analytical models were used to validate the modeling techniques employed in this study. Because of insufficient data on the combined events of fire following an earthquake separate validations were performed for the fire and seismic analysis. These validation models are presented in Sections 4.3.2 and 4.3.3, respectively. In addition, Section

4.3.4 describes an eigenvalue analysis that was performed on the line element models of both frames and the results compared to results presented in Ghassemieh (2012) on the same frame configurations. The mesh convergence study performed for this project is also presented in Section 4.3.5.

4.3.2 Heat Transfer Validation

In order to validate the modeling technique used for the heat transfer analysis two analytical models were created to calculate the temperature distribution within a steel plate. Since conduction was the only heat transfer mechanism used in the study the validation models were limited to only consider conduction. An ABAQUS model of a 36-ft by 24-ft steel plate was created to determine the temperature distribution throughout the plate when a temperature boundary condition was placed along one of its edges. The temperature boundary condition was constrained to follow the time-temperature curve shown in Figure 4-10. For this analysis the same techniques described in Section 4.2.2 were employed. It should be noted that the heat transfer validation model was performed primarily by Mehrdad Memari who is a fellow graduate student at Colorado State University working on similar models and as such the validation model was applicable to this study.

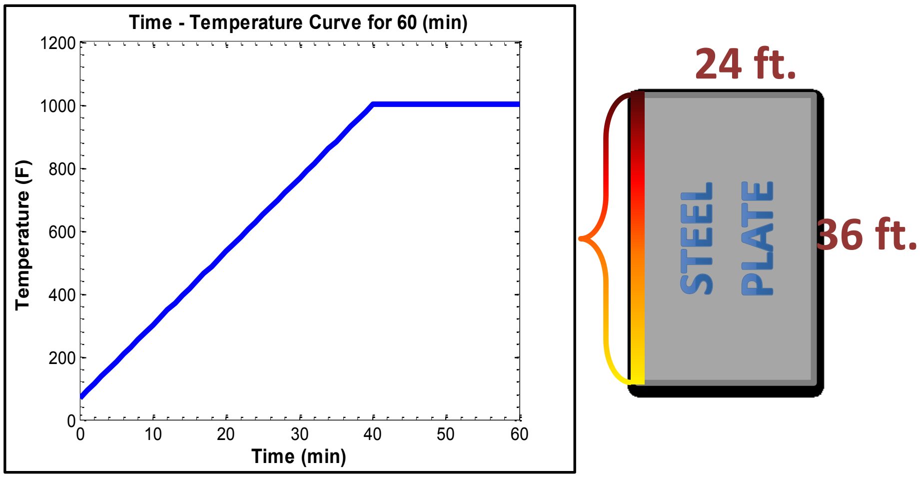

Figure 4-10. Depiction of Heat Transfer Validation Model

The results of this analysis were then compared to results from a computational fluid dynamics (CFD) code developed in Matlab (2012) to analyze the same scenario. Because of the complexities associated with the CFD code, 2-D instead of 3-D conduction was analyzed. The CFD code utilizes a finite-difference numerical method to determine nodal temperatures throughout the plate. When comparing the results from the two analyzes the temperature distribution was nearly identical throughout the entirety of the time-temperature curve.

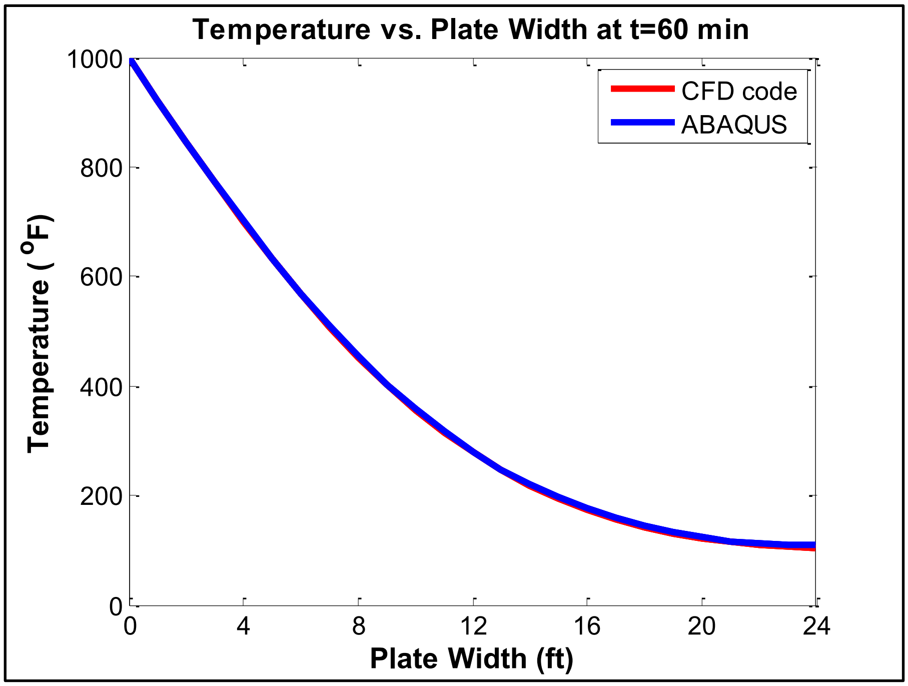

Figure 4-11. Comparison of the Temperature Distribution along the Width of the Plate at the end of the Time-Temperature Curve

4.3.3 Mechanical Response Validation

A three-dimensional finite element model of a beam-column subassembly that is representative of specimen LS-1 tested under the SAC project (SAC, 2000) was developed to validate the mechanical analyzes models. The same material properties, modeling techniques and assumptions implemented for this study were utilized for the development of the model. The subassembly was exposed to the same cyclic loading that was employed by the SAC project and the action and displacement properties compared. Very good agreement was found between the finite element model and the experimental results obtained from the SAC project. A comparison of the moment-rotation relationship and observable deformations are presented in Figures 4-12 and 4-13, respectively.

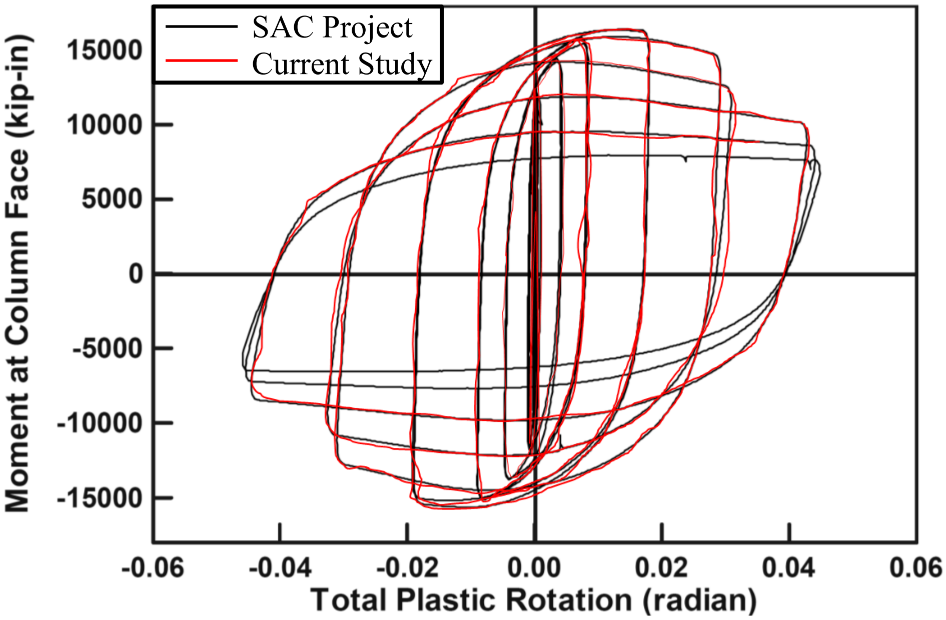

Figure 4-12. Comparison of Moment-Rotation Relationship Between the Finite Element Model (red) and the Experimental Test (black) (SAC, 2000)

It should be noted that the finite element model began to diverge at the first of the final three cycles in the cyclic loading and was terminated at this point. Excessive buckling and strength degradation observed in the experimental testing at this point in the test made convergence unlikely in the finite element models.

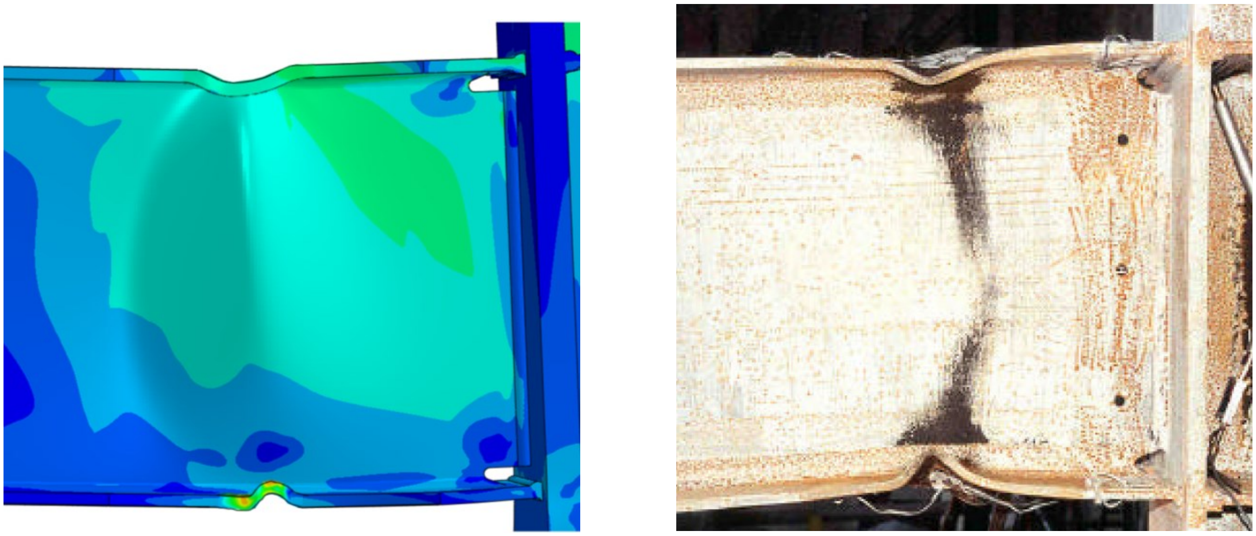

Figure 4-13. Comparison of Deformation in the Reduced Beam Section Between the Finite Element Model (left) and the Experimental Test (right) (SAC, 2000)

4.3.4 Modal Analysis

An eigenvalue analysis was performed on both frames and the natural period of vibration and mode shapes were compared to a previous study by Ghassemieh and Kiani (2012) on the same frames. It was found that natural period of vibration was within 1.3% of the values presented by Ghassemieh for the first 3 modes of vibration for both frames and within 15% for the first eight modes; furthermore the anticipated mode shapes were also captured. A depiction of the mode shapes can be seen in Figure 4-14 and a comparison of the natural period of vibration values obtained in this study and the values presented by Ghassmieh can be found in Table 4-2.

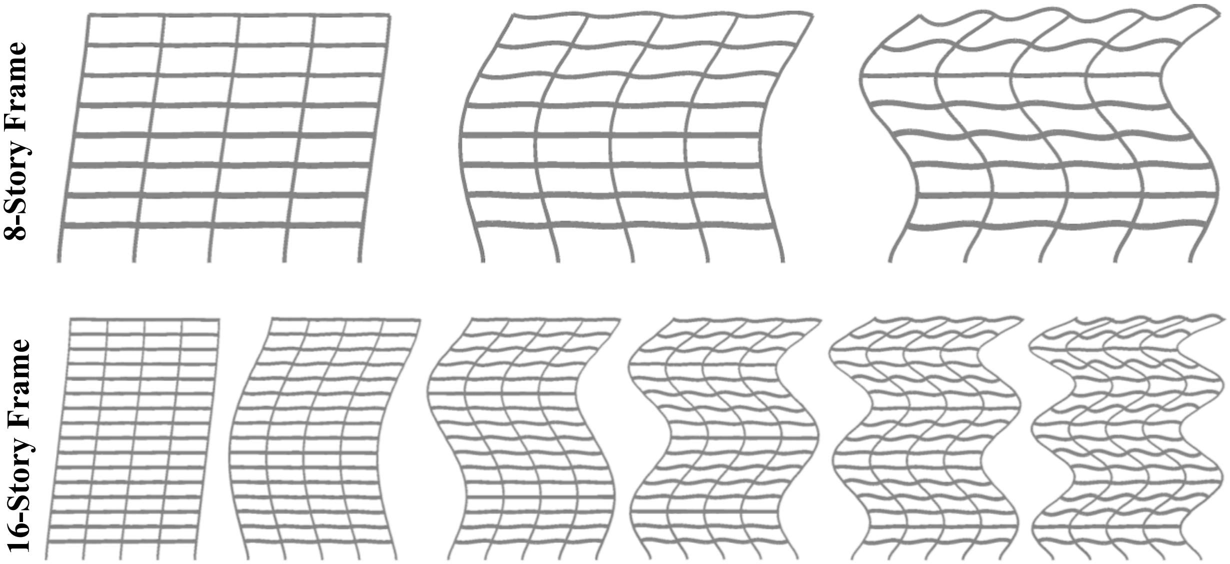

Figure 4-14. Mode Shapes of 8-Story and 16-Story Frames

Table 4-2. Comparison of Natural Period of Vibration (sec)

Mode	8-Story			16-Story		
	Ghassemieh (2012)	Current Study	% Diff.	Ghassemieh (2012)	Current Study	% Diff.
1	2.487	2.468	0.764	3.430	3.451	0.612
2	0.917	0.926	0.981	1.230	1.245	1.220
3	0.497	0.510	2.616	0.709	0.712	0.465
4	0.327	0.338	3.364	0.498	0.511	2.610
5	0.227	0.237	4.405	0.362	0.387	6.906
6	0.166	0.176	6.024	0.283	0.302	6.714
7	0.131	0.142	8.397	0.227	0.250	10.132
8	0.127	0.139	9.449	0.186	0.201	8.065

4.3.5 Mesh Convergence Study

The mesh density used in both the line element frame models and the 3-D continuum element beam-column subassembly models was determined by analyzing the convergence of results of several simulations. For both models (2-D and 3-D) the convergence study compared the results of an earthquake and fire analysis to ensure that each scenario used for this project are taken under consideration. The line element models were initially discretized based on an element length of 24-inches and reduced until the roof drift angle, base shear and interstory drift angle (IDA) converged at a single value. An earthquake simulation and a separate fire simulation were performed on both frames (8-story and 16-story) and the values from these analyses compared. A summary of these analyses can be seen in Table 4-3. For both the 8-story and 16-story frames the values converged at an element length of 6”. For the thermal analysis of the line element frames the models were discretized for compatibility with the earthquake and fire simulation.

Table 4-3. Convergence Study of Line-Element Models

Model	Element Length	Earthquake Simulation			Fire Simulation		
		Roof Drift (in)	Max. IDA (rad)	Norm. Base Shear	Roof Drift (in)	Max. IDA (rad)	Norm. Base Shear
8-Story	24"	12.26850	0.04567	4.10354	8.56789	0.01236	1.67890
	18"	14.10878	0.05252	4.71907	9.85307	0.01421	1.93074
	12"	14.81421	0.05620	5.04941	9.95160	0.01521	2.06589
	8"	14.94754	0.05653	5.07263	10.04117	0.01517	2.05349
	6"	15.02228	0.05699	5.11321	10.12150	0.01531	2.06992
16-Story	24"	27.52350	0.06323	2.36124	24.57890	0.02356	1.01230
	18"	30.82632	0.07461	2.62097	26.79100	0.02804	1.06292
	12"	35.45027	0.08580	3.01412	30.80965	0.03224	1.22235
	8"	37.22278	0.08409	2.95383	31.11775	0.03450	1.23091
	6"	37.55779	0.08398	2.94999	31.33557	0.03435	1.22751

Mesh discretization for the three-dimensional beam-column subassembly models were initially based on suggestions by Garlock (2010). Starting with that configuration the mesh was reduced until convergence was reached for nodal stress values in the critical regions of the connection which included the weld access hole, beam-column welds, reduced beam section of the flange, and several points within the panel zone region of the column. Figure 4-15 provides a depiction of some of the regions analyzed for the convergence study.

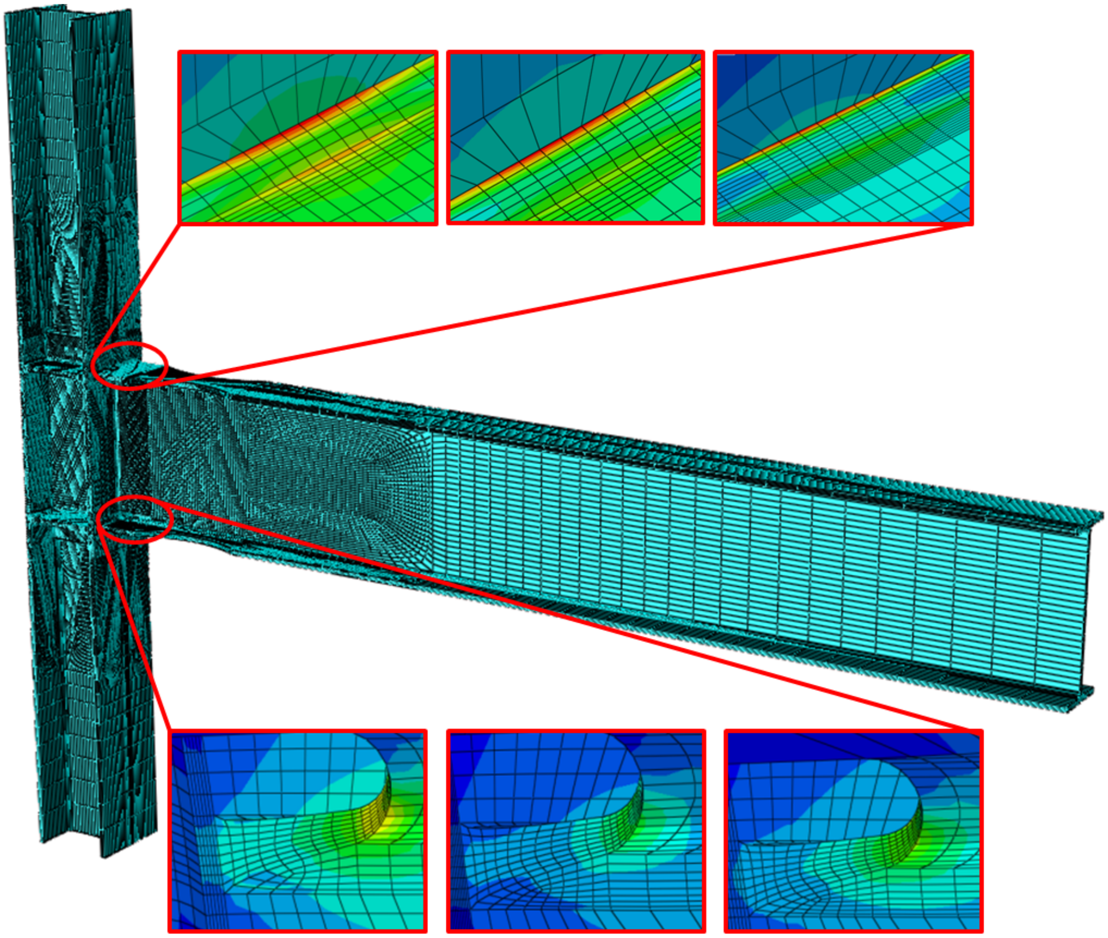

Figure 4-15. Mesh Convergence Study of 8-Story Beam-Column Subassembly

To ensure convergence was reached for the earthquake simulation a cyclic load was placed on the beam tip of both subassemblies (8-story and 16-story) and the stress values evaluated. Because of the computational cost associated with analyses that impose high demand on the 3-D continuum element models the cyclic loading was restrained to a maximum displacement of 1.5 inches. The final mesh density was selected once the stress values in all of the selected regions reached a constant value. Convergence for the fire simulation was analyzed in the same manner but instead of cyclic loading a temperature distribution with a maximum temperature of 1200 °F was imposed on the subassemblies. From these two analyses it was found that the earthquake simulation models control the density of both subassemblies. A summary of the study is provided in Table 4-4. For the thermal analysis of the three-dimensional subassemblies the models were discretized for compatibility with the earthquake and fire simulation.

Table 4-4. Convergence Study of 3-D Continuum Element Models

Model	Mesh Density	Earthquake Simulation				Fire Simulation			
		WAH (psi)	BCW (psi)	RBS (psi)	PZ (psi)	WAH (psi)	BCW (psi)	RBS (psi)	PZ (psi)
8-Story	Initial	23606	33621	12795	29658	21010	29923	11387	26396
	2x	27147	38664	14714	34107	24161	34411	13095	30355
	3x	28505	41371	14817	36494	25369	36820	14012	32480
	4x	28539	41784	14830	36859	25420	37925	14096	32675
	5x	28796	41279	14903	36988	25623	38456	14124	32773
16-Story	Initial	24787	35302	13434	31141	25842	36805	14006	32467
	2x	27761	41657	15853	34566	28943	43430	16527	36038
	3x	31925	47905	18230	39751	33284	49944	19006	41444
	4x	33521	51258	19507	42534	34948	53441	20337	44345
	5x	34192	52796	19682	46362	38094	55044	20117	44287
	6x	34705	54908	19820	48216	38284	55704	20379	45173

* All values are maximum principle stresses within the specified region at the same time in the analysis

** WAH = Weld Access Hole
BCW = Beam-Column Weld
RBS = Reduce Beam Section
PZ = Panel Zone

4.4 Summary

The finite-element modeling techniques employed for this research are presented in this chapter, this included a detailed description of the line element models, a discussion of the 3-D continuum element beam-column subassembly models, and finally a description of the validation models implemented for this study. Key points presented in this chapter are summarized below:

- The line element models of both the 8-story and 16-story frames were developed to determine the nodal displacement values for the earthquake simulation as well as the constraint stiffness values for the fire simulations.

- Two models were created of each beam-column subassembly and a fire analysis and FFE analysis was ran on both models.
- Nodal temperature data used for the fire and FFE analysis were calculated through a heat transfer analysis.
- The fire analysis was performed on both beam-column subassemblies and considered three different boundary condition configurations to simulate the restraint imposed by the surrounding frame.
- The FFE analysis was run on both subassemblies and included a dynamic earthquake simulation for all ten earthquake records followed by a fire simulation that included realistic boundary conditions to simulate the restraint imposed by the surrounding frame.
- Validation models were analyzed to ensure the modeling techniques employed in this study produced accurate results. This included a heat transfer validation model, earthquake simulation validation model, modal analysis on the line element models and a mesh convergence study for both the line element and 3-D continuum element models.

CHAPTER 5
SIMULATION RESULTS AND OBSERVATIONS

5.0 Overview

This chapter presents the results from the 3-D continuum element beam-column subassembly models discussed in Chapters 3 and 4. Results from the heat transfer analysis as well as the fire and fire following an earthquake simulations are presented and discussed. Section 5.1.1 presents steel temperature data and the variation of temperature-dependent material properties for several critical regions within the subassemblies throughout the entirety of the fire simulation. Results from the sequentially coupled fire and FFE simulations are then presented in Sections 5.1.2 and 5.1.3, respectively. Following these sections a comparison of the results to current design standards is presented.

5.1 Results

The critical regions of the beam-column subassemblies that were selected to discuss in detail in the following sections are depicted in Figure 5-1. Values for points BCW-TF and BCW-BF are taken from the beam-column flange welds at the top and bottom flanges of the beam, respectively. Values for the WAH-T and WAH-B regions are taken from the top and bottom weld access holes, respectively. The PZ region is taken as a 6-inch by 6-inch region corresponding to the middle of the panel zone in the beam-column joint. Regions RBS-TF and RBS-BF are taken as the top and bottom flanges of the reduced section on the beam, respectively. Region RBS-W is a 6-inch by 6-inch region of the reduced beam section at the mid-depth of the beam web. Region BCW-TW is taken as the upper portion of the beam web column flange full penetration weld.

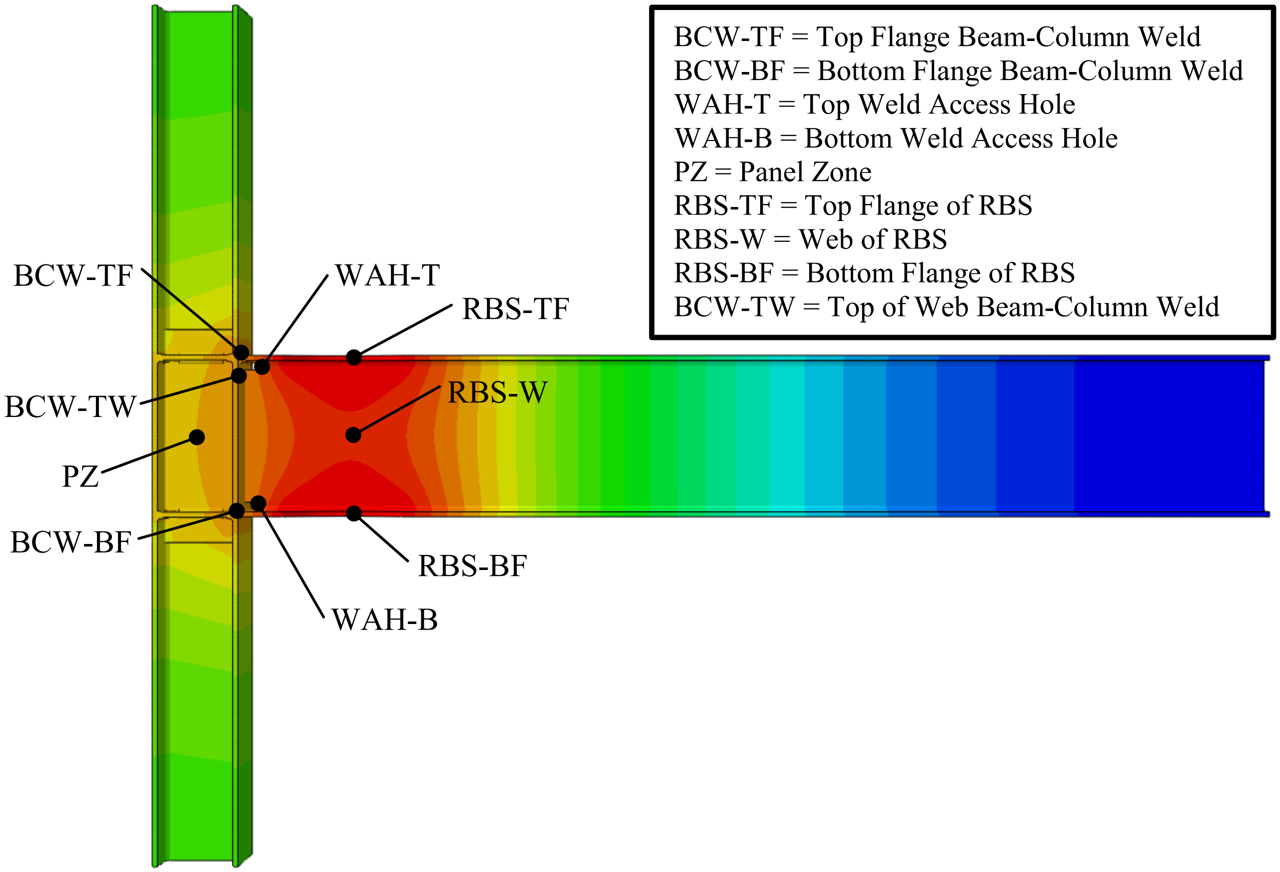

Figure 5-1. Location of Critical Regions Discussed in the Analysis Results

5.1.1 Heat Transfer Simulation

The following section presents results from the numerical heat transfer simulations discussed in Section 4.2.2. Figures 5-2 through 5-5 present the average recorded nodal temperature values from the heat transfer simulations of the selected regions for the 8-story and 16-story subassembly models for both the fire and FFE. In order to keep the plots from becoming to convoluted regions that share similar values with other locations are excluded. A legend is provided in the upper right hand corner of all of the figures, which indicates what points were incorporated.

When examining the temperature values seen in the thermal analysis performed for the fire only simulations it can be seen that the bottom flange of the RBS (RBS-BF) follows the time-temperature curve exactly. This is expected since the thermal loading was applied by forcing the surface temperature of the bottom flange of the beam to follow the time-temperature curve. For the 8-story subassembly, temperatures in all of the critical regions reach their peak values at approximately 3,600 seconds into the simulation, which corresponds to the end of constant temperature portion of the time-temperature curve. The associated lag time between the time-temperature curve reaching within 10% of its peak value of 1652 ºF and the steel temperature of the selected regions reaching within 10% of their peak value is approximately 2,400 seconds. As the ambient temperature rapidly falls between 3,600 seconds and 18,000 seconds into the simulation the steel temperature in the critical regions also declines at a similar rate. This can be attributed to heat loss in these sections through conductive heat transfer to cooler regions of the steel beam and column, as well as convective and radiative heat transfer to the cooling ambient environment simulated by forcing the bottom flange of the beam and outer flange of the column to follow the cooling portion of the time-temperature curve.

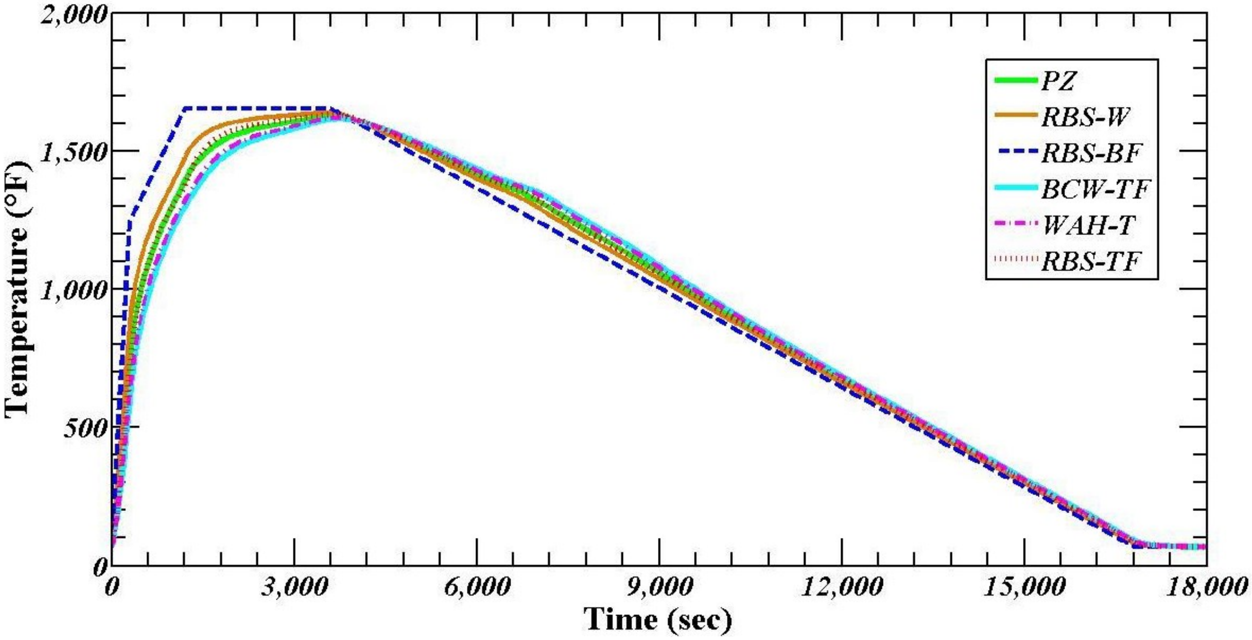

Figure 5-2. Nodal Temperature Values for 8-Story Fire Thermal Analysis

When examining the temperature values presented in Figure 5-3 for the 16-story fire thermal analysis it can be seen that there is a larger time lag between temperatures in the bottom flange of the RBS and the other critical regions. This is expected since the members in the 16-story subassembly are substantially larger than those in the 8-story. Because of this same reason the maximum temperatures in these regions never reach the maximum temperature of the fire, with the web of the RBS only reaching 1540 ºF and the beam-column top flange weld reaching a maximum temperature of only 1377 ºF.

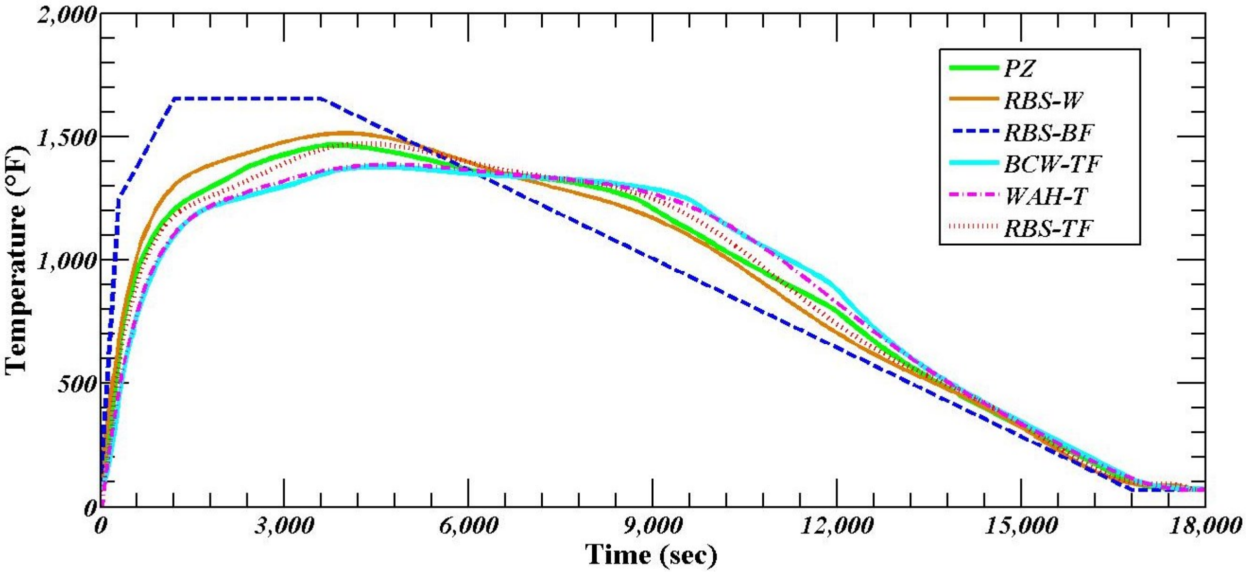

Figure 5-3. Nodal Temperature Values for 16-Story Fire Thermal Analysis

For the FFE simulations, the symmetric nature of the applied temperature boundary condition creates nearly identical temperature values in the top and bottom beam-column welds, top and bottom weld access holes and top and bottom RBS flanges. Because of this the top regions were excluded from the figures to keep them from becoming too convoluted to read. Much like the fire thermal analysis, it can be seen that the nodal temperature in the exposed, or unprotected, region of the beams are identical to the ambient temperature history provided by the time-temperature curve. This behavior is expected since a thermal boundary condition was placed on those regions to force the nodal temperatures to follow the time-temperature curve. Much like the 8-story fire analysis, the temperatures in all of the critical regions for the 8-story FFE simulation reach their peak values at approximately 3,600 seconds into the model which corresponds to the end of the constant temperature portion of the time-temperature curve. The associated lag time and rate of cooling also has similar properties to those seen in the fire analysis. The biggest difference between the fire and FFE simulations is in the regions experiencing the highest temperature values. For the FFE analysis the RBS portion of the beam has considerably higher temperatures during the heating phase of the fire and the panel zone region has lower temperatures during this phase when compared to the fire simulation.

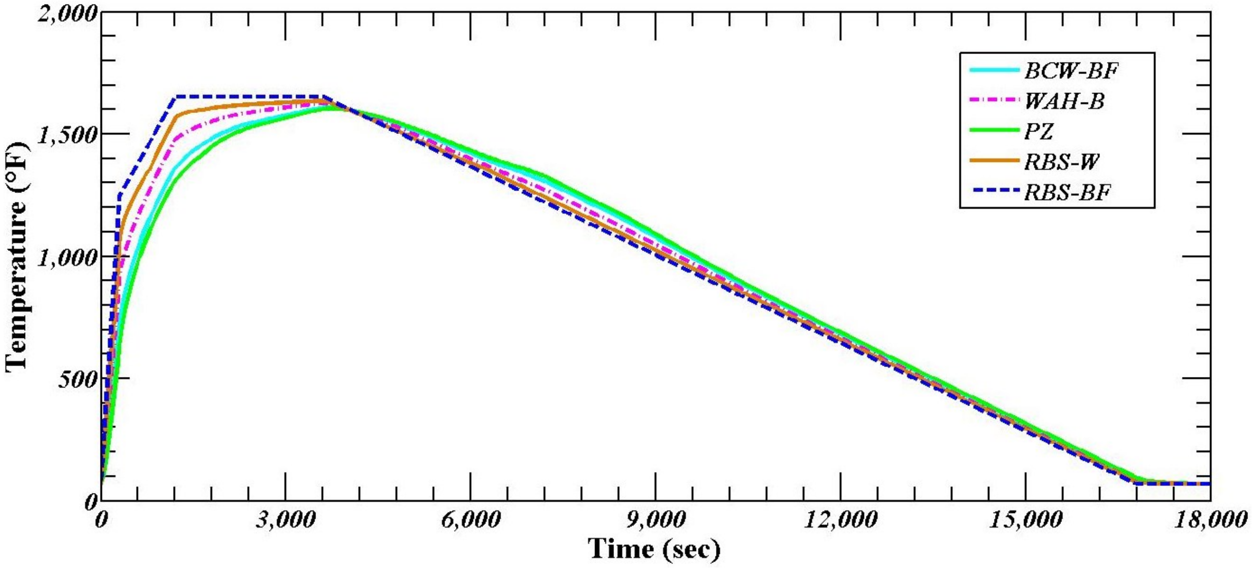

Figure 5-4. Nodal Temperature Values for 8-Story FFE Thermal Analysis

The 16-story FFE thermal analysis also has very similar behavior to the 16-story fire anlaysis with the biggest difference again being the regions experiencing the highest temepratures. Much like the 8-story FFE thermal simulation, the web of the reduced beam section and panel zone experience higher and lower temperatures, respectively, than what was seen in the fire simulation.

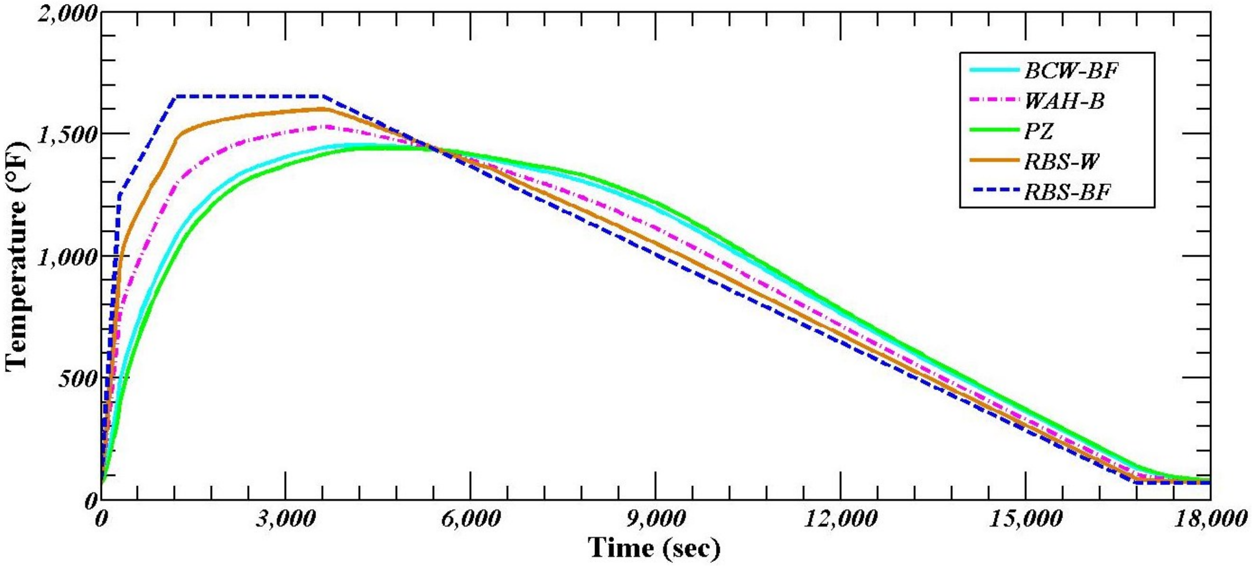

Figure 5-5. Nodal Temperature Values for 16-Story FFE Thermal Analysis

The change in material properties over the course of the fire simulations are presented in Figures 5-6 through 5-9. Normalized values for the modulus of elasticity, yield stress, thermal conductivity and specific heat are provided. The values are normalized based on their room temperature values before the fire starts. Just like the nodal temperature plots, the points that have very similar material property values are excluded to keep the figures legible. A legend is provided in the upper right hand corner of all figures which indicates what points were included. When examining the plots emphasis should be given to the reduction in yield stress and modulus of elasticity. For both of the 8-story simulations it can be seen that yield stress drops to 6% of its room temperature value in most of the regions examined at approximately 3,600 seconds into the simulation. However, for the 16-story simulations only the regions with directly exposed surfaces reach this level of strength loss.

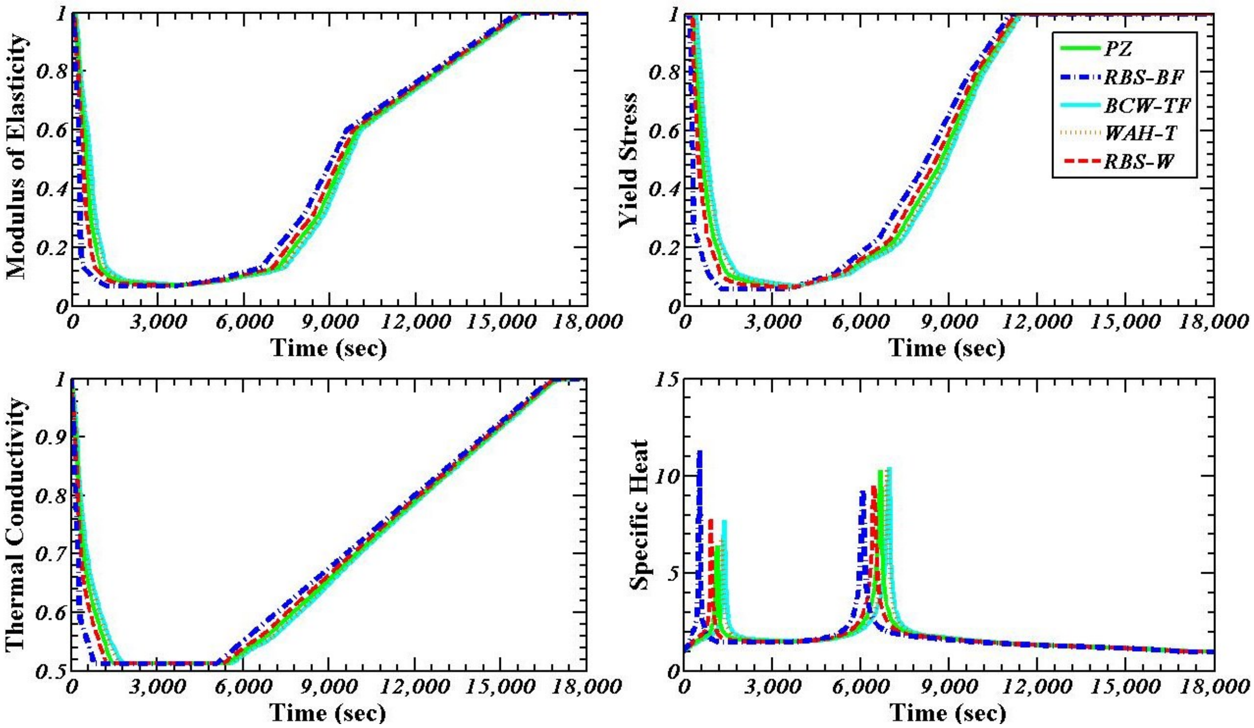

Figure 5-6. Material Property Degradation for 8-Story Fire Thermal Analysis

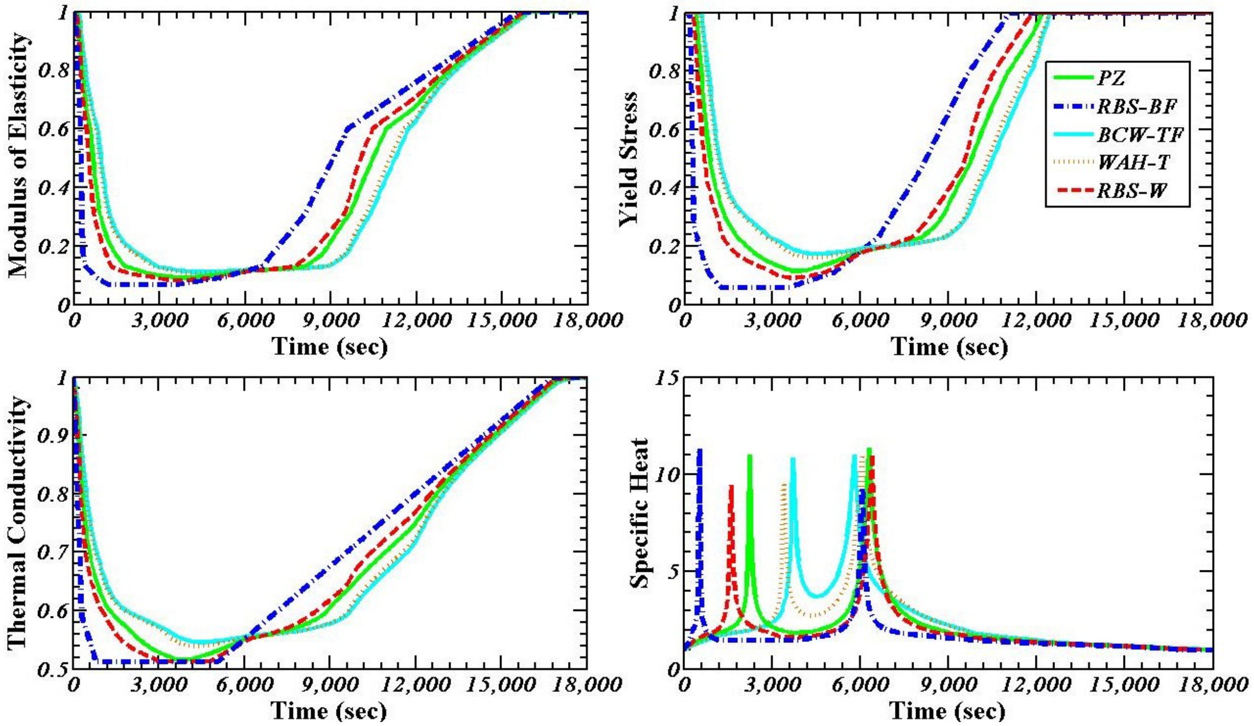

Figure 5-7. Material Property Degradation for 16-Story Fire Thermal Analysis

Similar behavior is seen in the FFE thermal analysis compared to fire only analysis and as expected the most notable difference comes from the variation of material degradation between different regions.

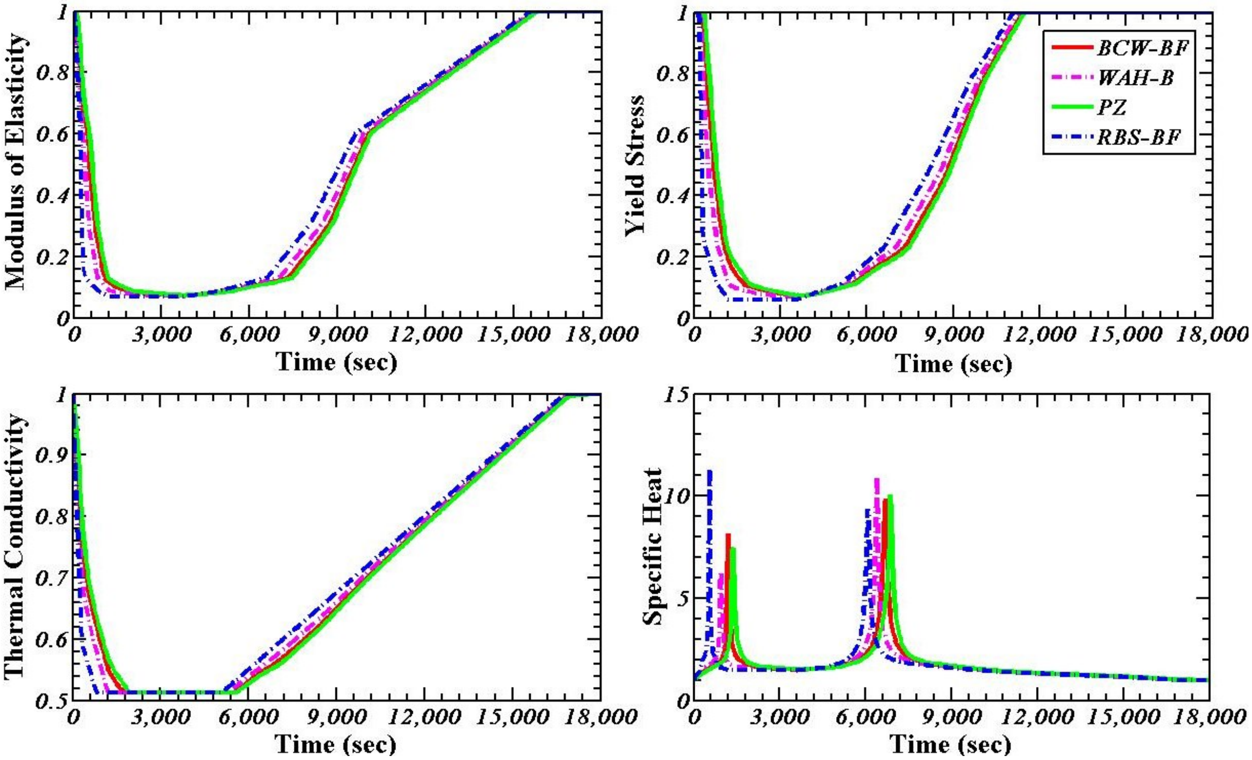

Figure 5-8. Material Property Degradation for 8-Story FFE Thermal Analysis

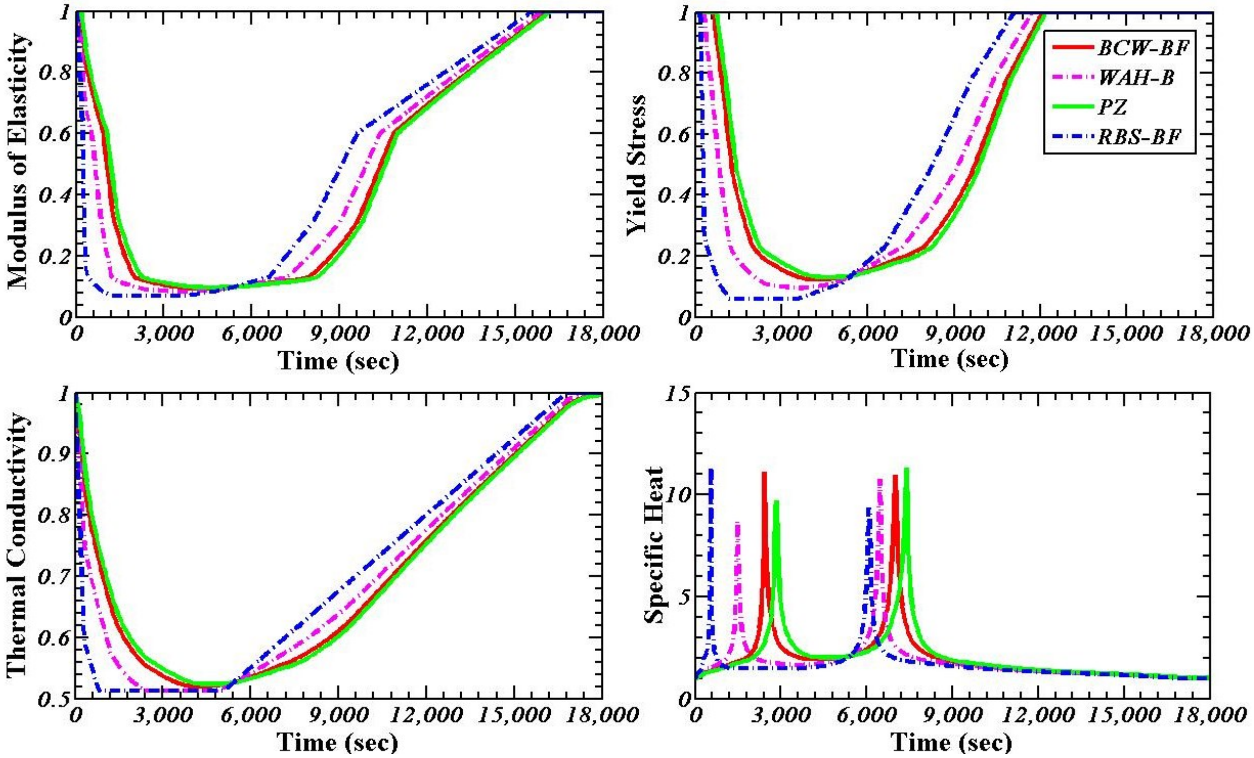

Figure 5-9. Material Property Degradation for 16-Story FFE Thermal Analysis

5.1.2 Fire Analysis Results

The following section provides results from the mechanical fire simulations performed on both beam-column subassemblies. For both subassemblies three different boundary conditions were placed at the tips of the beam and column so that the effects of constraints could be examined. The first boundary condition, which will be referred to as realistic, consists of fully coupled constraints that incorporate all planar degrees of freedom. These constraints were updated throughout the simulation to represent the variation of constraint provided by the frame throughout the fire and is thought to provide the most realistic representation. The second boundary condition, termed lateral, is similar to the realistic boundary condition but the horizontal stiffness provided by the frame at the tips of the column and vertical constraint at the beam end are replaced with a fixed boundary condition. The third boundary condition, referred to as fixed, constrains the tips of the beam and column to be fixed in all applicable degrees of freedom during the entirety of the analysis. This boundary condition is thought to bound the problem, providing the highest demands on the subassembly.

When examining the response of the subassemblies during the simulations some interesting behavior is observed between the different constraint configurations. The most notable is the difference in deformation, shown in Figure 5-10, that occurs within the joint depending on the boundary condition. For the 8-story fire simulations, no noticeable deformation is seen in the realistic or lateral boundary condition models. The demand imposed on these models is relatively small and as a result the members are able to resist any excessive deformation throughout the entirety of the fire. Despite the small demand, notable difference in the stress distribution between the realistic and lateral boundary condition models can be seen. When all of the tips of the beam and column are fully fixed, twisting of the column is observed and lateral-torsional buckling occurs in the column directly below the beam-column joint. The change in behavior is expected since the fully fixed boundary condition does not allow for any thermal expansion, creating extremely high demands in the members. Column twisting is typically caused as a result of beam lateral torsional buckling in deep column connections. However, no noticeable buckling occurred in the beam so the cause of the twisting action is thought to come from the thermal expansion of the column, which resulted in lateral torsional buckling below the beam-column joint which led to the twisting action. A depiction of the deformed shapes during the peak of the fire is shown in Figure 5-10.

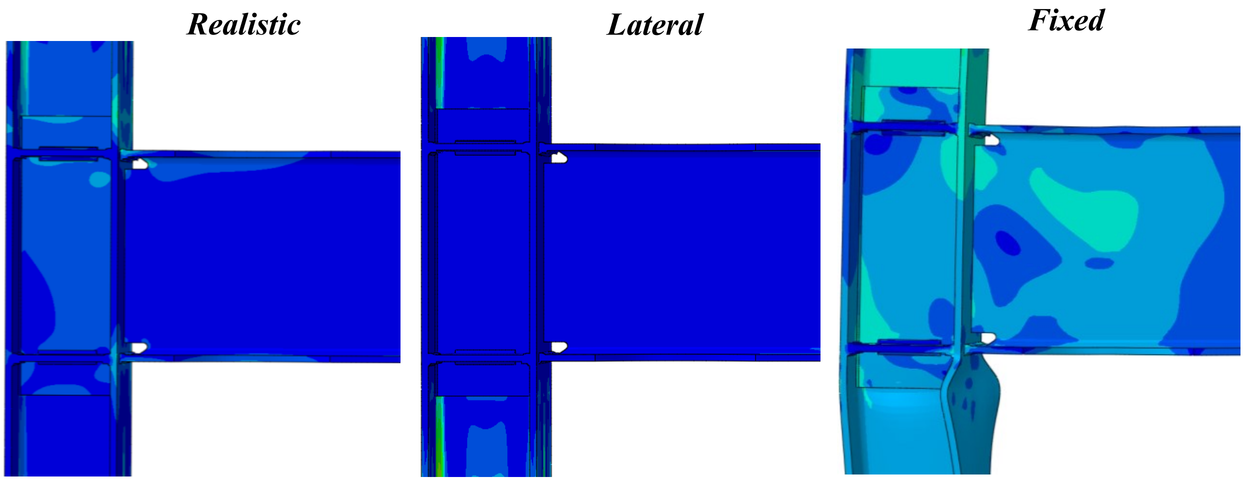

Realistic *Lateral* *Fixed*

Figure 5-10. Deformation at Peak of Fire for 8-Story Fire Simulation for Various Boundary Conditions

The effect of boundary conditions on the damage patterns observed in the 16-story fire simulations can be clearly seen (Figure 5-11). The figure shows local buckling in the flange and web of the beam in the reduced section for all three sets of boundary conditions. However, the extent of deformation varies between each constraint configuration. It can be seen that the deformation in the realistic model is the least of the three, with relatively small amounts of observable distortion occurring in the web and bottom flange of the reduced section. The lateral boundary condition model resulted in substantial local buckling in the web and upper flange of the RBS as well as less notable buckling of the bottom flange. The fixed boundary condition model, which imposes the highest demand on the members, resulted in the largest notable distortion with extensive local buckling occurring in the top flange and web of the RBS. Figure 5-11 provides a depiction of the observed damage for the 16-story fire simulations at the peak of the fire.

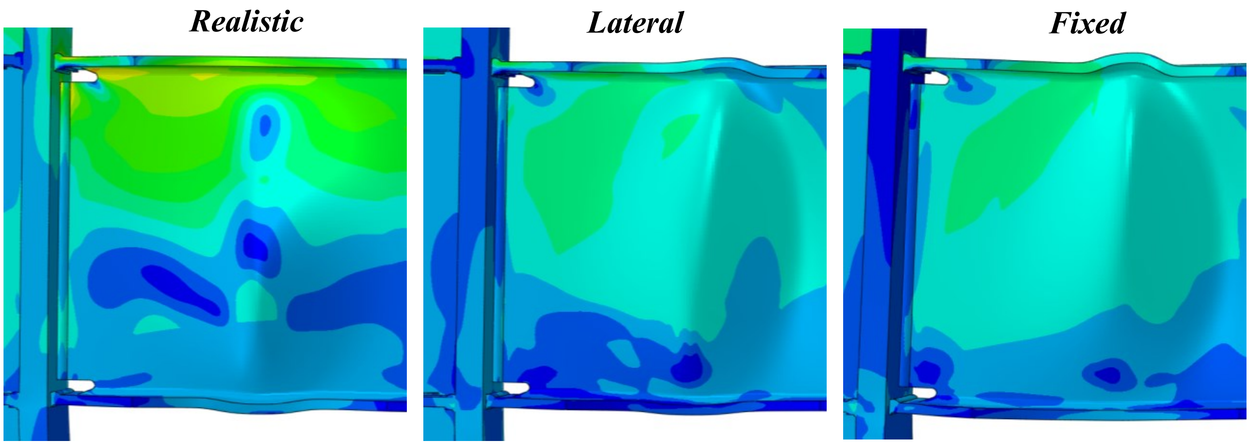
Realistic *Lateral* *Fixed*

Figure 5-11. Deformation at Peak of Fire for 16-Story Fire Simulation for Various Boundary Conditions

Another interesting behavior that is seen by examining the extent of deformation in the 16-story models during the fire is the damage that occurs during the cooling phase. When comparing the visible damage at the initial heating phase, the peak of the fire and then the cooling phase it can be seen that the substantial demand continues to be imposed on the subassembly throughout the entirety of the fire with significant deformations observed during the cooling phase. This is depicted in Figure 5-12.

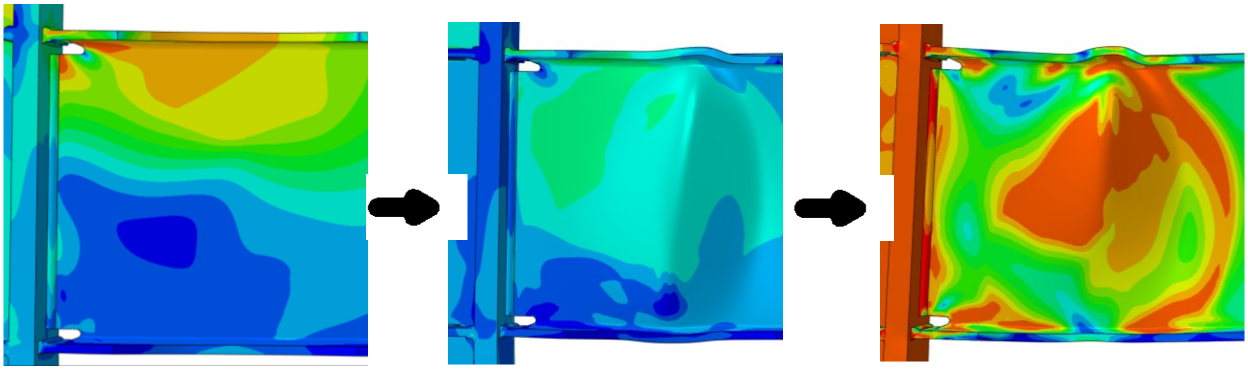

Figure 5-12. Deformation at Initial Stages of the Heating Phase (left), During the Peak of the Fire (middle) and During the Cooling Phase (right) for 16-Story Fire Simulation

When examining the localized stresses in the critical regions of the 8-story subassembly, it becomes obvious that relatively little demand is being imposed on the members. While this behavior is unexpected for such a high temperature fire it is plausible and can be attributed to the location of the selected member within the frame. At the chosen level relatively little gravity load is supported by the columns, and member sections are small compared to lower levels causing far less constraint against thermal expansion and contraction. This is behavior is confirmed when examining the stiffness values determined by the previously discussed constraint analysis which are substantially smaller than values determined for the 16-story frame.

However, some interesting observations can still be made regarding the evolution of stress values throughout the fire, particularly in the fixed models which do not include the constraint imposed by the frame. It can be seen that stress values at the very early stages of the fire are substantial, particularly before material strength degradation begins. Early in the fire, the members have not yet become sufficiently hot to experience a significant reduction in modulus of elasticity or yield strength, and therefore maintain a high axial stiffness. Although material degradation does not occur until temperatures of several hundred degrees Fahrenheit are achieved, thermal expansion starts immediately with the start of heating. The combination of thermal expansion and high axial stiffness in the early stages of a fire results in high stress concentrations early in the heating. Furthermore, it can be seen that large stress demands also occur during the cooling phase of the fire and large residual stresses are present at the end of the fire. This behavior is illustrated in Figure 5-13, which shows the evolution of stress values in the beam-column weld and reduced beam section for the 8-story model. Since yielding of the material is of particular concern the von Mises stress values were selected to be plotted. The von Mises stress is a yield criteria, which combines all three principal stress values in a region to determine if yielding is likely to occur.

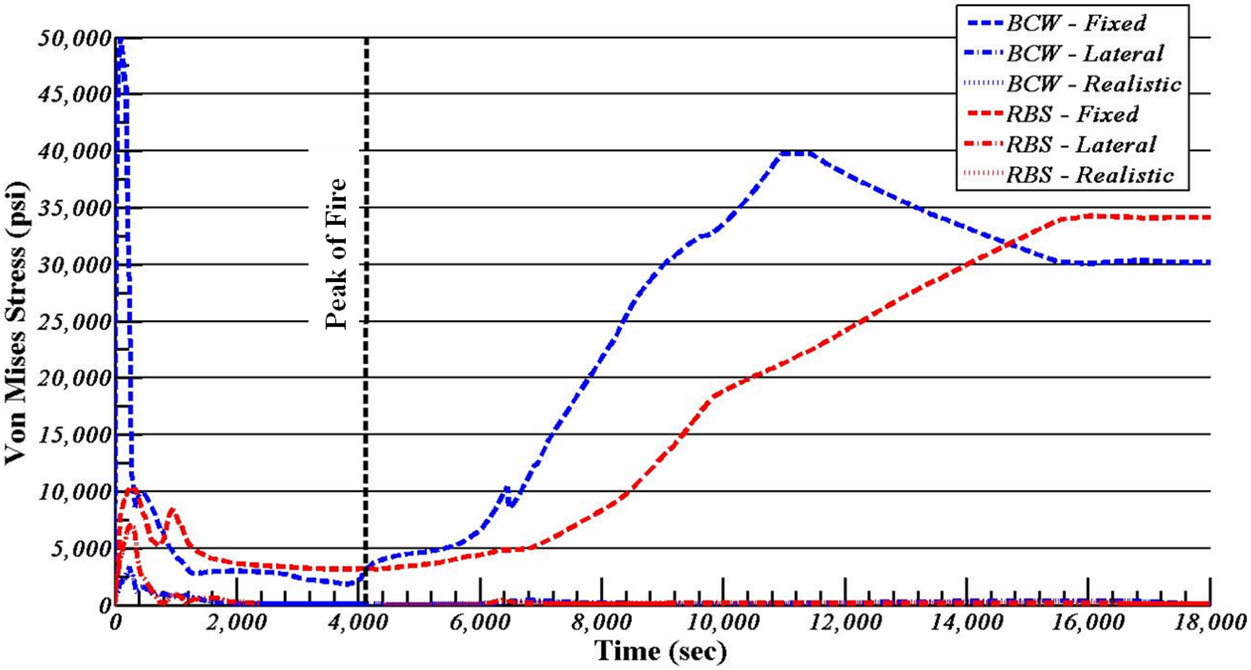

Figure 5-13. Von Mises Stress Values at Critical Locations for 8-Story Fire Simulations

For the 16-story models, the fire simulations created substantially larger stress concentrations than seen in the 8-story models. However, the same observations can be made regarding the evolution of stress values throughout the fire. As expected stress values in the critical regions rise substantially during the initial stages of the fire until material degradation starts to occur and cause the values to drop. As the fire transitions into the cooling phase the material regains its strength properties and the stress values begin to increase again. Much like the 8-story fixed models, the stress values during the initial period of the fire are substantial and considerable residual stresses are observed at the end of the fire. The most significant observations in the 16-story fire simulations are the difference in the stress values as a result of the variation in boundary conditions. The fixed model is thought to bound the problem, creating the highest possible demand on the structure, while the realistic model is designed to provide accurate representation of the actual behavior. When comparing the stress values between these models and the lateral models it can be seen that the lateral models overestimate the stress values in the critical regions. This phenomenon is shown in Figure 5-14, which provides stress values throughout the fire simulation in the beam-column weld and reduced beam section for all three boundary conditions.

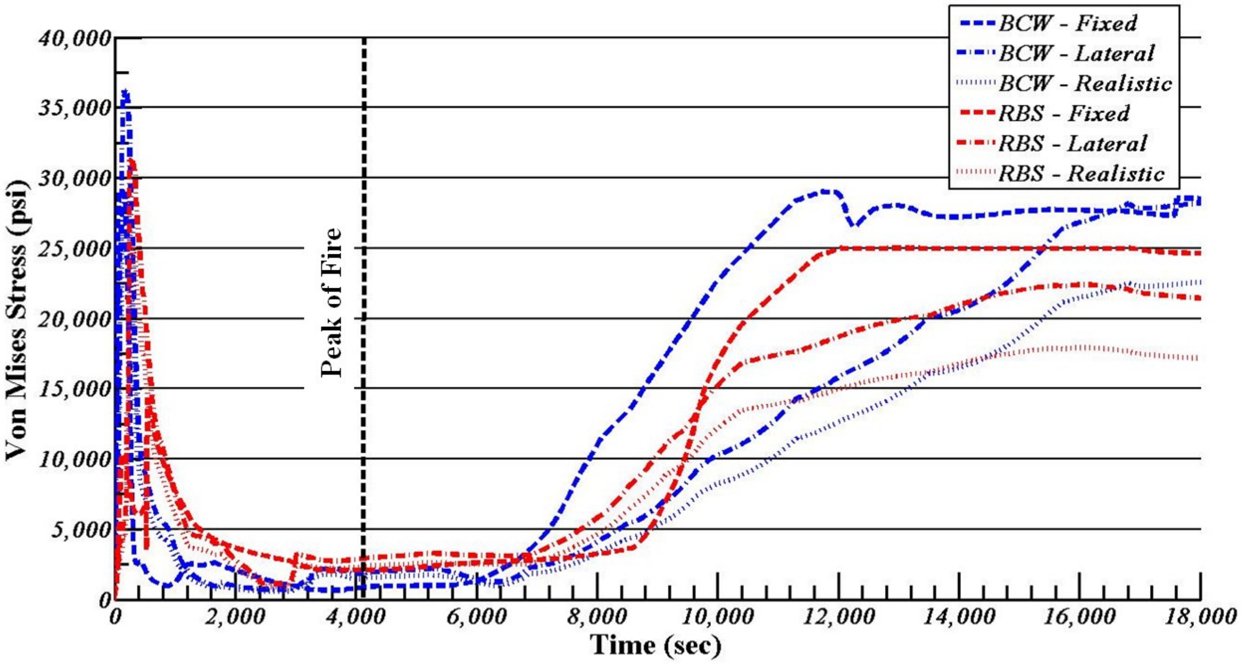

Figure 5-14. Von Mises Stress Values at Critical Locations for 16-Story Fire Simulation

This same behavior is further emphasized when comparing axial forces in the beams of the 16-story models over the course of the fire. The observed demand is plotted in Figure 5-15. The axial load in the lateral model is substantially higher than the realistic model, clearly demonstrating that the exclusion of horizontal constraint at the column tips provides a rather conservative estimate of the demand on the subassembly. It is also observed that the axial forces in the beams reach very high values during the early stages of the heating phase and that even after the specimen has cooled to its original temperature, residual forces remain in the beam.

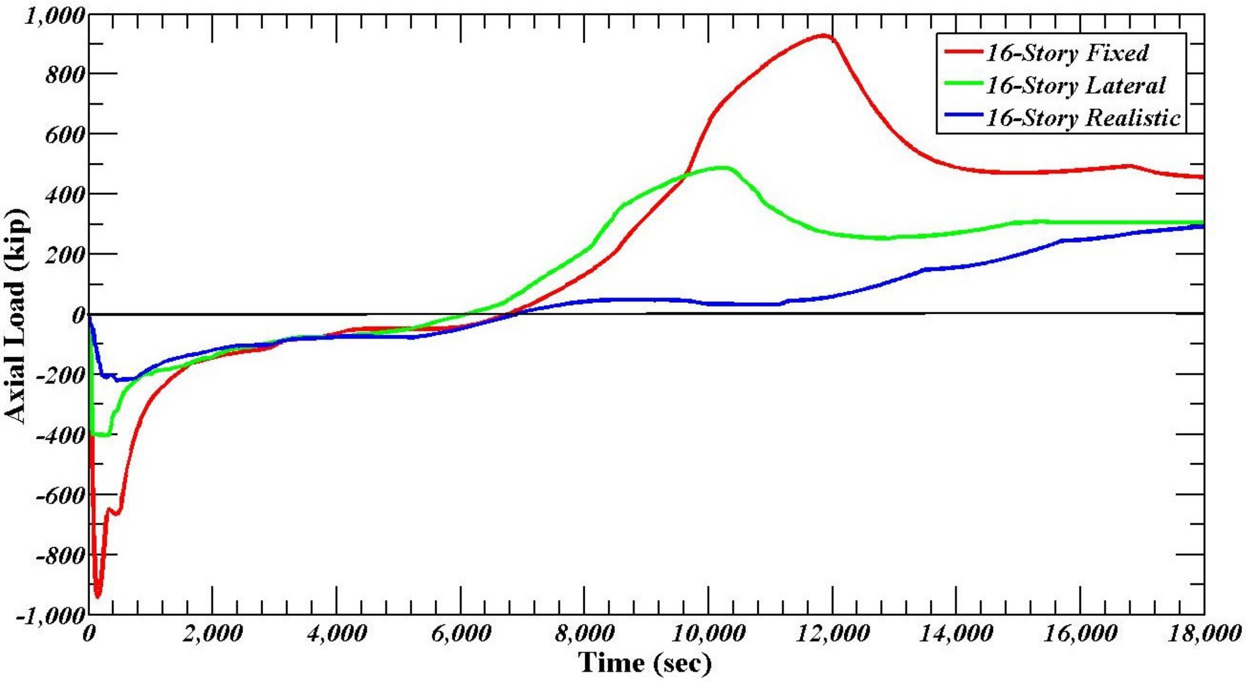

Figure 5-15. Beam Axial Load During Fire

The axial demand in the columns of the different 16-story subassembly models do not follow the same trends seen in Figures 5-14 and 5-15. Because the axial constraint imposed at the tips of the columns does not change between the lateral and realistic models nearly identical demand is imposed. This is depicted in Figure 5-16 which includes an inset for the values from the fixed model. These values were not plotted on the same axes because the demand in the fixed model is magnitudes larger than the lateral and realistic models which make it difficult to observe the trends in all three when plotted on the same figure.

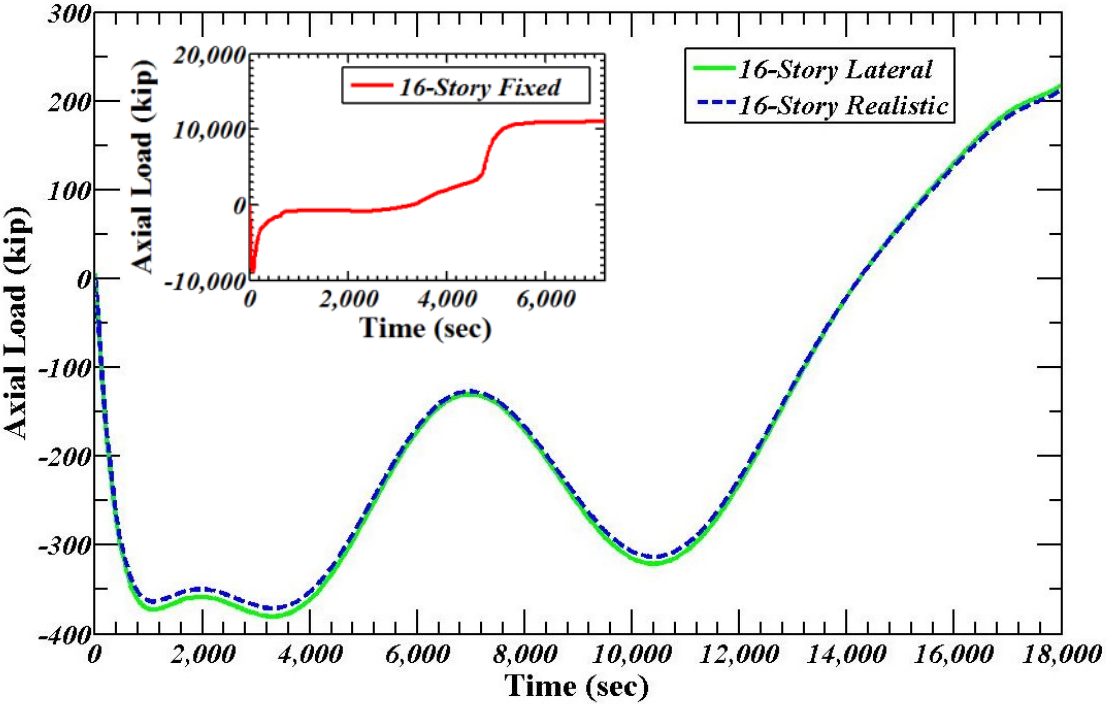

Figure 5-16. Column Axial Load During Fire

The finite element model utilized for both the fire and FFE analyses is not able to capture the occurrence of fractures in the subassemblies. Because of this the evaluation of the potential for fracture was based on the relative values of a rupture index (RI). The RI is defined as:

$$RI = \frac{\varepsilon_p/\varepsilon_y}{exp\left(1.5\frac{p}{q}\right)} \qquad \text{(Equation 5-1)}$$

Where,
ε_p = Equivalent Plastic Strain
ε_y = Yield Strain
p = Hydrostatic Pressure
q = Von Mises Stress

The RI was computed for all of the previously mentioned critical regions of the subassemblies. The maximum values of the RI at the three main stages of the fire simulation for several of the critical regions of all three 16-story models are provided in Figure 5-17. Very high values are seen in the top flange of the reduced beam section during the initial heating phase in both the fixed and lateral models whereas the highest values for the realistic model occurred in the bottom flange of the reduced beam section. As the fire progresses the overall trend is an increase in RI with maximum values occurring during the cooling phase.

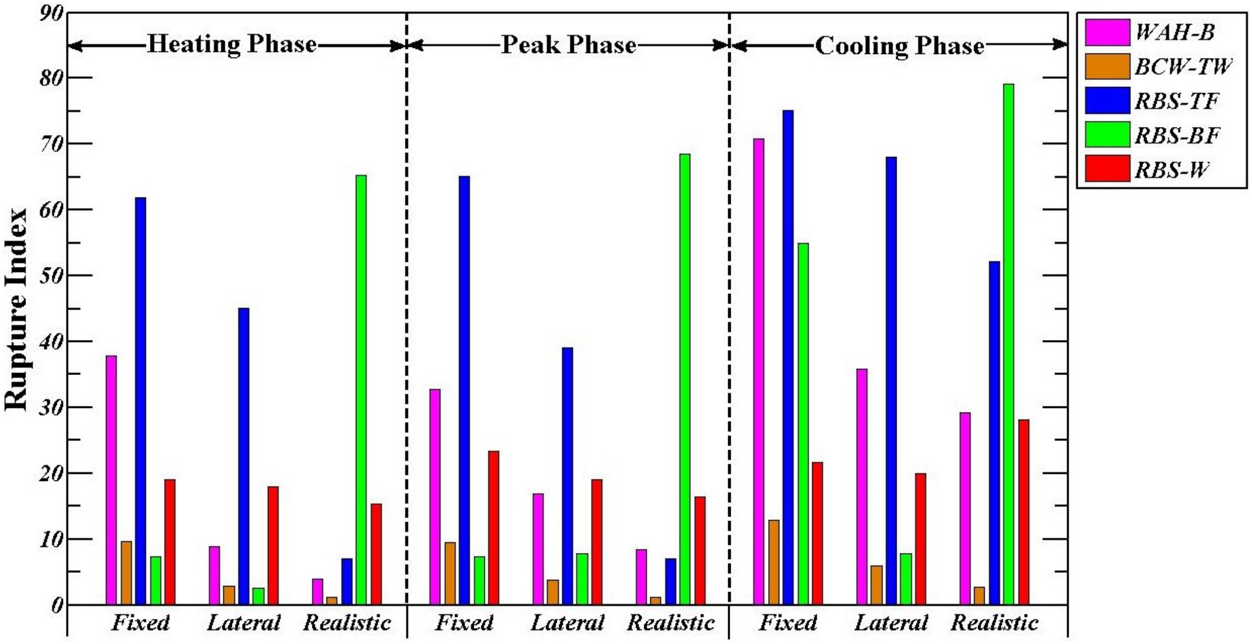

Figure 5-17. Maximum Rupture Index for 16-Story Subassembly During the Various Phases of the Fire Simulation

5.1.3 Fire Following an Earthquake Analysis Results

The following section provides results from the FFE simulations performed on both beam-column subassemblies. When examining the behavior of the subassemblies during the simulations some key observations can be made regarding typical failure modes. For the 8-story models, two failure modes were observed during the earthquake simulations; flange and web local buckling in the reduced section of the beam and buckling of the doubler plate in the panel zone region. Of the ten earthquake simulations performed eight of them resulted in at least some buckling in the RBS and the other two caused buckling of the doubler plate. The buckling of the flange and web of the RBS is a typical behavior for moment resting connections with RBS and is how the joint is designed to behave during high seismic demand. Yielding in the panel zone region is somewhat less common but has been seen in numerous experimental tests (Chi 2002, Lee 2005) on RBS. Furthermore, the design procedure outlined in FEMA 350 (FEMA 2000), which is what the design of the members are based on, is set up to ensure that yielding of the panel zone initiates at the same time as flexural yielding of the beam so the observed behavior is probable. In addition, high stress values were also observed in the weld access hole and beam-column welds at the top and bottom flange of the beams. This is expected since one of the most commonly observed failures in connections with RBS is fractures in these regions. Figure 5-18 provides a depiction of the typical failure modes observed during the earthquake portions of the FFE simulations.

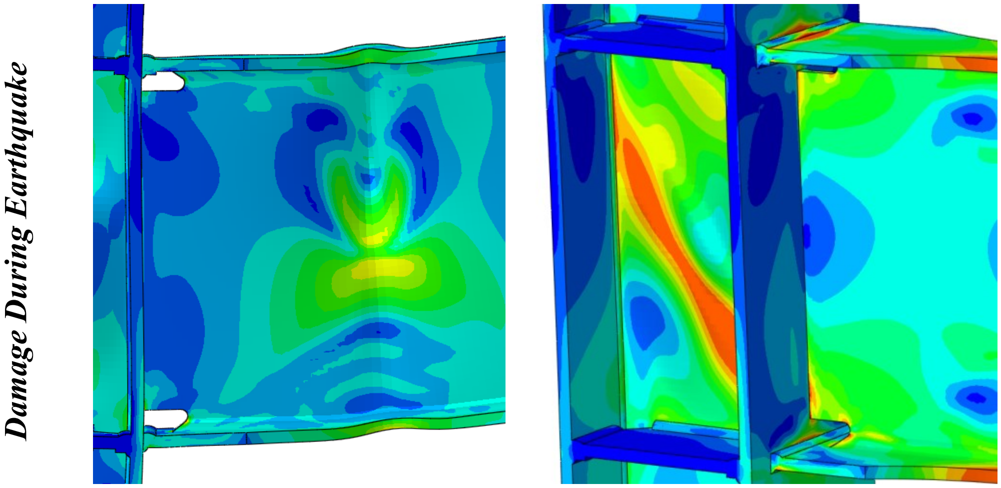

Figure 5-18. Observed Damage During the Earthquake Portion of the FFE Simulations for the 8-Story Subassembly

Much like the fire simulations the fire portion of the FFE simulations produced relatively little demand on the 8-story subassemblies. However, some flange and web local buckling as well as lateral torsional buckling was seen in three of the ten 8-story subassemblies. In all three of these models the buckling occurred at or near the peak of the fire when the thermal expansion of the beam was at its highest. For the three models that demonstrated this behavior different buckling modes were present, all a combination of either web or flange local buckling and lateral torsional buckling. Examples of the different buckling modes observed during the fire simulation are presented in Figure 5-19. These different modes combined with the fact that over half of the models didn’t show any substantial plastic deformation during the fire point towards the fact that the earthquake induced damage played a significant role in the behavior of the joint during the subsequent fire.

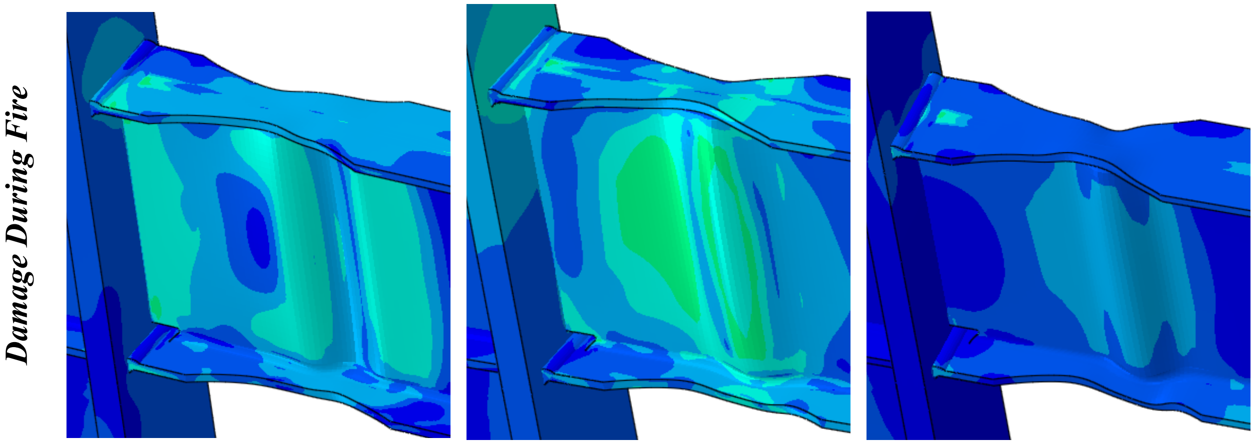

Figure 5-19. Observed Damage During the Fire Portion of the FFE Simulations for the 8-Story Subassembly

The demand imposed on the 16-story subassemblies during the earthquake simulation was far more variable than in the 8-story models. While yielding did occur in several key locations for all of the models, including the weld access hole and the reduced beam section, permanent deformation was only observed in three of the ten earthquakes. This included buckling in the web of the reduced beam section during the Imperial Valley earthquake, and local flange buckling in the reduced beam section during the Loma Prieta and Koceali earthquake simulations, these deformations are depicted in Figure 5-20.

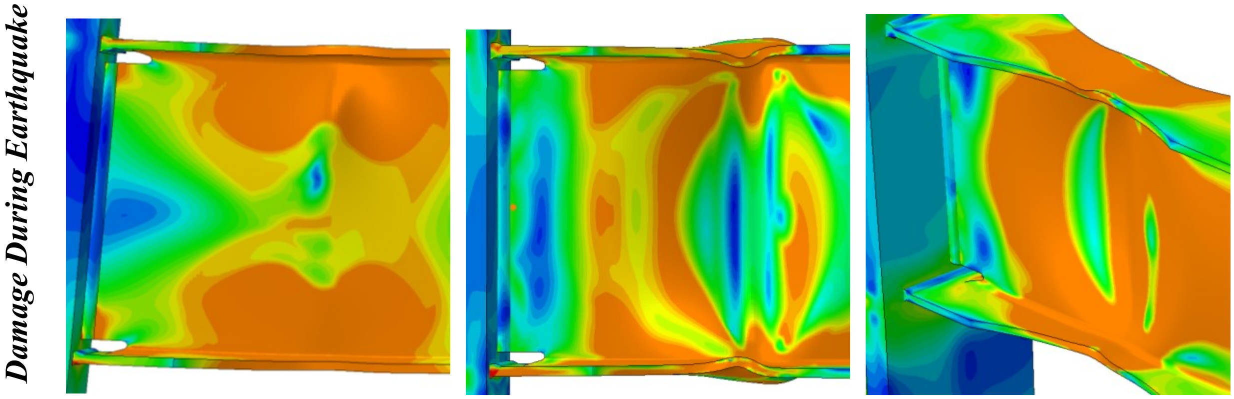

Figure 5-20. Observed Damage During the Earthquake Simulation for the 16-Story Subassembly

The demand imposed during the subsequent fire analysis did produce significant deformation in all of the models, particularly in the reduced beam section. Both lateral torsional buckling as well as localized web buckling was generated during the fire simulations. This behavior is shown in Figure 5-21.

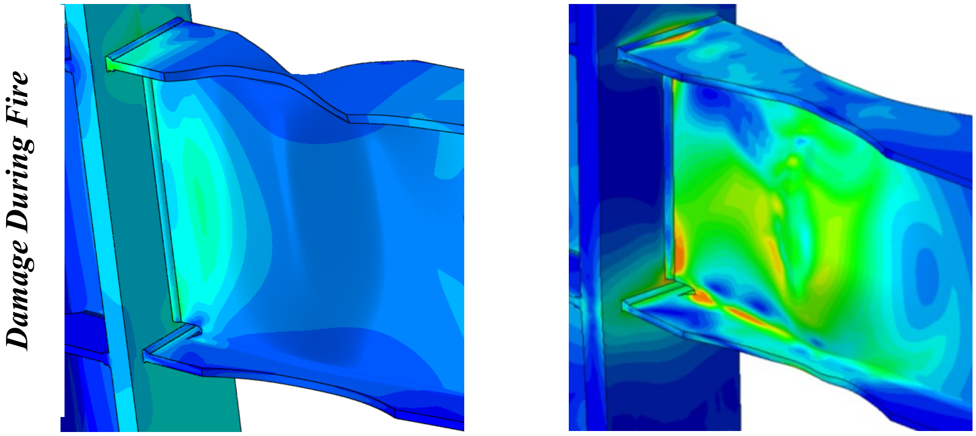

Figure 5-21. Observed Damage During the Fire Portion of the FFE Simulations for the 16-Story Subassembly

The stress values seen in the critical regions of the 8-story subassemblies during the earthquake simulations are presented in Figures 5-22 and 5-23. Since yielding of the material is of particular concern the von Mises stress values were selected as the yield criteria. For the earthquake simulation portion of the analyzes stress values are not able to be accurately averaged since the earthquake demand varies from record to record, so instead examples that illustrate typical behavior are provided. For the 8-story subassemblies the Imperial Valley and Kocaeli earthquake simulations were selected as representative examples since they depict the two typical failure modes observed during the simulations. The Imperial Valley earthquake resulted in yielding and failure of the panel zone region and not the RBS. This is evident in Figure 5-22 which shows low von Mises stress values in the RBS web and stress values in the panel zone reaching the yield point numerous times throughout the earthquake.

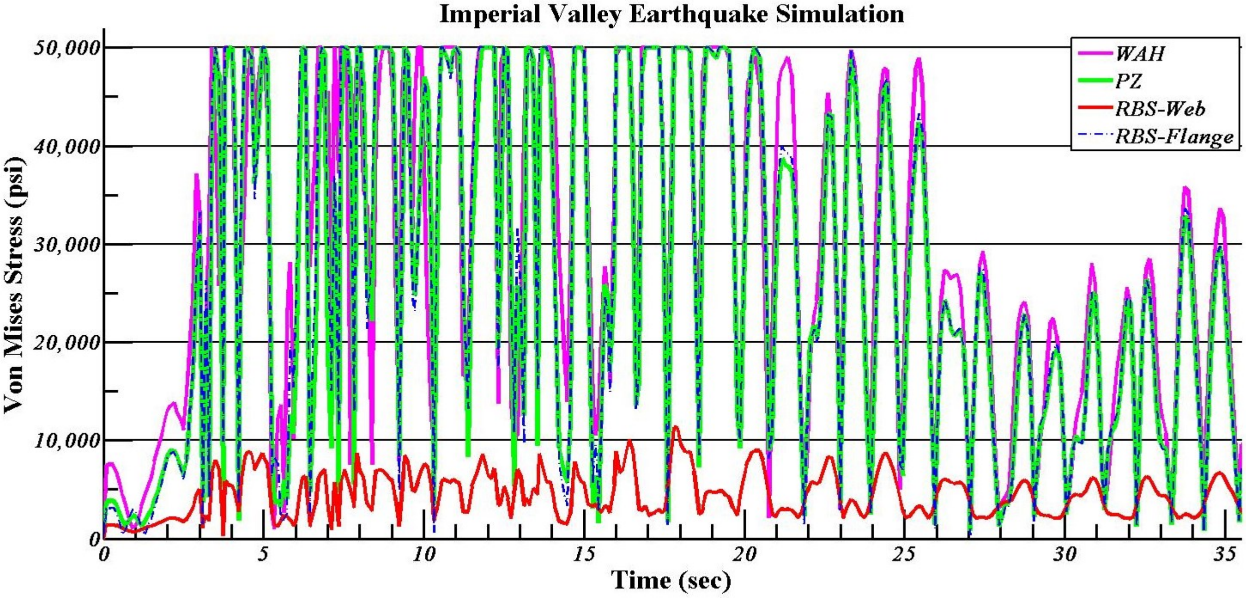

Figure 5-22. Von Mises Stress Values at Critical Locations for 8-Story Imperial Valley Earthquake Simulation

The second observed failure mode, flange and web local buckling in the reduced section of the beam, was seen during the Kocaeli earthquake. Relatively high stress values in the web of the RBS were observed for models that experienced this failure mode and far fewer cycles caused stress values to reach yielding in the panel zone. This is depicted in Figure 5-23.

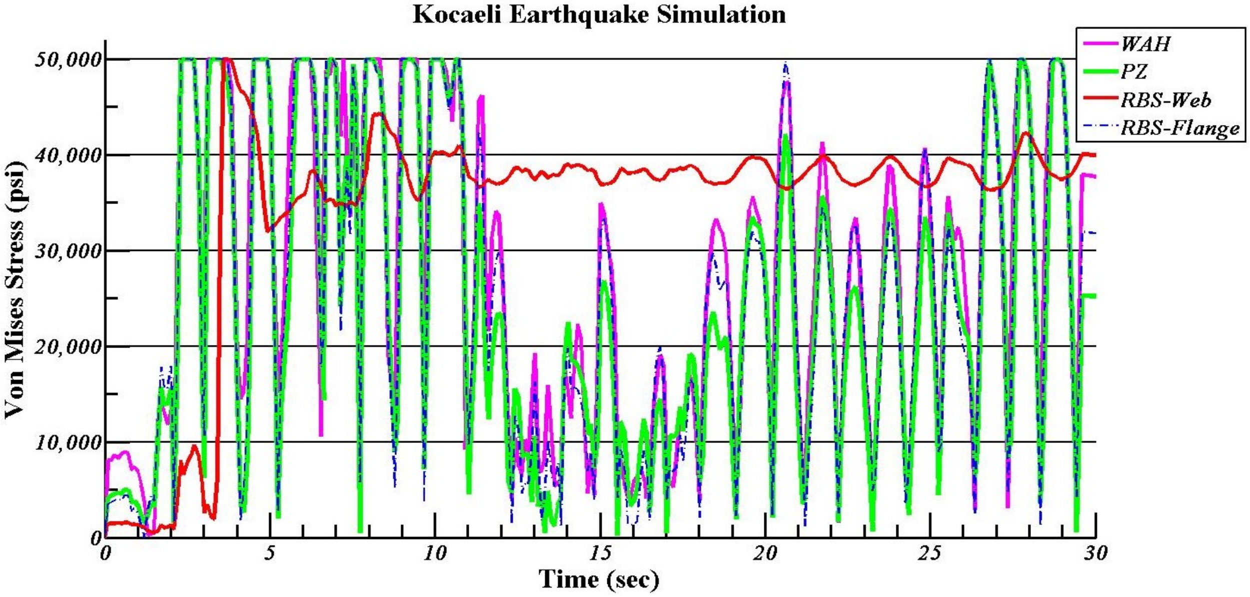

Figure 5-23. Von Mises Stress Values at Critical Locations for 8-Story Kocaeli Earthquake Simulation

The maximum rupture index, which is discussed in section 5.1.2, was also examined to gain a better understanding of the demand imposed by the various earthquakes. This provides valuable insight into the extent and location of damage sustained during the earthquake simulations, which can be used to gain a better understanding of the behavior during the subsequent fire simulations. When examining maximum values of the RI, which are provided in Figure 5-24, it can be seen that considerable variation exists between earthquakes, furthermore the location experiencing the highest demand also differs.

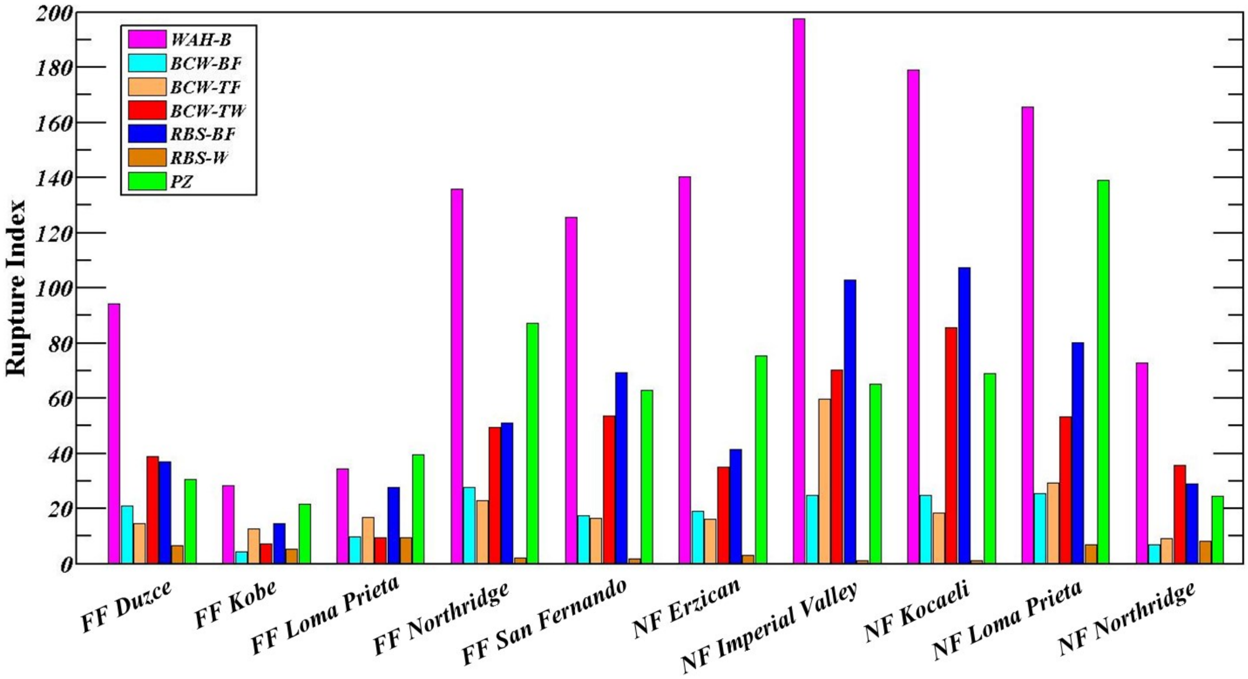

Figure 5-24. Maximum Rupture Index During 8-Story Earthquake Simulations

For the 16-story subassembly models stresses imposed during the various earthquakes displayed similar trends to those seen in the 8-story models. Very high stresses are seen in the weld access holes and the flanges of the reduced beam section. However, the panel zone region did not experience the same level of demand seen in the 8-story models. These behaviors are depicted in Figures 5-25 and 5-26, which plot the von Mises stress values in various regions of the subassemblies during the Imperial Valley and Duzce earthquake simulations, respectively.

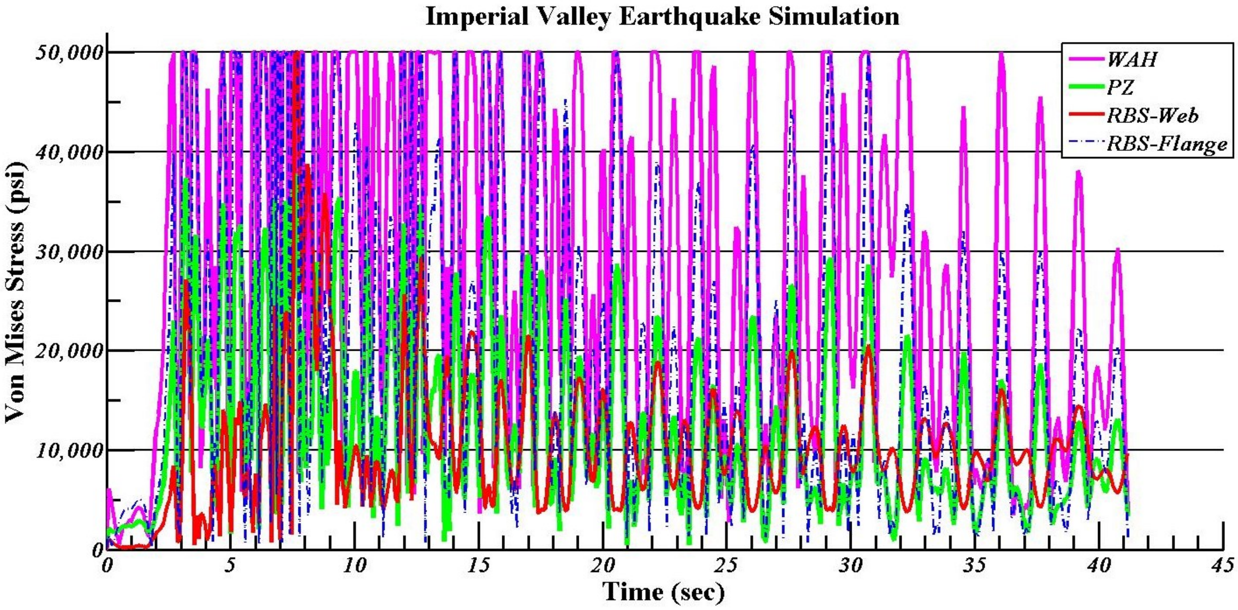

Figure 5-25. Von Mises Stress Values at Critical Locations for 16-Story Imperial Valley Earthquake Simulation

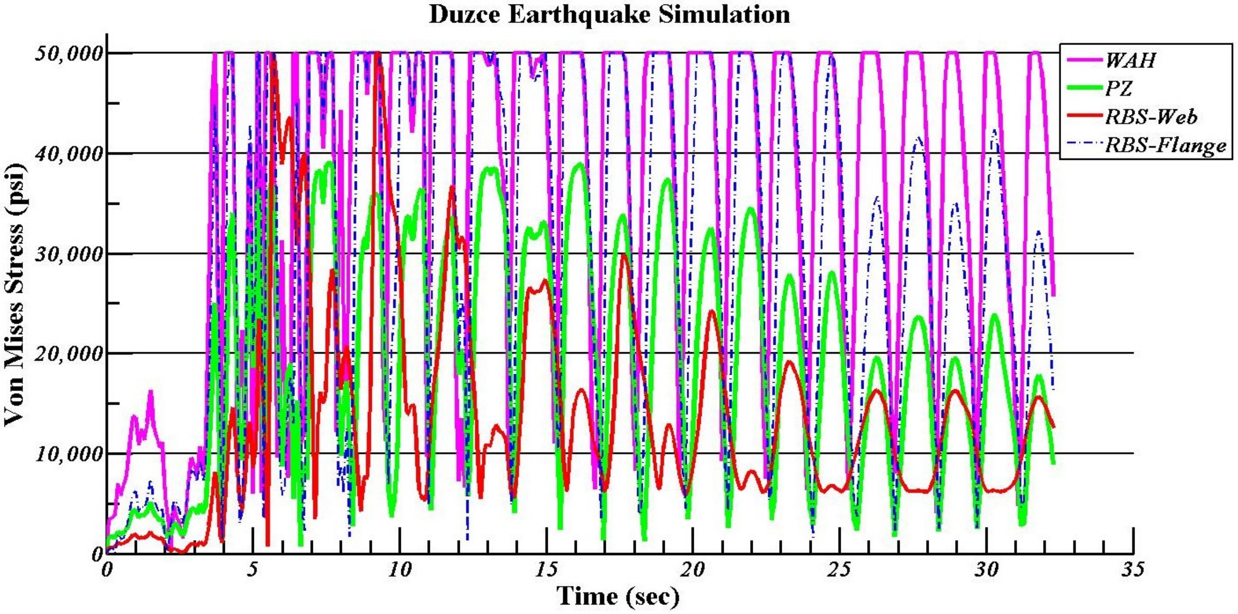

Figure 5-26. Von Mises Stress Values at Critical Locations for 16-Story Duzce Earthquake Simulation

The maximum rupture index was also examined for the 16-story subassemblies during the various earthquake simulations to gain a better understanding of the demand imposed on the members. When examining maximum values of the RI, which are provided in Figure 5-27, considerable variation is observed between earthquakes.

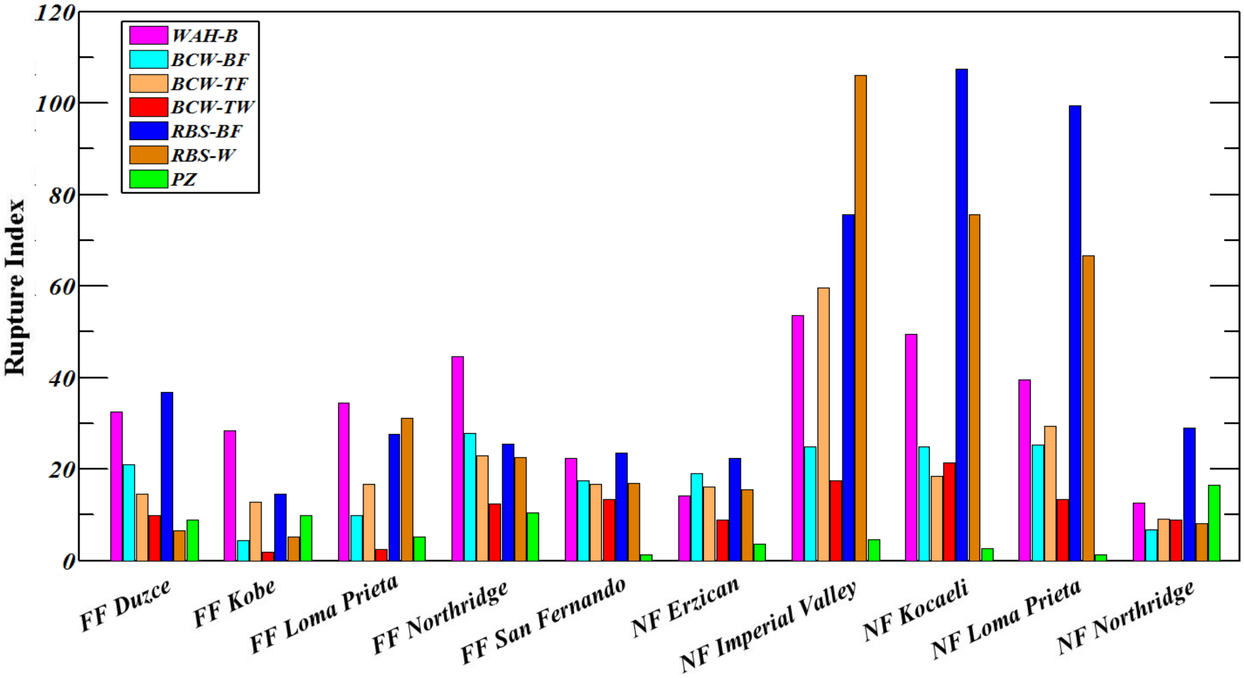

Figure 5-27. Maximum Rupture Index During 16-Story Earthquake Simulations

When examining the stress values during the fire portions of the FFE simulations, it is important to keep in mind the effect of material degradation on the magnitude of stresses. As expected, stress values increase significantly during the initial stages of the fire as a result of the initial thermal expansion that occurs before a temperature of 750 ºF, which is when strength begins to degrade in steel. Once this temperature is reached, the strength of the material begins to diminish to a low point that occurs near the peak of the fire. As the fire burns out and the temperature of the metal decreases, the strength is regained and as a result stress values rise. Figures 5-28 and 5-29 provide average von Mises stress values at critical locations during the entirety of the fire simulations for both the 8-story and 16-story models.

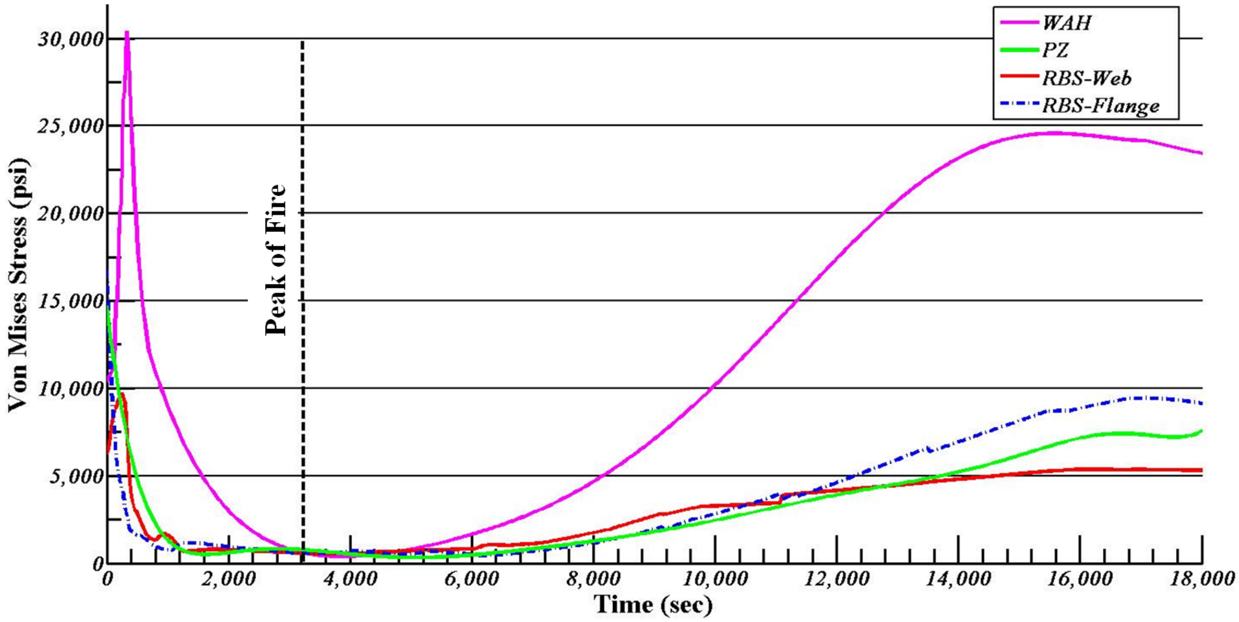

Figure 5-28. Average Von Mises Stress Values at Critical Locations for 8-Story Post-Earthquake Fire Simulation

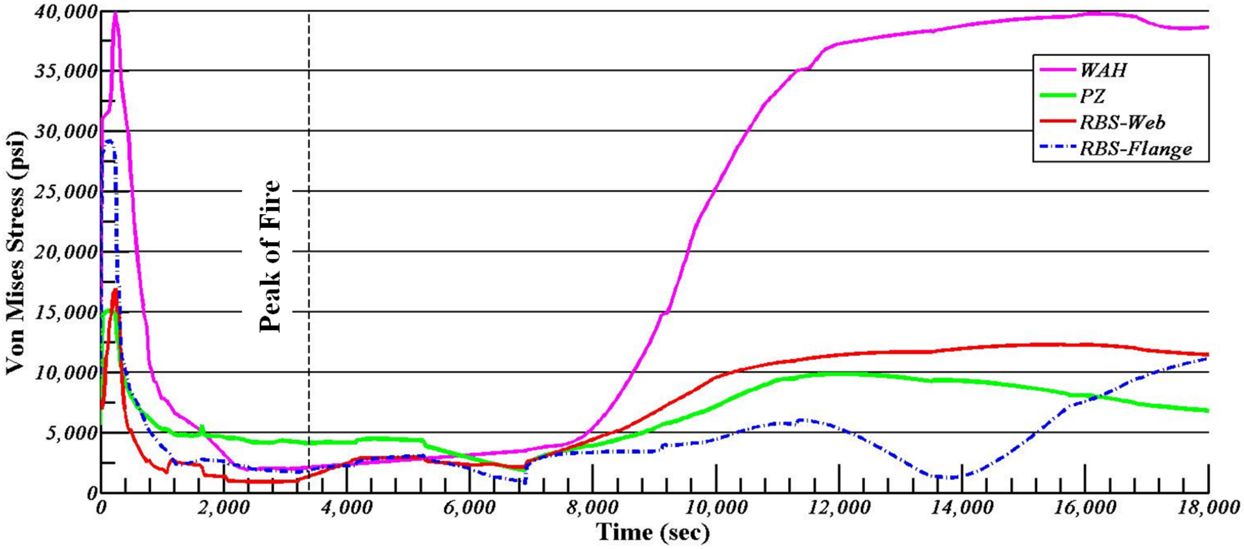

Figure 5-29. Average Von Mises Stress Values at Critical Locations for 16-Story Post-Earthquake Fire Simulation

Since the majority of structural damage during a fire is a result of the expansion and contraction of members the axial loads experienced during the fire are of particular importance. Values seen in both the 16-story and 8-story subassembly beams and columns are presented in Figures 5-30 and 5-31, respectively. These plots highlight the fact that relatively little demand was imposed on the 8-story subassembly during the fire. However, the 16-story subassembly experienced very high axial forces in both the beam and column members. When examining the axial loads in the beam it can be seen that very large values are produced during the early portion of the heating phase, but maximum demand does not occur until later into the cooling phase of the fire.

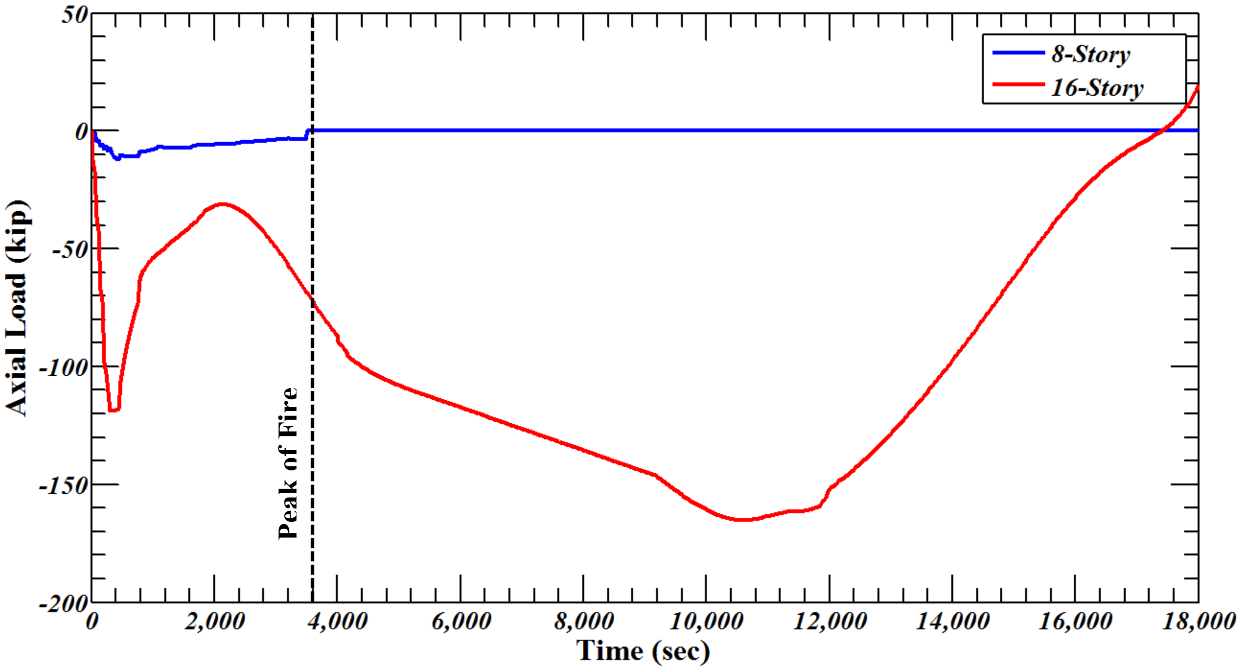

Figure 5-30. Average Beam Axial Load During Post-Earthquake Fire

A much different behavior is observed in the columns of the 16-story subassembly than in the beams. The peak axial force is reached near the end of the heating phase with relatively little demand seen during the cooling phase of the fire.

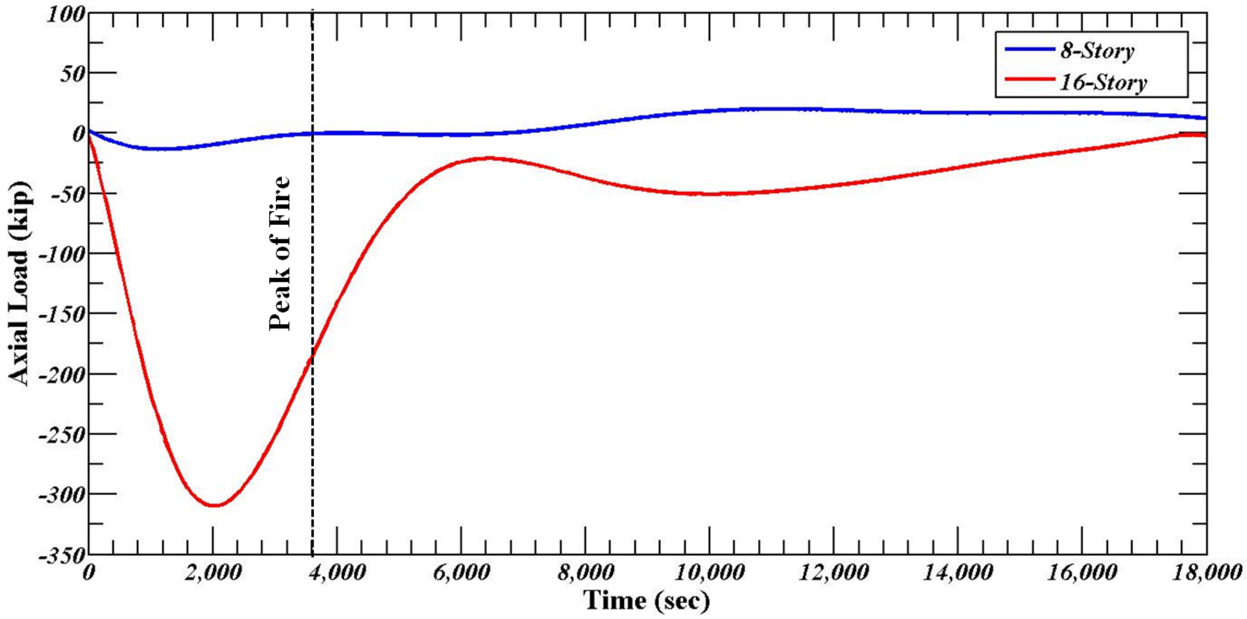

Figure 5-31. Average Column Axial Load During Post-Earthquake Fire

5.2 Combined Axial and Moment Loads

The structural demand imposed on beam and column members during a fire often create axial and flexural loading that is not considered during the design process. These loads can combine to create structural failures that are very difficult to predict based on the current prescriptive design methodology used for structural fire engineering. The design of members subjected to simultaneous axial force and flexure is based on Chapter H of the AISC Steel Manual (AISC 2012). This chapter presents a simplified interaction curve that was developed to ensure members are able to withstand the combined forces, the curve is based on the following AISC equations:

$$
\begin{aligned}
&For\ \frac{P_r}{P_c} \geq 0.2 \\
&\qquad \frac{P_r}{P_c} + \frac{8}{9}\left(\frac{M_{rx}}{M_{cx}} + \frac{M_{ry}}{M_{cy}}\right) \leq 1.0 \\
&For\ \frac{P_r}{P_c} < 0.2 \\
&\qquad \frac{P_r}{2P_c} + \left(\frac{M_{rx}}{M_{cx}} + \frac{M_{ry}}{M_{cy}}\right) \leq 1.0
\end{aligned}
\qquad \text{(Equation 5-2)}
$$

Where,

P_r is the required axial compressive strength
P_c is the available axial compressive strength
M_r is the required flexural strength
M_c is the available flexural strength

It can be seen that the beam-column interaction equation includes both the required axial forces and moments, and the available capacities based on member sizing. For this study the required axial forces and moments were taken as the actual forces observed during the simulations to determine if the demand exceeded the design strength. Furthermore, the available capacity of the members changes throughout the fire as material degradation occurs. In order to determine the available strength based on the AISC guidelines the average nodal temperatures of the member at the cross section where the highest flexural demand occurred was taken and the available strength based on the determined temperature at that point in the analysis calculated. These values were then plotted for both the fire simulations as well as the FFE simulations along with the AISC interaction curve for comparison. This can be seen in Figures 5-32 and 5-33, respectively. For the purpose of the fire simulations, the 8-story model was excluded since the imposed demand was found to be insignificant. The demand imposed during the 16-story fire simulations proved excessive with values reaching up to twice the calculated capacity for axial loading. Maximum values for each phase of the fire for both the beam and column are provided below.

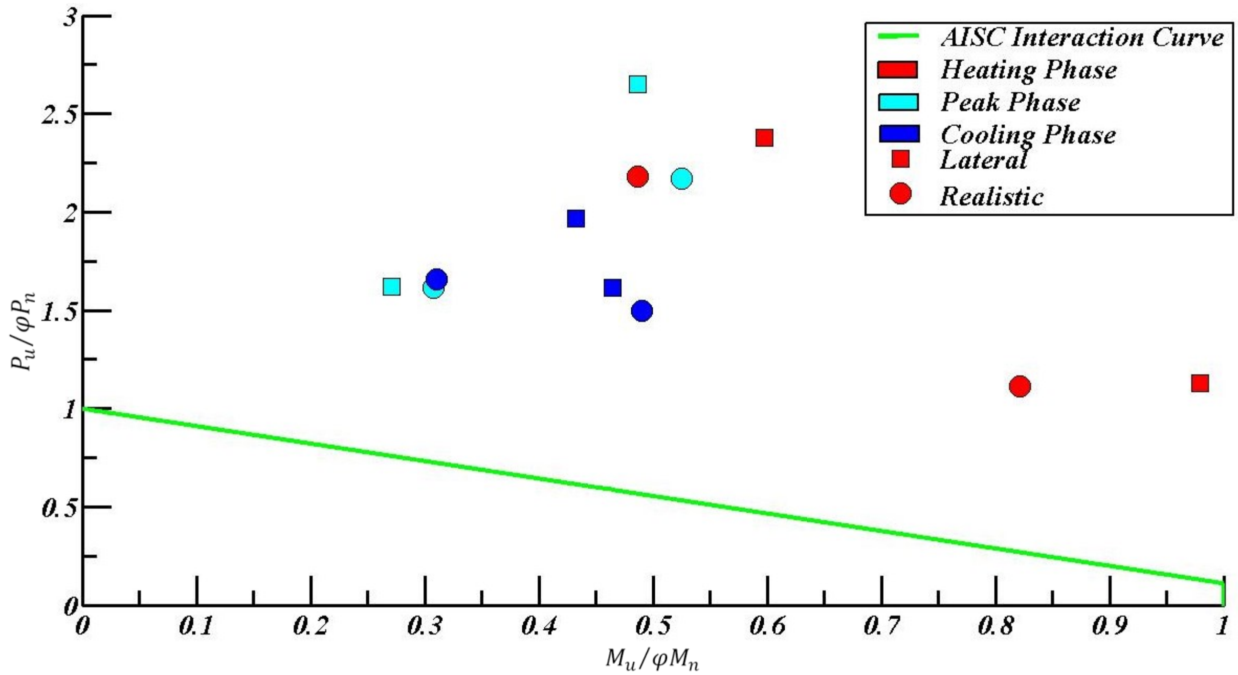

Figure 5-32. Comparison of Results to AISC Design Specifications for Members Subjected to Flexural and Axial Forces for 16-Story Fire Simulations

The axial and flexural demand during the FFE simulations for both the beam and column members of the 8-story and 16-story models are plotted against the AISC interaction curve in Figure 5-33. It can be seen that the demand imposed on the 8-story subassembly during the entirety of the simulations fell within the bounds of the interaction curve, as did the demand imposed on the 16-story subassembly during the earthquake portion of the simulations. However, the demand created during the fire portion of the FFE analyses proved excessive, particularly the axial forces, and fall outside the bounds of the interaction curve.

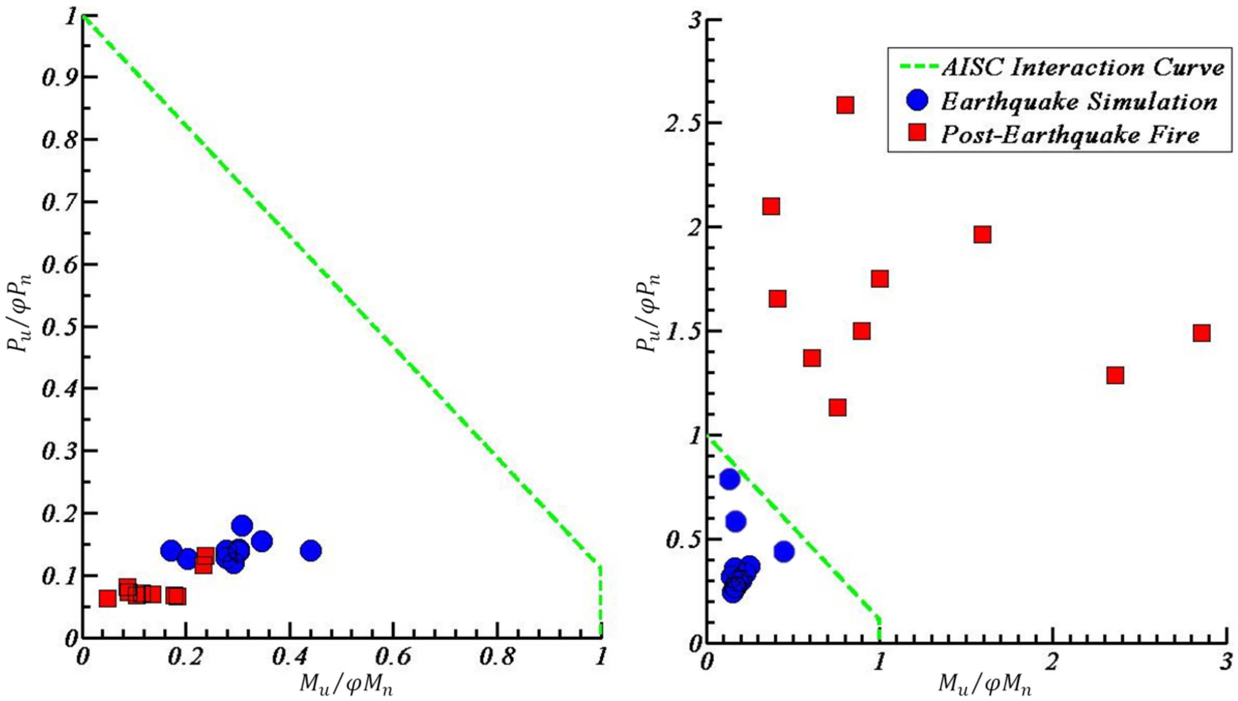

Figure 5-33. Comparison of Results to AISC Design Specifications for Members Subjected to Flexural and Axial Forces for 8-Story (left) and 16-Story (right) FFE Simulations

5.3 Summary

In this chapter, the response of two beam-column subassemblies exposed to fire and fire following an earthquake was presented. The parameters discussed included observed damage patterns, von Mises stresses in critical regions of the connection, rupture index values seen during the earthquake and fire simulations, and the magnitude of axial demand imposed on the beams and columns during the fire. In addition, the imposed demand on the subassemblies when exposed to fire as well as FFE are compared to the nominal strength values specified by the AISC steel construction manual (AISC, 2012). A summary of conclusions that can be taken from these results as well as recommendations based on this study are presented in the following chapter.

CHAPTER 6
SUMMARY, CONCLUSIONS AND RECOMMENDATIONS

6.0 Overview

The primary objective of this research was to expand the knowledge base on the behavior of steel moment resisting connections during exposure to fire as well as fire following an earthquake (FFE). In this thesis, a numerical study on the mechanical response of steel moment-resisting connections with reduced beam sections (RBS) during fire as well as FFE was presented. A new methodology for the evaluation of moment-resisting connections subjected to both events is proposed and implemented. The methodology includes conducting thermal analysis to determine probable temperature distributions during a representative fire, performing global-level frame analysis to determine the expected seismic behavior of the structure and define constraint demands on beam-column subassemblies during the fire, and finally detailed mechanical simulations of beam-column subassemblies during fire and FFE. This chapter provides a summary of the study, conclusions that can be drawn from the research, recommendations based on the findings of the project as well as suggestions for additional work that should be performed.

6.1 Summary of Study

The following section provides a brief overview of the research tasks performed for the study.

- Two moment resisting frames designed for the Los Angeles region were selected to be analyzed during a fire as well as a fire following an earthquake. The test structures are representative of typical office buildings located in California and are 8-stories and 16-stories in height.

- The lateral force resisting system for the test structures both consisted of perimeter steel special moment frames with welded beam-column connections with reduced beam sections. Performance requirements and detailing standards for the frames and connections were checked based on the guidelines of IBC-06 (IBC, 2006), ASCE/SEI 7-05 (ASCE/SEI, 2005), and ANSI/AISC (2005a, 2005b, 2005c).
- The design-basis seismic hazards for the structure were determined based on the guidelines of IBC-06 and ASCE/SEI 7-05. Gravity load demands for the dynamic simulation were based on the expected (or probable) load case presented in IBC-06 (IBC, 2006).
- An suite of ten earthquake ground motions records was created from the PEER-NGA database (PEER-NGA, 2011) using the guidelines in FEMA P695. Normalization and scaling of the records was performed following the guidelines of FEMA P695.
- A compartment fire model was selected from the work of Garlock (2008) to be used for the fire simulation.
- Temperature dependent material properties for A992 steel were implemented based on the suggestions of Eurocode 3 (EC3, 2005). A damage model based on the work of Johnson and Cook (1983) was also incorporated.
- Fire protection was neglected during the fire simulations and damage to passive fire protection during the FFE simulations was assumed based on the work of Braxtan and Pessiki (2009, 2011a, 2011b).
- A nonlinear dynamic response model for each lateral force resisting frame was developed in the finite element software ABAQUS (ABAQUS, 2012) to study the seismic response and constraint properties of the system. The structures were idealized as half-system

submodels composed of a nonlinear lateral resisting frame connected to a leaning column substructure. Panel zone behavior, reduced beam sections and inherent damping were all included in the models.

- Beam-column subassemblies from each frame were selected to be analyzed in detail. High-fidelity models were developed for both of the selected joints in the nonlinear finite element software ABAQUS (ABAQUS, 2012). These models were used to study transient heat flow and mechanical response during exposure to fire and FFE. A sequentially coupled thermomechanical analysis was used to perform the fire simulations and a displacement controlled stress analysis was utilized for the earthquake evaluation.
- Time dependent mechanical boundary condition models were developed to evaluate the influence of various levels of restrained thermal expansion on the response of the selected beam-column subassemblies during fire exposure. Three boundary condition cases were evaluated to determine the effect of the constraint on the subassemblies.

6.2 Conclusions

It is clear that predicting the force and deformation demands on beam-column subassemblies in fire and FFE is complex and is affected by many variables. Some preliminary conclusions that can be made from these analyses are as follows:

- Elastic modulus and yield stress of the critical regions not directly exposed to the fire were reduced to 8% and 9% of their values at normal ambient temperature for the 8-story fire models, 12% and 14% for the 16-story fire models, 10% and 11% for the 8-story FFE models and 14% and 16% for the 16-story FFE models.

- Very large axial forces can develop in beams during a fire. These forces are then transmitted through the beam-column connection, which is concerning since this is not accounted for in room temperature design, where shear forces and rotational demand are typically what control the connection design.
- Axial force in the beam, which is transmitted to the connection, is typically compressive in the early stages of a fire due to thermal expansion of the beam. The peak axial compression force can occur very early in a fire. Early in the fire, the beam has not yet become sufficiently hot to experience a significant reduction in modulus of elasticity or yield strength, and therefore maintains a high axial stiffness. Although reductions in strength do not occur until temperatures of several hundred degrees Fahrenheit are reached, thermal expansion starts immediately with the increase of temperature. The combination of thermal expansion and high axial stiffness in the early stages of a fire results in large compressive forces early in the heating. The analyses conducted showed that high axial compressive forces often occur at temperatures as low as 200 to 400°F.
- As heating of the beam continues, the compression force reduces as the beam loses stiffness and as the beam begins to sag. The axial force can turn into tension as heating continues and the beam sags and develops catenary action.
- The magnitude of the compression appears to be limited by the local buckling capacity of the beam at elevated temperatures. During the cooling phase of the fire and after complete cool down, very large tensile forces can develop in the beam, column and the connection, which in theory could cause connection failure. Significant residual forces and deformations may remain in the beam and column after a fire.

- The structural response of steel beams, columns and connections during the event of a fire as well as FFE can be predicted with reasonable accuracy using finite element analysis. When subjected to fire, steel elements can undergo very large deformations and experience yielding at low load levels. Consequently, predicting the elevated temperature structural response of steel members and connections generally requires consideration of nonlinear geometry, inelasticity, and temperature dependent nonlinear material properties. These factors can be accommodated by advanced finite element programs such as ABAQUS, which was used in this study. These capabilities, however, are generally not available in commercial structural analysis software typically used for building design. This likely represents a barrier to the more widespread use of engineered structural fire safety solutions for most building design applications.

6.3 Recommendations

In this study numerical investigations were carried out to evaluate the performance of moment resisting connections with RBS under fire and post-earthquake fire exposure. The results of the study highlight the significance of including realistic boundary conditions during fire simulations and points towards their being a substantial potential for extensive damage to occur in unprotected steel frames during fire as well as protected steel frames during fire following an earthquake. Based on these findings recommendations are presented on design implications, future research and potential improvements to the current study.

6.3.1 Design Implications

The results of these analyses, although preliminary, raise some concerns about structural-fire safety approaches used in current practice, particularly in highly seismic regions. Current U.S. practice for structural-fire safety relies on testing of structural components at elevated temperature according to the requirements of ASTM E119 (ASTM 2000). Based on these analyses, there may be several shortcomings of the E119 testing approach. First, ASTM E119 does not require testing of connections. It only requires testing of structural members (beams, girders, columns, etc.). Consequently, the performance of connections in fire is not explicitly addressed in U.S. building codes. Secondly, the standard ASTM E119 fire exposure does not include the cooling stage of a fire. As is clear from the analyses conducted in this study the cooling stage can be the most demanding phase of a fire, and failure can occur during cooling. Finally, a primary criterion for determining the amount of fireproofing required for a beam according to ASTM E119 is to limit the temperature of the beam to about 600 °F. This is based on the assumption that the beam will retain sufficient strength at this temperature to maintain support of gravity loads. However, as shown by these analyses, very large forces are developed at temperatures well below 600 °F. Consequently, even though a beam is insulated to satisfy the ASTM E119 testing criteria, they may still be vulnerable to failure when subjected to fire. This is further exacerbated by the likelihood of insulation spalling and debonding during a seismic event leaving the structural member directly exposed to the high temperatures of fire. Overall, there is reason to question the adequacy and safety of current U.S. building code requirements when it comes to structural fire design.

In terms of developing improved design practices for structural-fire safety of steel buildings, developing simplified methods for estimating force and deformation demands represents an important need. In this research, the forces and deformations developed during a fire and a fire following an earthquake were estimated by using very detailed three-dimensional finite element models. This approach is impractical for routine design practice. Considerable supplementary work is needed to develop approaches for evaluating structural performance in fire that is suitable for design practice.

6.3.2 Future Work

Based on the findings of this study, several areas have been identified where supplementary research could provide useful information. Future work directions should include the following:

- Further work is needed in developing a uniform definition of yield strength of steel at elevated temperatures. Because steel loses its characteristic yield plateau at elevated temperature, defining yield strength becomes more subjective. The literature review indicated that previous researchers as well as building standards have used a variety of different definitions of yield strength. This can lead to significantly different values of yield strength for the same stress-strain curve.
- A factor that introduces considerable uncertainty in heat transfer analysis of steel members subjected to fire is the lack of data on temperature dependent thermal properties of commercially available insulation materials, including spray applied fire resistive materials, gypsum board, fiber board, intumescent coatings, etc. The data needed includes thermal conductivity, specific heat capacity, and density. These properties are needed

over the full range of temperatures of interest in structural-fire engineering analysis, which typically goes up to about 1800 °F.

- Large-scale cyclic tests of SFRM insulated beam-column subassemblies should be performed to evaluate the seismic performance of thermal insulation in beam-column connections with reduced beam sections.
- Additional numerical studies of entire building system response during post-earthquake fire exposure, considering various building configurations, seismic hazard levels, and fire exposure conditions should be conducted. The interaction of temperature effects in the gravity frames, floor system, and the lateral force resisting elements should be addressed, including temperature-induced large displacement response in the floor system, temperature-induced softening of moment-frame and gravity-frame beam-column connections, and dynamic impact from falling debris.
- Simpler analysis techniques are needed to evaluate the adequacy of connections in buildings subjected to fire. Considerable additional work is needed to develop simpler approaches for connection evaluation under fire conditions that are suitable for design practice.

6.3.3 Research Improvements

Based on the findings of this research, several issues have been identified where improvements to the study can be made. Future work directions should include the following:

- The models require further validation before results can be trusted and recommendations implemented. This should include a combination of experimental testing and more numerical simulations.

- One of the key factors not included in the analysis was explicit modeling of fracture phenomena in the connection. The occurrence of fracture in the members could be approximately inferred from predictions of very large localized deformations in an element. However, the behavior of the subassembly after the onset of fracture could not be accurately predicted by the finite element models developed for this research.
- The subassemblies and frames investigated included only bare steel with no concrete slab. The effect of the concrete slab on the behavior of the structure should be investigated since the slab will affect the location of the neutral axis in the connection, which will likely change the onset of yielding. Furthermore, the concrete slab covering the beams top flange has the potential to act as a heat sink, absorbing energy from the beam during the heating phase which could affect the thermal analysis results.
- A parametric study should be implemented to gain a better understanding on the effect of the various components in the model. This should include various fire scenarios as well as different fire locations throughout the frame, different connection configurations that are common in highly seismic regions, and varying material properties.
- A more realistic thermal analysis that incorporates the convection and radiation heat transfer mechanisms should be implemented. This simulation should include the passive fire protection expected to be on the beams and columns as well as the concrete slab supported by the beams. This model should then be calibrated based on experimental data on steel temperatures observed during various fire tests to assure accurate results.
- Global behavior of the frame during the fire portion of the simulations should be evaluated to assure that no critical response behavior is being missed. For instance, it is common to see partial or total collapse of beams and floor systems during a fire causing

load distribution to change throughout the structure. This is not something that is captured with the subassembly models.

- High-temperature creep should be included in the material model since it has been shown to have a significant influence on the fire resistance of steel structures. Despite its significance, high temperature creep in structural steel is not explicitly accounted for in stress-strain relationships and thus wasn’t incorporated into the models in this study. In some situations neglecting this might lead to unconservative fire resistance predictions. Furthermore, no data exists on temperature dependent material properties of steel during the cooling phase of a fire causing researchers to assume the same properties as the heating phase. This may prove unconservative and should be updated with more realistic material models once available.

REFERENCES

Aasen, B. “An experimental study on steel columns behaviour at elevated temperatures.” (1985)The Norwegian Inst. of Technol., Trondheim, Norway.

ABAQUS *v6.11*, (2012). Dassault Systems, Providence, RI. (www.simulia.com).

Adan, Scott M. and Reaveley, Lawrence D. “The Reduced Beam Section Moment Connection without Continuity Plates” (2004)13th World Conference of Earthquake Engineering

Alavi, Babak, and Helmut Krawinkler. "Consideration of near-fault ground motion effects in seismic design." (2000) Proceedings of the 12th World Conference on Earthquake Engineering.

Ali, F. A., D. O'Connor, and A. Abu-Tair. "Explosive spalling of high-strength concrete columns in fire." Magazine of Concrete Research 53.3 (2001): 197-204.

Ali, Faris A., et al. "The effect of axial restraint on the fire resistance of steel columns." Journal of Constructional Steel Research 46 (1998): 305-306.

Al-Jabri, Khalifa Saif, et al. "Behaviour of steel and composite beam-column connections in fire." Journal of Constructional Steel Research 46.1 (1998): 308-309.

Anderson, J. and Duan, X. “Repair/Upgrade Procedures for Welded Beam to Column Connections” (PEER 98/03). Pacific Earthquake Engineering Research Center, May (1998)

ANSI/AISC 341-05: “Seismic Provisions for Structural Steel Buildings.” (2005a). American Institute of Steel Construction, Chicago, IL.

ANSI/AISC 358-05: “Prequalified Connections for Special and Intermediate Steel Moment Frames for Seismic Applications.” (2005b) American Institute of Steel Construction, Chicago, IL.

ANSI/AISC 360-05: “Specification for Structural Steel Buildings.” (2005c). American Institute of Steel Construction, Chicago, IL.

ASCE/SEI 7-05: “Minimum Design Loads for Buildings and Other Structures.” (2005). American Society of Civil Engineers, Reston, VA.

ASTM A992/A992M-11. American Society of Testing and Materials (ASTM), (2011)West Conshohocken, PA.

ASTM E119-00a: “Standard Test Methods for Fire Tests of Building Construction and Materials.” (2000a). American Society of Testing and Materials (ASTM), West Conshohocken, PA.

ASTM E736-00: “Standard Test Method for Cohesion/Adhesion of Sprayed Fire-Resistive Materials Applied to Structural Members.” (2000b). American Society of Testing and Materials (ASTM), West Conshohocken, PA.

Atila Zekioglu, S. E., et al. "Designing after Northridge." Modern Steel Construction (1997).

AutoCAD v2012. (2012). Autodesk, San Rafael, CA. (www.autodesk.com).

Baker, Jack W. "Quantitative classification of near-fault ground motions using wavelet analysis." Bulletin of the Seismological Society of America 97.5 (2007): 1486-1501.

Barnett, C. R. "BFD curve: a new empirical model for fire compartment temperatures." Fire Safety Journal 37.5 (2002): 437-463.

Beitel, Jesse J., and Nestor Iwankiw. “Analysis of needs and existing capabilities for full-scale fire resistance testing.” US Department of Commerce, National Institute of Standards and Technology, (2002).

Bhowmick, Madan, and Satish Chandra Bera. "An approach to optimum combustion control using parallel type and cross-limiting type technique." Journal of Process Control (2011).

Brandow, Gregg, et al. "AN ALTERNATIVE PROCEDURE FOR SEISMIC ANALYSIS AND DESIGN OF TALL BUILDINGS LOCATED IN THE LOS ANGELES REGION." (2008)

Braxtan, N.L. (2009). “Post-Earthquake Fire Performance of Steel Moment-Frame Building Columns”, PhD Dissertation, Department of Civil and Environmental Engineering, Lehigh University, Bethlehem, PA.

Braxtan, N.L. and Pessiki, S. (2011a), “Bond Performance of SFRM on Steel Plates Subjected to Tensile Yielding”, Journal of Fire Protection Engineering, Vol. 21(1), pp. 37-55.

Braxtan, N.L. and Pessiki, S. (2011b), “Postearthquake Fire Performance of Sprayed Fire-Resistive Material on Steel Moment Frames”, Journal of Structural Engineering, American Society of Civil Engineers, Vol. 137, No. 9, pp. 946-953.

British Steel. (1999). “The Behavior of Multi-Storey Steel Framed Buildings in Fire”, (1999). STC Technical Report, Swinden Technology Centre, Rotherham, South Yorkshire, UK.

BS EN 1991-1-2:2002. Eurocode 1: actions on structures: Part 1–2 General actions—structures exposed to fire; 2002.

California Building Code. (2010). California Building Standards Commission, Sacramento, CA.

Chambers, Janice J., Shaheed Almudhafar, and Frank Stenger. "Effect of reduced beam section frame elements on stiffness of moment frames." Journal of Structural Engineering 129.3 (2003): 383-393.

Chen, J., Young, B., and Uy, B. _2006_. “Behavior of high strength structural steel at elevated temperatures.” J. Struct. Eng., 132_12_, 1948–1954.

Chen, S.J., Yeh, C.H. and Chu, J.M, "Ductile Steel Beam-to-Column Connections f or Seismic Resistance," Journal of Structural Engineering, Vol. 122, No. 11, November 1996, pp. 1292-1299.

Cheol-Ho Lee, Jae-Hoon Kim, Seismic design of reduced beam section steel moment connections with bolted web attachment, Journal of Constructional Steel Research, Volume 63, Issue 4, April 2007, Pages 522-531, ISSN 0143-974X, 10.1016/j.jcsr.2006.06.030.

Chi, Brandon, and Chia-Ming Uang. "Cyclic response and design recommendations of reduced beam section moment connections with deep columns." Journal of Structural Engineering 128.4 (2002): 464-473.

Choe, Lisa, et al. "Fundamental Behavior of Steel Beam-Columns and Columns under Fire Loading: Experimental Evaluation." Journal of Structural Engineering 137.9 (2011): 954-966.

Cooke, G. M. E. "An introduction to the mechanical properties of structural steel at elevated temperatures." Fire safety journal 13.1 (1988): 45-54.

Corley, Gene. World Trade Center building performance study: data collection, preliminary observations, and recommendations. Federal Emergency Management Agency, 2002.

Cousins, W., and W. Smith. "Estimated losses due to post-earthquake fire in three New Zealand cities." Proceedings, New Zealand Society of Earthquake Engineering Conference. 2004.

D.T. Pachoumis, E.G. Galoussis, C.N. Kalfas, I.Z. Efthimiou, Cyclic performance of steel moment-resisting connections with reduced beam sections — experimental analysis and finite element model simulation, Engineering Structures, Volume 32, Issue 9, September 2010, Pages 2683-2692, ISSN 0141-0296, 10.1016/j.engstruct.2010.04.038.

Dai, X. H., Y. C. Wang, and C. G. Bailey. "Numerical modelling of structural fire behaviour of restrained steel beam–column assemblies using typical joint types." Engineering Structures 32.8 (2010): 2337-2351.

Della Corte, G., B. Faggiano, and F. MAZZOLANI. "On the structural effects of fire following an earthquake." Improvement of Building's Structural Quality by new Technologies-COST C12 Final Conference Proceedings, Taylor and Francis, London. 2005.

Della Corte, G., R. Landolfo, and F. M. Mazzolani. "Post-earthquake fire resistance of moment resisting steel frames." Fire Safety Journal 38.7 (2003): 593-612.

Dharma, Ronny Budi, and Kang-Hai Tan. "Rotational capacity of steel I-beams under fire conditions Part II: Numerical simulations." Engineering structures 29.9 (2007): 2403-2418.

DiNenno, Philip J. SFPE handbook of fire protection engineering. Quincy, MA: National Fire Protection Association, 1988.

EC1: Actions on Structures – Part 1.2: General Actions – Actions on Structures Exposed to Fire. (2002). British Standards Institution, London, UK.

Engelhardt, M.D. and Venti, M., Unpublished preliminary test reports for SAC Phase 2 tests, University of Texas at Austin, 1999. "

Engelhardt, M.D., Winneberger, T., Zekany, A.J. and Potyraj, T.J., "Experimental Investigation of Dogbone Moment Connections," Proceedings; 1997 National Steel Construction Conference, American Institute of Steel Construction, May 7-9, 1997, Chicago.

Engelhardt, M.D., Winneberger, T., Zekany, A.J. and Potyraj, T.J., "The Dogbone Connection, Part II, Modem Steel Construction, August 1996.

Engelhardt, Michael D., et al. "Behavior and design of radius-cut, reduced beam section connections." Rep. No. 00/17, SAC, Sacramento, Calif. (2000).

Englehardt, M. D., et al. "Experimental investigation of dogbone moment connections." American Institute of Steel Construction, Inc.(USA), (1997): 12.

European Committee for Standardization. _2005_. "General rules—Structural fire design, EN1993-1-2." Eurocode 3, Brussels.

Faggiano, B., and D. Gregorgio. "Assessment of the robustness of structures subjected to fire following earthquake through a performance-based approach." Urban habitat constructions under catastrophic events (2010).

Faggiano, B., et al. "Fire analysis on steel portal frames damaged after earthquake according to performance based design." Urban Habitat Constructions under Catastrophic Events, COST C26 Workshop, Prague, Czech Republic. 2007.

Faggiano, B., et al. "Post-earthquake fire resistance of moment resisting steel frames." Proceedings of the Eurosteel Conference on Steel and Composite Structures, Maastricht, The Netherlands. 2005.

Faggiano, B., M. Esposto, and F. M. Mazzolani. "Risk assessment of steel structures under fire." Proc. 14th World Conference on Earthquake Engineering, Beijing, PR of China, paper. No. S19-015. 2008.

Feasey, Roger, and Andrew Buchanan. "Post-flashover fires for structural design." Fire Safety Journal 37.1 (2002): 83-105.

Federal Emergency Management Agency (FEMA 461). "Interim Testing Protocols for Determining the Seismic Performance Characteristics of Structural and Nonstructural Components." (2007).

FEMA 350: Recommended Seismic Design Criteria for New Steel Moment-Frame Buildings. (2000). Federal Emergency Management Agency, Washington, D.C.

FEMA, P. "695. Quantification of Building Seismic Performance Factors." Federal Emergency Management Agency: Washington DC (2009).

Franssen, Jean-Marc, et al. "Stability of steel columns in case of fire: experimental evaluation." Journal of structural engineering 124.2 (1998): 158-163.

Fry, G., Unpublished preliminary test reports for SAC Phase 2 tests, Texas A & M University, 1999.

Fu, Qiang, and Charles Menun. "Seismic-environment-based simulation of near-fault ground motions." Proc. 13th World Conference on Earthquake Engineering. 2004.

Garlock, Maria E. Moreyra, and Spencer E. Quiel. "The behavior of steel perimeter columns in a fire." Proceedings of the 2005 Structures Congress and the 2005 Forensic Engineering Symposium, New York. 2005.

Gilton, Chad S., and Chia-Ming Uang. "Cyclic response and design recommendations of weak-axis reduced beam section moment connections." Journal of Structural Engineering 128.4 (2002): 452-463.

Grubbs, Kristin Victoria. The effect of the dogbone connection on the elastic stiffness of steel moment frames. Diss. University of Texas at Austin, 1997.

Haselton, C. B., et al. "Selecting and scaling earthquake ground motions for performing response-history analysis." Proceedings of the 15th World Conference on Earthquake Engineering. 2012.

International Building Code. (2006). International Code Council, Inc., Country Club Hills, IL.

ISO. (1975). ‘‘Fire resistance tests-elements of building construction.’’ International Standard ISO 834, Geneva.

Iwankiw, N. R., and J. Mohammadi. "Elastic in-plane stiffness for a circular cut reduced beam section (RBS)." ENGINEERING JOURNAL-AMERICAN INSTITUTE OF STEEL CONSTRUCTION 41.1 (2004): 23-36.

Iwankiw, N.R., and Carter, C., "The Dogbone: A New Idea to Chew On," Modern Steel Construction, April 1996.

Janss, J. , and Minne, R. (1982). “Buckling of steel columns in fire conditions.” Fire Safety J. , 4 (4), 227–235.

Jin, Jun, and Sherif El-Tawil. "Seismic performance of steel frames with reduced beam section connections." Journal of Constructional Steel Research 61.4 (2005): 453-471.

Jones, Scott L., Gary T. Fry, and Michael D. Engelhardt. "Experimental evaluation of cyclically loaded reduced beam section moment connections.” Journal of Structural Engineering 128.4 (2002): 441-451.

Keller, Wesley J., and Stephen Pessiki. "Effect of earthquake-induced damage to spray-applied fire-resistive insulation on the response of steel moment-frame beam-column connections during fire exposure." Journal of Fire Protection Engineering 22.4 (2012): 271-299.

Kelly, Elizabeth J., and Raymond N. Tell. "A Method for Evaluating Fire After Earthquake Scenarios for Single Buildings." (2011).

Kim, Kee-Dong, and Michael D. Engelhardt. "Nonprismatic beam element for beams with RBS connections in steel moment frames." Journal of Structural Engineering 133.2 (2007): 176-184.

Kirby, B. R., and Preston, R. R. _1988_. “High temperature properties of hot-rolled, structural steels for use in fire engineering design studies.” Fire Saf. J., 13, 27–37.

Kitjasateanphun, T., et al. "Inelastic analysis of steel frames with reduced beam sections." The Structural Design of Tall Buildings 10.4 (2001): 231-244.

Kochalski, Gregory, and Jason Ericksen. "Steelwise-Prequalified Seismic Moment Connections-Here's a visual summary of the seismic requirements for two prequalified moment connections." Modern Steel Construction 47.1 (2007): 55.

Kodur, Venkatesh, Mahmud Dwaikat, and Rustin Fike. "High-temperature properties of steel for fire resistance modeling of structures." Journal of Materials in Civil Engineering 22.5 (2010): 423-434.

Lars, Bostrom. "Time-temperature Curves." Time-temperature Curves. SP, n.d. Web. 03 Jan. 2013. <http://www.sp.se/en/index/services/firetest_building/fire_constructions/fireresist/timetemperature/Sidor/default.aspx>.

Lee, Cheol-Ho, et al. "Effects of panel zone strength and beam web connection method on seismic performance of reduced beam section steel moment connections." Journal of Structural Engineering 131.12 (2005): 1854-1865.

Lee, Kihak, and Douglas A. Foutch. "Performance evaluation of damaged steel frame buildings subjected to seismic loads." Journal of Structural Engineering 130.4 (2004): 588-599.

Lee, Selina, et al. "Fire following earthquake—Reviewing the state-of-the-art of modeling." Earthquake Spectra 24.4 (2008): 933-967.

Li, G.-Q., Jiang, S.-C., Yin, Y.-Z., Chen, K., and Li, M.-F. _2003_. “Experimental studies on the properties of constructional steel at elevated temperatures.” J. Struct. Eng., 129_12_, 1717–1721.

Li, Guo-Qiang, and Shi-Xiong Guo. "Experiment on restrained steel beams subjected to heating and cooling." Journal of Constructional Steel Research 64.3 (2008): 268-274.

Lie, T. T., and K. H. Almand. "A method to predict the fire resistance of steel building columns." Engineering Journal 27.4 (1990): 158-167.

Lim, L., A. Buchanan, and P. Moss. "Experimental testing and numerical modelling of two-way concrete slabs under fire conditions." Journal of the Structural Engineering Society 15.2 (2002): 12-26.

Liu, T. C. H., M. K. Fahad, and J. M. Davies. "Experimental investigation of behaviour of axially restrained steel beams in fire." Journal of Constructional Steel Research 58.9 (2002): 1211-1230.

Ma, Zhongcheng, and Pentti Mäkeläinen. "Parametric temperature–time curves of medium compartment fires for structural design." Fire Safety Journal 34.4 (2000): 361-375.

Mesquita, L. M. R., et al. "Experimental and numerical research on the critical temperature of laterally unrestrained steel I beams." Journal of Constructional Steel Research 61.10 (2005): 1435-1446.

Meyer, Peter. "Other Fires in Steel-Structure Buildings." Serendipity. Serendipity, 15 Feb. 2012. Web. 03 Jan. 2013. <http://www.serendipity.li/wot/other_fires/other_fires.htm>.

Milke, James. "An Overview of Fire Protection in Buildings." (2002).

Moncada, Jaime A. "Fire Unchecked." NFPA. NFPA Journal, Mar.-Apr. 2005. Web. 26 May 2012.

Moore, Kevin S., James O. Malley, and Michael D. Engelhardt. Design of Reduced Beam Section (RBS) moment frame connections. Steel Committee of California, 1999.

Newman, G. M. "Structural fire engineering investigation of Broadgate phase 8 fire." Steel Construction Institute, Ascot (1991).

Newman, Gerald M., Jef T. Robinson, and Colin G. Bailey. Fire safe design: A new approach to multi-story steel-framed buildings. Steel Construction Institute, 2000.

NIST NCSTAR 1-3D: Mechanical Properties of Structural Steel, Federal Building and Fire Safety Investigation of the of the Work Trade Center Disaster. (2005). National Institute of Standards and Technology, Gaithersburg, MD.

NIST. (2011). Selecting and Scaling Earthquake Ground Motions for Performing Response-History Analyses (NIST GCR 11-917-15). National Institute of Standards and Technology, Gaithersburg, MD.

NIWA, HIRONORI. "Investigation of Windsor Building Fire in Spain." Report of Obayashi Corporation Technical Research Institute (CD-ROM) 70 (2006): 11-2.

Nouanegue, H. F., A. Muftuoglu, and E. Bilgen. "Heat transfer by natural convection, conduction and radiation in an inclined square enclosure bounded with a solid wall." International Journal of Thermal Sciences 48.5 (2009): 871-880.

Olesen, F. B. (1980). “Fire tests on steel columns.” Inst. of Build. Technol. and Struct. Engr., Aalborg, Denmark.

Outinen, J. (2007). “Mechanical properties of structural steels at high temperatures and after cooling down. ” Doctoral dissertation, Laboratory of Steel Structures Publications, Helsinki Univ. of Technology, Helsinki, Finland.

Pachoumis, D. T., et al. "Cyclic performance of steel moment-resisting connections with reduced beam sections—experimental analysis and finite element model simulation." Engineering Structures 32.9 (2010): 2683-2692.

Pacific Earthquake Engineering Research Center. “Tall Buildings Initiative: Guidelines for Performance Based Seismic Design of Tall Buildings”. (2010)

PEER-NGA Strong Ground Motion Database. (2011). (www.peer.berkeley.edu/nga/)

Plumier, A., "New Idea for Safe Structures in Seismic Zones," IABSE Symposium - Mixed Structures Including New Materials, Brussels, 1990.

Plumier, A., "The Dogbone: Back to the Future," Engineering Journal, American Institute of Steel Construction, Inc. 2nd Quarter 1997.

Popov, E.P., Yang, T.S. and Chang, S.P., "Design of Steel MRF Connections Before and After 1994 Northridge Earthquake," International Conference on Advances in Steel Structures, Hong Kong, December 11-14, 1996. Also in: Engineering Structures, 20(12), 1030-1038, 1998.

Quintiere, J. G. "Growth of fire in building compartments." Fire standards and safety, ASTM STP 614 (1977): 131-167.

Ren, A. Z., and X. Y. Xie. "The simulation of post-earthquake fire-prone area based on GIS." Journal of fire sciences 22.5 (2004): 421-439.

Ricles, J. M., et al. "Seismic performance of deep column-to-beam welded reduced beam section moment connections." Connections in Steel Structures V (2004).

Routley, J. Gordon, Charles Jennings, and Mark Chubb. "High-Rise Office Building Fire, One Meridian Plaza, Philadelphia, Pennsylvania." FEMA (Federal Emergency Management Agency) (1991).

Scawthorn, Charles R. The Shake Out Scenario Supplemental Study: Fire Following Earthquake. SPA Risk LLC, 2008.

Schaffer, E. L. "Structural fire protection." ASCE, 1992.

Selamet, Serdar, and Maria E. Garlock. "A Comparison between the Single Plate and Angle Shear Connection Performance under Fire." Structures Congress 2011. ASCE, 2011.

Selamet, Serdar, and Maria Garlock. "Guidelines for modeling three dimensional structural connection models using finite element methods." International Symposium: Steel Structures: Culture & Sustainability. 2010.

Shahi, Shrey K., and Jack W. Baker. "An empirically calibrated framework for including the effects of near-fault directivity in probabilistic seismic hazard analysis." Bulletin of the Seismological Society of America 101.2 (2011): 742-755.

Shen, J., T. Kitjasateanphun, and W. Srivanich. "Seismic performance of steel moment frames with reduced beam sections." Engineering Structures 22.8 (2000): 968-983.

Steel, British. "The behaviour of multi-storey steel framed buildings in fire." A European Joint Research Program (1999).

Steels, Prestressing. "Elevated-temperature tensile and creep properties of some structural and prestressing steels." Fire Test Performance: A Symposium Presented at the Winter Meeting, American Society for Testing and Materials, Denver, Colo., 2-7 Feb. 1969. Vol. 464. ASTM International, 1970.

Takagi, Jiro, and Gregory G. Deierlein. "Strength design criteria for steel members at elevated temperatures." Journal of Constructional Steel Research 63.8 (2007): 1036-1050.

Tan, Kang-Hai, and Zhen-Hai Qian. "Experimental behaviour of a thermally restrained plate girder loaded in shear at elevated temperature." Journal of Constructional Steel Research 64.5 (2008): 596-606.

Tremblay, R., Tchebotarev, N. and Filiatrault, A., "Seismic Performance of RBS Connections for Steel Moment Resisting Frames: Influence of Loading Rate and Floor Slab," Proceedings, Stessa '97, August 4-7, 1997, Kyoto, Japan.

Uang, C.M., Unpublished preliminary test reports for SAC Phase 2 RBS tests, University of California at San Diego, December 1998 and February 1999.

Uang, Chia-Ming, and Chao-Chin Fan. "Cyclic stability criteria for steel moment connections with reduced beam section." Journal of Structural Engineering 127.9 (2001): 1021-1027.

Usmani, A. S., et al. "Fundamental principles of structural behaviour under thermal effects." Fire Safety Journal 36.8 (2001): 721-744.

Vandamme, M., and Janss, J. (1981). “Buckling of axially loaded steel columns in fire conditions.” IABSE Periodica, 3/1981, 82–95.

Venture, SAC Joint. Recommended seismic design criteria for new steel moment-frame buildings. Federal Emergency Management Agency, 2000.

Villaverde, Juan Antonio Trilleros, Sonia Mato Díaz, and Irene Huertas González. "Temperature Field on Structural Carbon Steel under Fire Conditions." Journal of Materials Science and Engineering 1.6 (2011): 25-35.

Wang, Guojian, and Jiayun Yang. "Influences of glass flakes on fire protection and water resistance of waterborne intumescent fire resistive coating for steel structure." Progress in Organic Coatings 70.2 (2011): 150-156.

Wang, Y. C. "An analysis of the global structural behaviour of the Cardington steel-framed building during the two BRE fire tests." Engineering Structures 22.5 (2000): 401-412.

Wickstrom, U. "Comments on calculation of temperature in fire-exposed bare steel structures in EN 1993-1-2: Eurocode 3—design of steel structures—Part 1–2: general rules—structural fire design." Fire Safety Journal 40.2 (2005): 191-192.

Yassin, Hany, A. Bagachi, and Venkatesh Kodur. "Structural performance of stud walls under normal and post-earthquake fire exposure." Proc., Structures Congress. New York: ASCE, 2008.

Yin, Y. Z., and Y. C. Wang. "A numerical study of large deflection behaviour of restrained steel beams at elevated temperatures." Journal of Constructional Steel Research 60.7 (2004): 1029-1047.

Yin, Y. Z., and Y. C. Wang. "Analysis of catenary action in steel beams using a simplified hand calculation method, Part 1: theory and validation for uniform temperature distribution." Journal of Constructional Steel Research 61.2 (2005): 183-211.

Yu, Cheng, and Benjamin W. Schafer. "Distortional buckling tests on cold-formed steel beams." Journal of structural engineering 132.4 (2006): 515-528.

Yu, Qi Song, Chad Gilton, and Chia-Ming Uang. Cyclic response of RBS moment connections: Loading sequence and lateral bracing effects. Vol. 99. No. 13. Dept. of Structural Engineering, Univ. of California, San Diego, 2000.

Zehfuß, J., and D. Hosser. "A parametric natural fire model for the structural fire design of multi-storey buildings." Fire safety journal 42.2 (2007): 115-126.

Zekioglu, A., Mozaffarian, H., and Uang, C.M., "Moment Frame Connection Development and Testing for the City of Hope National Medical Center," Building to Last- Proceedings of Structures Congress XV, ASCE, Portland, April 1997.

Zekioglu, A., Mozaffarian, H., Chang, K.L., Uang, C.M. and Noel, S., "Designing After Northridge," Modem Steel Construction, March 1997.

Zhang, Xiaofeng, and James M. Ricles. "Seismic behavior of reduced beam section moment connections to deep columns." Journal of structural engineering 132.3 (2006): 358-367.

APPENDIX A

REDUCED BEAM SECTION MOMENT CONNECTIONS EXPERIMENTAL TESTING SUMMARY

Table A-1. Summary of Experimental Testing on RBS Moment Connections

Source	Specimen Label	Column	Beam	Beam Web Connection	Beam Flange Connection	RBS Design	θ_p (%)	Comments
Chen 1996	YC-1	Built-up Box: 19.7"x19.7"x7.9" L_c = 87" A572 Gr. 50 F_y = 56 ksi F_u = 82 ksi	Built-up W shape d=23.6" b_f=11.8" t_f=0.79" t_w=0.47" L_b=73" A36 steel F_{y-f}= 40 ksi F_{u-f}= 66 ksi F_{y-w} = 40 ksi F_{u-w} = 65 ksi	Bolted: 7-7/8" A325	SS-FCAW E70T-7 No weld tabs used	Tapered cut L_1 = 2" L_{RBS}=13.8" FR=20%	2.4	Fracture of beam flange initiating at weld access hole
Chen 1996	YC-2					Tapered cut L_1 = 2" L_{RBS}=17.7" FR=25%	2.9	Fracture of beam flange initiating at weld access hole
Chen 1996	PC-1					Tapered cut L_1 = 4.7" L_{RBS}=15.7" FR = 34%	4.1	Fracture of beam flange initiating at weld access hole
Chen 1996	PC-2					Tapered cut L_1 = 4.7", L_{RBS} = 17.7", FR = 42%	4.8	Fracture of beam flange initiating at weld access hole
Chen 1996	PC-3					Tapered cut L_1 = 4.7" L_{RBS}=17.7" FR = 42%	3.8	Fracture of beam flange initiating at weld access hole
Iwankiw 1996	DBT-1A-99-176	W14x176 A572 Gr. 50 L_c=168" F_{y-w}=55.6 ksi F_{u-w}=70.7 ksi	W30x99 A572 Gr. 50 L_b=138" F_{y-w}=61.6 ksi F_{u-w}=82.8 ksi	Bolted: 7-1" A325	SS-FCAW E70TG-K2, backing bar removed at bottom flange	Tapered cut L_1 = 7.5" L_{RBS} = 20.25" FR = 45%	2.8	No failure, test stopped due to limitations in test setup
Iwankiw 1996	DBT-1B-99-176	W14x176 A572 Gr. 50 L_c=168" F_{y-w} = 55.5 ksi F_{u-w} = 71.8 ksi	W30x99 A572 Gr. 50 L_b=138" F_{y-w}=51.5 ksi F_{u-w}=72.1 ksi				4.0	No failure, test stopped due to limitations in test setup
Iwankiw 1996	DBT-2A-150-257	W14x257 A572 Gr. 50 L_c=168" F_{y-w} = 59.6 ksi F_{u-w} = 75.2 ksi	W36x150 A572 Gr. 50 L_b=138" F_{y-w}=60.2 ksi F_{u-w}=72.3 ksi	Bolted: 9-1" A325		Tapered cut L_1 = 9" L_{RBS} = 24" FR = 45%	3.5	Fracture of beam top flange near groove weld
Iwankiw 1996	DBT-2B-150-257	W14x257 A572 Gr. 50 L_c=168" F_{y-w}=64.5 ksi F_{u-w}=83.2 ksi	W36x150 A572 Gr. 50 L_b=138" F_{y-w}=62.9 ksi F_{u-w}=83.1 ksi				1.7	Fracture of beam top flange weld, propogated to divot-type fracture of column flange

Notation

F_{y-f} = Flange yield stress from coupon tests
F_{u-f} = Flange ultimate stress from coupon tests
F_{y-w} = Web yield stress from coupon tests
F_{u-w} = Web ultimate stress from coupon tests
L_b = Length of beam, measured from load application point to face of column
L_o = Length of column
L_1 = Distance from face of column to start of RBS cut
L_{RBS} = Length of RBS cut
FR = Flange Reduction = (area of flange removed/original flange area) x100
(Flange Reduction reported at narrowest section of RBS)
θ_p = Maximum plastic rotation developed for at least one full cycle of loading, measured with respect to the face of the column (based on occurrence of fracture or based on end of loading)
r = Radius of reduced beam section cut

Table A-1. Summary of Experimental Testing on RBS Moment Connections (Continued)

Source	Specimen Label	Column	Beam	Beam Web Connection	Beam Flange Connection	RBS Design	θ_p (%)	Comments
Zekioglu 1997	ARUP-1	W14x426 A572 Gr. 50 L_c=136"	W36x150 A572 Gr. 50, L_b=132", F_{y-f}= 55.5 ksi, F_{u-f}= 73 ksi, F_{y-w} = 62.5 ksi, F_{u-w} = 77 ksi	Welded (heavy shear tab groove welded to column and fillet welded to beam web)	SS-FCAW E70TG-K2, backing bar left in place w/ seal weld at top flange, backing bar removed at bottom flange	Tapered cut, L_1 = 9", L_{RBS} = 24", FR = 44%, top & bottom flanges reinforced with vertical ribs	3.5	Flange fracture at minimum section of RBS
Zekioglu 1997	COH-1	W14x455 A572 Gr. 50, L_c=136", F_{y-f}= 55 ksi, F_{u-f}= 84 ksi, F_{y-w} = 54 ksi, F_{u-w} = 86 ksi	W27x178 A572 Gr. 50, L_b=132", F_{y-f}= 44 ksi, F_{u-f}= 62 ksi, F_{y-w} = 46 ksi, F_{u-w} = 62 ksi			Tapered cut, L_1 = 7", L_{RBS} = 20", FR = 38%, top & bottom flanges reinforced with vertical ribs	3.5	Flange fracture at minimum section of RBS
Zekioglu 1997	COH-2						3.8	Flange fracture at minimum section of RBS
Zekioglu 1997	COH-3	W14x455 A572 Gr. 50, L_c=136", F_{y-f}= 55 ksi, F_{u-f}= 84 ksi, F_{y-w} = 54 ksi, F_{u-w} = 86 ksi, Beam connected to column web	W33x152 A572 Gr. 50, L_b=132", F_{y-f}= 57.6 ksi, F_{u-f}= 78.5 ksi, F_{y-w} = 62 ksi, F_{u-w} = 84.5 ksi			Tapered cut L_1 = 9" L_{RBS} = 26" FR = 43% top & bottom flanges reinforced with vertical ribs	3.2	Flange fracture at minimum section of RBS
Zekioglu 1997	COH-4						4.0	Flange fracture at minimum section of RBS
Zekioglu 1997	COH-5		W33x152 A572 Gr. 50, L_b=132", F_{y-f}= 62.8 ksi, F_{u-f}= 86 ksi, F_{y-w} = 69.1 ksi, F_{u-w} = 93.7 ksi				1.8	Flange fracture at minimum section of RBS
Engelhardt 1996, 1997	DB1	W14x426 A572 Gr. 50, L_c=136"	W36x160 L_b=134", F_{y-f}= 54.7 ksi, F_{u-f}= 75.6 ksi, F_{y-w} = 53.5 ksi, F_{u-w} = 79.2 ksi	Welded (beam web groove welded to column)	SS-FCAW E71T-8, backing bar left in place w/ seal weld at top flange, backing bar removed at bottom flange	Constant Cut L_1 = 9", L_{RBS} = 19.5", FR = 40%	2.0	Flange fracture at RBS
Engelhardt 1996, 1997	DB2	W14x426 A572 Gr. 50, L_c=136", F_{y-f}= 50 ksi, F_{u-f}= 74.5 ksi, F_{y-w} = 50 ksi, F_{u-w} = 75 ksi	W36x150 L_b=134", F_{y-f}=41.4 ksi, F_{u-f}= 58.7 ksi, F_{y-w} = 47.1 ksi, F_{u-w} = 61.8 ksi			Radius cut L_1 = 9", L_{RBS} = 27", FR = 40%	3.0	Testing Stopped due to limitations of test setup
Engelhardt 1996, 1997	DB3	W14x426 A572 Gr. 50, L_c=136"	W36x170 L_b=134", F_{y-f}= 58 ksi, F_{u-f}= 73 ksi, F_{y-w} = 58.5 ksi, F_{u-w} = 76.7 ksi			Radius cut L_1 = 9", L_{RBS} = 27", FR = 40%	3.8	Testing Stopped due to limitations of test setup
Engelhardt 1996, 1997	DB4	W14x426 A572 Gr. 50, L_c=136", F_{y-f}= 50 ksi, F_{u-f}= 74.5 ksi, F_{y-w} = 50 ksi, F_{u-w} = 75 ksi	W36x194 L_b=134", F_{y-f}= 38.5 ksi, F_{u-f}= 58.6 ksi, F_{y-w} = 43.6 ksi, F_{u-w} = 59.8 ksi			Radius cut L_1 = 9", L_{RBS} = 27", FR = 38%	3.7	Testing Stopped due to limitations of test setup
Engelhardt 1996, 1997	DB5	W14x257 A572 Gr. 50, L_c=136" F_{y-f}= 48.7 ksi, F_{u-f}= 69 ksi, F_{y-w} = 49.4 ksi, F_{u-w} = 66.2 ksi	W30x148 L_b=134", F_{y-f}= 46.6 ksi, F_{u-f}= 64.5 ksi, F_{y-w} = 48.5 ksi, F_{u-w} = 65.4 ksi			Radius cut L_1 = 5", L_{RBS} = 25", FR = 38%	4.0	Testing Stopped due to limitations of test setup, significant column panel zone yielding

Table A-1. Summary of Experimental Testing on RBS Moment Connections (Continued)

Source	Specimen Label	Column	Beam	Beam Web Connection	Beam Flange Connection	RBS Design	θ_p (%)	Comments
Popov 1996	DB1	W14x257 A572 Gr. 50 L_c=132"	W36x135 A36 Steel L_b=134.5"	Not Available	SS-FCAW E71T-8 (details of backing and weld tabs not available)	Radius cut L_1 = 8" L_{RBS} = 28" FR = 40%	3.0	1-5/16" thk. cover plates welded across flanges to form box. Testing Stopped due to limitations of test setup
Anderson 1997	AD13	W16x77 A36 Lc=100"	W21x68 A36 Steel L_b=83"	Welded	Downhand (flate) complete penetration	Perforated Beam Section: eight holes with increasing diameters (2@1"ø, 2@1 1/4"ø , 2@1 1/2"ø and 2@1 3/4"ø) having a one inch edge to edge clearance between holes and a 1/4 inch clearance on the edge of the flange. The smaller hole is located nearest the column.	2.5	Specimen sustained 20 cycles. Failure occurred on the second cycle at a displacement of 2.5" (4% rot.) by the formation of a crack in the weld at the top flange of the beam. The crack appeared to start in the web cope and then propagate outward to the edges
Tremblay 1997	S-1	W14x120 A572 Gr. 50 L_c=120"	W530x82 (Canadian Designation) d=20.8", b_f=8.2", t_f=0.52", t_w=0.37", wt. = 54 lb/ft L_b=142" CSA G40.41-350W steel F_{y-f}= 52.4 ksi F_{u-f}= 76.6 ksi F_{y-w} = 57.5 ksi F_{u-w} = 81 ksi	Bolted: 5-1" A325	SS-FCAW E71T-8, backing bar left in place w/ seal weld at top flange, backing bar removed at bottom flange	Radius cut L_1 = 4.7" L_{RBS} = 15.7" FR = 55%	9.0	Specimen loaded monotonically, testing stopped due to limitations of test setup
Tremblay 1997	S-2A						3.6	Testing Stopped due to limitations of test setup
Tremblay 1997	SC-1						3.4	Composite slab included, testing stopped due to limitations of test setup
Tremblay 1997	S-3						2.0	Statically applied simulated earthquake loading, testing stopped due to reaching end of simulated earthquake loading, no connection
Tremblay 1997	S-4						2.0	Dynamically applied simulated earthquake loading. testing stopped due to reaching end of simulated earthquake loading, no connection failure
Tremblay 1997	SC-2						2.0	Composite slab included, Dynamically applied simulated earthquake loading, testing stopped due to reaching end of simulated earthquake loading, no connection failure

Table A-1. Summary of Experimental Testing on RBS Moment Connections (Continued)

Source	Specimen Label	Column	Beam	Beam Web Connection	Beam Flange Connection	RBS Design	θ_p (%)	Comments
Uang 1998	LS-1	W14x176 A572 Gr. 50 L_c=150" F_{y-f}=55.5 ksi F_{u-f}=74.0 ksi F_{y-w}=54.0 ksi F_{u-w}=73.1 ksi	W30x99 A572 Gr. 50 L_b=141" F_{y-f}=54.0 ksi F_{u-f}=71.9 ksi F_{y-w}=58.0 ksi F_{u-w}=74.8 ksi	Welded (beam web groove welded to column)	SS-FCAW E70T-6, backing bar left in place w/ seal weld at top flange, backing bar removed at bottom flange	Radius cut L_1=7" L_{RBS}=20" FR=50%	4.0	No connection failure
Uang 1998	LS-2						+1.0 / -5.0	Near field loading protocol where the specimen was subjected to peak pulses corresponding to 6% story drift ratio. Loading was repeated six times and the specimen eventually failed due to low cycle fatigue fracture at the narrowest section in the RBS.
Uang 1998	LS-3						-1.0 / +5.0	Near field loading protocol where the specimen was subjected to peak pulses corresponding to 6% story drift ratio. Loading was repeated four times and the specimen eventually failed due to low cycle fatigue fracture at the narrowest section in the RBS.
Uang 1998	LS-4						4.0	No connection failure, testing stopped due to limitations of test setup
Engelhardt 1999	DBBW Beam 1	W14x398 A572 Gr. 50 L_c=146" F_y = 53.0 ksi F_u = 73.0 ksi (based on CMTR)	W36x150 A572 Gr. 50 L_b=141" F_{y-f}=54.3 ksi F_{u-f}=68.8 ksi F_{y-w}=59.4 ksi F_{u-w}=72.0 ksi	Bolted: 10-1" A490	SS-FCAW E70T-6, backing bar left in place w/ seal weld at top flange, backing bar removed at bottom flange	Radius cut L_1=9" L_{RBS}=27" FR=50%	4.0	No connection failure, testing stopped due to limitations of test setup, curciform type specimens with beams attached to each column flange
Engelhardt 1999	DBBW Beam 2						4.0	No connection failure, testing stopped due to limitations of test setup, curciform type specimens with beams attached to each column flange
Engelhardt 1999	DBBW-C Beam 1						5.0	Low cycle fatigue fracture in RBS, cruciform type specimens
Engelhardt 1999	DBBW-C Beam 2						3.8	Fracture of bottom beam flange adjacent to groove weld, fracture initiated at weld access hole, cruciform type specimens
Fry 1999	DBBW Beam 1	W14x398 A572 Gr. 50 L_c=144" F_y = 53.0 ksi F_u = 73.0 ksi (based on CMTR)	W36x150 A572 Gr. 50 L_b=141" F_{y-f}=54.3 ksi F_{u-f}=68.8 ksi F_{y-w}=59.4 ksi F_{u-w}=72.0 ksi	Welded (beam web groove welded to column)	SS-FCAW E70T-6, backing bar left in place w/ seal weld at top flange, backing bar removed at bottom flange	Radius cut L_1=9" L_{RBS}=27" FR=50%	3.5	No connection failure, testing stopped due to limitations of test setup, cruciform type specimens
Fry 1999	DBBW Beam 2						3.5	No connection failure, testing stopped due to limitations of test setup, cruciform type specimens
Fry 1999	DBBW-C Beam 1						5.0	Low cycle fatigue fracture in RBS, cruciform type specimens
Fry 1999	DBBW-C Beam 2						5.0	Low cycle fatigue fracture in RBS, cruciform type specimens
Moore 1999	WG-1	W14x311 A913 Gr. 65 L_c=152" F_{y-f}=69.0 ksi F_{u-f}=88.3 ksi F_{y-w}=68.0 ksi F_{u-w}=86.5 ksi	W33x201 A572 Gr. 50 L_b=160.5" F_{y-f}=52.0 ksi F_{u-f}=72.8 ksi F_{y-w}=51.5 ksi F_{u-w}=68.0 ksi	Bolted: 13-1" A490	SS-FCAW E70TG-K2, backing bar removed at bottom flange	Radius cut L_1=9.3" L_{RBS}=25" FR=54%	2.9	5/8" doubler plates (A572 Gr. 50) provided on each side of column web. Fracture of RBS at local buckle in RBS
Moore 1999	WG-2						2.9	5/8" doubler plates (A572 Gr. 50) provided on each side of column web. No connection failure, test stopped due to limitations of test setup

Table A-1. Summary of Experimental Testing on RBS Moment Connections (Continued)

Source	Specimen Label	Column	Beam	Beam Web Connection	Beam Flange Connection	RBS Design	θ_p (%)	Comments
Moore 1999	WG-3	W14x550 A913 Gr. 65, L_c=152", F_{y-f}=67.0 ksi, F_{u-f}=86.8 ksi, F_{y-w}=68.1 ksi, F_{u-w}=87.6 ksi	W36x300 A572 Gr. 50, L_b=159", F_{y-f}=56.0 ksi, F_{u-f}=72.9 ksi, F_{y-w}=56.7 ksi, F_{u-w}=74.5 ksi	Bolted: 13-1" A490	SS-FCAW E70TG-K2, backing bar removed at bottom flange	Radius cut L_1=9.3" L_{RBS}=25" FR=54%	3.5	No connection failure, test stopped due to limitations of test setup
Moore 1999	WG-4						4.5	No connection failure, test stopped due to limitations of test setup
Jones 2000	DBWW	W14x398 L_c=144"	W36x150 L_b=144"	Field welded to the column flange with complete joint penetration single bevel groove weld.	Flanges were field welded with complete joint penetration single bevel groove welds. Bottom flange backing bars were removed and a reinforcing fillet was placed at the root of the groove weld. Top flange backing bars were left in place and sealed with a fillet weld at	Radius cut L_1 = 9" L_{RBS}=27" FR=40%	NA	Column base pinned to the floor and beam ends restrained from moving vertically by bearing guides supported by vertical reaction frames. In both specimens, saturation load corresponded to local buckling of the beam webs and flanges in the RBS region.
Jones 2000	DBBWSPZ	W14x398 3/4" Doubler plates on both sides of the column web L_c=144"	W36x150 L_b=144"	Bolted to shear tabs that had been shop welded to the column flanges		Radius cut L_1=9" L_{RBS}=27" FR=40%	NA	
Jones 2002	1B	W14x398 A572 Gr. 50, L_c=146", F_{y-f}=352.0 Mpa, F_{u-f}=492.0 Mpa, F_{y-w}=331 Mpa, F_{u-w}=488 Mpa	W36x150 A572 Gr. 50, L_b=150", F_{y-f}=374.0 Mpa, F_{u-f}=474.0 Mpa, F_{y-w}=410 Mpa, F_{u-w}=497 Mpa	Bolted	Beam flanges were field welded to the column flanges with complete joint penetration single bevel groove welds. The bottom flange backing bars were removed and a small reinforcing fillet was placed at the root of the groove weld. The top flange backing bars were left in place and sealed with a fillet weld at its base.	Radius cut FR = 50%	3.0	Strength degraded to 80% of peak strength due to beam instability
Jones 2002	1C	W14x398 A572 Gr. 50, L_c=46", F_{y-f}=352.0 Mpa, F_{u-f}=492.0 Mpa, F_{y-w}=331 Mpa, F_{u-w}=488 Mpa	W36x150 A572 Gr. 50, L_b=150", F_{y-f}=374.0 Mpa, F_{u-f}=474.0 Mpa, F_{y-w}=410 Mpa, F_{u-w}=497 Mpa	Bolted		Radius cut FR = 50%	3.8	Strength degraded to 80% of peak strength due to beam instability and fracture of beam bottom flange near weld
Jones 2002	2B	W14x398 A572 Gr. 50, L_c=146", F_{y-f}=352.0 Mpa, F_{u-f}=492.0 Mpa, F_{y-w}=331 Mpa, F_{u-w}=488 Mpa	W36x150 A572 Gr. 50, L_b=150", F_{y-f}=374.0 Mpa, F_{u-f}=474.0 Mpa, F_{y-w}=410 Mpa, F_{u-w}=497 Mpa	Welded		Radius cut FR = 50%	3.0	Strength degraded to 80% of peak strength due to beam instability
Jones 2002	2C	W14x398 A572 Gr. 50, L_c=146", F_{y-f}=352.0 Mpa, F_{u-f}=492.0 Mpa, F_{y-w}=331 Mpa, F_{u-w}=488 Mpa,	W36x150 A572 Gr. 50, L_b=150", F_{y-f}=374.0 Mpa, F_{u-f}=474.0 Mpa, F_{y-w}=410 Mpa, F_{u-w}=497 Mpa	Welded		Radius cut FR = 50%	3.0	Strength degraded to 80% of peak strength due to beam instability
Jones 2002	3B	W14x283 A572 Gr. 50, L_c=146", F_{y-f}=380.0 Mpa, F_{u-f}=519.0 Mpa, F_{y-w}=376 Mpa, F_{u-w}=520 Mpa	W36x150 A572 Gr. 50, L_b=150", F_{y-f}=374.0 Mpa, F_{u-f}=474.0 Mpa, F_{y-w}=410 Mpa, F_{u-w}=497 Mpa	Bolted		Radius cut FR = 40%	3.0	Strength degraded to 80% of peak strength due to beam instability and fracture of beam bottom flange near weld
Jones 2002	3C	W14x283 A572 Gr. 50, L_c=146", F_{y-f}=380.0 Mpa, F_{u-f}=519.0 Mpa, F_{y-w}=376 Mpa, F_{u-w}=520 Mpa	W36x150 A572 Gr. 50, L_b=150", F_{y-f}=374.0 Mpa, F_{u-f}=474.0 Mpa, F_{y-w}=410 Mpa, F_{u-w}=497 Mpa	Bolted		Radius cut FR = 40%	4.6	Fracture of beam top and bottom flanges near weld and fracture of beam bottom flange near weld
Jones 2002	4B	W14x398 A572 Gr. 50, L_c=46", F_{y-f}=352.0 Mpa, F_{u-f}=492.0 Mpa, F_{y-w}=331 Mpa, F_{u-w}=488 Mpa	W36x150 A572 Gr. 50, L_b=150", F_{y-f}=374.0 Mpa, F_{u-f}=474.0 Mpa, F_{y-w}=410 Mpa, F_{u-w}=497 Mpa	Bolted		Radius cut FR = 50%	2.0	(2) 19 mm thick doubler plates. Failed due to global instability. Out-of-plane column tip displacement exceeded the in-plane displacement after 0.03 rad of total story drift.
Jones 2002	4C	W14x398 A572 Gr. 50, L_c=46", F_{y-f}=352.0 Mpa, F_{u-f}=492.0 Mpa, F_{y-w}=331 Mpa, F_{u-w}=488 Mpa	W36x150 A572 Gr. 50, L_b=150", F_{y-f}=374.0 Mpa, F_{u-f}=474.0 Mpa, F_{y-w}=410 Mpa, F_{u-w}=497 Mpa	Bolted		Radius cut FR = 50%	3.0	(2) 19 mm thick doubler plates. Strength degraded to 80% of peak strength due to beam instability

Table A-1. Summary of Experimental Testing on RBS Moment Connections (Continued)

Source	Specimen Label	Column	Beam	Beam Web Connection	Beam Flange Connection	RBS Design	θ_p (%)	Comments
Chi 2002	DC-1	W27x146 A992 L_c=146" F_{y-f}=358.0 MPa F_{u-f}=474.0 MPa F_{y-w}=344 MPa F_{u-w}=433 Mpa	W36x150 A992 L_b=150" F_{y-f}=400.0 MPa F_{u-f}=455.0 MPa F_{y-w}=359 MPa F_{u-w}=445 Mpa	The beam webs were field welded to the column flange with complete joint penetration single bevel groove welds. The shear plate was bolted to the beams with (4) 1" dia. A325 H.S.B	Beam flanges were field welded to the column flanges with complete joint penetration single bevel groove welds. The bottom flange backing bars were removed and a small reinforcing fillet was placed at the root of the groove weld. The top flange backing bars were left in place and sealed with a fillet weld at its base.	Radius cut L_1 = 9" L_{RBS} = 30" FR = 50%	3.0	SAC loading. Yielding observed in panel zone first. Web local buckling in RBS region then occurred, followed by lateral-torsional buckling and flange local buckling. Yielding of the doubler plate that was contained in the panel zone was evident. Test was stopped due to the twisting of column.
Chi 2002	DC-2	W27x194 A992 L_c=146" F_{y-f}=427.0 MPa F_{u-f}=453.0 MPa F_{y-w}=435 MPa F_{u-w}=449 Mpa	W36x150 A992 L_b=150" F_{y-f}=400.0 MPa F_{u-f}=455.0 MPa F_{y-w}=359 MPa F_{u-w}=445 Mpa			Radius cut L_1 = 9" L_{RBS} = 30" FR = 50%	3.0	SAC loading. Yielding observed in panel zone first. Web local buckling in RBS region then occurred, followed by lateral-torsional buckling and flange local buckling. Specimen reached 0.03 rad total plastic rotation before strength degraded below 80% of nominal plastic moment. Panel zone contributed 0.005 rad plastic rotation. Test was stopped after one complete cycle at 5% drift was completed due to significant strength degradation and column twisting.
Chi 2002	DC-3	W27x194 A992 L_c=146" F_{y-f}=427.0 MPa F_{u-f}=453.0 MPa F_{y-w}=435 MPa F_{u-w}=449 Mpa	W36x150 A992 L_b=150" F_{y-f}=400.0 MPa F_{u-f}=455.0 MPa F_{y-w}=359 MPa F_{u-w}=445 Mpa			Radius cut L_1 = 10.5" L_{RBS} = 24" FR = 43%	2.8	SAC loading. Yielding observed in panel zone first. Web local buckling in RBS region then occurred, followed by lateral-torsional buckling and flange local buckling. Continuity plates had also yielded. Buckling amplitudes were smaller than first two specimens because of low slenderness ratios. Out-of-plane deformation of the column flange due to column twisting reached 16 mm at 4% drift. JTotal plastic rotation was 0.028 rad of which the panel zone contributed 0.007 rad.
Adan 2004	RBS1	W14x283 A572 Gr. 50 Lc=150" Fy = 56.3 ksi Fu = 78.5 ksi	W30x132 A572 Gr. 50 Lc=150" Fy = 55.6 ksi Fu = 74.1 ksi	The beam webs were field welded to the column flange with complete joint penetration single bevel groove weld	The beam flanges were field welded to the column flange with complete joint penetration single bevel groove weld	Radius cut r= 21" FR = 40%	NA	SAC loading. Initial yielding was visually observed during step #4. Whitewash flaking initiated in the beam web, near the thinnest section of the reduced flange. At step #6, localized buckling of the beam web occurred. With each subsequent downward cycle, lateral torsional buckling occurred in the beam bottom flange. The lateral torsional buckling mode twisted the bottom flange outward. At step #8, localized buckling of the beam occurred in the reduced flange. At load higher load steps, severe web buckling was observed in the beam web and on the upward cycles, buckling was also observed in the beam top flange.Ultimately, all specimens fractured shortly after load step #9. There was no significant weld damage in any of the beam-to-column welds. No evidence of weld failure was observed in any of the tests.
	RBS2	W14x283 A572 Gr. 50 L_c=150" F_y=56.3 ksi F_u=78.5 ksi	W30x132 A572 Gr. 50 L_b=150" F_y=55.6 ksi F_u=74.1 ksi				NA	
	RBS3	W18x211 A572 Gr. 50 L_c=150" F_y=51.8 ksi F_u=70.3 ksi	W30x132 A572 Gr. 50 L_b=150" F_y=55.6 ksi F_u=74.1 ksi				NA	
	RBS4	W18x211 A572 Gr. 50 L_c=150" F_y=51.8ksi F_u=70.. ksi	W30x132 A572 Gr. 50 L_c=150" F_y=55.6 ksi F_u=74.1 ksi				NA	

Table A-1. Summary of Experimental Testing on RBS Moment Connections (Continued)

Source	Specimen Label	Column	Beam	Beam Web Connection	Beam Flange Connection	RBS Design	θ_p (%)	Comments
Ricles 2004	1	W36x230 L_c=156" F_{y-f}=356.0 MPa F_{u-f}=496.0 MPa F_{y-w}=393.0 MPa F_{u-w}=514.0 Mpa	W36x150 L_b=144" F_{y-f}=343.0 MPa F_{u-f}=478.0 MPa F_{y-w}=378.0 MPa F_{u-w}=492.0 MPa	CJP groove field welds utilized E71T-8 electrodes. No run off tabs were used for the vertical beam web CJP groove welds.	CJP groove field welds utilized E70T-6. The run off tabs for the beam flanges were removed following the placement of the CJP groove welds, and the weld at the edges of the beam flanges ground to a smooth transition. The backing bar of the top flange weld was left in place and a reinforcement fillet weld was provided between the bottom surface of the backing bar and the column flange using the E71T-8 electrode. The beam bottom flange backing bar was removed using the airarc process, back gouged, and reinforced with a fillet weld using an E71T-8 electrode.	Radius cut	4.0	Composite floor slab with total thickness of 133 mm included. The combined effect of cyclic local buckling and lateral flange displacement resulted in a gradual deterioration in specimen capacity to occur during subsequent cycles where the story drift amplitude was increased. The lateral displacement of the bottom beam flange occurred when it was in compression, and caused some column twist to develop. The maximum column twist among the specimens with a floor slab at 4% story drift was 0.037 rads. (SPEC-4). 4% story drift is the drift at which connections are judged for qualification for seismic use by the AISC Seismic Provisions (4). SPEC-4, like the other specimens, developed a flange fracture in the RBS where extensive local flange buckling had occurred. This occurred at a story drift of 6%, and was caused by local buckling in the beam flange that led to large cyclic strains, resulting in a low cycle fatigue failure. SPEC-6, which had a supplemental brace and lateral bracing attached to the beam that is parallel to the test beam, had minimal deterioration in capacity as well as column twist (0.004 rads. at 4% story drift). The reduced amount of deterioration in the capacity of SPEC-6 was due to the specimen having a weaker panel zone than the other specimens.
Ricles 2004	2	W27x194 L_c=156" F_{y-f}=372.0 MPa F_{u-f}=520.0 MPa F_{y-w}=378.0 MPa F_{u-w}=492.0 Mpa	W36x150 L_b=144" F_{y-f}=343.0 MPa F_{u-f}=478.0 MPa F_{y-w}=378.0 MPa F_{u-w}=492.0 MPa			Radius cut	4.0	
Ricles 2004	3	W27x194 L_c=156" F_{y-f}=356.0 MPa F_{u-f}=497.0 MPa F_{y-w}=403.0 MPa F_{u-w}=521.0 Mpa	W36x150 L_b=144" F_{y-f}=356.0 MPa F_{u-f}=508.0 MPa F_{y-w}=396.0 MPa F_{u-w}=506.0 MPa			Radius cut	5.0	
Ricles 2004	4	W36x150 L_c=156" F_{y-f}=356.0 MPa F_{u-f}=508.0 MPa F_{y-w}=396.0 MPa F_{u-w}=506.0 Mpa	W36x150 L_b=144" F_{y-f}=365.0 MPa F_{u-f}=508.0 MPa F_{y-w}=396.0 MPa F_{u-w}=506.0 MPa			Radius cut	4.0	
Ricles 2004	5	W27x146 L_c=156" F_{y-f}= 363.0 MPa F_{u-f}= 499.0 MPa F_{y-w} = 399.0 MPa F_{u-w} = 513.0 Mpa	W30x108 L_b=144" F_{y-f}= 344.0 MPa F_{u-f}= 471.0 MPa F_{y-w} = 353.0 MPa F_{u-w} = 469.0 MPa			Radius cut	5.0	
Ricles 2004	6	W24x131 L_c=156" F_{y-f}= 334.0 MPa F_{u-f}= 499.0 MPa F_{y-w} = 359.0 MPa F_{u-w} = 493.0 Mpa	W30x108 L_b=144" F_{y-f}= 344.0 MPa F_{u-f}= 471.0 MPa F_{y-w} = 353.0 MPa F_{u-w} = 469.0 MPa			Radius cut	4.0	

Table A-1. Summary of Experimental Testing on RBS Moment Connections (Continued)

Source	Specimen Label	Column	Beam	Beam Web Connection	Beam Flange Connection	RBS Design	θ_p (%)	Comments
Lee 2005	DB700-SW	W17x271 L_c=3500 mm F_{y-f}= 343.0 MPa F_{u-f}= 512.0 MPa F_{y-w} = 358.0 MPa F_{u-w} = 520.0 Mpa	W27x123 L_b=3597 mm F_{y-f}= 304.0 MPa F_{u-f}= 455.0 MPa F_{y-w} = 364.0 MPa F_{u-w} = 480.0 MPa	Welded	Beam flanges were field welded to the column flanges with complete joint penetration single bevel groove welds. The bottom flange backing bars were removed and a small reinforcing fillet was placed at the root of the groove weld. The top flange backing bars were left in place and sealed with a fillet weld at its base.	Radius cut L_1=175 mm L_{RBS}=525 mm FR=37%	NA	SAC loading. Excellent rotation capacity without fracture.
Lee 2005	DB700-MW	W17x271 L_c=3500 mm F_{y-f}= 343.0 MPa F_{u-f}= 512.0 MPa F_{y-w} = 358.0 MPa F_{u-w} = 520.0 Mpa	W27x123 L_b=3597 mm F_{y-f}= 304.0 MPa F_{u-f}= 455.0 MPa F_{y-w} = 364.0 MPa F_{u-w} = 480.0 MPa	Welded		Radius cut L_1 = 175 mm L_{RBS} = 525 mm FR = 37%	NA	SAC loading. Significant yielding of the panel zone
Lee 2005	DB700-SB	W17x271 L_c=3500 mm F_{y-f}= 343.0 MPa F_{u-f}= 512.0 MPa F_{y-w} = 358.0 MPa F_{u-w} = 520.0 Mpa	W27x123 L_b=3597 mm F_{y-f}= 304.0 MPa F_{u-f}= 455.0 MPa F_{y-w} = 364.0 MPa F_{u-w} = 480.0 MPa	Bolted		Radius cut L_1 = 175 mm L_{RBS} = 525 mm FR = 37%	NA	SAC loading. Performed poorly due to brittle fracture across the beam flange at the weld access hole. This suggests the possibility of web bolt slippage.
Lee 2005	DB700-MB	W17x271 L_c=3500 mm F_{y-f}= 343.0 MPa F_{u-f}= 512.0 MPa F_{y-w} = 358.0 MPa F_{u-w} = 520.0 Mpa	W27x123 L_b=3597 mm F_{y-f}= 304.0 MPa F_{u-f}= 455.0 MPa F_{y-w} = 364.0 MPa F_{u-w} = 480.0 MPa	Bolted		Radius cut L_1 = 175 mm L_{RBS} = 525 mm FR = 37%	NA	SAC loading. Performed poorly due to brittle fracture across the beam flange at the weld access hole
Lee 2005	DB600-MW1	W16x115 L_c=3500 mm F_{y-f}= 358.0 MPa F_{u-f}= 525.0 MPa F_{y-w} = 374.0 MPa F_{u-w} = 531.0 Mpa	W24x70 L_b=3597 mm F_{y-f}= 326.0 MPa F_{u-f}= 467.0 MPa F_{y-w} = 343.0 MPa F_{u-w} = 473.0 MPa	Welded		Radius cut L_1 = 150 mm L_{RBS} = 510 mm FR = 40%	NA	SAC Loading. All welded-web specimens in Set number 2 exhibited satisfactory connection ductility.
Lee 2005	DB600-MW2	W16x115 L_c=3500 mm F_{y-f}= 358.0 MPa F_{u-f}= 525.0 MPa F_{y-w} = 374.0 MPa F_{u-w} = 531.0 Mpa	W24x70 L_b=3597 mm F_{y-f}= 326.0 MPa F_{u-f}= 467.0 MPa F_{y-w} = 343.0 MPa F_{u-w} = 473.0 MPa	Welded		Radius cut L_1 = 150 mm L_{RBS} = 390 mm FR = 40%	NA	
Lee 2005	DB600-SW1	W24x100 L_c=3500 mm F_{y-f}= 343.0 MPa F_{u-f}= 512.0 MPa F_{y-w} = 358.0 MPa F_{u-w} = 520.0 Mpa	W24x70 L_b=3597 mm F_{y-f}= 326.0 MPa F_{u-f}= 467.0 MPa F_{y-w} = 343.0 MPa F_{u-w} = 473.0 MPa	Welded		Radius cut L_1 = 150 mm L_{RBS} = 450 mm FR = 40%	NA	
Lee 2005	DB600-SW2	W24x100 L_c=3500 mm F_{y-f}= 374.0 MPa F_{u-f}= 534.0 MPa F_{y-w} = 405.0 MPa F_{u-w} = 546.0 Mpa	W24x80 L_b=3597 mm F_{y-f}= 295.0 MPa F_{u-f}= 447.0 MPa F_{y-w} = 333.0 MPa F_{u-w} = 471.0 MPa	Welded		Radius cut L_1 = 150 mm L_{RBS} = 450 mm FR = 40%	NA	

Table A-1. Summary of Experimental Testing on RBS Moment Connections (Continued)

Source	Specimen Label	Column	Beam	Beam Web Connection	Beam Flange Connection	RBS Design	θ_p (%)	Comments
Lee 2007	DB1	H-428x407x20x35 Lc=3500 mm Fy = 313.0 Mpa	H-700x300x13x24 L_b=3597 mm F_y = 313.0 Mpa	Bolted: (12) F10T-6-M27	SS-FCAW E71T-8, backing bar left w/ weld at top, backing bar removed at bottom	Radius cut L_l = 175 mm L_{RBS} = 525 mm FR = 40%	5.0	SAC standard loading protocol for cyclic loading. The test specimen developed excellent connection cyclic rotation capacity up to 5% story drift without fracture. After one complete cycle loading of 5% story drift, testing was terminated due to concerns about possible damage to the test setup.
Pachoumis 2010	RBSa	HE 300B L_c=1797 mm F_{y-f}=310.0 MPa F_{u-f}=430.0 Mpa	HE 180A L_b=1200 mm F_{y-f}=310.0 MPa F_{u-f}=430.0 Mpa	Welded	Welded	Radius cut L_l = 144 mm L_{RBS} = 128.25 mm FR = 40%	3.0	SAC standard loading protocol for cyclic loading. The value of the geometrical parameter a was greater (80%bf) than the upper limits recommended by EC8 or FEMA. A real plastic hinge developed at the RBS area. The ductility, in terms of rotation, was greater than the 0.03 rad, a rotation which is sometimes considered as the upper limit of the ' required in practice. Initial yielding occurred during the first cycle at 1:0 y, with yielding observed at the bottom flange. It should be noted that during that cycle the beam-to-column interface remained in the elastic area. Progressing through the loading history, yielding started to propagate along the RBS bottom flange. During the second cycle at 2:0 y, yielding was also observed at the top flange of the RBS. Due to the limitation of the test set-up, after the second cycle at 3:0 y, the test was continued monotonically. During that loading, local buckling of the bottom flange developed, which became more pronounced with each successive loading. Initiation of web buckling appeared close to the yielded bottom flange.
Pachoumis 2010	RBSb					Radius cut L_l = 72mm L_{RBS} = 102.6 mm FR = 40%	5.0	SAC standard loading protocol for cyclic loading. Initial yielding occurred during the fourth cycle at 1:0 y, with significant yielding observed at the bottom flange. Progressing through the loading history, yielding started to propagate along the RBS bottom flange. Web buckling was not noted. During the first cycle at 1:5 y, yielding was also observed at the top flange of the RBS. During the cycle at 3:0 y, severe flange local buckling developed, which became more pronounced with each successive loading cycle. After the second cycle at 4:0 y, the test was continued monotonically until the specimen reached the 0.12 rad rotation. Testing was stopped at this point due to the limitations in the test set-up. No failure occurred in specimen RBSb.

APPENDIX B

CONNECTION DESIGN

Reduced Beam Section Connection Design (8-Story)

Units:
$kip := 1000lbf \quad ksi := 1000psi \quad kcf := kip \cdot ft^{-3}$

Beam and Column Design Using a Wide Flange:

$F_y := 50 \cdot ksi \quad E := 29000ksi \quad F_u := 65ksi \quad c_{pr} := 1.15 \quad R_y := 1.1 \quad L_{bay} := 30ft \quad P := 16.898kip$

Beam Dimensions

Using a W27X102

$w_{b\_b} := 102 \frac{lbf}{ft} \quad d_{\_b} := 27.1in \quad b_{f\_b} := 10in \quad t_{w\_b} := .515in \quad t_{f\_b} := .83in$

$I_{x\_b} := 3620in^4 \quad I_{y\_b} := 139in^4 \quad A_{g\_b} := 30in^2 \quad Z_{x\_b} := 305in^3$

Column Dimensions

Using a W14X109

$w_{b\_c} := 176 \frac{lbf}{ft} \quad d_{\_c} := 14.3in \quad b_{f\_c} := 14.6in \quad t_{w\_c} := .525in \quad t_{f\_c} := .86in$

$I_{x\_c} := 1240in^4 \quad I_{y\_c} := 447in^4 \quad A_{g\_c} := 32$

Step #1 - Length and Location of Beam Flange Reduction

$a_{min} := 0.5 \cdot b_{f\_b} = 5 \cdot in \quad a_{max} := 0.75 \cdot b_{f\_b} = 7.5 \cdot in \quad a_{select} := 7in$

$b_{min} := 0.65 \cdot d_{\_b} = 17.615 \cdot in \quad b_{max} := 0.85 \cdot d_{\_b} = 23.035 \cdot in \quad b_{select} := 20in$

Step #2 - Depth of Flange Reduction

$c_b := 0.25 \cdot b_{f\_b} = 2.5 \cdot in$

$Z_{rbs} := Z_{x\_b} - 4 \cdot c_b \cdot t_{f\_b} \cdot \left(0.5 \cdot d_{\_b} - 0.5 \cdot t_{f\_b}\right) = 195.98 \cdot in^3$

$x_b := a_{select} + 0.5 \cdot b_{select} = 17 \cdot in$

$L_{plastic} := L_{bay} - 2 \cdot x_b = 326in$

$M_{pr\_b} := c_{pr} \cdot R_y \cdot Z_{rbs} \cdot F_y = 1032.975kip \cdot ft$

$$V_{p\_b} := \frac{\left(w_{b\_b} \cdot \frac{L_{plastic}^{\;2}}{2} + 2 \cdot M_{pr\_b} + P \cdot \frac{L_{plastic}}{2}\right)}{L_{plastic}} = 85.882kip$$

$M_{f\_b} := M_{pr\_b} + V_{p\_b} \cdot x_b = 1154.641kip \cdot ft$

Check if c_b is acceptable: $Check_{cb} := if\left(M_{f\_b} < c_{pr} \cdot R_y \cdot Z_{x\_b} \cdot F_y, "OK", "Increase C"\right)$ $\boxed{Check_{cb} = "OK"}$

Step #3 - Calculate M_f and M_c based on the Final RBS Dimensions

$$S_{rbs} := \frac{\left(b_{f\_b} - 2 \cdot c_b\right) \cdot d_{\_b}^{\,2}}{6} - \left(b_{f\_b} - 2 \cdot c_b - t_{w\_b}\right) \cdot \frac{\left(d_{\_b} - 2 \cdot t_{f\_b}\right)^3}{6 \cdot d_{\_b}} = 157.865 \cdot in^3$$

$$C_y := \frac{1}{c_{pr} \cdot \left(\frac{Z_{rbs}}{S_{rbs}}\right)} = 0.7$$

$$M_{yf} := C_y \cdot M_{f\_b} = 9705.207 \cdot kip \cdot in$$

$$M_{\_c} := M_{pr\_b} + V_{p\_b} \cdot \left(x_b + \frac{d_{\_c}}{2}\right) = 14469.748 \cdot kip \cdot in$$

Step #4 - Calculate the Shear at the Column Face

$$V_g := 500kip$$

$$V_f := 2 \cdot \left(\frac{M_{yf}}{L_{bay} - d_{\_c}}\right) + V_g = 556.148 \cdot kip$$

Weld Acces Hole Geometry:

$a_1 := 45deg$ $\quad a_2 := t_{f\_b} = 0.83 \cdot in$ $\quad a_3 := 0.75in$ $\quad a_4 := 1in$ $\quad a_5 := 3 \cdot t_{f\_b} = 2.49 \cdot in$

Continuity Plates Requirement:

$$t_{cf} := 0.4 \cdot \sqrt{1.8 \cdot b_{f\_b} \cdot t_{f\_b}} = 1.546 \cdot in$$

$$t_{cf2} := \frac{b_{f\_b}}{6} = 1.667 \cdot in$$

Check if continuity plate is required: $Check_{cp} := if\left(t_{f\_c} < t_{cf2}, "Yes", "No"\right)$ $\quad \boxed{Check_{cp} = "Yes"}$

Doubler Plates Requirement:

$$t_{pz} := \frac{\left[C_y \cdot M_{\_c} \cdot \left[\frac{\left(144in - d_{\_b}\right)}{144in}\right]\right]}{0.9 \cdot 0.6 \cdot 50000psi \cdot R_y \cdot d_{\_c} \cdot \left(d_{\_b} - t_{f\_b}\right)} = 0.737 \cdot in \qquad t_{w\_c} = 0.525 \cdot in$$

Check if doubler plate is required: $Check_{cp} := if\left(t_{w\_c} < t_{pz}, "Yes", "No"\right)$ $\quad \boxed{Check_{cp} = "Yes"}$

$$t_{cp} := t_{pz} - t_{w\_c} = 0.212 \cdot in$$

AISC-ASD89 Check:

$$V_p := 0.9 \cdot 0.6 \cdot F_y \cdot d_{\_c} \cdot t_{w\_c} = 202702.5 \cdot lbf$$

$$t_p := \frac{V_p}{\left(0.6 \cdot 0.9 \cdot F_y \cdot d_{\_c}\right)} - \frac{3 \cdot b_{f\_c} \cdot t_{f\_c}^{\,2}}{d_{\_c} \cdot d_{\_b}} = 0.441 \cdot in$$

Design Code - FEMA 350

Beam Information:

Selected a W30x99 steel beam

$\text{Width} := 10.5\text{in} \quad \text{Depth} := 29.7\text{in} \quad R_y := 1.3 \quad W_b := 99\frac{\text{lbf}}{\text{ft}} \quad Z_e := 312\text{in}^3 \quad f_y := 50\text{ksi} \quad f_u := 65\text{ksi}$

$L_e := 20\text{ft} \quad L_p := 15.9\text{ft} \quad M_p := f_y \cdot Z_e \quad P := 20\text{kip}$

Column Information:

Selected a W14x176 steel column

$\text{Width}_c := 15.7\text{in} \quad \text{Depth}_c := 15.2\text{in} \quad W_c := 176\frac{\text{lbf}}{\text{ft}} \quad Z_c := 320\text{in}^3 \quad f_y := 50\text{ksi} \quad f_u := 65\text{ksi}$

$A_g := 51.8\text{in}^2 \quad P_{uc} := 20\text{kip}$

Column/Beam Bending Strength Ratio:

$$C_{pr} := \frac{\left(f_y + f_u\right)}{2 \cdot f_y} \qquad \text{Mpr} := C_{pr} \cdot R_y \cdot Z_e \cdot f_y \qquad \text{Mpr} = 1.944 \times 10^3 \cdot \text{kip} \cdot \text{ft}$$

$$V_p := \frac{\left(\text{Mpr} + \text{Mpr} + P \cdot L_p \cdot 0.5 + W_b \cdot L_p{}^2 \cdot 0.5\right)}{L_p} \qquad V_p = 255.252\text{kip}$$

$$M_c := \text{Mpr} + V_p \cdot 2.05\text{ft} \qquad M_c = 2.467 \times 10^3 \cdot \text{kip} \cdot \text{ft}$$

$$M_{pc} := 2Z_c \cdot \left(f_y - \frac{P_{uc}}{A_g}\right) \qquad M_{pc} = 2.646 \times 10^3 \cdot \text{kip} \cdot \text{ft}$$

$$\text{Check} := \text{if}\left(\frac{M_{pc}}{M_c} > 1, \text{"ok"}, \text{"redesign"}\right) \qquad \text{Check} = \text{"ok"}$$

Reduced Beam Section Connection Design (16-Story)

Units: $\text{kip} := 1000\text{lbf} \quad \text{ksi} := 1000\text{psi} \quad \text{kcf} := \text{kip}\cdot\text{ft}^{-3}$

Beam and Column Design Using a Wide Flange:

$F_y := 50\cdot\text{ksi} \quad E := 29000\text{ksi} \quad F_u := 65\text{ksi} \quad c_{pr} := 1.15 \quad R_y := 1.1 \quad L_{bay} := 30\text{ft} \quad P := 16.898\text{kip}$

Beam Dimensions

Using a W36x160

$w_{b\_b} := 160\,\frac{\text{lbf}}{\text{ft}} \quad d_{\_b} := 36\text{in} \quad b_{f\_b} := 12\text{in} \quad t_{w\_b} := .65\text{in} \quad t_{f\_b} := 1.02\text{in}$

$I_{x\_b} := 9760\text{in}^4 \quad I_{y\_b} := 295\text{in}^4 \quad A_{g\_b} := 47\text{in}^2 \quad Z_{x\_b} := 624\text{in}^3$

Column Dimensions

Using a W14X398

$w_{b\_c} := 398\,\frac{\text{lbf}}{\text{ft}} \quad d_{\_c} := 18.3\text{in} \quad b_{f\_c} := 16.6\text{in} \quad t_{w\_c} := 1.77\text{in} \quad t_{f\_c} := 2.85\text{in}$

$I_{x\_c} := 1240\text{in}^4 \quad I_{y\_c} := 447\text{in}^4 \quad A_{g\_c} := 117$

Step #1 - Length and Location of Beam Flange Reduction

$a_{min} := 0.5\cdot b_{f\_b} = 6\cdot\text{in} \quad a_{max} := 0.75\cdot b_{f\_b} = 9\cdot\text{in} \quad a_{select} := 7\text{in}$

$b_{min} := 0.65\cdot d_{\_b} = 23.4\cdot\text{in} \quad b_{max} := 0.85\cdot d_{\_b} = 30.6\cdot\text{in} \quad b_{select} := 20\text{in}$

Step #2 - Depth of Flange Reduction

$c_b := 0.25\cdot b_{f\_b} = 3\cdot\text{in}$

$Z_{rbs} := Z_{x\_b} - 4\cdot c_b\cdot t_{f\_b}\cdot\left(0.5\cdot d_{\_b} - 0.5\cdot t_{f\_b}\right) = 409.922\cdot\text{in}^3$

$x_b := a_{select} + 0.5\cdot b_{select} = 17\cdot\text{in}$

$L_{plastic} := L_{bay} - 2\cdot x_b = 326\cdot\text{in}$

$M_{pr\_b} := c_{pr}\cdot R_y\cdot Z_{rbs}\cdot F_y = 2160.633\cdot\text{kip}\cdot\text{ft}$

$$V_{p\_b} := \frac{\left(w_{b\_b}\cdot\frac{L_{plastic}^{\;2}}{2} + 2\cdot M_{pr\_b} + P\cdot\frac{L_{plastic}}{2}\right)}{L_{plastic}} = 169.687\cdot\text{kip}$$

$M_{f\_b} := M_{pr\_b} + V_{p\_b}\cdot x_b = 2401.023\cdot\text{kip}\cdot\text{ft}$

Check if c_b is acceptable: $\text{Check}_{cb} := \text{if}\left(M_{f\_b} < c_{pr}\cdot R_y\cdot Z_{x\_b}\cdot F_y, \text{"OK"}, \text{"Increase C"}\right)$ $\boxed{\text{Check}_{cb} = \text{"OK"}}$

Step #3 - Calculate M_f and M_c based on the Final RBS Dimensions

$$S_{rbs} := \frac{(b_{f\_b} - 2\cdot c_b)\cdot d_{\_b}^2}{6} - (b_{f\_b} - 2\cdot c_b - t_{w\_b})\cdot\frac{(d_{\_b} - 2\cdot t_{f\_b})^3}{6\cdot d_{\_b}} = 325.93\cdot in^3$$

$$C_y := \frac{1}{c_{pr}\cdot\left(\frac{Z_{rbs}}{S_{rbs}}\right)} = 0.691$$

$$M_{yf} := C_y\cdot M_{f\_b} = 19920.6\cdot kip\cdot in$$

$$M_{\_c} := M_{pr\_b} + V_{p\_b}\cdot\left(x_b + \frac{d_{\_c}}{2}\right) = 30364.915\cdot kip\cdot in$$

Step #4 - Calculate the Shear at the Column Face

$$V_g := 500kip$$

$$V_f := 2\cdot\left(\frac{M_{yf}}{L_{bay} - d_{\_c}}\right) + V_g = 616.597\cdot kip$$

Weld Acces Hole Geometry:

$a_1 := 45deg$ $a_2 := t_{f\_b} = 1.02\cdot in$ $a_3 := 0.75in$ $a_4 := 1in$ $a_5 := 3\cdot t_{f\_b} = 3.06\cdot in$

Continuity Plates Requirement:

$$t_{cf} := 0.4\cdot\sqrt{1.8\cdot b_{f\_b}\cdot t_{f\_b}} = 1.878\cdot in$$

$$t_{cf2} := \frac{b_{f\_b}}{6} = 2\cdot in$$

Check if continuity plate is required: $Check_{cp} := if(t_{f\_c} < t_{cf2}, "Yes", "No")$ $Check_{cp} = "No"$

Doubler Plates Requirement:

$$t_{pz} := \frac{\left[C_y\cdot M_{\_c}\cdot\left[\frac{(144in - d_{\_b})}{144in}\right]\right]}{0.9\cdot 0.6\cdot 50000psi\cdot R_y\cdot d_{\_c}\cdot(d_{\_b} - t_{f\_b})} = 0.828\cdot in$$ $t_{w\_c} = 1.77\cdot in$

Check if doubler plate is required: $Check_{cp} := if(t_{w\_c} < t_{pz}, "Yes", "No")$ $Check_{cp} = "No"$

$$t_{cp} := t_{pz} - t_{w\_c} = -0.942\cdot in$$

AISC-ASD89 Check:

$$V_p := 0.9\cdot 0.6\cdot F_y\cdot d_{\_c}\cdot t_{w\_c} = 874557\cdot lbf$$

$$t_p := \frac{V_p}{(0.6\cdot 0.9\cdot F_y\cdot d_{\_c})} - \frac{3\cdot b_{f\_c}\cdot t_{f\_c}^2}{d_{\_c}\cdot d_{\_b}} = 1.156\cdot in$$

Design Code - FEMA 350

Beam Information:

Selected a W36x160 steel beam

$\text{Width} := 12\text{in} \quad \text{Depth} := 36\text{in} \quad R_y := 2.5 \quad W_b := 160\,\frac{\text{lbf}}{\text{ft}} \quad Z_e := 77.3\text{in}^3 \quad f_y := 50\text{ksi} \quad f_u := 65\text{ksi}$

$L_e := 20\text{ft} \quad L_p := 15.9\text{ft} \quad M_p := f_y \cdot Z_e \quad P := 20\text{kip}$

Column Information:

Selected a W14x398 steel column

$\text{Width}_c := 16.6\text{in} \quad \text{Depth}_c := 18.3\text{in} \quad W_c := 398\,\frac{\text{lbf}}{\text{ft}} \quad Z_c := 801\text{in}^3 \quad f_y := 50\text{ksi} \quad f_u := 65\text{ksi}$

$A_g := 117\text{in}^2 \quad P_{uc} := 20\text{kip}$

Column/Beam Bending Strength Ratio:

$$C_{pr} := \frac{(f_y + f_u)}{2 \cdot f_y} \qquad Mpr := C_{pr} \cdot R_y \cdot Z_e \cdot f_y \qquad Mpr = 925.99 \cdot \text{kip} \cdot \text{ft}$$

$$V_p := \frac{\left(Mpr + Mpr + P \cdot L_p \cdot 0.5 + W_b \cdot L_p^{\,2} \cdot 0.5\right)}{L_p} \qquad V_p = 127.749 \cdot \text{kip}$$

$$M_c := Mpr + V_p \cdot 2.05\text{ft} \qquad M_c = 1.188 \times 10^3 \cdot \text{kip} \cdot \text{ft}$$

$$M_{pc} := 2Z_c \cdot \left(f_y - \frac{P_{uc}}{A_g}\right) \qquad M_{pc} = 6.652 \times 10^3 \cdot \text{kip} \cdot \text{ft}$$

$$\text{Check} := \text{if}\left(\frac{M_{pc}}{M_c} > 1, \text{"ok"}, \text{"redesign"}\right) \qquad \text{Check} = \text{"ok"}$$

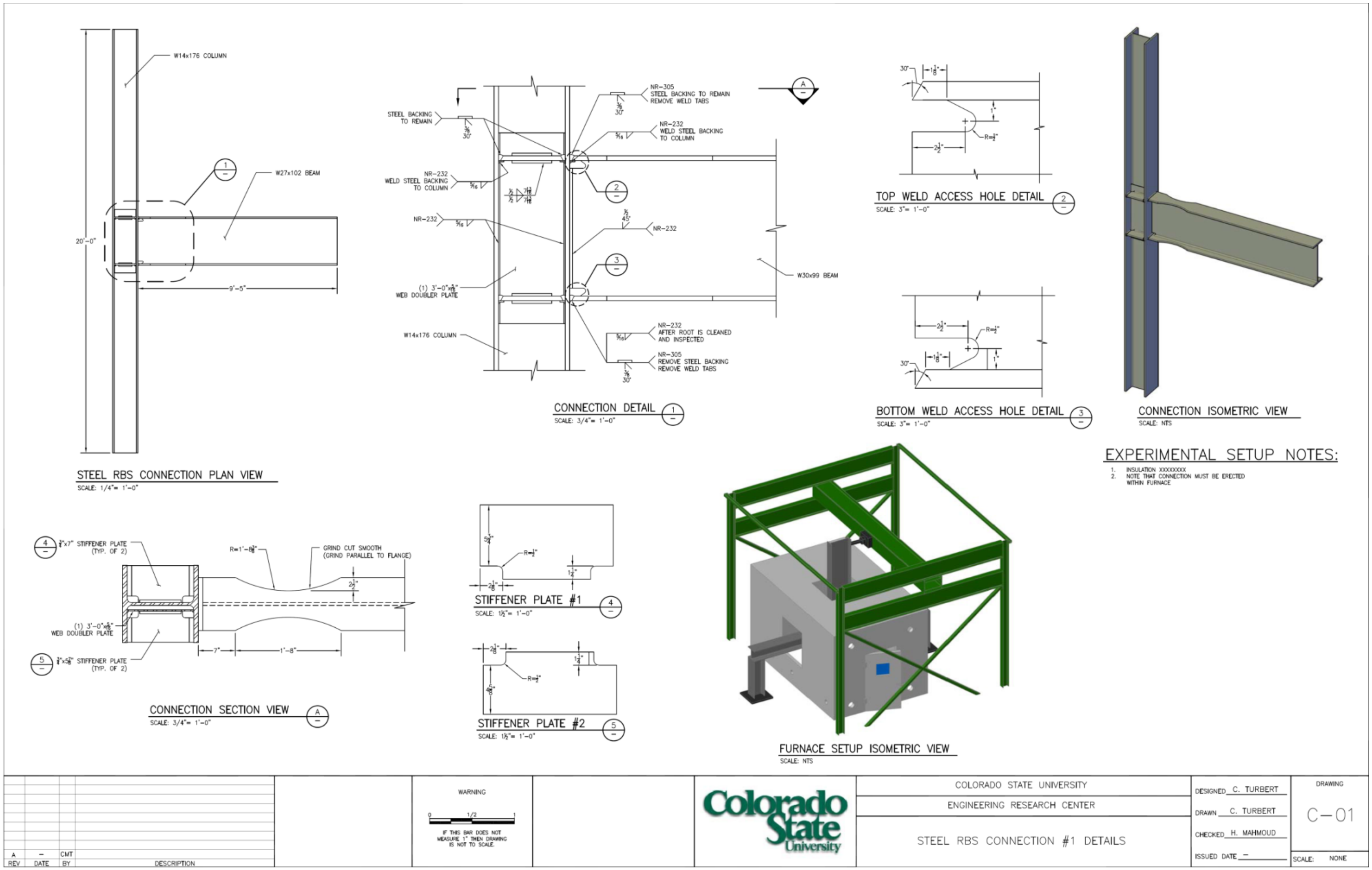

EXPERIMENTAL SETUP NOTES:

1. INSULATION XXXXXXXX
2. NOTE THAT CONNECTION MUST BE ERECTED WITHIN FURNACE

*Note: Drawings were made for experimental testing that is to be performed on the two beam-columns subassemblies. Because of this the member lengths provided in the drawings were adjusted to accommodate experimental setup restrictions.

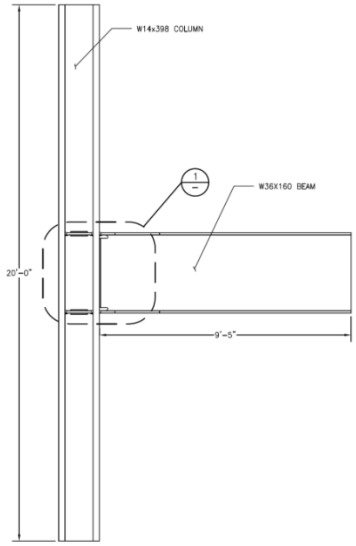

STEEL RBS CONNECTION PLAN VIEW

SCALE: 1/4"= 1'-0"

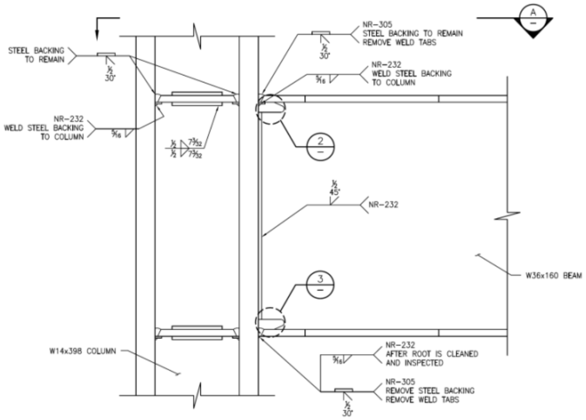

CONNECTION DETAIL ①

SCALE: 3/4"= 1'-0"

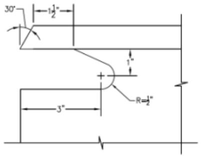

TOP WELD ACCESS HOLE DETAIL ②

SCALE: 3"= 1'-0"

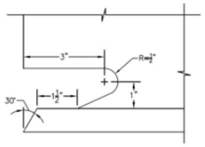

BOTTOM WELD ACCESS HOLE DETAIL ③

SCALE: 3"= 1'-0"

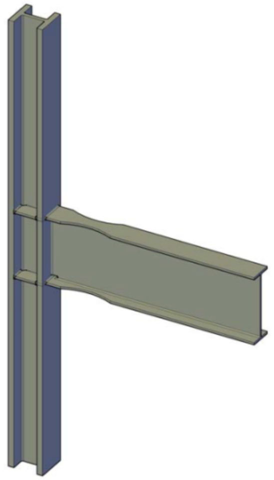

CONNECTION ISOMETRIC VIEW

SCALE: NTS

EXPERIMENTAL SETUP NOTES:

1. INSULATION XXXXXXXX
2. NOTE THAT CONNECTION MUST BE ERECTED WITHIN FURNACE

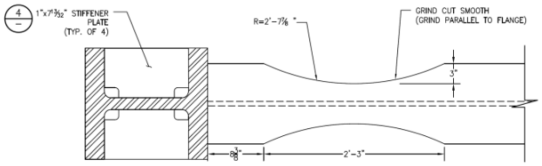

CONNECTION SECTION VIEW Ⓐ

SCALE: 3/4"= 1'-0"

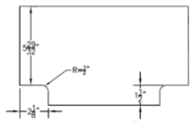

STIFFENER PLATE #1 ④

SCALE: 1½"= 1'-0"

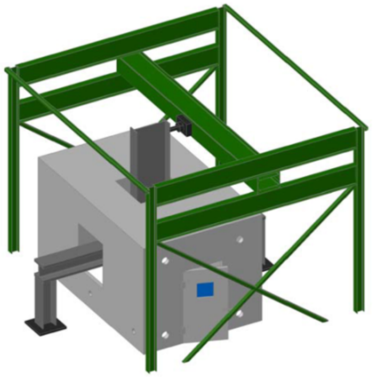

FURNACE SETUP ISOMETRIC VIEW

SCALE: NTS

A – CMT
REV DATE BY DESCRIPTION

WARNING
0 1/2 1
IF THIS BAR DOES NOT MEASURE 1" THEN DRAWING IS NOT TO SCALE.

Colorado State University

COLORADO STATE UNIVERSITY
ENGINEERING RESEARCH CENTER
STEEL RBS CONNECTION #2 DETAILS

DESIGNED C. TURBERT
DRAWN C. TURBERT
CHECKED H. MAHMOUD
ISSUED DATE –

DRAWING C–02
SCALE: NONE

*Note: Drawings were made for experimental testing that is to be performed on the two beam-columns subassemblies. Because of this the member lengths provided in the drawings were adjusted to accommodate experimental setup restrictions.

APPENDIX C

EARTHQUAKE RECORDS

Earthquake Record Selection

All records are obtained from FEMA-P695 Ground Motion Record Set. The following section provides a brief description of the selection of earthquake records from this set. It includes a general overview of both the Far-Field and Near-Field record sets including pertinent tables taken from FEMA-P695. It then describes the objective taken into consideration during the selection process and finally the selected records.

- **Far-Field**: ≥ 10 km
    - The twenty-two records are taken from 14 events that occurred between 1971 and 1999. Of the 14 events, eight were United States (California) earthquakes and six were from five different foreign countries. Event magnitudes range from M6.5 to M7.6 with an average magnitude of M7.0 for the Far-Field record set.
    - Sixteen sites are classified as Site Class D (stiff soil sites) and the remaining six are classified as Site Class C (very stiff soil sites). Fifteen records are from events of predominantly strike-slip faulting and the remaining seven records are from events of predominantly thrust (or reverse) faulting.
    - Site-source distances are given for the closest distance to fault rupture, Campbell R distance, and Joyner-Boore horizontal distance to the surface projection of the rupture. Based on the average of Campbell and Boore-Joyner fault distances, the minimum site-source distance is 11.1 km, the maximum distance is 26.4 km and the average distance is 16.4 km for the Far-Field record set.
    - Peak ground acceleration values vary from 0.21g to 0.82g with an average PGAmax of 0.43g. Peak ground velocity values vary from 19 cm/second to 115 cm/second with an average PGVmax of 46 cm/second.
    - Normalization factors vary from 0.41 to 2.10. After normalization, peak ground acceleration values vary from 0.18g to 0.58g with an average PGAmax of 0.40g. Peak ground velocity values vary from 36 cm/second to 54 cm/second with an average PGVmax of 42 cm/second. Table A-5 shows that normalization of the records (by PGVPEER) has reduced the dispersion in PGVmax to a level consistent with that of PGAmax without appreciably affecting average values of PGAmax or PGVmax for the record set.

Table C-1. Summary of Earthquake Event and Recording Station Data for the Far-Field Record Set (FEMA-P695, 2009)

ID No.	Earthquake			Recording Station	
	M	Year	Name	Name	Owner
1	6.7	1994	Northridge	Beverly Hills - Mulhol	USC
2	6.7	1994	Northridge	Canyon Country-WLC	USC
3	7.1	1999	Duzce, Turkey	Bolu	ERD
4	7.1	1999	Hector Mine	Hector	SCSN
5	6.5	1979	Imperial Valley	Delta	UNAMUCSD
6	6.5	1979	Imperial Valley	El Centro Array #11	USGS
7	6.9	1995	Kobe, Japan	Nishi-Akashi	CUE
8	6.9	1995	Kobe, Japan	Shin-Osaka	CUE
9	7.5	1999	Kocaeli, Turkey	Duzce	ERD
10	7.5	1999	Kocaeli, Turkey	Arcelik	KOERI
11	7.3	1992	Landers	Yermo Fire Station	CDMG
12	7.3	1992	Landers	Coolwater	SCE
13	6.9	1989	Loma Prieta	Capitola	CDMG
14	6.9	1989	Loma Prieta	Gilroy Array #3	CDMG
15	7.4	1990	Manjil, Iran	Abbar	BHRC
16	6.5	1987	Superstition Hills	El Centro Imp. Co.	CDMG
17	6.5	1987	Superstition Hills	Poe Road (temp)	USGS
18	7.0	1992	Cape Mendocino	Rio Dell Overpass	CDMG
19	7.6	1999	Chi-Chi, Taiwan	CHY101	CWB
20	7.6	1999	Chi-Chi, Taiwan	TCU045	CWB
21	6.6	1971	San Fernando	LA - Hollywood Stor	CDMG
22	6.5	1976	Friuli, Italy	Tolmezzo	--

Table C-2. Summary of Site and Source Data for the Far-Field Record Set (FEMA-P695, 2009)

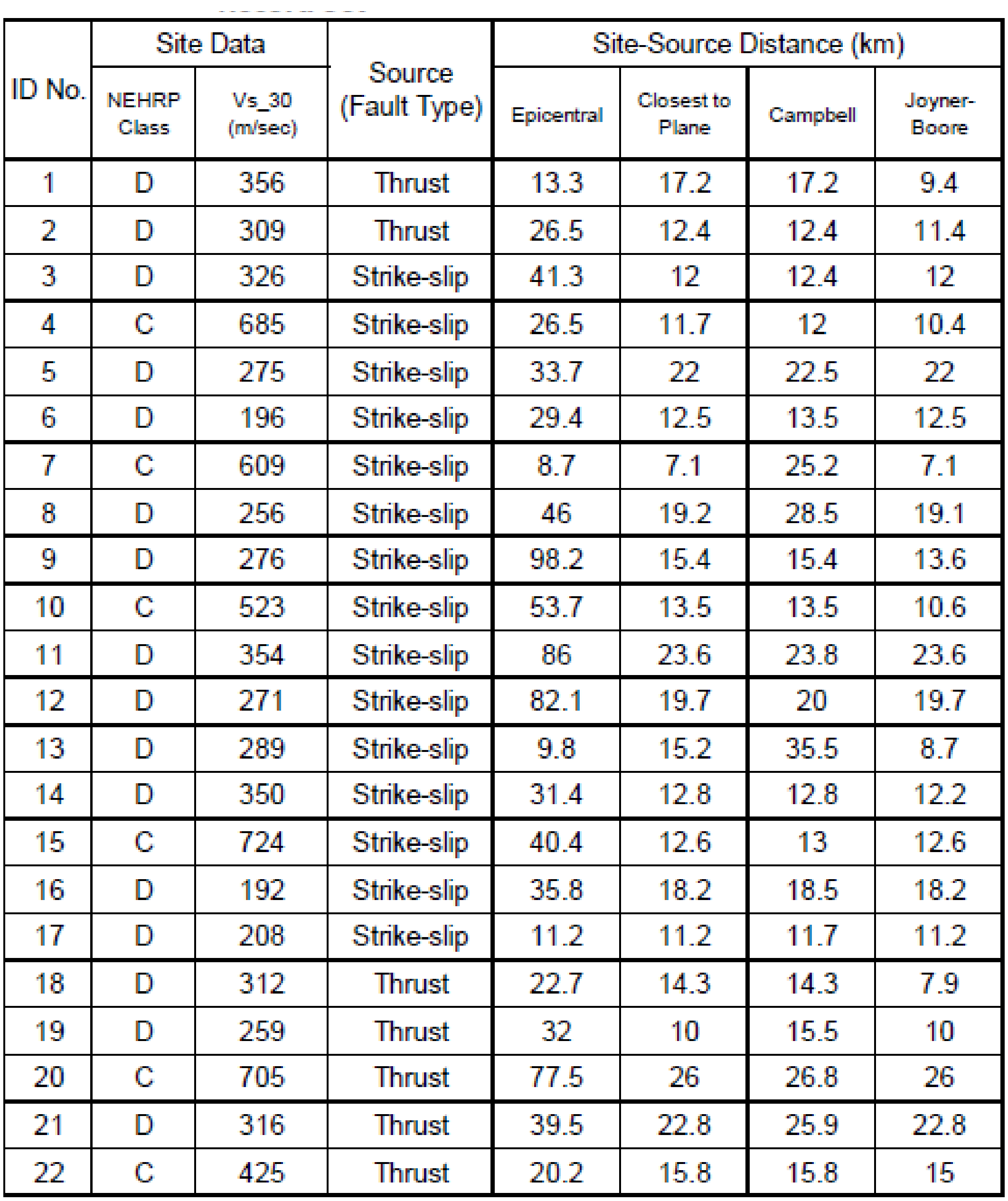

ID No.	Site Data		Source (Fault Type)	Site-Source Distance (km)			
	NEHRP Class	Vs_30 (m/sec)		Epicentral	Closest to Plane	Campbell	Joyner-Boore
1	D	356	Thrust	13.3	17.2	17.2	9.4
2	D	309	Thrust	26.5	12.4	12.4	11.4
3	D	326	Strike-slip	41.3	12	12.4	12
4	C	685	Strike-slip	26.5	11.7	12	10.4
5	D	275	Strike-slip	33.7	22	22.5	22
6	D	196	Strike-slip	29.4	12.5	13.5	12.5
7	C	609	Strike-slip	8.7	7.1	25.2	7.1
8	D	256	Strike-slip	46	19.2	28.5	19.1
9	D	276	Strike-slip	98.2	15.4	15.4	13.6
10	C	523	Strike-slip	53.7	13.5	13.5	10.6
11	D	354	Strike-slip	86	23.6	23.8	23.6
12	D	271	Strike-slip	82.1	19.7	20	19.7
13	D	289	Strike-slip	9.8	15.2	35.5	8.7
14	D	350	Strike-slip	31.4	12.8	12.8	12.2
15	C	724	Strike-slip	40.4	12.6	13	12.6
16	D	192	Strike-slip	35.8	18.2	18.5	18.2
17	D	208	Strike-slip	11.2	11.2	11.7	11.2
18	D	312	Thrust	22.7	14.3	14.3	7.9
19	D	259	Thrust	32	10	15.5	10
20	C	705	Thrust	77.5	26	26.8	26
21	D	316	Thrust	39.5	22.8	25.9	22.8
22	C	425	Thrust	20.2	15.8	15.8	15

Table C-3. Summary of PEER-NGA Database Information and Parameters of Recorded Ground Motions for the Far-Field Record Set (FEMA-P695, 2009)

ID No.	PEER-NGA Record Information				Recorded Motions	
	Record Seq. No.	Lowest Freq (Hz.)	File Names - Horizontal Records		PGA_{max} (g)	PGV_{max} (cm/s.)
			Component 1	Component 2		
1	953	0.25	NORTHR/MUL009	NORTHR/MUL279	0.52	63
2	960	0.13	NORTHR/LOS000	NORTHR/LOS270	0.48	45
3	1602	0.06	DUZCE/BOL000	DUZCE/BOL090	0.82	62
4	1787	0.04	HECTOR/HEC000	HECTOR/HEC090	0.34	42
5	169	0.06	IMPVALL/H-DLT262	IMPVALL/H-DLT352	0.35	33
6	174	0.25	IMPVALL/H-E11140	IMPVALL/H-E11230	0.38	42
7	1111	0.13	KOBE/NIS000	KOBE/NIS090	0.51	37
8	1116	0.13	KOBE/SHI000	KOBE/SHI090	0.24	38
9	1158	0.24	KOCAELI/DZC180	KOCAELI/DZC270	0.36	59
10	1148	0.09	KOCAELI/ARC000	KOCAELI/ARC090	0.22	40
11	900	0.07	LANDERS/YER270	LANDERS/YER360	0.24	52
12	848	0.13	LANDERS/CLW-LN	LANDERS/CLW-TR	0.42	42
13	752	0.13	LOMAP/CAP000	LOMAP/CAP090	0.53	35
14	767	0.13	LOMAP/G03000	LOMAP/G03090	0.56	45
15	1633	0.13	MANJIL/ABBAR--L	MANJIL/ABBAR--T	0.51	54
16	721	0.13	SUPERST/B-ICC000	SUPERST/B-ICC090	0.36	46
17	725	0.25	SUPERST/B-POE270	SUPERST/B-POE360	0.45	36
18	829	0.07	CAPEMEND/RIO270	CAPEMEND/RIO360	0.55	44
19	1244	0.05	CHICHI/CHY101-E	CHICHI/CHY101-N	0.44	115
20	1485	0.05	CHICHI/TCU045-E	CHICHI/TCU045-N	0.51	39
21	68	0.25	SFERN/PEL090	SFERN/PEL180	0.21	19
22	125	0.13	FRIULI/A-TMZ000	FRIULI/A-TMZ270	0.35	31

- **Near-Field**: ≤ 10 km
    - NF-Pulse: Strong pulses
    - NF-No Pulse: No pulses
    - The Near-Field record set includes twenty-eight records (56 individual components) selected from the PEER-NGA database using the criteria from Section A.7 of this appendix. Fourteen records have pulses (Pulse subset) and fourteen records do not have pulses (No-Pulse subset), as judged by wavelet analysis classification of the records (Baker, 2007).
    - The twenty-eight records are taken from 14 events that occurred between 1976 and 2002. Of the 14 events, seven were United States earthquakes (six in California) and seven were from five different foreign countries. Event magnitudes range from M6.5 to M7.9 with an average magnitude of M7.0.
    - Eleven sites are classified as Site Class D (stiff soil sites), fifteen are classified as Site Class C (very stiff soil sites), and the remaining two are classified as Site Class B (rock sites). Fourteen records are from events of predominantly strike-slip faulting and the remaining fourteen records are from events of predominantly thrust (or reverse) faulting. Based on the average of Campbell and Boore-Joyner fault distances, the minimum site-source distance is 1.7 km, the maximum distance is 8.8 km, and the average distance is 4.2 km.
    - Peak ground acceleration values range from 0.22g to 1.43g with an average PGAmax of 0.60g. Peak ground velocity values range from 30 cm/second to 167 cm/second with an average PGVmax of 84 cm/second.
    - Normalization factors vary from 0.57 to 2.79. After normalization, peak ground acceleration values range from 0.19g to 1.50g with an average PGAmax of 0.60g. Peak ground velocity values range from 50 cm/second to 115 cm/second with an average PGVmax of 80 cm/second. Table A-7 shows that normalization of the records (by PGVPEER) has substantially reduced the dispersion in PGVmax without greatly affecting average values of PGAmax or PGVmax, or the dispersion in PGAmax.

Table C-4. Summary of Earthquake Event and Recording Station Data for the Near-Field Record Set (FEMA-P695, 2009)

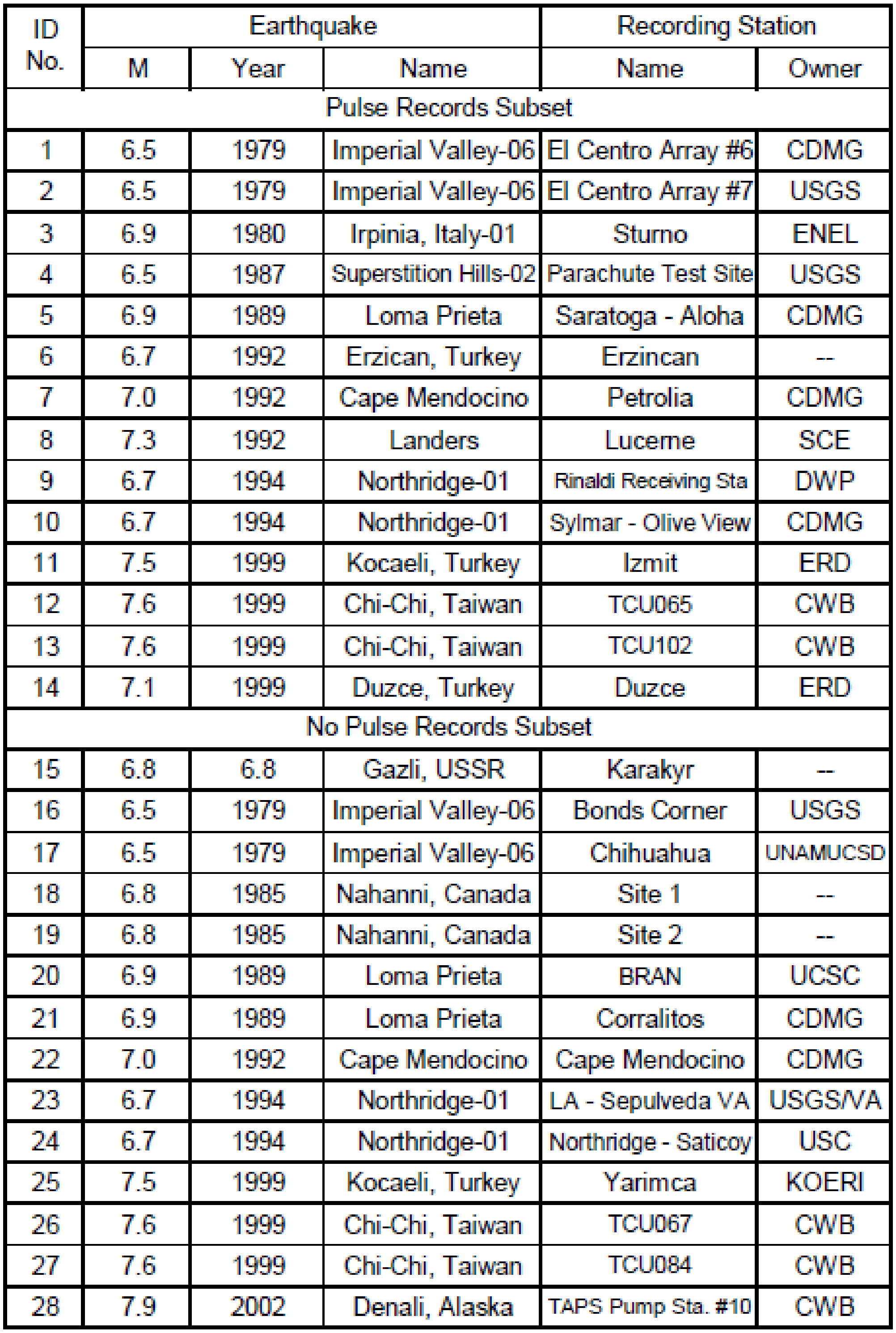

ID No.	Earthquake			Recording Station	
	M	Year	Name	Name	Owner
			Pulse Records Subset		
1	6.5	1979	Imperial Valley-06	El Centro Array #6	CDMG
2	6.5	1979	Imperial Valley-06	El Centro Array #7	USGS
3	6.9	1980	Irpinia, Italy-01	Sturno	ENEL
4	6.5	1987	Superstition Hills-02	Parachute Test Site	USGS
5	6.9	1989	Loma Prieta	Saratoga - Aloha	CDMG
6	6.7	1992	Erzican, Turkey	Erzincan	--
7	7.0	1992	Cape Mendocino	Petrolia	CDMG
8	7.3	1992	Landers	Lucerne	SCE
9	6.7	1994	Northridge-01	Rinaldi Receiving Sta	DWP
10	6.7	1994	Northridge-01	Sylmar - Olive View	CDMG
11	7.5	1999	Kocaeli, Turkey	Izmit	ERD
12	7.6	1999	Chi-Chi, Taiwan	TCU065	CWB
13	7.6	1999	Chi-Chi, Taiwan	TCU102	CWB
14	7.1	1999	Duzce, Turkey	Duzce	ERD
			No Pulse Records Subset		
15	6.8	6.8	Gazli, USSR	Karakyr	--
16	6.5	1979	Imperial Valley-06	Bonds Corner	USGS
17	6.5	1979	Imperial Valley-06	Chihuahua	UNAMUCSD
18	6.8	1985	Nahanni, Canada	Site 1	--
19	6.8	1985	Nahanni, Canada	Site 2	--
20	6.9	1989	Loma Prieta	BRAN	UCSC
21	6.9	1989	Loma Prieta	Corralitos	CDMG
22	7.0	1992	Cape Mendocino	Cape Mendocino	CDMG
23	6.7	1994	Northridge-01	LA - Sepulveda VA	USGS/VA
24	6.7	1994	Northridge-01	Northridge - Saticoy	USC
25	7.5	1999	Kocaeli, Turkey	Yarimca	KOERI
26	7.6	1999	Chi-Chi, Taiwan	TCU067	CWB
27	7.6	1999	Chi-Chi, Taiwan	TCU084	CWB
28	7.9	2002	Denali, Alaska	TAPS Pump Sta. #10	CWB

Table C-5. Summary of Site and Source Data for the Near-Field Record Set (FEMA-P695, 2009)

ID No.	Site Data		Source (Fault Type)	Site-Source Distance (km)			
	NEHRP Class	Vs_30 (m/sec)		Epicentral	Closest to Plane	Campbell	Joyner-Boore
Pulse Records Subset							
1	D	203	Strike-slip	27.5	1.4	3.5	0.0
2	D	211	Strike-slip	27.6	0.6	3.6	0.6
3	B	1000	Normal	30.4	10.8	10.8	6.8
4	D	349	Strike-slip	16.0	1.0	3.5	1.0
5	C	371	Strike-slip	27.2	8.5	8.5	7.6
6	D	275	Strike-slip	9.0	4.4	4.4	0.0
7	C	713	Thrust	4.5	8.2	8.2	0.0
8	C	685	Strike-slip	44.0	2.2	3.7	2.2
9	D	282	Thrust	10.9	6.5	6.5	0.0
10	C	441	Thrust	16.8	5.3	5.3	1.7
11	B	811	Strike-slip	5.3	7.2	7.4	3.6
12	D	306	Thrust	26.7	0.6	6.7	0.6
13	C	714	Thrust	45.6	1.5	7.7	1.5
14	D	276	Strike-slip	1.6	6.6	6.6	0.0
No Pulse Records Subset							
15	C	660	Thrust	12.8	5.5	5.5	3.9
16	D	223	Strike-slip	6.2	2.7	4.0	0.5
17	D	275	Strike-slip	18.9	7.3	8.4	7.3
18	C	660	Thrust	6.8	9.6	9.6	2.5
19	C	660	Thrust	6.5	4.9	4.9	0.0
20	C	376	Strike-slip	9.0	10.7	10.7	3.9
21	C	462	Strike-slip	7.2	3.9	3.9	0.2
22	C	514	Thrust	10.4	7.0	7.0	0.0
23	C	380	Thrust	8.5	8.4	8.4	0.0
24	D	281	Thrust	3.4	12.1	12.1	0.0
25	D	297	Strike-slip	19.3	4.8	5.3	1.4
26	C	434	Thrust	28.7	0.6	6.5	0.6
27	C	553	Thrust	8.9	11.2	11.2	0.0
28	C	553	Strike-slip	7.0	8.9	8.9	0.0

Table C-6. Summary of PEER-NGA Database Information and Parameters of Recorded Ground Motions for the Near-Field Record Set (FEMA-P695, 2009)

ID No.	PEER-NGA Record Information				Recorded Motions	
	Record Seq. No.	Lowest Freq (Hz.)	File Names - Horizontal Records		PGA_{max} (g)	PGV_{max} (cm/s.)
			FN Component	FP Component		
Pulse Records Subset						
1	181	0.13	IMPVALL/H-E06_233	IMPVALL/H-E06_323	0.44	111.9
2	182	0.13	IMPVALL/H-E07_233	IMPVALL/H-E07_323	0.46	108.9
3	292	0.16	ITALY/A-STU_223	ITALY/A-STU_313	0.31	45.5
4	723	0.15	SUPERST/B-PTS_037	SUPERST/B-PTS_127	0.42	106.8
5	802	0.13	LOMAP/STG_038	LOMAP/STG_128	0.38	55.6
6	821	0.13	ERZIKAN/ERZ_032	ERZIKAN/ERZ_122	0.49	95.5
7	828	0.07	CAPEMEND/PET_260	CAPEMEND/PET_350	0.63	82.1
8	879	0.10	LANDERS/LCN_239	LANDERS/LCN_329	0.79	140.3
9	1063	0.11	NORTHR/RRS_032	NORTHR/RRS_122	0.87	167.3
10	1086	0.12	NORTHR/SYL_032	NORTHR/SYL_122	0.73	122.8
11	1165	0.13	KOCAELI/IZT_180	KOCAELI/IZT_270	0.22	29.8
12	1503	0.08	CHICHI/TCU065_272	CHICHI/TCU065_002	0.82	127.7
13	1529	0.06	CHICHI/TCU102_278	CHICHI/TCU102_008	0.29	106.6
14	1605	0.10	DUZCE/DZC_172	DUZCE/DZC_262	0.52	79.3
No Pulse Records Subset						
15	126	0.06	GAZLI/GAZ_177	GAZLI/GAZ_267	0.71	71.2
16	160	0.13	IMPVALL/H-BCR_233	IMPVALL/H-BCR_323	0.76	44.3
17	165	0.06	IMPVALL/H-CHI_233	IMPVALL/H-CHI_323	0.28	30.5
18	495	0.06	NAHANNI/S1_070	NAHANNI/S1_160	1.18	43.9
19	496	0.13	NAHANNI/S2_070	NAHANNI/S2_160	0.45	34.7
20	741	0.13	LOMAP/BRN_038	LOMAP/BRN_128	0.64	55.9
21	753	0.25	LOMAP/CLS_038	LOMAP/CLS_128	0.51	45.5
22	825	0.07	CAPEMEND/CPM_260	CAPEMEND/CPM_350	1.43	119.5
23	1004	0.12	NORTHR/0637_032	NORTHR/0637_122	0.73	70.1
24	1048	0.13	NORTHR/STC_032	NORTHR/STC_122	0.42	53.2
25	1176	0.09	KOCAELI/YPT_180	KOCAELI/YPT_270	0.31	73.0
26	1504	0.04	CHICHI/TCU067_285	CHICHI/TCU067_015	0.56	91.8
27	1517	0.25	CHICHI/TCU084_271	CHICHI/TCU084_001	1.16	115.1
28	2114	0.03	DENALI/ps10_199	DENALI/ps10_289	0.33	126.4

- **Objectives**
  - **ASCE/SEI 7-05**: "ground motions shall consist of pairs of appropriate horizontal ground motion acceleration components that shall be selected and scaled from individual recorded events."
  - **Very Strong Ground Motions**: "The records should represent very strong ground motions corresponding to the MCE motion. In high seismic regions where buildings are at greatest risk, few recorded ground motions are intense enough, and often significant upward scaling of the records is required."
  - **Large Number of Records: "**The number of records in the set should be "statistically" sufficient such that the results of collapse evaluations adequately describe both the median value and record-to-record (RTR) variability of collapse capacity." (Wen & Wu 2001 and Dr. Mahmoud's Thesis)
  - **Structure Type Independent: "**The records should be broadly applicable to collapse evaluation of a variety of structural systems (i.e., systems that have different dynamic response properties, performance characteristics, etc.). Accordingly, records should not depend on period, or other building-specific properties of the structure."
  - **Site Hazard Independent: "**The records should be broadly applicable to collapse evaluation of structures located at different sites (i.e., sites with different ground motion hazard functions, site and source conditions, etc.). Accordingly, records should not depend on hazard de-aggregation, or other site- or hazard-dependent properties."
- **Spectral Shape Considerations**
  - "In essence, the shape of the spectrum of rare ground motions drops off more rapidly at periods both greater and less than the fundamental period of interest (i.e., has less energy), as compared to spectra of other (less rare) records. The amount by which spectral shape can influence the collapse ratio is a function of the "rareness" of the ground motions. For ductile structures located in coastal California, accounting for this spectral shape effect can cause a 40% to 60% increase in the collapse margin ratio (i.e. median collapse capacity)."
  - "The ground motion record sets do not (could not) directly incorporate the effect of spectral shape. Direct incorporation of spectral shape would necessarily require records to be selected based on the fundamental period of the structure, resulting in a different set of records for each structure of differing period. Rather, collapse margin ratios calculated using the ground motion record sets are adjusted for spectral shape effects based on structure deformation capacity and seismic design category, described in Section 7.4, using factors developed in Appendix B."
- **Earthquake Selection (Maximum Considered and Design)**
  - ACSE ground motions based on seismic design category (A-low to E-highest)
    - Design Earthquake
    - Occupancy Category (I or II)
  - The seismic provisions of ASCE/SEI 7-05 define MCE demand in terms of mapped values of short-period spectral acceleration, SS, and 1-second spectral acceleration, S1, site coefficients, Fa and Fv, and a standard response spectrum shape. For seismic design of the structural system, ASCE/SEI 7-05 defines the DE demand as two-thirds of the MCE demand. Archetypical systems are designed for DE ground motions and evaluated for collapse using the corresponding set of MCE ground motions.

- **Record Selection Criteria**
  - **Source Magnitude –** M ≥ 6.5
  - **Source Type –** Strike-Slip and Reverse (Thrust) Sources
  - **Site Conditions –** Soft Rock (Site Class C) or Stiff Soil (Site Class D)
  - **Site-Source Distance** – Far and Near Field Records
  - **Number of Records per Event** – Not more than 2 per set
  - **Strongest Ground Motion Records** – PGA > 0.2g and PGV > 15 cm/s
  - **Strong Motion Instrument Capability –** Instruments with valid frequency content of at least 4 sec
  - **Strong Motion Instrument Location –** Free-Field Locations (or ground floor of small building)
- **Selected Records**
  - Far-Field
    - Northridge – LOS000 - #2 – 12.4km – 0.410g – 1.636 sf
    - Ducze – BOL000 - #3 – 12.0km – 0.728g – 0.929 sf
    - Loma Prieta – CAP090 - #13(2) – 15.2km – 0.443g – 1.542 sf
    - Kobe – SHI090 - #8(2) – 19.2 km – 0.212g – 1.731 sf
    - San Fernando –SF038 - #21 – 3.9km – 0.644g – 1.339 sf
  - Near-Field
    - Imperial Valley – HBCR233 - #16 – 2.7km – 0.76g – 1.002 sf
    - Loma Prieta – CLS038 - #21 – 3.9km – 0.644g – 1.339 sf
    - Erzican – EZERZ - #6 – 4.4km - 0.496g – 0.997 sf
    - Kocaeli – IZT080 - #11 – 7.2km – 0.222g – 2.347 sf
    - Northridge– LOS000 - #2 – 12.0km – 0.728g – 0.929 sf
- **Scaling Method**
  - **Normalization of Records -** Ground motion records are normalized by peak ground velocity (PGV) to remove unwarranted record-to-record variability. Normalization is an inherent feature of record sets described in this appendix. Users of the Methodology need only scale the record set as required for collapse evaluation. Individual records (of a given set) are "normalized" by their respective peak ground velocities. In essence, some records are factored upwards (and some factored downwards), while maintaining the same overall ground motion strength of the record set. Normalization by peak ground velocity is a simple way to remove unwarranted variability between records due to inherent differences in event magnitude, distance to source, source type and site conditions, while still maintaining the inherent aleatory (i.e., record-to-record) variability necessary for accurately predicting collapse fragility.
  - **Scaling of Record Sets -** For collapse evaluation, the set of (normalized) records is collectively increased (or decreased) in strength (e.g., algebraic scaling of each record by the same factor) as required to determine median collapse (i.e., the record set is scaled such that 50 percent of the records cause collapse of archetype analysis model of interest).
    - Record normalization and record set scaling to match a particular level of ground motions parallels the ground motion scaling requirements of Section 16.1.3.2 of ASCE/SEI 7-05, with the notable exception that the median value of the scaled record set need only match the MCE demand at the fundamental period, T, rather than over the range of periods required by ASCE/SEI 7-05.

Table C-7. Median 5%-Damped Spectral Acceleration of Normalized Far-Field and Near-Field Record Sets and Scaling Factors for Anchoring the Normalized Far-Field Record Set to MCE Spectral Demand (FEMA-P695, 2009)

Period $T = C_u T_a$ (seconds)	Median Value of Normalized Record Set, S_{NRT} (g)		Scaling Factors for Anchroing Far-Field Record Set to MCE Spectral Demand			
	Near-Field Set	Far-Field Set	Dmax	Cmax	Bmax	
				Dmin	Cmin	Bmin
0.25	0.936	0.779	1.93	0.96	0.64	0.32
0.3	1.020	0.775	1.94	0.97	0.65	0.32
0.35	0.939	0.761	1.97	0.99	0.66	0.33
0.4	0.901	0.748	2.00	1.00	0.67	0.33
0.45	0.886	0.749	2.00	0.89	0.59	0.30
0.5	0.855	0.736	2.04	0.82	0.54	0.27
0.6	0.833	0.602	2.49	0.83	0.55	0.28
0.7	0.805	0.537	2.40	0.80	0.53	0.27
0.8	0.739	0.449	2.50	0.83	0.56	0.28
0.9	0.633	0.399	2.50	0.83	0.56	0.28
1.0	0.571	0.348	2.59	0.86	0.58	0.29
1.2	0.476	0.301	2.49	0.83	0.55	0.28
1.4	0.404	0.256	2.51	0.84	0.56	0.28
1.6	0.356	0.208	2.70	0.90	0.60	0.30
1.8	0.319	0.168	2.98	0.99	0.66	0.33
2.0	0.284	0.148	3.05	1.02	0.68	0.34
2.2	0.258	0.133	3.08	1.03	0.68	0.34
2.4	0.230	0.118	3.18	1.06	0.71	0.35
2.6	0.210	0.106	3.28	1.09	0.73	0.36
2.8	0.190	0.091	3.53	1.18	0.79	0.39
3.0	0.172	0.080	3.75	1.25	0.83	0.42
3.5	0.132	0.063	4.10	1.37	0.91	0.46
4.0	0.104	0.052	4.29	1.43	0.95	0.48
4.5	0.086	0.046	4.34	1.45	0.96	0.48
5.0	0.072	0.041	4.43	1.48	0.98	0.49

1. Spectral acceleration values and scaling factors may be based on linear interpolation for periods not listed in the table.

Scaling of Earthquake Records

All earthquake records were normalized and scaled in accordance with FEMA-P695. The following section provides data on the scaling of the record sets. A comparison of the MCE response spectrum to the normalized and scaled earthquake records is provided in Chapter 3.

Table C-8. Ground Motion Record Set Summary and Normalization and Scaling Information

Far-Field Record Set

ATC63 #	Earthquake	Year	Magnitude	NEHRP Class	Source	Epicentral Distance (km)	Lowest Freq.	PGA (g)	PGV (cm/s)	Medain PGV	NM	Scale Factor (8)	Scale Factor (16)
2	Northridge	1994	6.7	D	Thrust	26.5	0.13	0.48	45	38	0.84444	2.0177	2.468
3	Duzce	1999	7.1	D	Strike-slip	41.3	0.06	0.82	62		0.6129		
8	Kobe	1995	6.9	D	Strike-slip	46	0.13	0.24	38		1		
13	Loma Prieta	1989	6.9	D	Strike-slip	9.8	0.13	0.53	35		1.08571		
21	San Fernando	1971	6.6	D	Thrust	39.5	0.25	0.21	19		2		

Near-Field Record Set

ATC63 #	Earthquake	Year	Magnitude	NEHRP Class	Source	Epicentral Distance (km)	Lowest Freq.	PGA (g)	PGV (cm/s)	Medain PGV	NM	Scale Factor (8)	Scale Factor (16)
6	Erzican	1992	6.7	D	Strike-slip	9	0.13	0.49	95.5	45.5	0.47644	2.65	2.782
11	Kocaeli	1999	7.5	B	Strike-slip	5.3	0.13	0.22	29.8		1.52685		
16	Imperial Valley	1979	6.5	D	Strike-slip	6.2	0.13	0.76	44.3		1.02709		
21	Loma Prieta	1989	6.9	C	Strike-slip	7.2	0.25	0.51	45.5		1		
9	Northridge	1994	6.7	D	Thrust	10.9	0.11	0.87	167.3		0.27197		

APPENDIX D

ENGINEERING RESEARCH CENTER (ERC) TEST FURNACE SETUP

D-1 Introduction

Interest in the effects of fire on various structures has significantly increased over the last several years. Historically a prescriptive approach to structural fire safety in the form of codes has been utilized, while this helps to solve the problems associated with designing structures for fire loading to a certain extent, the current process is thought to be inadequate. The validity of the prescriptive approach and its level of safety is now a concern due to the development of performance-based approaches which are able to account for the various stages and development process that occur when a structure is on fire. This new design approach has opened up an entire field of research aimed to gain a better understanding of the actual behavior and performance of structural systems when exposed to fire. This new area of research is the reason behind the design and implementation of the new Engineering Research Center (ERC) fire testing furnace. The fire testing furnace was created from an existing environmental chamber by lining the chamber with insulation and cutting holes into the sides and top of the furnace to allow various sized specimen to be supported and loaded from outside the furnace. The use of the chamber allows for precise control over the temperature within the compartment as well as an ability to test a wide range of specimen sizes. A large steel frame surrounds the furnace and is designed to support a 200-kip actuator which can be used to load the test specimen. This setup allows not only fire loading to be imposed on various specimens but also mechanical loading which can allow for simulating multi-hazard events such as a fire following an earthquake. This will be the first fire testing furnace of its size to be implemented by a university in the United States. A picture of the test setup is provided in Figure D-1.

Figure D-1. Engineering Research Center Fire Testing Furnace

D-2 Completed Tasks

The following sections provide an overview of the various tasks that have been completed on the design and construction of the fire testing furnace. A description of the task, materials used and personnel involved is provided. Tasks are presented in the order they were completed.

D-2.1 Environmental Chamber Retrofit

Task 1 consisted of retrofitting the existing Environmental Chamber at the ERC so it is suitable to be used as a fire testing furnace. The first part of this task was removing two 4’x4’ sections from either side of the existing chamber as well as one 4’x4’ section from the roof of the chamber. The second part of this task was removing the existing light framing from the interior of the chamber and sealing off any vulnerable portions exposed from its removal. The final part of this task was cleaning the area around the chamber to allow easy access for other components of the setup. The first part of the task, removing the three 4’x4’ sections, was performed by the ERC shop staff under the supervision of Junior Garza based on provided drawings. The drawing created for this task is presented in Figure D-2. Removing the existing lighting and cleaning the chamber and the surrounding area was performed without outside assistance.

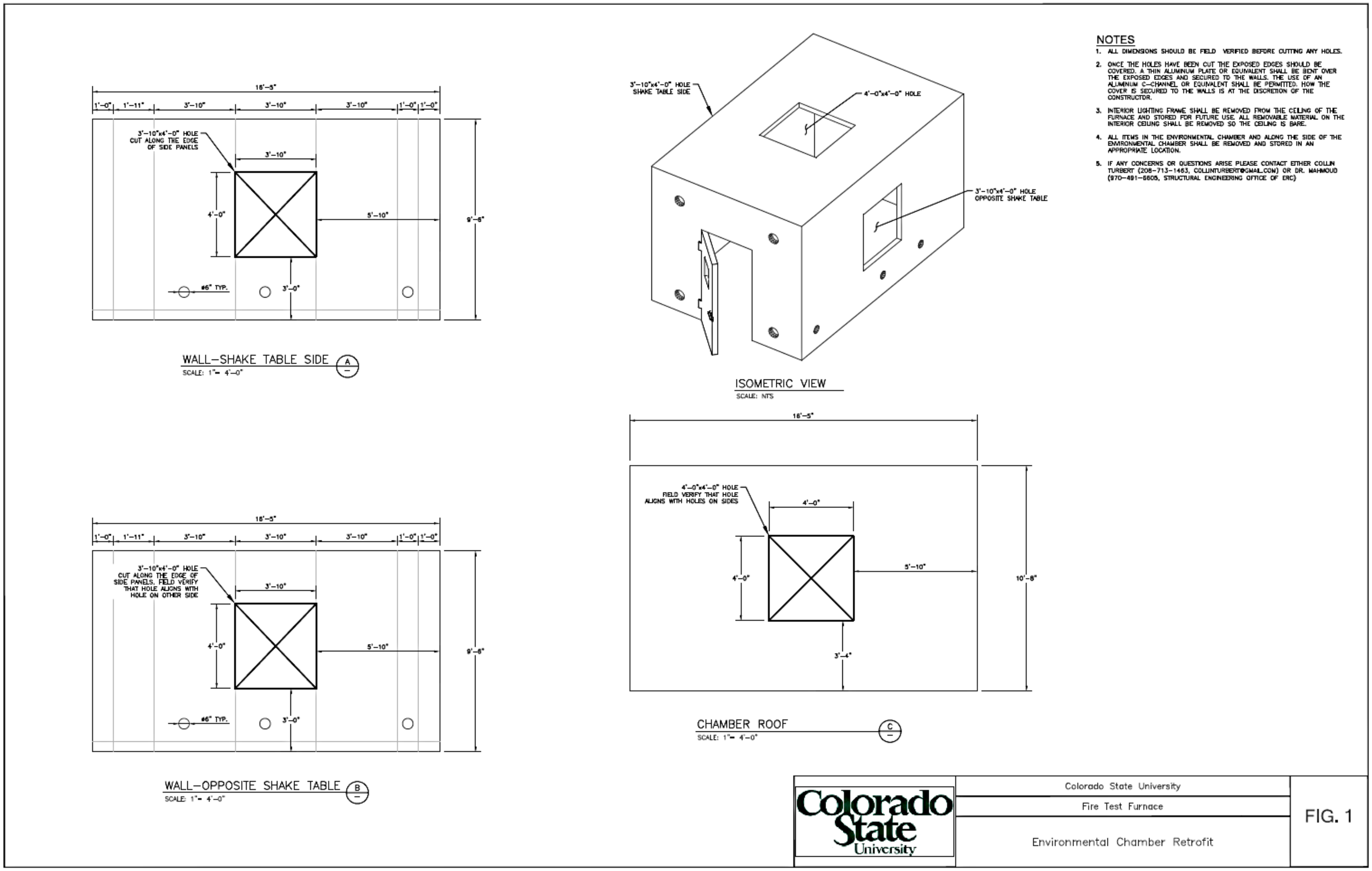

NOTES

1. ALL DIMENSIONS SHOULD BE FIELD VERIFIED BEFORE CUTTING ANY HOLES.
2. ONCE THE HOLES HAVE BEEN CUT THE EXPOSED EDGES SHOULD BE COVERED. A THIN ALUMINUM PLATE OR EQUIVALENT SHALL BE BENT OVER THE EXPOSED EDGES AND SECURED TO THE WALLS. THE USE OF AN ALUMINUM C–CHANNEL OR EQUIVALENT SHALL BE PERMITTED. HOW THE COVER IS SECURED TO THE WALLS IS AT THE DISCRETION OF THE CONSTRUCTOR.
3. INTERIOR LIGHTING FRAME SHALL BE REMOVED FROM THE CEILING OF THE FURNACE AND STORED FOR FUTURE USE. ALL REMOVABLE MATERIAL ON THE INTERIOR CEILING SHALL BE REMOVED SO THE CEILING IS BARE.
4. ALL ITEMS IN THE ENVIRONMENTAL CHAMBER AND ALONG THE SIDE OF THE ENVIRONMENTAL CHAMBER SHALL BE REMOVED AND STORED IN AN APPROPRIATE LOCATION.
5. IF ANY CONCERNS OR QUESTIONS ARISE PLEASE CONTACT EITHER COLLIN TURBERT (208–713–1463, COLLINTURBERT@GMAIL.COM) OR DR. MAHMOUD (970–491–6605, STRUCTURAL ENGINEERING OFFICE OF ERC)

Figure D2. Furnace Retrofit Drawing (11”x17”)

D-2.2 Acquisition of Project Material

Task 2 consisted of purchasing the ceramic heating plates, control panel, thermocouples and Kaowool insulation to be used for the project. All items were purchased from E&M sales. The selection of the ceramic heating plates and control panel were based on discussions with Greg Curnow of E&M sales as well as consideration for the objectives of this project. The initial purchase included the following items:

- (6) Ceramic Plate Heaters
    - Rated at 240/240 volts
    - 11,500 watts
    - Up to 1875° F
    - For use in dry air
- (1) Control Panel
    - 480 V AC
    - 100 amp
    - 36”x36”x12” NEMA 12 Enclosure on Mobile Stand
    - 3 controllers for 3 zones of control
    - 10 ft. power cord and plug-in
    - Alarm lights in the event of a shorted heater
- (3) Thermocouples
    - Construction style 20
    - Sheath diameter 1/8”
    - Fiberglass w/ SS overbraid, 24 GA
- (1) Thermocouple Wire
    - Rated to 2200° F
    - 250 ft.
- (10) Kaowool Insulation Blanket
    - 2’x25’x1”
    - Rated to 2400° F

In addition to this initial purchase two supplementary purchases of Kaowool insulation were made. It was decided that the initial order would be fairly conservative on the amount of insulation since the actual amount needed was hard to determine at that time. This resulted in an additional two purchases of six and then four rolls of Kaowool insulation blanket. Several other smaller items also had to be obtained including adhesive and clamps for installing the insulation.

D-2.3 Ceramic Heating Plate Cases

Once the heating plates were purchased and delivered protective casing had to be made to store the plates. The plates are extremely fragile and expensive so keeping them protected from incidental damage was an essential part of the project. For this task six wood cases were built for storing and protecting the plates. It should be noted that Jeffery Newcomer helped with the building process.

D-2.4 Design of Support Frame

The design of the steel frame used to support the 200-kip actuator was performed and checked based on current standards and practice. The finite element program SAP2000 was used to determine all design loads on the structure. The frame was initially being used to support a vertical actuator used for loading specimen perpendicular to the ground. To retrofit the frame so it could be used for a 200-kip actuator that applies loading in the horizontal plane several changes had to be made. First the support beam of the structure, which consists of two W24x55 wide flange members, had to be flipped such that the strong axis was placed in the loading direction. This beam also had to be strengthened to withstand the expected loading from the actuator which was done by welding two 0.5" plates to the exterior of the beam. In addition lateral x-bracing had to be added to support the structure. The design calculations and a depiction of the SAP2000 finite element model are provided below.

Columns Design Check

Units: $kip := 1000 lbf$ $ksi := 1000 psi$ $kcf := kip \cdot ft^{-3}$ $\gamma_w := 62.4 pcf$

Beam Design Using a Wide Flange:

Dimensions

Distance Supported by Beam $L := 16.5 ft$

Using a W8X28 $w_b := 28 \frac{lbf}{ft}$ $d := 8.06 in$ $tw := .285 in$ $Ix := 98 in^4$ $A_g := 8.24 in^2$ $r_{min} := 1.62 in$ $S_x := 24.3 in^3$

$F_y := 50 \cdot ksi$ $E := 29000 ksi$ $F_u := 65 ksi$ $Iy := 21.7 in^4$ $h := 6.125 in$ $S_y := 6.63 in^3$

Loads

Maximum Shear $V := 55.25 kip$

Maximum Moment $M := 51.5 kip \cdot ft$

Maximum Deflection $\Delta_{max} := .0129 ft$

Maximum Compression $C := 55 kip$

Minor Axis Shear $Vmin := 2.54 kip$

Maximum Tension $T := 50.37 kip$

Minor Axis Moment $Mmin := 4.69 kip \cdot ft$

Calculations

Max Allowable Deflection $\Delta_{max.Allow} := \frac{L}{360}$ $\Delta_{max.Allow} = 0.55 \cdot in$

Check Deflection $Check_{def} := if(\Delta_{max} \le \Delta_{max.Allow}, "OK", "REDESIGN")$ $Check_{def} = "OK"$

Yielding Stress $F_b := \frac{M}{S_x}$ $F_b = 25.43 ksi$

Yield Capacity Used $Capacity_1 := \frac{F_b}{F_y}$ $Capacity_1 = 0.509$

Check Bending Stress in Beam $Check_{bending} := if(F_b < F_y \cdot 0.6, "OK", "REDESIGN")$ $Check_{bending} = "OK"$

Yielding Stress Minor $F_{bmin} := \frac{Mmin}{S_y}$ $F_{bmin} = 8.49 ksi$

Yield Capacity Used Minor $Capacity_2 := \frac{F_{bmin}}{F_y}$ $Capacity_2 = 0.17$

Check Minor Bending Stress in Beam $Check_{bendingmin} := if(F_{bmin} < F_y \cdot 0.6, "OK", "REDESIGN")$ $Check_{bendingmin} = "OK"$

Check Shear $Aw := d \cdot tw$ $Cv := 1$

Shear Variables $Vn := 0.6 F_y \cdot Aw \cdot Cv$ $Aw = 2.297 in^2$ $Vn = 68.913 kip$

Shear Strength $Check_{shear} := if\left(V < \frac{Vn}{1.5}, "OK", "REDESIGN"\right)$ $Check_{shear} = "REDESIGN"$

Check Shear Minor $Aw := d \cdot tw$ $Cv := 1$

Shear Variables $Vn := 0.6 \cdot F_y \cdot Aw \cdot Cv$ $Aw = 2.297 \cdot in^2$ $Vn = 68.913 \cdot kip$

Shear Strength Minor

$$\text{Check}_{\text{shearmin}} := \text{if}\left(\text{Vmin} < \frac{\text{Vn}}{1.5}, \text{"OK"}, \text{"REDESIGN"}\right)$$

$\text{Check}_{\text{shearmin}} = \text{"OK"}$

Check Tension

Yielding or Rupture

$$\text{Check}_{\text{tension}} := \text{if}\left[\frac{\left(F_y \cdot A_g\right)}{1.67} > \frac{\left(F_u \cdot A_g\right)}{2}, \text{"RUPTURE"}, \text{"YEILD"}\right]$$

$\text{Check}_{\text{tension}} = \text{"YEILD"}$

Check for tensile yielding

$\text{Pn} := F_y \cdot A_g \qquad \Omega t := 1.67$

$$\text{Check}_{\text{tensile}} := \text{if}\left(\frac{\text{Pn}}{\Omega t} > T, \text{"OK"}, \text{"REDESIGN"}\right)$$

$\text{Check}_{\text{tensile}} = \text{"OK"}$

Check Compression

Check Slenderness

$$\lambda p := 3.76 \cdot \sqrt{\frac{E}{F_y}} = 90.553 \qquad \lambda r := 5.70 \cdot \sqrt{\frac{E}{F_y}} = 137.274 \qquad \frac{h}{tw} = 21.491$$

Compresssion

$$K := 1 \qquad K \cdot L = 16.5\,\text{ft} \qquad \frac{K \cdot L}{r_{\min}} = 122.222$$

$$\text{Check} := \text{if}\left(\frac{K \cdot L}{r_{\min}} < 200, \text{"OK"}, \text{"BAD"}\right)$$

$\text{Check} = \text{"OK"}$

$$F_e := \frac{\pi^2 \cdot E}{\left(\frac{K \cdot L}{r_{\min}}\right)^2} \qquad F_e = 19.16 \cdot \text{ksi}$$

$$F_{cr} := 0.877 \cdot F_e \quad F_{cr} = 16.803 \cdot \text{ksi} \quad C_{cr} := 0.6 \cdot F_{cr} \cdot A_g \quad C_{cr} = 83.076 \cdot \text{kip}$$

$$\text{Check}_{\text{comp}} := \text{if}\left(C_{cr} > C, \text{"OK"}, \text{"REDESIGN"}\right)$$

$\text{Check}_{\text{comp}} = \text{"OK"}$

Check Buckling

$$P_{cr} := \frac{\pi^2 \cdot E \cdot A_g}{\left(\frac{K \cdot L}{r_{\min}}\right)^2} \qquad P_{cr} = 157.879 \cdot \text{kip}$$

$$\text{Check}_{\text{buck}} := \text{if}\left(P_{cr} > C, \text{"OK"}, \text{"REDESIGN"}\right)$$

$\text{Check}_{\text{buck}} = \text{"OK"}$

Support Beam Design Check

Units: $\text{kip} := 1000\text{lbf}$ $\text{ksi} := 1000\text{psi}$ $\text{kcf} := \text{kip}\cdot\text{ft}^{-3}$ $\gamma_w := 62.4\text{pcf}$

Beam Design Using a Wide Flange:

Dimensions

Distance Supported by Beam $L := 21\text{ft}$

Using W21X50

$w_b := 50\dfrac{\text{lbf}}{\text{ft}}$ $d := 20.8\text{in}$ $tw := .38\text{in}$ $Ix := 984\text{in}^4$ $A_g := 14.7\text{in}^2$ $S_x := 94.5\text{in}^3$

$F_y := 50\cdot\text{ksi}$ $E := 29000\text{ksi}$ $F_u := 65\text{ksi}$ $Iy := 24.9\text{in}^4$ $h := 18.405\text{in}$ $r_{min} := 1.62\text{in}$ $S_y := 7.64\text{in}^3$

Loads

Maximum Shear	$V := 14.1\text{kip}$		
Maximum Moment	$M := 86.9\text{kip}\cdot\text{ft}$	Maximum Deflection	$\Delta_{max} := .019\text{ft}$
Maximum Compression	$C := 31.7\text{kip}$	Minor Axis Shear	$Vmin := 1.77\text{kip}$
Maximum Tension	$T := 33.1\text{kip}$	Minor Axis Moment	$Mmin := 16.34\text{kip}\cdot\text{f}$

Calculations

Max Allowable Deflection	$\Delta_{max.Allow} := \dfrac{L}{360}$	$\Delta_{max.Allow} = 0.7\cdot\text{in}$
Check Deflection	$Check_{def} := \text{if}\left(\Delta_{max} \le \Delta_{max.Allow}, \text{"OK"}, \text{"REDESIGN"}\right)$	$\boxed{Check_{def} = \text{"OK"}}$
Yielding Stress	$F_b := \dfrac{M}{S_x}$	$F_b = 11.03\text{ksi}$
Yield Capacity Used	$Capacity_1 := \dfrac{F_b}{F_y}$	$Capacity_1 = 0.221$
Check Bending Stress in Beam	$Check_{bending} := \text{if}\left(F_b < F_y\cdot 0.6, \text{"OK"}, \text{"REDESIGN"}\right)$	$\boxed{Check_{bending} = \text{"OK"}}$
Yielding Stress Minor	$F_{bmin} := \dfrac{Mmin}{S_y}$	$F_{bmin} = 25.66\text{ksi}$
Yield Capacity Used Minor	$Capacity_1 := \dfrac{F_{bmin}}{F_y}$	$Capacity_1 = 0.513$
Check Minor Bending Stress in Beam	$Check_{bendingmin} := \text{if}\left(F_{bmin} < F_y\cdot 0.6, \text{"OK"}, \text{"REDESIGN"}\right)$	$\boxed{Check_{bendingmin} = \text{"OK"}}$
Check Shear	$Aw := d\cdot tw$ $Cv := 1$	
Shear Variables	$Vn := 0.6F_y\cdot Aw\cdot Cv$	$Aw = 7.904\,\text{in}^2$ $Vn = 237.12\text{kip}$
Shear Strength	$Check_{shear} := \text{if}\left(V < \dfrac{Vn}{1.5}, \text{"OK"}, \text{"REDESIGN"}\right)$	$Check_{shear} = \text{"OK"}$
Check Shear Minor	$Aw := d\cdot tw$ $Cv := 1$	
Shear Variables	$Vn := 0.6\cdot F_y\cdot Aw\cdot Cv$	$Aw = 7.904\cdot\text{in}^2$ $Vn = 237.12\cdot\text{kip}$

Shear Strength Minor

$$\text{Check}_{\text{shearmin}} := \text{if}\left(\text{Vmin} < \frac{\text{Vn}}{1.5}, \text{"OK"}, \text{"REDESIGN"}\right) \qquad \text{Check}_{\text{shearmin}} = \text{"OK"}$$

Check Tension

Yielding or Rupture

$$\text{Check}_{\text{tension}} := \text{if}\left[\frac{\left(F_y \cdot A_g\right)}{1.67} > \frac{\left(F_u \cdot A_g\right)}{2}, \text{"RUPTURE"}, \text{"YEILD"}\right] \qquad \text{Check}_{\text{tension}} = \text{"YEILD"}$$

Check for tensile yielding

$$\text{Pn} := F_y \cdot A_g \qquad \Omega t := 1.67$$

$$\text{Check}_{\text{tensile}} := \text{if}\left(\frac{\text{Pn}}{\Omega t} > T, \text{"OK"}, \text{"REDESIGN"}\right) \qquad \text{Check}_{\text{tensile}} = \text{"OK"}$$

Check Compression

Check Slenderness

$$\lambda p := 3.76 \cdot \sqrt{\frac{E}{F_y}} = 90.553 \qquad \lambda r := 5.70 \cdot \sqrt{\frac{E}{F_y}} = 137.274 \qquad \frac{h}{tw} = 48.434$$

Compresssion

$$K := 1 \qquad K \cdot L = 21\,\text{ft} \qquad \frac{K \cdot L}{r_{\text{min}}} = 155.556 \qquad \text{Check} := \text{if}\left(\frac{K \cdot L}{r_{\text{min}}} < 200, \text{"OK"}, \text{"BAD"}\right)$$

$$F_e := \frac{\pi^2 \cdot E}{\left(\frac{K \cdot L}{r_{\text{min}}}\right)^2} \qquad F_e = 11.828 \cdot \text{ksi} \qquad \text{Check} = \text{"OK"}$$

$$F_{cr} := 0.877 \cdot F_e \quad F_{cr} = 10.374 \cdot \text{ksi} \quad C_{cr} := 0.6 \cdot F_{cr} \cdot A_g \quad C_{cr} = 91.494 \cdot \text{kip}$$

$$\text{Check}_{\text{comp}} := \text{if}\left(C_{cr} > C, \text{"OK"}, \text{"REDESIGN"}\right) \qquad \text{Check}_{\text{comp}} = \text{"OK"}$$

Check Buckling

$$P_{cr} := \frac{\pi^2 \cdot E \cdot A_g}{\left(\frac{K \cdot L}{r_{\text{min}}}\right)^2} \qquad P_{cr} = 173.878 \cdot \text{kip} \quad \text{Check}_{\text{buck}} := \text{if}\left(P_{cr} > C, \text{"OK"}, \text{"REDESIGN"}\right)$$

$$\text{Check}_{\text{buck}} = \text{"OK"}$$

Loading Beam Design Check

Units: $kip := 1000lbf$ $ksi := 1000psi$ $kcf := kip \cdot ft^{-3}$ $\gamma_w := 62.4pcf$

Beam Design Using a Wide Flange:

Dimensions

Distance Supported by Beam $L := 21ft$

Using two W24X55 $w_b := 110\frac{lbf}{ft}$ $d := 23.6in$ $tw := .79in$ $Ix := 2700in^4$ $A_g := 32.4in^2$ $S_x := 228in^3$

$F_y := 50 \cdot ksi$ $E := 29000ksi$ $F_u := 65ksi$ $Iy := 260in^4$ $h := 6.125in$ $r_{min} := 1.62in$ $S_y := 37in^3$

Loads

Maximum Shear	$V := 100kip$		
Maximum Moment	$M := 1050kip \cdot ft$	Maximum Deflection	$\Delta_{max} := .111ft$
Maximum Compression	$C := 5kip$	Minor Axis Shear	$Vmin := 3kip$
Maximum Tension	$T := 5kip$	Minor Axis Moment	$Mmin := 35kip \cdot ft$

Calculations

Max Allowable Deflection $\Delta_{max.Allow} := \frac{L}{360}$ $\Delta_{max.Allow} = 0.7 \cdot in$

Check Deflection $Check_{def} := if(\Delta_{max} \le \Delta_{max.Allow}, "OK", "REDESIGN")$ $Check_{def} = "REDESIGN"$

Yielding Stress $F_b := \frac{M}{S_x}$ $F_b = 55.26ksi$

Yield Capacity Used $Capacity_1 := \frac{F_b}{F_y}$ $Capacity_1 = 1.105$

Check Bending Stress in Beam $Check_{bending} := if(F_b < F_y \cdot 0.6, "OK", "REDESIGN")$ $Check_{bending} = "REDESIGN"$

Add 1/2" Plate to both sides of beams $S_{xnew} := 433in^3$

Yielding Stress New $F_{bnew} := \frac{M}{S_{xnew}}$ $F_{bnew} = 29.1 \cdot ksi$

Yield Capacity Used New $Capacity_2 := \frac{F_{bnew}}{F_y}$ $Capacity_2 = 0.582$

Check Bending Stress in Beam New $Check_{bendingn} := if(F_{bnew} < F_y \cdot 0.6, "OK", "REDESIGN")$ $Check_{bendingn} = "OK"$

Yielding Stress Minor $F_{bmin} := \frac{Mmin}{S_y}$ $F_{bmin} = 11.35ksi$

Yield Capacity Used Minor $Capacity_1 := \frac{F_{bmin}}{F_y}$ $Capacity_1 = 0.227$

Check Minor Bending Stress in Beam $Check_{bendingmin} := if(F_{bmin} < F_y \cdot 0.6, "OK", "REDESIGN")$ $Check_{bendingmin} = "OK"$

Check Shear $Aw := d \cdot tw \qquad Cv := 1$

Shear Variables $Vn := 0.6 \cdot F_y \cdot Aw \cdot Cv \qquad Aw = 18.644 \cdot in^2 \qquad Vn = 559.32 \cdot kip$

Shear Strength $Check_{shear} := if\left(V < \frac{Vn}{1.5}, \text{"OK"}, \text{"REDESIGN"}\right) \qquad Check_{shear} = \text{"OK"}$

Check Shear Minor $Aw := d \cdot tw \qquad Cv := 1$

Shear Variables $Vn := 0.6 \cdot F_y \cdot Aw \cdot Cv \qquad Aw = 18.644 \cdot in^2 \qquad Vn = 559.32 \cdot kip$

Shear Strength Minor $Check_{shearmin} := if\left(Vmin < \frac{Vn}{1.5}, \text{"OK"}, \text{"REDESIGN"}\right) \qquad Check_{shearmin} = \text{"OK"}$

Check Tension

Yielding or Rupture

$$Check_{tension} := if\left[\frac{(F_y \cdot A_g)}{1.67} > \frac{(F_u \cdot A_g)}{2}, \text{"RUPTURE"}, \text{"YEILD"}\right] \qquad Check_{tension} = \text{"YEILD"}$$

Check for tensile yielding

$$Pn := F_y \cdot A_g \qquad \Omega t := 1.67$$

$$Check_{tensile} := if\left(\frac{Pn}{\Omega t} > T, \text{"OK"}, \text{"REDESIGN"}\right) \qquad Check_{tensile} = \text{"OK"}$$

Check Compression

Check Slenderness

$$\lambda p := 3.76 \cdot \sqrt{\frac{E}{F_y}} = 90.553 \qquad \lambda r := 5.70 \cdot \sqrt{\frac{E}{F_y}} = 137.274 \qquad \frac{h}{tw} = 7.753$$

Compresssion

$$K := 1 \qquad K \cdot L = 21\,ft \qquad \frac{K \cdot L}{r_{min}} = 155.556 \qquad Check := if\left(\frac{K \cdot L}{r_{min}} < 200, \text{"OK"}, \text{"BAD"}\right)$$

$$F_e := \frac{\pi^2 \cdot E}{\left(\frac{K \cdot L}{r_{min}}\right)^2} \qquad F_e = 11.828 \cdot ksi \qquad Check = \text{"OK"}$$

$$F_{cr} := 0.877 \cdot F_e \quad F_{cr} = 10.374 \cdot ksi \quad C_{cr} := 0.6 \cdot F_{cr} \cdot A_g \quad C_{cr} = 201.661 \cdot kip$$

$$Check_{comp} := if\left(C_{cr} > C, \text{"OK"}, \text{"REDESIGN"}\right) \qquad Check_{comp} = \text{"OK"}$$

Check Buckling

$$P_{cr} := \frac{\pi^2 \cdot E \cdot A_g}{\left(\frac{K \cdot L}{r_{min}}\right)^2} \qquad P_{cr} = 383.241 \cdot kip \quad Check_{buck} := if\left(P_{cr} > C, \text{"OK"}, \text{"REDESIGN"}\right)$$

$$Check_{buck} = \text{"OK"}$$

Cross Brace Design Check

Units: $kip := 1000 lbf$ $ksi := 1000 psi$ $kcf := kip \cdot ft^{-3}$ $\gamma_w := 62.4 pcf$

Cross Brace Design Using a HSS Section:

Dimensions

Distance Supported by Beam $L := 20 ft$

Using a HSS 4x4x1/4 $w_b := 12.18 \frac{lbf}{ft}$ $d := 4 in$ $tw := .25 in$ $Ix := 7.8 in^4$ $A_g := 3.37 in^2$ $r_{min} := 1.52 in$ $S_x := 3.9 in^3$

$F_y := 50 \cdot ksi$ $E := 29000 ksi$ $F_u := 65 ksi$ $Iy := 7.8 in^4$ $h := 6.125 in$ $S_y := 3.9 in^3$

Loads

Maximum Shear $V := .15 kip$

Maximum Moment $M := 1.1 kip \cdot ft$ Maximum Deflection $\Delta_{max} := .0083 ft$

Maximum Compression $C := 66.8 kip$ Minor Axis Shear $Vmin := .15 kip$

Maximum Tension $T := 66.9 kip$ Minor Axis Moment $Mmin := 1.1 kip \cdot ft$

Calculations

Max Allowable Deflection $\Delta_{max.Allow} := \frac{L}{360}$ $\Delta_{max.Allow} = 0.667 in$

Check Deflection $Check_{def} := if(\Delta_{max} \le \Delta_{max.Allow}, "OK", "REDESIGN")$ $Check_{def} = "OK"$

Yielding Stress $F_b := \frac{M}{S_x}$ $F_b = 3.38 ksi$

Yield Capacity Used $Capacity_1 := \frac{F_b}{F_y}$ $Capacity_1 = 0.068$

Check Bending Stress in Beam $Check_{bending} := if(F_b < F_y \cdot 0.6, "OK", "REDESIGN")$ $Check_{bending} = "OK"$

Yielding Stress Minor $F_{bmin} := \frac{Mmin}{S_y}$ $F_{bmin} = 3.38 ksi$

Yield Capacity Used Minor $Capacity_2 := \frac{F_{bmin}}{F_y}$ $Capacity_2 = 0.068$

Check Minor Bending Stress in Beam $Check_{bendingmin} := if(F_{bmin} < F_y \cdot 0.6, "OK", "REDESIGN")$ $Check_{bendingmin} = "OK"$

Check Shear $Aw := d \cdot tw$ $Cv := 1$

Shear Variables $Vn := 0.6 F_y \cdot Aw \cdot Cv$ $Aw = 1 \cdot in^2$ $Vn = 30 \cdot kip$

Shear Strength $Check_{shear} := if\left(V < \frac{Vn}{1.5}, "OK", "REDESIGN"\right)$ $Check_{shear} = "OK"$

Check Shear Minor $Aw := d \cdot tw$ $Cv := 1$

Shear Variables $Vn := 0.6 \cdot F_y \cdot Aw \cdot Cv$ $Aw = 1 \cdot in^2$ $Vn = 30 \cdot kip$

Shear Strength Minor

$\text{Check}_{\text{shearmin}} := \text{if}\left(\text{Vmin} < \frac{\text{Vn}}{1.5}, \text{"OK"}, \text{"REDESIGN"}\right)$ $\text{Check}_{\text{shearmin}} = \text{"OK"}$

Check Tension

Yielding or Rupture

$\text{Check}_{\text{tension}} := \text{if}\left[\frac{(F_y \cdot A_g)}{1.67} > \frac{(F_u \cdot A_g)}{2}, \text{"RUPTURE"}, \text{"YEILD"}\right]$ $\text{Check}_{\text{tension}} = \text{"YEILD"}$

Check for tensile yielding

$\text{Pn} := F_y \cdot A_g$ $\Omega t := 1.67$

$\text{Check}_{\text{tensile}} := \text{if}\left(\frac{\text{Pn}}{\Omega t} > T, \text{"OK"}, \text{"REDESIGN"}\right)$ $\text{Check}_{\text{tensile}} = \text{"OK"}$

Check Compression

Check Slenderness

$\lambda p := 1.12 \cdot \sqrt{\frac{E}{F_y}} = 26.973$ $\lambda r := 1.40 \cdot \sqrt{\frac{E}{F_y}} = 33.716$ $\frac{h}{tw} = 24.5$

Compresssion

$K := 1$ $K \cdot L = 20\,\text{ft}$ $\frac{K \cdot L}{r_{\min}} = 157.895$ $\text{Check} := \text{if}\left(\frac{K \cdot L}{r_{\min}} < 200, \text{"OK"}, \text{"BAD"}\right)$

$F_e := \frac{\pi^2 \cdot E}{\left(\frac{K \cdot L}{r_{\min}}\right)^2}$ $F_e = 11.481 \cdot \text{ksi}$ $\text{Check} = \text{"OK"}$

$F_{cr} := 0.877 \cdot F_e$ $F_{cr} = 10.068 \cdot \text{ksi}$ $C_{cr} := 0.6 \cdot F_{cr} \cdot A_g$ $C_{cr} = 20.358 \cdot \text{kip}$

$\text{Check}_{\text{comp}} := \text{if}\left(C_{cr} > C, \text{"OK"}, \text{"REDESIGN"}\right)$ $\text{Check}_{\text{comp}} = \text{"REDESIGN"}$

Check Buckling

$P_{cr} := \frac{\pi^2 \cdot E \cdot A_g}{\left(\frac{K \cdot L}{r_{\min}}\right)^2}$ $P_{cr} = 38.689 \cdot \text{kip}$ $\text{Check}_{\text{buck}} := \text{if}\left(P_{cr} > C, \text{"OK"}, \text{"REDESIGN"}\right)$

$\text{Check}_{\text{buck}} = \text{"REDESIGN"}$

Use Braces at midpoint

$\text{Lnew} := 10\text{ft}$

$F_{\text{enew}} := \frac{\pi^2 \cdot E}{\left(\frac{K \cdot \text{Lnew}}{r_{\min}}\right)^2}$ $F_{\text{enew}} = 45.922 \cdot \text{ksi}$

$F_{\text{crnew}} := 0.877 \cdot F_{\text{enew}}$ $F_{cr} = 10.068 \cdot \text{ksi}$ $C_{\text{crnew}} := 0.6 \cdot F_{\text{crnew}} \cdot A_g$ $C_{\text{crnew}} = 81.434 \cdot \text{ki}$

$\text{Check}_{\text{compnew}} := \text{if}\left(C_{\text{crnew}} > C, \text{"OK"}, \text{"REDESIGN"}\right)$ $\text{Check}_{\text{compnew}} = \text{"OK"}$

$P_{\text{crnew}} := \frac{\pi^2 \cdot E \cdot A_g}{\left(\frac{K \cdot \text{Lnew}}{r_{\min}}\right)^2}$ $P_{\text{crnew}} = 154.758 \cdot \text{kip}$ $\text{Check}_{\text{bucknew}} := \text{if}\left(P_{\text{crnew}} > C, \text{"OK"}, \text{"REDESIGN"}\right)$

$\text{Check}_{\text{bucknew}} = \text{"OK"}$

Angle Design Check

Member

Units:

$kip := 1000 lbf \quad ksi := 1000 psi \quad kcf := kip \cdot ft^{-3}$

Modulus of Elasticity of Steel $E := 29000 ksi$

Yield Stress of Steel $F_y := 36 ksi$

Tensile Stress of Steel $F_u := 58 ksi$

Factor of Safety for Flexural Members $\Omega := 1.67$

Maximum Loading:

Length of Member $L_m := 4 ft$

Maximum Deflection $\Delta_{max} := .001 ft$

Axial Load $a := 5.91 kip$ $\quad a = 5910 ft \cdot \frac{lbf}{ft}$

Shear Force $R_1 := .58 kip$ $\quad R_1 = 580 lbf$

Moment at Center of Member $M := .16 kip \cdot ft$ $\quad M = 160 lbf \cdot ft$

Check Yield Stress:

3 x3x 1/2

Angle Properties $A := 2.75 in^2$ $\quad I := 2.2 in^4$ $\quad S_x := 1.06 in^3$ $\quad r := .895 in$ $\quad Z := 1.91 in^3$ $\quad b := 3 in$ $\quad t := \frac{1}{2} in$

Check Deflection $CheckDefl := if\left(\Delta_{max} \le \frac{L_m}{360}, "OK", "Redesign"\right)$ $\quad \frac{L_m}{360} = 0.1 \cdot in$ $\quad \Delta_{max} = 0.012 in$ $\quad \boxed{CheckDefl = "OK"}$

Moment Yielding $M_y := F_y \cdot S_x$ $\quad M_y = 3.2 \cdot kip \cdot ft$

Nominal Flexural Strength for 1 Angles $M_n := \frac{(1.5 \cdot M_y)}{\Omega}$ $\quad \boxed{M_n = 2.9 \cdot kip \cdot ft}$

Yield Capacity Used $Capacity := \frac{M}{M_n}$ $\quad Capacity = 0.06$

Check Bending Stress in Plate $Check_{yield} := if(M < M_n, "OK", "REDESIGN")$ $\quad \boxed{Check_{yield} = "OK"}$

$Cv := 1 \quad Aw := b \cdot t$

Nominal Shear Strength $Vn := 0.6 F_y \cdot Cv \cdot Aw$ $\quad Vn = 32.4 kip$ $\quad Aw = 1.5 \cdot in^2$

Allowable Shear Strength $\frac{Vn}{1.67} = 19.4 kip$

Shear Strength Check $Check_{shear} := if\left(R_1 < \frac{Vn}{1.67}, "OK", "REDESIGN"\right)$ $\quad \boxed{Check_{shear} = "OK"}$

Check Lateral Torsional Buckling of Angle:

Unbraced Length $L_b := 4\text{ft} + 0\text{in}$

$C_b := 1$

Elastic Lateral-Tosional Buckling Moment Max Tension at Toe
$$M_e := \frac{0.66 \cdot E \cdot b^4 \cdot t \cdot C_b}{L_m^2} \cdot \left[\sqrt{1 + 0.78 \cdot \left(\frac{L_m \cdot t}{b^2}\right)^2} + 1\right]$$
equation (F10 − 4b) $M_e = 99.8 \cdot \text{kip} \cdot \text{ft}$

Check If Lateral-Torsional Buckling Applies (b) CheckALTBb := if($M_e > M_y$,"L-T-B Applies","M.n_LTB2 Does Not Apply")

CheckALTBb = "L-T-B Applies"

Nominal Flexural Strength Based on Lateral Torsional Buckling For
$$M_{n\_LTB2} := \frac{\left[\left(1.92 - 1.17 \cdot \sqrt{\frac{M_y}{M_e}}\right) \cdot M_y\right]}{\Omega}$$

$M_{n\_LTB2} = 3.258 \cdot \text{kip} \cdot \text{ft}$

Check Lateral Torsioinal Buckling CHLTB := if($M_{n\_LTB2} > M$,"OK","Redesign")

CHLTB = "OK"

SAP2000 Model:

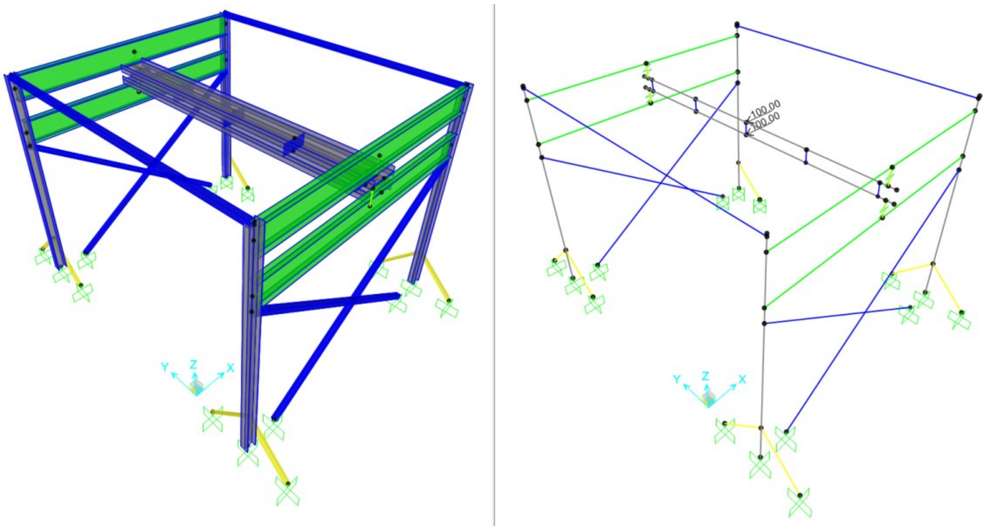

Figure D-3. SAP2000 Finite Element Model: 3-D (right) and Frame Span Loads (right)

D-2.5 Lining of Testing Furnace

In order to keep the furnace walls from seeing extreme temperatures and contain the heat within the furnace the walls had to be lined with insulation. The purchased Kaowool insulation was used for this task. A high temperature adhesive was used to line all of the interior walls, ceiling, and floor of the testing furnace. Covers for the three openings which allow for the furnace to be completely open (all three holes open) as well as close off any or all of the holes were also created.

D-2.6 Control Panel Power Hook-up

The control panel required 480 V at 100 amps of power. The panel came with a 10 foot power cord that had a pin and sleeve type plug-in at its end. The current power supply at the ERC had to initially be checked to insure it could produce this much power. Once that was confirmed Junior Garza was utilized to retrofit an existing electrical panel to deliver the required power. This retrofit included installing a compatible connection point so that the existing power cord could be plugged into the panel.

D-3 Remaining Tasks

The following sections provide a summary of the remaining tasks to be completed for the project. For several of these tasks a considerable amount of work has already been performed and several are currently in the process of being implemented, the status of each task is provided in the titles of the sections. For the tasks currently underway, in addition to a brief overview, the current state as of the submission of this thesis is presented.

D-2.1 Electric Wiring (In Progress)

The electrical wiring from the control panel to the ceramic heating plates was another component that needed to be considered during the setup. Because the ceramic plates would be placed within the furnace the wiring needs to either be protected from seeing elevated temperatures or be able to operate under high temperatures. This task is currently in the design phase and is being worked on through a joint effort with CSU Facilities. Rochelle Mellott is the lead electrical engineer working on the design of the power hook up.

D-2.1 Ceramic Heating Plate Support (In Progress)

When developing the furnace priority was given to having a mobile setup that allows the heating plates to not only be moved to any location within the furnace but also throughout the lab. This requires a way of supporting the heating plates that allows the plates to be moved vertically and horizontally, and that can be unplugged and moved to any location within the lab. Several preliminary designs have been made on this setup and the final design is currently being worked on. Coordination with Junior Garza is prudent for this task since he will likely build the units.

D-2.1 Calibration of System

Once the electrical wiring to the heating plates has been installed and the plate support system has been constructed the system will have to be calibrated. This will include learning the program to control the power input to the plates as well as analyzing the achieved temperature gradients within the furnace. Furthermore, the temperature distribution throughout the surrounding lab will have to be evaluated to insure no damage to existing systems will occur.

This will also include verifying that the applied insulation will provide an effective thermal barrier to the walls of the furnace.

D-2.1 Strain Measurement Device (Partially Completed)

One of the biggest issues with performing fire testing within a furnace is finding instrumentation for data acquisition that can withstand the high temperatures. The ability to capture strain values at critical regions of the specimen being tested is of particular concern. Two main alternatives have been identified and invest aged for this purpose. The first option was to use high temperature strain gauges that can withstand the elevated temperatures within the furnace. While several options exist that would meet the requirements of the project they are very expensive and typically can only be used for one test before having to be replaced. The second option was to place high temperature cameras within the furnace and use an image processing software to calculate strain values. For this option several high temperature cameras were analyzed and at the time of this thesis the best option appeared to be the CANTY Minitemp high temperature camera. Several image processing software options were also investigated with emphasis given to free programs. Two free Matlab codes were utilized and a series of 2-D strain tests were performed to analyze the programs. A simple tension test was performed on 20 steel rod specimen and pictures taken during the test. The pictures were then input into the programs and the values obtained compared to values taken using a strain gauge during the test. Good agreement was found for both programs. However, taking this from 2-D to 3-D strain measurements presents several new obstacles that have not been addressed yet and still need attention.

D-2.1 Actuator Setup (Partially Completed)

The actuator that will be used to provide loading at the top of the furnace still needs to be installed. The hosing up to the actuator location and the control setup for the actuator have been installed but the connection to the support beam and the actual installation of the actuator still need to be performed.

D-2.1 Specimen Support System (Partially Completed)

For the initial tests the thought is to perform cyclic loading on a beam-column subassembly followed by heating of the furnace to provide a fire simulation. In order to perform this test support for the specimen must be provided at the outside of the furnace. Importance has been placed on providing support that doesn't overconstrain the specimen and allows for a realistic representation of the constraint the specimen would actually see. Several preliminary design ideas have been evaluated on how to perform this task but further investigation is required.

D-4 Project Personnel

Table D1 provides a brief summary of the various personnel involved in the project. The table includes a short description of their role in the project as well as contact information.

Table D-1. Summary of Project Personnel

Name	Title	Project Role	Phone #	Email Address
Dr. Hussam Mahmoud	Assistant Professor Colorado State University Civil and Environmental Engineering	Project supervisor in charge of the design and setup of the fire testing furnace. Oversaw all work to date performed for the furnace setup	(970) 491-6605	hussam.mahmoud@colostate.edu
Collin Turbert	Graduate Research Assistant Colorado State University Civil and Environmental Engineering	Lead graduate research assistant working for Dr. Mahmoud on the setup of the furnace. Performed tasks described in Section D-2	(208) 713-1463	collinturbert@gmail.com
Mehrdad Memari	Graduate Research Assistant Colorado State University Civil and Environmental Engineering	Graduate research assistant working for Dr. Mahmoud. Oversaw a large portion of the work done to date	NA	mehrdad.memari@gmail.com
Jeffrey Newcomer	Undergraduate Research Assistant Colorado State University Civil and Environmental Engineering	Undergraduate research assistant working for Dr. Mahmoud. Worked under the supervision of Collin Turbert helping build the ceramic heating plate cases, lining the furnace with insulation, and design of the specimen support system	NA	jnewcome@rams.colostate.edu
Junior Garza	ERC Shop Foreman	Performed numerous tasks during the setup including the environmental chamber retrofit, construction of the support frame, and the power hook-up to the control panel	(970) 491-8664	garza@engr.colostate.edu
Dr. Christopher Thornton	Associate Professor Director Engineering Research Center Civil and Environmental Engineering	Providing oversight on several aspects of the project including the wiring of the control panel to the heating plates as well as several of the previously mentions remaining tasks	(970) 491-8394	thornton@engr.colostate.edu
Eric March	Asbestos/Lead Coordinator Health and Safety Coordinator Colorado State University	Providing oversight and advice on all safety and workplace related hazards	(970) 491-4833	eric.march@colostate.edu
Barry Willier	Project Manager Facilities Management Colorado State University	Project manager in charge of the design and construction of the electrical wiring from the control panel to the heating plates	(970) 491-6567	barry.willier@colostate.edu

Table D-1. Summary of Project Personnel (cont.)

Name	Title	Project Role	Phone #	Email Address
Jesse Parker	Facilities Coordinator Colorado State University College of Engineering	General oversight and correspondence on the work done by facilities for the project.	(970) 491-3885	jesse.parker@colostate.edu
Greg Curnow	Sales Representative E&M Sales	Sales contact at E&M Sales used for purchasing the control panel, heating plates, thermocouples and insulation (Tania Difeo has also a point of contact)	(303) 979-5000 X235	gcurnow@e-msales.com
Tom Glanz	President Glanz Electrical Contracting, Inc.	Initially involved in the design of the electrical wiring from the control panel to the ceramic heating plates	(970) 482-5218	TGlanz@glanzelectric.com
Rochelle Mellott	Electric Utility Engineer Facilities Management Colorado State University	Lead electrical engineer currently working on the design and construction of the electrical wiring from the control panel to the heating plates	(970) 491-0161	rochelle.mellot@colostate.edu